

A chemical genetic approach to identify new treatments for melanoma

By

Kimberley Marie Hanson

A thesis submitted to the University of East Anglia for the degree
of Doctor of Philosophy

The University of East Anglia, Norwich
School of Biological Sciences

June 2015

Number of words: 51,751

© This copy of the thesis has been supplied on condition that anyone who consults it is understood to recognise that its copyright rests with the author and that use of any information derived there-from must be in accordance with current UK Copyright Law. In addition, any quotation or extract must include full attribution.

Abstract

Melanoma is the most deadly form of skin cancer which develops from the pigment producing cells called melanocytes. Unlike the majority of other cancers, the incidence rates of melanoma are still on the rise and the few treatment options currently available are being hindered by resistance. A recent chemical genetic screen carried out in *Xenopus laevis* embryos identified that the already FDA approved drug leflunomide used for rheumatoid arthritis patients also holds potential therapeutic value in treating melanoma. This thesis shows the results of a new successful chemical genetic and cell based viability screen of the NCI Diversity set II library. 13 potential novel targets for treating melanoma were identified.

This thesis also further characterised the function of leflunomide and showed that leflunomide reduces the number of viable cells in both wild type and BRAF^{V600E} mutant melanoma cell lines. Further experiments revealed leflunomide reduces cell proliferation and causes cells to arrest in G1 of the cell cycle. Cell death assays showed leflunomide to cause apoptosis coupled with a stable mitochondrial membrane potential at 25 and 50 μ M leflunomide. However at 100 μ M the number of apoptotic cells decreased and an increase in the number of viable cells with a hyperpolarised mitochondrial membrane potential was observed. To determine if leflunomide had the potential to be used in combination with other melanoma drugs, it was tested in combination with the MEK inhibitor selumetinib. This combination showed a synergistic effect in the majority of the cell lines tested. The M375 melanoma cell line produced strong synergy values across all of the combinations of leflunomide and selumetinib tested. This combination led to an enhanced decrease in tumour size when tested *in vivo* in a mouse xenograft model when compared to either drug alone.

Key words; Melanoma, BRAF^{V600E}, leflunomide, cell viability, selumetinib, synergy, combination index value, NCI Diversity Set II, *Xenopus laevis*.

Contents page

Abstract	2
Contents page	3-7
List of figures	8-14
List of tables	15
Abbreviation list	16-18
Acknowledgments	19
Chapter 1: Introduction	20
– 1.1 Melanoma	20
– 1.1.1 Normal melanocyte development	20
– 1.1.2 Melanocytes and melanoma	21-22
– 1.1.3 The MAPK pathway and melanoma	22-23
– 1.1.4 Homeostatic negative feedback regulation of the MAPK pathway	24-25
– 1.1.5 Mutations in the MAPK pathway	26-28
– 1.1.6 The PI3K pathway and melanoma	28-30
– 1.1.7 The CDKN2A locus and melanoma	30
– 1.1.8 C-KIT and melanoma	30-31
– 1.1.9 G α subunits and melanoma	32
– 1.2 Therapeutic targeting	32-33
– 1.2.1 Immunotherapy	33
– 1.2.2 Ipillimumab	33-35
– 1.2.3 PD-1 antibody treatment	36-37
– 1.2.4 Small molecule MAPK pathway inhibitors	37
– 1.2.5 Vemurafenib	37-38
– 1.2.6 MEK inhibitors	38-40
– 1.2.7 Paradoxical ERK activation and vemurafenib resistance phenomena	40-44
– 1.3 Combinatorial therapies and future approaches	44

– 1.3.1 Combined immunotherapy	45-46
– 1.3.2 Combined BRAF inhibitors and immunotherapy	46-47
– 1.3.3 Combined BRAF inhibitors and MEK inhibitors	47-49
– 1.3.4 Triple agent combination	49-50
– 1.3.5 Intermittent treatment to overcome BRAF inhibitor resistance	50-51
– 1.4 Chemical genetics	52
– 1.4.1 Chemical genetic screens	52
– 1.4.2 Model organisms for chemical genetic screens	53-54
– 1.5 Leflunomide	54-56
Aims	57
Chapter 2: Materials and methods	58
– 2.1 Frequently used solutions	58-59
– 2.2 Cell lines and cell culture	60
– 2.3 Mycoplasma PCR	60-61
– 2.4 Drugs and compounds	61
– 2.5 Cell viability assays	61-63
– 2.6 BrdU proliferation assay	63-64
– 2.7 Cell cycle analysis	64
– 2.8 Annexin V apoptosis assay	64-65
– 2.9 JC1 mitochondrial membrane ($\Delta(\Psi)$) potential assay	65
– 2.10 Mitotracker green	65-66
– 2.11 Combinatorial cell viability assays	66-67
– 2.12 Calculation of drug synergy	67
– 2.13 Western blots	67-72
– 2.14 Preliminary mouse study	72
– 2.15 Mouse xenograft study	72
– 2.16 Testes isolation	73
– 2.17 Generation of <i>X.laevis</i> eggs and <i>in vitro</i> fertilisation	73
– 2.18 De-jellying of the embryo	73
– 2.19 Embryo fixing	74
– 2.20 Compounds used in chemical genetic screen	74

– 2.21 Chemical genetic screen using <i>X.laevis</i>	74
– 2.22 Observing the embryo	75
– 2.23 Analysis of the chemical screen	75
– 2.24 Validation of compounds	75
– 2.25 Cell viability assays on NCI ‘hit’ compounds	76

**Chapter 3: Chemical genetic screen of the NCI diversity set II library
in *X.laevis* embryos succeeded by a cell-based screen** **77**

– 3.1 Introduction	77-78
– 3.2 Results	78
– 3.2.1 Phenotypic scoring criteria of the chemical genetic screen	78-79
– 3.2.2 Summary of results of the chemical genetic screen of the NCI Diversity set II library on <i>X.laevis</i> embryos	79-82
– 3.2.3 Compounds categorised into the total pigment loss phenotype	83-84
– 3.2.4 Compounds categorised into the partial pigment phenotype	85-87
– 3.2.5 Compounds categorised into the abnormal melanophore morphology phenotype	88-89
– 3.2.6 Compounds categorised into the abnormal melanophore migration phenotype	90-91
– 3.2.7 Compounds classified into the abnormal general morphology phenotype	92-93
– 3.2.8 Compounds classified into the abnormal eye development phenotype	94-95
– 3.2.9 Compounds classified into the edema phenotype	96
– 3.2.10 Compounds classified into the blistering phenotype	97
– 3.2.11 Dose-response assays on the 72 ‘hit’ compounds	98-99
– 3.2.12 Cell-based cell viability screen on the 72 ‘hit’ compounds	100-103
– 3.2.13 Statistical analysis of the IC ₅₀ ’s generated between the A375, RD1 and HEK293 cell lines	104-108
– 3.3 Discussion	108-112

Chapter 4: Characterising the function of leflunomide as an effective melanoma drug	113
– 4.1 Introduction	113-115
– 4.2 Results	116
– 4.2.1 Cell viability assays	116-121
– 4.2.2 Visualisation of leflunomide treated A375 cells	121-122
– 4.2.3 BrdU proliferation assay	123-124
– 4.2.4 Cell cycle analysis	124-129
– 4.2.5 Annexin V assay	129-134
– 4.2.6 JC-1 mitochondrial membrane ($\Delta(\Psi)$) potential assay	134-136
– 4.2.7 Mitotracker green staining	137-140
– 4.3 Discussion	141-148
Chapter 5: Investigating the possibility of using leflunomide in combination with selumetinib to treat melanoma	149
– 5.1 Introduction	149
– 5.2 Results	150
– 5.2.1 Selumetinib cell viability assays	150-152
– 5.2.2 Western blot detection for phospo-ERK and total ERK	153
– 5.2.3 Leflunomide and selumetinib combinatorial cell viability assays	154-165
– 5.2.4 Calculation of drug synergy between leflunomide and selumetinib	165-178
– 5.2.5 Pre-treatment of the melanoma cells for 24 hours with leflunomide or selumetinib cell viability assays	178-188
– 5.2.6 Pre-treatment of the melanoma cells for 24 hours with leflunomide or selumetinib and calculation of drug synergy	189-198
– 5.2.7 Western blots detecting for apoptotic markers in leflunomide and selumetinib treated cells	199-200
– 5.2.8 Pilot mice study	201-204
– 5.2.9 Mouse xenograft study	204-209
– 5.3 Discussion	210-219

Chapter 6: Overall Summary and future directions 220-225

References 226-249

List of figures

Chapter 1: Introduction

- 1.1. Progression of melanocyte transformation 22
- 1.2. A schematic diagram of the homeostatic negative feedback loops of the MAPK pathway 25
- 1.3. The MAPK signalling cascade 26
- 1.4. The molecular pathogenesis of melanoma with regards to RAS activation 29
- 1.5. The CDKN2A locus and molecular function of the tumour suppressors ARF and INK4A 31
- 1.6. T-cell activation and mechanism of action of ipilimumab 34
- 1.7. Mechanism underlying BRAF inhibition in cells harbouring the BRAF^{V600E} mutation and paradoxical signalling of the MAPK pathway caused by SBI's 42
- 1.8. Schematic representation of the mechanism driving BRAF inhibitor resistance 44
- 1.9. The proposed model of the theory behind intermittent drug delivery and the onset of resistance 51
- 1.10. The effect of A771723 on melanoma cell viability and mouse xenograft 56

Chapter 2: Materials and methods

- 2.1. Experimental design of how the cell viability assays were carried out 63
- 2.2. Experimental design of the combinatorial cell viability assays whereby leflunomide and selumetinib were added either at the same time or 24 hour pre-treatment 67
- 2.3. Illustration showing how to assemble a transfer cassette 70

Chapter 3: Chemical genetic screen of the NCI diversity set II library in *X.laevis* embryos succeeded by a cell-based screen

- 3.1. Annotation of an *X.laevis* embryo showing the anterior of the embryo to the left and the posterior to the right 78
- 3.2. Summary of the phenotypes produced from the ‘hit’ compounds in the chemical genetic screen of the NCI diversity set II library 82
- 3.3. NCI compounds that caused a total loss of pigment in *X.laevis* embryos 84
- 3.4. NCI compounds that caused a partial loss of pigment in *X.laevis* embryos 86-87
- 3.5. NCI compounds that caused abnormal melanophore morphology in *X.laevis* embryos 89
- 3.6. NCI compounds that caused abnormal melanophore migration in *X.laevis* embryos 91
- 3.7. NCI compounds that caused abnormal general morphology in *X.laevis* embryos 93
- 3.8. NCI compounds that caused abnormal eye development in *X.laevis* embryos 94-95
- 3.9. NCI compounds that caused edema in *X.laevis* embryos 96
- 3.10. NCI compounds that caused blistering in *X.laevis* embryos 97
- 3.11. Dose response curves of NCI compounds showing cell viability of the A375, RD1 and HEK293 cell lines per compound 101-102
- 3.12. Statistical analysis of 11 of the NCI compounds comparing the cell viability for DMSO control to the 1×10^{-9} M for each of the compounds 105
- 3.13. Data used for the statistical analysis for the comparison of the IC_{50} 's for the A375, RD1 and HEK293 cell lines 107-108

Chapter 4: Characterising the function of leflunomide as an effective melanoma drug

- 4.1. A schematic diagram of the *de novo* pyrimidine synthesis Pathway of rUMP 114
- 4.2. Cell viability data for the A375 melanoma cell line in response to a range of leflunomide concentrations analysed by two different reagents 116
- 4.3. Leflunomide caused a dose-dependent decrease in cell viability in eight human melanoma cell lines 118
- 4.4. Leflunomide reduced cell viability at a similar rate in wildtype BRAF melanoma cells and BRAF^{V600E} mutant cell lines 120
- 4.5. Leflunomide caused a dose-dependent decrease in cell viability in melanocytes, HEK293 and RD1 cells 121
- 4.6. Phenotypic images of A375 cells treated with leflunomide for 72 hours 122
- 4.7. Percentage of BrdU positive A375 cells after 72 hours treatment with leflunomide 124
- 4.8. Representative DNA histogram plots of the cell cycle analysis performed on A375 cells treated for 72 hours with leflunomide 125
- 4.9. Cell cycle phase distribution for A375 cells treated for 72 hours with leflunomide 126
- 4.10. Representative data showing the distribution of cells in each phase of the cell cycle 128
- 4.11. Representative pseudo plots of cell death analysis determined by flow cytometry 130
- 4.12. Graph quantifying the percentage of A375 cells that are viable, early apoptotic, late apoptotic and necrotic after 72 hours of treatment with leflunomide 131
- 4.13. Increasing concentrations of leflunomide caused a dose-dependent increase in the fold change in time compared to the DMSO control 133
- 4.14. Representative JC-1 plots measuring mitochondrial

–	membrane potential determined by flow cytometry	135
–	4.15. Graph quantifying the intensity of red and green fluorescence of JC-1 dye determined by flow cytometry	136
–	4.16. Representative data plot showing the intensity of green fluorescence for DMSO, 25, 50 and 100 μ M leflunomide treated A375 cells	138
–	4.17. Quantification of the fold change of the intensity of green fluorescence between 25, 50 and 100 μ M leflunomide treated A375 cells and DMSO control cells	139
–	4.18. Increasing concentrations of leflunomide caused an increase in the fold change in time compared to the DMSO control	140

Chapter 5: Investigating the possibility of using leflunomide in combination with selumetinib to treat melanoma

–	5.1. Selumetinib caused a dose-dependent decrease in cell viability in eight human melanoma cells	151
–	5.2. Selumetinib had little effect on cell viability of the melanocytes (shown in black), HEK293 (shown in red) and RD1 (shown in blue) cell lines	152
–	5.3. Western blot analysis confirming the decrease in protein levels of phosphor-ERK upon treatment of 0.1 and 1 μ M selumetinib in A375 and M202 melanoma cell lines	153
–	5.4. The combination of leflunomide and selumetinib reduced cell viability in the M202 cell line	156
–	5.5. The combination of leflunomide and selumetinib reduced cell viability in the M285 cell line	157
–	5.6. The combination of leflunomide and selumetinib reduced cell viability in the M375 cell line	158
–	5.7. The combination of leflunomide and selumetinib reduced cell viability in the M296 cell line	159
–	5.8. The combination of leflunomide and selumetinib reduced cell viability in the A375 cell line	160
–	5.9. The combination of leflunomide and selumetinib reduced cell	

viability in the M229 cell line	161
– 5.10. The combination of leflunomide and selumetinib reduced cell viability in the SKmel28 cell line	162
– 5.11. The combination of leflunomide and selumetinib reduced cell viability in the SKmel5 cell line	163
– 5.12. A representative graph highlighting how the combination index values are to be interpreted	166
– 5.13. Combination index values for M202 melanoma cell line with leflunomide and selumetinib in combination at increasing concentrations	168
– 5.14. Combination index values for M285 melanoma cell line with leflunomide and selumetinib in combination at increasing concentrations	169
– 5.15. Combination index values for M375 melanoma cell line with leflunomide and selumetinib in combination at increasing concentrations	170
– 5.16. Combination index values for M296 melanoma cell line with leflunomide and selumetinib in combination at increasing concentrations	171
– 5.17. Combination index values for A375 melanoma cell line with leflunomide and selumetinib in combination at increasing concentrations	172
– 5.18. Combination index values for M229 melanoma cell line with leflunomide and selumetinib in combination at increasing concentrations	173
– 5.19. Combination index values for SKmel28 melanoma cell line with leflunomide and selumetinib in combination at increasing concentrations	174
– 5.20. Combination index values for SKmel5 melanoma cell line with leflunomide and selumetinib in combination at increasing concentrations	175
– 5.21. Sensitivity of the A375 melanoma cell line with pre-treatment for 24 hours with leflunomide, prior to the addition of selumetinib	181

- 5.22. Sensitivity of the A375 melanoma cell line with pre-treatment for 24 hours with selumetinib, prior to the addition of leflunomide 182
- 5.23. Sensitivity of the M229 melanoma cell line with pre-treatment for 24 hours with leflunomide, prior to the addition of selumetinib 183
- 5.24. Sensitivity of the M229 melanoma cell line with pre-treatment for 24 hours with selumetinib, prior to the addition of leflunomide 184
- 5.25. Sensitivity of the M375 melanoma cell line with pre-treatment for 24 hours with leflunomide, prior to the addition of selumetinib 185
- 5.26. Sensitivity of the M375 melanoma cell line with pre-treatment for 24 hours with selumetinib, prior to the addition of leflunomide 186
- 5.27. Sensitivity of the M285 melanoma cell line with pre-treatment for 24 hours with leflunomide, prior to the addition of selumetinib 187
- 5.28. Sensitivity of the M285 melanoma cell line with pre-treatment for 24 hours with selumetinib, prior to the addition of leflunomide 188
- 5.29. Combination index values for the A375 melanoma cell line with pre-treatment for 24 hours with leflunomide, prior to the addition of selumetinib 191
- 5.30. Combination index values for the A375 melanoma cell line with pre-treatment for 24 hours with selumetinib, prior to the addition of leflunomide 192
- 5.31. Combination index values for the M229 melanoma cell line with pre-treatment for 24 hours with leflunomide, prior to the addition of selumetinib 193
- 5.32. Combination index values for the M229 melanoma cell line with pre-treatment for 24 hours with selumetinib, prior to the addition of leflunomide 194
- 5.33. Combination index values for the M375 melanoma cell line

with pre-treatment for 24 hours with leflunomide, prior to the addition of selumetinib	195
– 5.34. Combination index values for the M375 melanoma cell line with pre-treatment for 24 hours with selumetinib, prior to the addition of leflunomide	196
– 5.35. Combination index values for the M285 melanoma cell line with pre-treatment for 24 hours with leflunomide, prior to the addition of selumetinib	197
– 5.36. Combination index values for the M285 melanoma cell line with pre-treatment for 24 hours with selumetinib, prior to the addition of leflunomide	198
– 5.37. Western blot analysis detecting the presence for anti and pro apoptotic markers in A375 melanoma cells	199
– 5.38. Results of the pilot study showing tumours for the A375, SKmel5 and M229 cell lines, but not for the M285 and M375 melanoma cell lines	203
– 5.39. Results of the repeated pilot study showing tumours for the M285 and M375 cell lines	205
– 5.40. The combination of leflunomide and selumetinib reduces the average tumour volume greater than either drug alone	207
– 5.41. The combination of leflunomide and selumetinib reduces tumour weight greater than either drug alone	208
– 5.42. Visualisation of the excised tumours from the mouse xenograft study	209

List of tables

Chapter 2: Materials and methods

- 2.1. The seeding densities for each cell line used for the cell viability assays 62
- 2.2. The different drug conditions A375 melanoma cells were subject to for detection of specific proteins by western blot 68
- 2.3. Composition of the resolving and stacking gels 69
- 2.4. Primary and secondary antibodies used in western blots on A375 melanoma cells (blocking solution, dilution factor and supplier also shown) 71

Chapter 3: Chemical genetic screen of the NCI diversity set II library in *X.laevis* embryos succeeded by a cell-based screen

- 3.1. Dose response data for NCI 133002 and NCI 111848 99
- 3.2. The generated IC₅₀'s for 32 of the NCI compounds for the A375, RD1 and HEK293 cell lines 103

Chapter 4: Characterising the function of leflunomide as an effective melanoma drug

- 4.1. The eight human melanoma cell lines used and their status for the BRAF^{V600E} mutation 117
- 4.2. IC₅₀ values for the eight melanoma cell lines, HEK293, RD1 cells and melanocytes in response to leflunomide 119
- 4.3. Quantification of the percentage of cells in each phase of the cell cycle 127

Chapter 5: Investigating the possibility of using leflunomide in combination with selumetinib to treat melanoma

- 5.1. IC₅₀ values for the eight melanoma cell lines, HEK293, RD1 cells and melanocytes in response to selumetinib 151
- 5.2. Summary of the combination index values for all eight melanoma cell lines 176

Abbreviation list

AKT	Protein kinase B
APC	Antigen-presenting cell
BIM	B-cell lymphoma 2 interacting mediator of cell death
BrdU	5-bromo-2'-deoxyuridine
BRIM	BRAF inhibitor in melanoma
BSA	Bovine serum albumin
CDKN2A	Cyclin-dependent kinase inhibitor 2A
CI	Combination index
CRD	Cysteine rich domain
CTLA-4	Cytotoxic T-lymphocyte antigen-4
Da	Daltons
DHODH	Dihydroorotate dehydrogenase
DMSO	Dimethyl sulfoxide
DUSPs	Dual-specificity phosphatases
EGFR	Epidermal growth factor receptor
ERK1/2	Extracellular-signal-regulated kinase 1 and 2
FA	Fraction affected
FDA	Food and Drug Administration
FSC	Forward scatter
GDP	Guanosine diphosphate
GEF	Guanine exchange factor
GOF	Gain of function
Gp100	Glycoprotein 100
GPCR	G-protein-coupled receptor
Grb2	Growth factor receptor-bound protein 2
GTP	Guanosine-5'-triphosphate
hCG	Human chorionic gonadotropin
HDM2	Human double minute 2
HEK293	Human Embryonic Kidney 293 cells
HePTP	Hematopoietic tyrosine phosphatase
IGF1R	Insulin-like growth factor 1 receptor
IRAE's	Immune-related adverse events

KA	Keratoacanthoma
MAPK	Mitogen-activated protein kinase
MCL-1	Myeloid cell leukemia.1
MEK1/2	Mitogen-activated protein kinase kinase 1 and 2
MHC	Major histocompatibility complex
MITF	Microphthalmia-associated transcription factor
MMP	Matrix metalloproteinases
MMR	Marc's modified Ringer's
MTD	Maximum tolerated dose
mTOR	Mammalian target of rapamycin
Mw	molecular weight
NCI	National Cancer Institute
OS	Overall survival
PARP	Poly (ADP-ribose) polymerase
PBS	Phosphate-buffered saline
PD-1	Programmed cell death protein-1
PDGFRβ	Platelet-derived growth factor receptor 1
PDK1	Phosphatidylinositol-dependent kinase-1
PD-L1	Programmed death-ligand 1
PDTX	Patient derived tumour xenografts
PFA	Paraformaldehyde
PFS	Progression-free survival
PI3K	Phosphoinositide 3-kinase
PIP₂	Phosphatidylinositol 4,5-bisphosphate
PIP₃	Phosphatidylinositol 3,4,5-trisphosphate
PLL	Poly-L-lysine
PMSG	Pregnant mare serum gonadotropin
PP2A	Protein phosphatase 2
PTEN	Phosphatase and tensin homolog
PUMA	p53 upregulated modulator of apoptosis
PVDF	Polyvinylidene difluoride
RA	Rheumatoid arthritis
RAF	Rapidly accelerated fibrosarcoma
RAS	Rat sarcoma

RB	Retinoblastoma protein
RBD	RAS binding domain
RCC	Renal cell carcinoma
RD1	Rhabdomyosarcoma
RGP	Radial growth phase
RPE	Retinal pigment epithelial
RTK	Receptor tyrosine kinase
rUMP	ribonucleotide uridine monophosphate
SARS	Structure-activity relationship studies
SBI's	Selective BRAF inhibitors
SCC	Squamous cell carcinoma
SCF	Stem cell factor
SCID	Severe combined immunodeficiency
SDS	Sodium dodecyl sulphate
SOS	Son of Sevenless
SPRY	Sprouty
<i>Spt5/spt6</i>	Suppressors of Ty 5 and 6
SSC	Side scatter
TAE	Tris-acetate-EDTA
TBST	Tris-buffered saline and Tween 20
TI	Therapeutic index
UV	Ultra-violet
VGP	Vertical growth phase

Acknowledgments

John Jarrold Trust and UEA – Thank you for providing the funds for this PhD

Dr Grant Wheeler - Thank you for being a great supervisor and all of the support over the past few years.

Dr Darren Sexton - Thank you for all of the help and advice regarding the flow cytometer.

Dr Stephen Robinson – Thank you for all of the help with the mice work.

Adam Hendry – Cheers for making Chapter 3 possible!

Wheeler and Munsterberg lab members, past and present – You have all been such a friendly bunch of people to work with. Thanks for listening to all of my lab talks and for all of the advice.

Mum, Dad, Jamie, Layla and Jam – Thank you to the best family I could ever ask for. A massive thank you for all of the support and the endless cups of tea to help me through my writing up!

Daisy and Bentley – My beautiful two dogs who have literally been by my side whilst I was writing up this thesis. I hope you enjoyed all of the late night walks, you are the best!

Poppy, Natalia, Trish, Hannah, Stef, Ayisha, Harpreet, Christina, Amanda – Each of you have all been amazing friends who have supported me every step of the way. Cheers for all of the fun times over the past 3 years.

I would like to dedicate this thesis to my Grandma and Grandad who both sadly passed away during my PhD. I hope I have done you proud.

Chapter 1: Introduction

1.1 Melanoma

1.1.1 Normal melanocyte development

Melanocytes are the specialised pigment-producing cells found predominately in the skin and eyes of humans and other vertebrates (Uong and Zon, 2010). Melanocytes are derived from a transient multipotent population of cells called the neural crest during embryogenesis. The neural crest is induced at the time of gastrulation in the ectoderm at the margins of the forming neural tube (Erickson and Reedy, 1998). Neural crest cells are initially multipotent. Gradually they become lineage-restricted giving rise to numerous different cell types such as smooth muscle, neurons of the peripheral nervous system, craniofacial bone and cartilage and melanocytes (Dorsky et al, 1998). The fate of neural crest cells is dependent upon the anatomical location they migrate to and the specific signals received there (Le Douarin et al, 2008).

Melanocytes migrate to and localise in the basal layer of the epidermis and in hair follicles (Slominski et al, 2004). In the epidermis melanocytes acquire a dendritic morphology allowing their cell projections to interact with surrounding keratinocytes at a ratio of approximately 1:40 (Cooper and Raible, 2009). This interaction with keratinocytes is vital for the homeostasis of melanocytes (Gray-Schopfer et al, 2007). Melanocytes play a key role in protecting our skin from ultra-violet (UV) induced DNA damage by producing and transferring melanin to keratinocytes in response to UV radiation, which results in the tanning process (Drummer and Flaherty, 2012). Ironically it is these melanocytes that are the precursors of melanoma, the most aggressive form of skin cancer (Gray-Schopfler et al, 2007).

1.1.2 Melanocytes and melanoma

Melanoma is the most deadly form of skin cancer. Unlike the majority of cancers, the incidence rates are still on the rise. Melanoma accounts for less than 5% of reported skin cancer cases but is perversely the cause of the majority of skin cancer deaths (Skin Cancer Foundation, 2012). In approximately 13,348 cases of malignant melanoma were diagnosed and in 2012, 2148 reported deaths from melanoma in 2012 in the UK (Cancer Research UK, 2012). Nonetheless if detected early the majority of melanomas are easily curable as, unlike other cancers, they are visible on the skin. It is only when melanoma has acquired the ability to spread to other parts of the body (often the brain, liver and lung) in later stages that it becomes incredibly hard to treat (Melanoma Research Foundation, 2012). The cause of melanoma tends to be a combination of exogenous (environmental) and endogenous (genetic) factors (Bandarchi et al, 2010).

A general consensus model for classical melanoma progression is shown in figure 1.1. Initially, melanocytes must become transformed allowing them to escape their tight regulation by keratinocytes (Gary-Schopfer et al, 2007). Consequently melanocytes can aberrantly proliferate resulting in the formation of benign nevi (or moles) within the epidermis that typically undergo cellular senescence. Once senescence is overcome or circumvented these nevi can then spread intra-epidermally referred to as the radial growth phase (RGP) (Zaidi et al, 2008). Melanomas within RGP (referred to as the primary melanoma) have low metastatic ability and are associated with good prognosis (Gaggioli and Sahain, 2007). The last stage called the vertical growth phase (VGP) is where cells have breached the basement membrane and invaded the underlying dermis. This transition to VGP is associated with poor prognosis as the cells have now acquired metastatic potential and can infiltrate the lymphatic or vascular systems and spread to distant metastatic sites (Gray-Schopfer et al, 2007). However it should be noted that not all metastatic melanomas progress through each of these stages and some can arise without a primary melanoma.

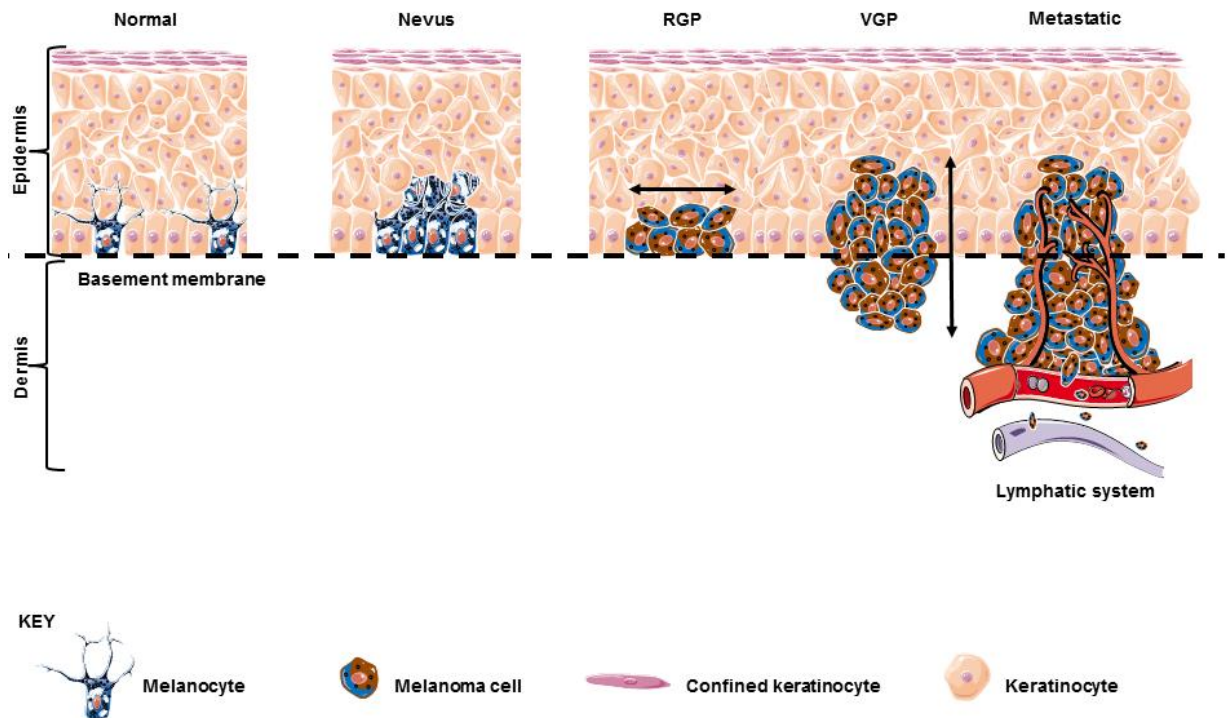


Figure 1.1. Progression of melanocyte transformation. Melanocytes undergo a series of stages to become malignant. The black arrows indicate the directional movement of melanocytes during radial growth phase (RGP) and vertical growth phase (VGP). Note that some malignant melanomas do not pass through the nevus stage. A nevus is a benign proliferation of melanocytes.

1.1.3 The MAPK pathway and melanoma

It has been established that many signalling pathways involved during melanocyte development are 'hijacked' in the development and progression of melanoma. One key pathway is the mitogen-activated protein kinase (MAPK) pathway (figure 1.2), in which receptor tyrosine kinases (RTK's) become activated upon the binding of extracellular growth factors, cytokines and hormone ligands. The cytoplasmic domain of RTK's consists of multiple tyrosine residues that are subject to phosphorylation, seven of which are auto phosphorylation sites. These tyrosine phosphorylation sites act as a recognition and assembly site for signalling adaptor proteins and guanine exchange factors (GEFs) (Ulrich and Schlessinger, 1990; Schlessinger, 2000; Pawson, 2002; Morandell et al, 2008). One such signalling adaptor protein is growth factor receptor bound protein 2 (Grb2). Grb2 consists of one SH2 domain and two SH3 domains. The SH2 domain allows the binding

of Grb2 to the tyrosine phosphorylated sites on RTK's in the cytoplasm. The remaining SH3 domains allow binding to proline rich regions on GEFs such as son of sevenless (SOS), forming a signalling complex (Li et al, 1993; Marshall CJ, 1996). The recruitment of Grb2 and SOS to RTK's brings SOS in close proximity to the plasma membrane bound small G-protein rat sarcoma (RAS). RAS is a member of the GTPase family and possess the intrinsic ability to hydrolyse guanosine-5'-triphosphate (GTP). In its inactive form RAS is bound to guanosine diphosphate (GDP) and in its active form is bound to GTP. Upon binding to SOS, SOS facilitates the activation of RAS by causing the dissociation of GDP from RAS, allowing the binding of GTP to RAS due to its 10-fold higher abundance compared with GDP in the cytoplasm (Quilliam et al, 1995; Downward J, 1996; Margarit et al, 2003).

Activated RAS binds with high affinity to rapidly accelerated fibrosarcoma (RAF) and causes RAF to translocate to the plasma membrane (Yajima et al, 2011; Drummer and Flaherty, 2012). For RAF to become fully activated, the effector binding domain of RAS must bind to two regions in the N-terminus of RAF; the RAS binding domain (RBD) and the cysteine rich domain (CRD). Both are necessary for RAF activation (Hu et al, 1995; Brtva et al, 1995). RAF is a serine/threonine kinase and in its active form initiates a phosphorylation cascade by phosphorylating and activating the downstream mitogen activated protein kinase kinase 1 and 2 (MEK1/2). RAF activates MEK1/2 by phosphorylating two serine residues conserved in the activation loop at positions 217 and 221. Phosphorylation at either residues results in partial activation of MEK1/2 (Alessi et al, 1994; Zheng et al. 1994; Kolch, 2000). Finally, activated MEK1/2 phosphorylates the extracellular-signal-regulated kinase 1 and 2 (ERK1/2). MEK1/2 are dual specificity kinases and can phosphorylate both serine/threonine and tyrosine residues. MEK1/2 activates ERK1/2 by phosphorylating both threonine and tyrosine residues of a conserved Thr-X-Tyr motif in the activation loop. Phosphorylation of both the threonine and tyrosine residues is required for ERK1/2 activation (Ferrel and Bhatt, 1994; Chen and Thorner, 2007, Kolch, 2000). The consequence

of activating this pathway is the regulation of cell proliferation, apoptosis, differentiation and survival (Solit and Rosen, 2010).

1.1.4 Homeostatic negative feedback regulation of the MAPK pathway

The MAPK pathway is subject to strict regulation predominately by homeostatic negative feedback mechanisms (Sturm et al, 2010). Several of these negative feedback mechanisms involve inhibitory phosphorylation of upstream components of the MAPK pathway, catalysed by ERK1/2 (figure 1.2). For example, ERK1/2 can phosphorylate some RTKs, which inhibits their kinase activity and dampens the signalling propagation (such as phosphorylation at Threonine 669 on epidermal growth factor receptor (EGFR)) (Heisermann et al, 1990; Li et al, 2008). ERK1/2 can also phosphorylate SOS at multiple sites which causes SOS to dissociate from GRB2 and ultimately inhibits RAS activation (Buday et al, 1995; Dong et al. 1996; Porfiri et al, 1996). RAF is also subject to phosphorylation by ERK1/2 at serine 289, 296 and 30. Inhibitory phosphorylation at these residues inhibits RAFs ability to phosphorylate its downstream target MEK1/2 (Dhougherty et al, 2005; Rushworth et al, 2006; Ritt et al, 2010). Finally ERK1/2 can phosphorylate MEK1/2 to prevent phosphorylation of ERK1/2. All of the above examples of ERK1/2 catalysed inhibitory phosphorylation of upstream components of the MAPK pathway provides a fast and short-term duration of negative control on the pathway (Caunt et al. 2015).

The MAPK pathway is also regulated by self-regulating homeostatic feedback controls via ERK1/2 induced transcription of Sprouty proteins (SPRY) and dual-specificity-phosphatases (DUSPs). SPRY proteins can dampen the MAPK signalling by either binding to the SOS-GRB2 complex inhibiting RAS activation or by interfering with the catalytic domain of RAF (McKay et al, 2007). DUSPs have the ability to dephosphorylate threonine and tyrosine residues on ERK1/2 and inactivating its intrinsic kinase activity. Specifically, DUSPs inactivate ERK by dephosphorylating the pT-E-pY motif

(Caunt et al, 2013; Owens et al, 2007; Caunt et al, 2015). The de novo expression of both SPRY and DUSPs exhibit a more long-term durable, however their induction is slower (Caut et al, 2015).

In addition to DUSPs, hematopoietic tyrosine phosphatase (HePTP) and protein phosphatase 2 (PP2A) have been implicated in dephosphorylating ERK1/2, rendering its activity (figure 1.2). HePTP and PP2A both dephosphorylate residues in the activation loop of ERK1/2, however HePTP specifically dephosphorylates tyrosine 187 and PP2A dephosphorylates threonine 185 (Zhou et al, 2002).

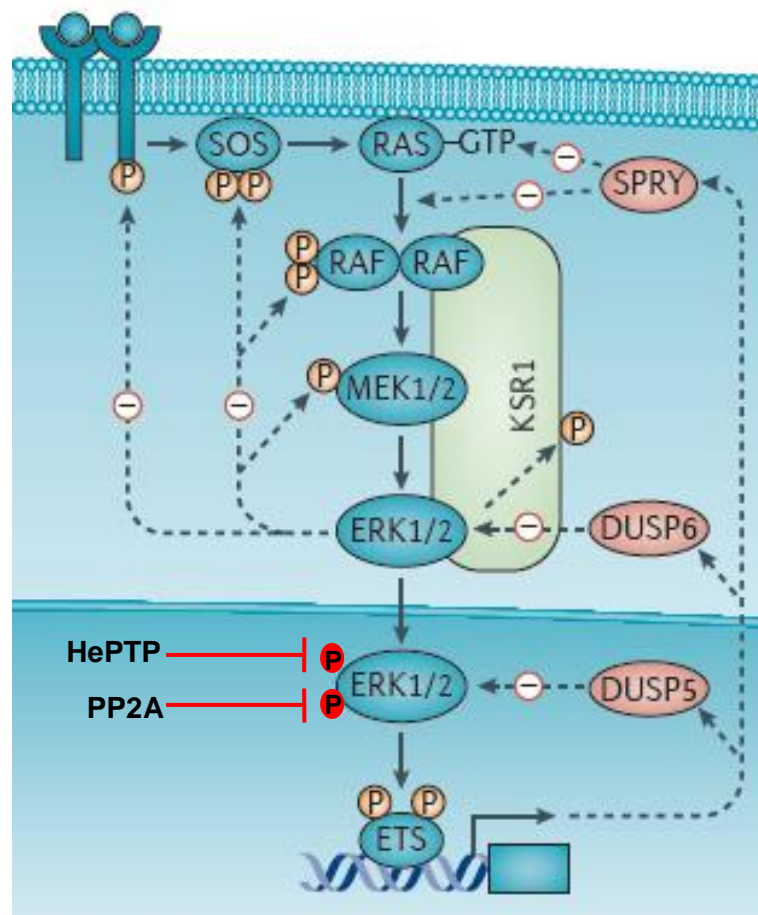


Figure 1.2. A schematic diagram of the homeostatic negative feedback loops of the MAPK pathway (adapted from Caunt et al, 2015).

1.1.5 Mutations in the MAPK pathway

In 2002, a seminal discovery was made which revolutionised the melanoma field and transformed our understanding of melanoma oncogenesis. Davies et al (2002) discovered that a component of the MAPK pathway was mutated in 50-70% of melanomas and 7% of a wide range of other cancers; the culprit being BRAF, one of the three isoforms of RAF. The most common mutation in BRAF is a substitution of a glutamic acid for a valine at position 600 (V600E). This mutation results in a 700-fold over activation of the BRAF kinase (Uong and Zon, 2010), thus over-stimulating cellular proliferation and survival, which are both essential features required for tumour growth (figure 1.3) (Gray-Schopfer et al, 2007).

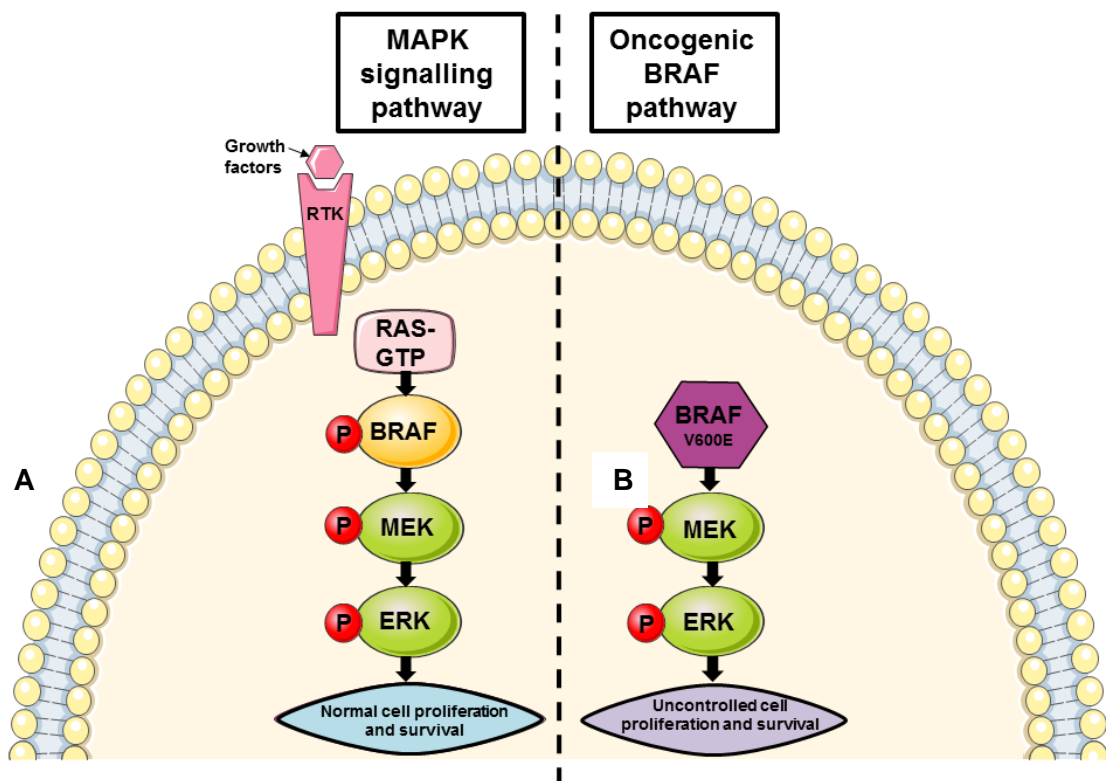


Figure 1.3. The MAPK signalling cascade. (A) MAPK signalling under wildtype and normal physiological conditions. (B) MAPK signalling in human melanomas that harbour the mutant BRAF^{V600E} mutation. The increase in cell proliferation and survival drives the growth of the tumour.

Approximately 80% of human nevi harbour the BRAF^{V600E} mutation (Kumar et al, 2004; Yazdi et al, 2003), but they rarely develop into metastatic melanomas. It stands to reason that the BRAF^{V600E} mutation occurs early on during melanoma oncogenesis and is not sufficient alone to cause malignancy, thus playing a role in activating this checkpoint or 'barrier'. Additional genetic hits or alterations must be acquired to overcome this barrier to form a malignancy (Tsao et al, 2012). This 'barrier' imposed by BRAF^{V600E} is more commonly known as oncogene-induced senescence. Senescence is a phenomenon whereby cells have reached their replicative capacity and can no longer progress through the cell cycle and become arrested. The idea of senescence was first introduced back in 1961 when the 'Hayflick limit' (replicative senescence) was first discovered in fibroblasts due to telomere shortening (Hayflick and Moorhead, 1961). The overexpression of an oncogene can induce premature senescence in normal cells acting as a mechanism to prevent malignant transformation (Zhang and Herlyn, 2012). The BRAF^{V600E} mutation is a perfect example of how an oncogene can participate in stimulating oncogene-induced senescence; a fail-safe mechanism similar to apoptosis.

However this concept that human nevi are arrested in senescence is being challenged as there is conflicting data distinguishing human nevi from metastatic melanomas using senescence markers. Tran et al (2012) have failed to show consistently, or at all, the staining of human nevi with reported senescence markers such as (SA)- β -galactosidase, promyelocytic leukemia protein and H3KMe3. This has raised a debate questioning whether oncogene-induced senescence is a pre-requisite for malignant transformation of melanocytes into melanoma cells. It has also highlighted that new biomarkers for senescent cells need to be identified to improve reliability of results (Zhang and Herlyn, 2012).

In melanoma the BRAF^{V600E} mutation is mutually exclusive with another component mutated in the MAPK pathway, NRAS, one of three isoforms of

RAS (Monzon and Dacey, 2012). Mutations in NRAS occur in 10-30% of melanomas with the most common mutation being a substitution of leucine for glutamine at position 61 (Q61L). This mutation in NRAS is a gain of function (GOF) mutation and results in constitutive activation of the Ras protein (Gray-Schopfer et al, 2007).

1.1.6 The PI3K pathway and melanoma

As well as RAS mutations having an effect on the MAPK pathway, it can also exert effects on the phosphoinositide-3-kinase (PI3K) pathway (figure 1.3) (Monzan and Dancey, 2012). The PI3K pathway is initiated by RTK's activating PI3K, although RAS can also directly activate PI3K (figure 1.4). Activated PI3K continues the signalling cascade by phosphorylating and converting the membrane lipid phosphatidylinositol (4,5) bisphosphate (PIP₂) to phosphatidylinositol (3,4,5) triphosphate (PIP₃). Both of these lipids are second messengers. PIP₃ subsequently activates phosphatidylinositol-dependent kinase 1 (PDK1) which activates the downstream effector Akt, a serine/threonine kinase (Cully et al, 2006). Akt phosphorylates a number of substrates, which results in cell survival, proliferation and angiogenesis. One such substrate is mammalian target of rapamycin (mTOR). This pathway is negatively regulated by Phosphatase and Tensin homolog (PTEN), which dephosphorylates PIP₃ back to PIP₂ and terminates the signalling cascade (Georgescu, 2010).

Considering the downstream cellular effects of the PI3K pathway it is no surprise that the pathway is hyper activated in melanoma. PI3K is rarely itself activated (approximately 3% of metastatic melanomas). The majority of mutations occur within the oncogene Akt and the tumour suppressor PTEN. Akt is overexpressed in around 60% of melanomas resulting in hyperactivity of the pathway (Gray-Schopfer et al, 2007). There are three isoforms of Akt with Akt3 being the primary isoform affected (Stahl et al. 2004). PTEN is located on chromosome 10q23 (Steck et al, 1997) and is frequently

inactivated by somatic loss of heterozygosity mutations (Georgescu, 2010). This inactivation of PTEN in melanomas releases the negative regulatory function it has on the pathway and thus the signalling pathway remains constitutively active.

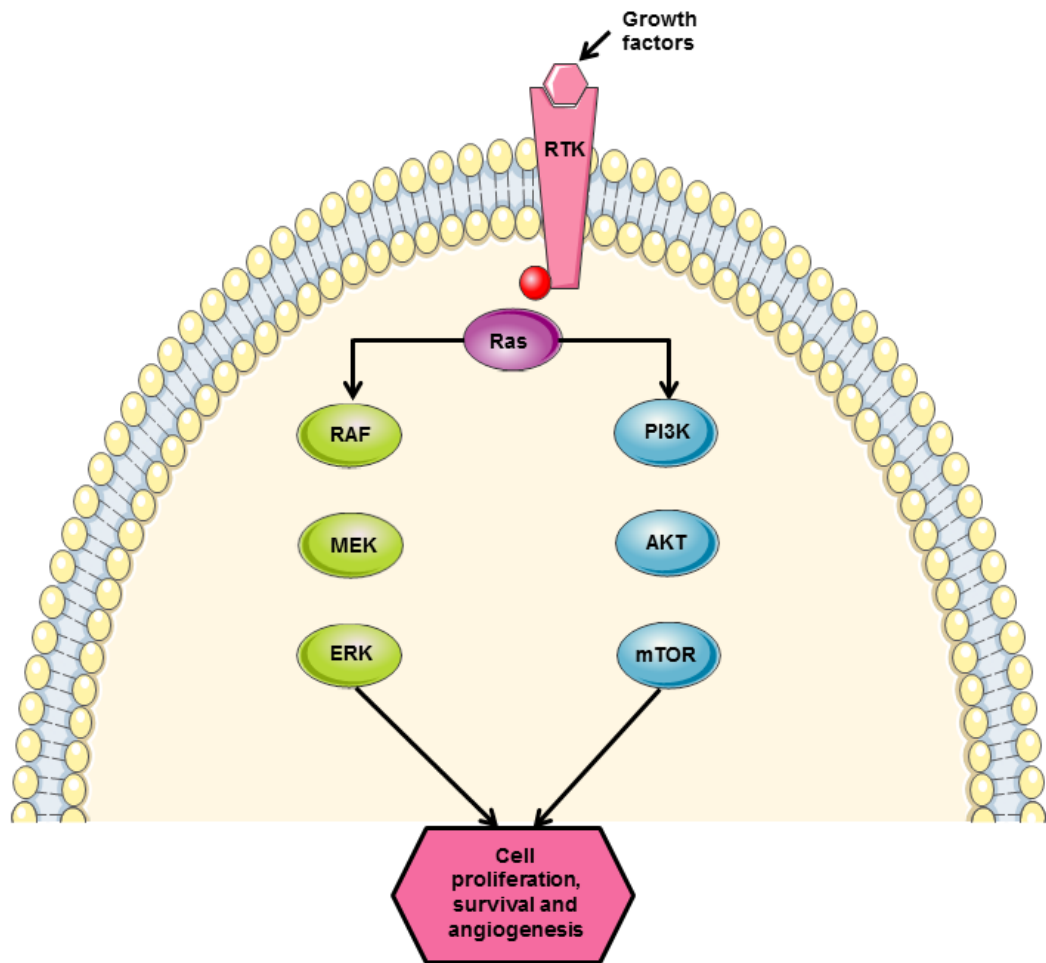


Figure 1.4. The molecular pathogenesis of melanoma with regards to RAS activation. MAPK and PI3K are independent signalling pathways, but simultaneous activation of these pathways via RAS causes defective cellular events, leading to melanoma (Monzon and Dancey, 2012).

Interestingly, PTEN and NRAS mutations are mutually exclusive to each other, but PTEN and BRAF mutations occur frequently with each other in around 20% of melanoma cases (Tsau et al, 2012). This suggests that PTEN could act as an oncogenic driver in the presence of BRAF^{V600E} mutation (Monzan and Dancey, 2012), alongside the fact that the MAPK and PI3K

pathway could act synergistically to increase cellular survival and malignancy (Atefi et al, 2011).

As well as these 'classical' mutations in the PI3K pathway, recent novel somatic mutations have been identified. These include mutations in the genes for mTOR, NFKB1 and PIK3R4, which may be new potential therapeutic targets (Shull et al, 2012).

1.1.7 The CDKN2A locus and melanoma

The cyclin-dependent kinase inhibitor 2A (CDKN2A) locus is located on chromosome 9p21 and encodes for two suppressors, INK4A (p16^{INK4A}) and ARF (p14^{ARF}). The CDKN2A locus consists of 4 exons and through alternative splicing results in the production of the two different tumour suppressors (figure 1.5) (Chin, 2003). In melanoma this CDKN2A locus is frequently deleted. INK4A binds to and sequesters the activity of CDK4/6, which consequently stops retinoblastoma (RB) protein from becoming phosphorylated. In this un-phosphorylated state, RB is bound to the transcription factor E2F, which causes G1 cycle arrest. The loss of the CDKN2A locus will result in the loss of INK4A; this allows G1 to S phase progression and thus a continuous entry into the cell cycle (Tsau et al, 2012). On the other hand ARF inhibits human double minute-2 (HDM2) protein and induces its degradation, which ultimately prevents the degradation of p53 caused by HDM2. p53 is a tumour suppressor involved in regulating the cell cycle. Loss of CDKN2A locus as seen in melanoma would cause uncontrolled degradation of p53 mediated by HDM2 and ultimately loss of cell cycle control and DNA repair (Law et al, 2012).

1.1.8 C-KIT and melanoma

C-KIT is a type III RTK for the ligand stem cell factor (SCF). The C-KIT locus is found on chromosome 4q11 (Curtin et al, 2006) and is either amplified or

mutated predominately in rare acral and mucosal melanomas on chronic sun-induced damaged skin (10-40%). Mutations in the C-KIT oncogene are activating mutations and most commonly occur in exons 11 and 13. Mutations in exon 11 code for the juxtamembrane domain and those in exon 13 code for the kinase domain of the C-KIT oncogene. Thus, both of these mutations results in constitutively active C-KIT kinase activity. However over 70% of the C-KIT mutations occur in exon 11 in the juxtamembrane domain, with the L576P mutation being the predominant mutation. C-KIT activates many pathways involved in differentiation pathway, proliferation and migration of melanocytes (such as the MAPK and PI3K pathway). Thus hyper activation of this receptor will allow optimal conditions for the growth of a tumour (Monzon and Damcey, 2012).

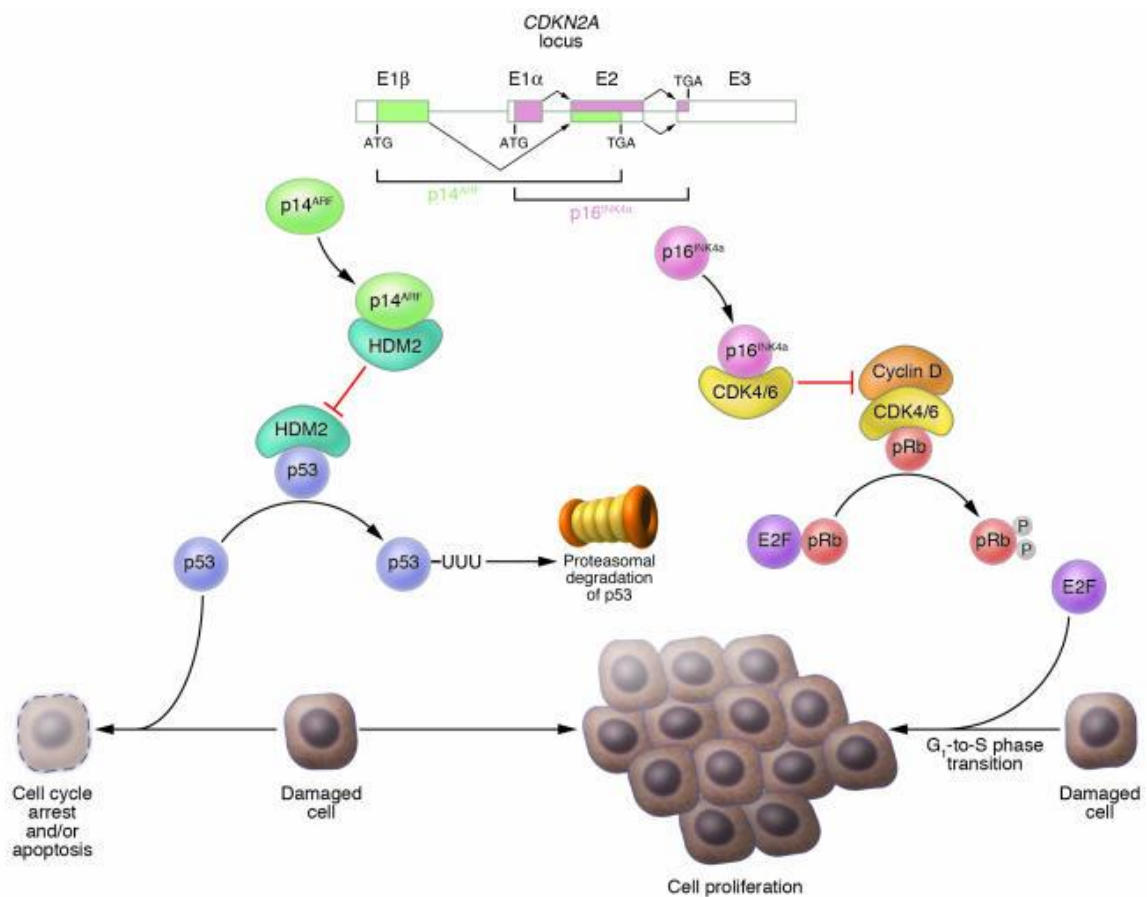


Figure 1.5. The CDKN2A locus and molecular function of the tumour suppressors ARF and INK4A. The CDKN2A locus consists of 4 exons (E), which through alternative splicing produces 2 tumour suppressor p14^{ARF} (in green) and p16^{INK4A} (in pink). Loss of the CDKN2A locus in melanoma disrupts the p53 and pRb pathways (Chudnovsky et al, 2005).

1.1.9 G α subunits and melanoma

G proteins are heterotrimeric guanine nucleotide binding proteins. G proteins transmit cellular signals from G-protein-coupled receptors (GPCR). Intracellular signalling through G proteins has been shown to be involved in the activation of the MAPK pathway (Johnson and Dhanasekaran, 1989; Goldsmith and Dhanasekaran, 2007). Two activating somatic mutations in the G-protein alpha subunit have been shown to frequently occur in uveal melanoma and blue nevi; GNAQ and GNA11 (Dorsam and Gutkind, 2007; Cárdenas-Navia et al, 2010). GNAQ mutations are seen in approximately 50% primary uveal melanoma, 28% metastatic uveal melanoma and 46-83% in blue nevi. GNA11 mutations are seen in approximately 34% primary uveal melanoma, 63% metastatic melanoma and 7% blue nevi. GNAQ and GNA11 mutations are mutually exclusive to each other; however the majority of both of these mutations occur within codon 209 in exon 5 of the gene (Onken et al, 2007; Van Raamsdonk et al, 2009; Van Raamsdonk et al, 2010; Bender et al, 2013). Both the GNAQ and GNA11 mutations are located in the catalytic GTP domain of the G α subunit which prevents GTP hydrolysis to GDP. Therefore either the GNAQ or GNA11 protein is kept in the active GTP bound conformation resulting in constitutive downstream signalling (Landis et al, 1989; Kalinec et al, 1992).

1.2 Therapeutic targeting

Many inhibitors against components of signalling cascades have been developed and undergone clinical trial evaluation, with the majority failing, for example ras farnesyl transferase inhibitors. Drug discovery into inhibitors that specifically targeted RAF kinases in melanoma initially identified sorafenib. However disappointing results from clinical trials of sorafenib revealed sorafenib to be a non-selective RAF inhibitor. Instead sorafenib was shown to be a multi-kinase inhibitor and displayed therapeutic efficacy for the treatment of renal cell carcinoma (RCC), hepatocellular cancer and thyroid cancer. In 2005, 2007 and 2013 the Food and Drug Administration (FDA) have since approved sorafenib for the treatment of RCC, hepatocellular

cancer and thyroid cancer respectively (U.S. Food and Drug Administration, 2015). However since 2011 major advances in the treatment of melanoma have been made, with the FDA approving six therapies in the EU, US and Japan; ipilimumab, pembrolizumab, nivolumab, vemurafenib, dabrafenib and trametinib.

1.2.1 Immunotherapy

1.2.2 Ipilimumab

Ipilimumab is a novel immunological treatment for unresectable and metastatic melanoma. Ipilimumab is a fully human monoclonal antibody against cytotoxic T-lymphocyte antigen-4 (CTLA-4) which utilises the T-cell response as its mechanism of action (Lipson and Drake, 2011).

T-cell activation requires two signals. The first signal being the presentation of an antigen in complex with a major histocompatibility complex (MHC) on an antigen presenting cell (APC) to a T-cell receptor and subsequent binding. This signal is amplified via the second signal whereby the co-stimulatory CD28 receptor on the T-cell binds with a B7 ligand (CD80 and CD86) on the APC. The now fully activated T-cell can elicit an immune response, such as T-cell proliferation and cytokine release (figure 1.6A) (Peggs et al, 2006). However, prolonged T-cell activation induces the upregulation of CTLA-4, a membrane bound receptor on the T-cell with antagonistic effects (Chambers et al, 2001; Mansh, 2011). CTLA-4 competes with CD28 for the binding of B7 ligands on APC'S, with which CTLA-4 has a much higher affinity for. Consequently an inhibitory signal is produced, downregulating T-cell activation and responses leading to a shutdown of the immune response and immune tolerance (figure 1.6.B) (Robert et al, 2009).

However, blocking the interaction of CTLA-4 with the B7 ligands can enhance the T-cell-induced antitumor immune response in patients. This is

how ipilimumab exerts its therapeutic effects. By blocking this interaction, no inhibitory signals by CTLA-4 are released, augmenting T-cell activation and proliferation and permitting the T-cell immune response to continue (figure 1.6.C). Thus, the patients' immune response against tumours is enhanced (Tarhini et al, 2010).

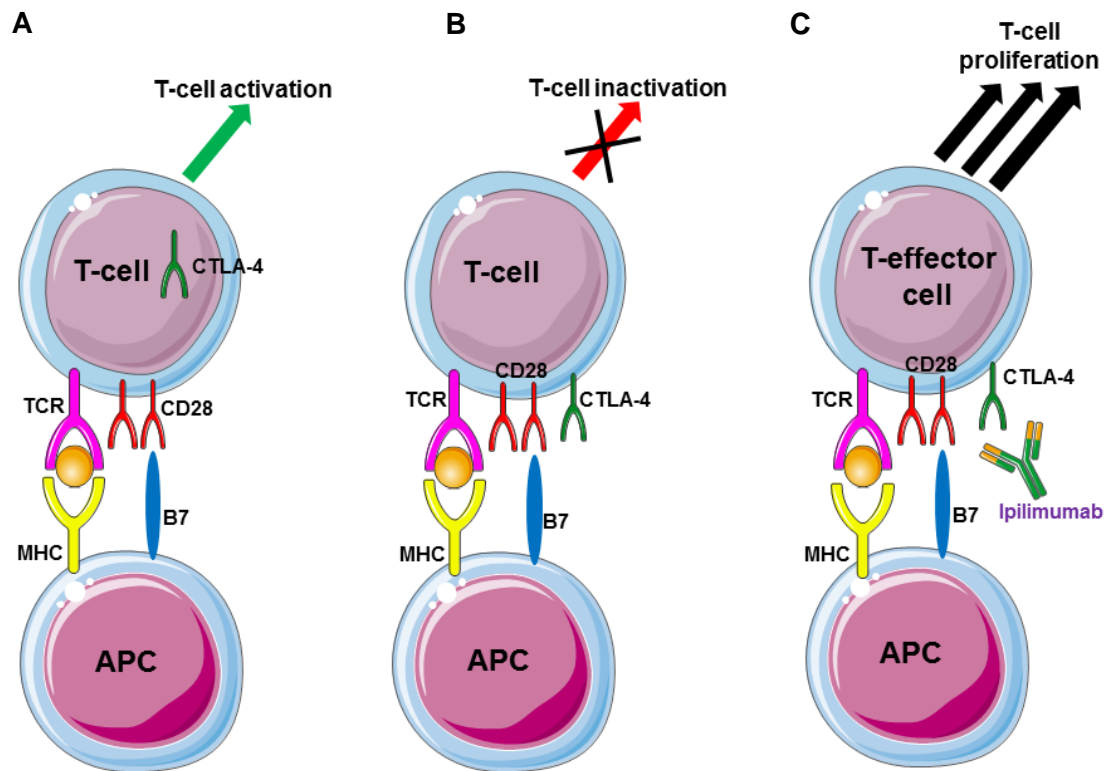


Figure 1.6. T-cell activation and mechanism of action of ipilimumab. T-cell receptor (TCR) shown in pink, major histocompatibility complex (MHC) shown in yellow. The receptors CD28 is shown in red and CTLA-4 in green. The ligand B7 is shown in blue.

The first trial looking into the potential benefits of ipilimumab was a randomized phase III double-blind study of 676 pre-treated patients for metastatic melanoma. Patients were assigned monotherapy of ipilimumab or a glycoprotein 100 (gp100) peptide vaccine or both in combination. The

primary end point was overall survival (OS). The median OS for patients receiving ipilimumab and gp100 was 10.1 months, an improvement compared to 6.4 months with patients receiving gp100 (Hodi et al, 2012). The success of this trial led to the FDA approval of ipilimumab in March 2011 at a dosage of 3mg/kg (Verschraegen, 2012).

The second randomised phase III double-blind trial involved 502 patients with previously untreated metastatic melanoma, comparing ipilimumab to dacarbazine. Patients were either assigned treatment of dacarbazine with ipilimumab or dacarbazine alone. The primary end point was OS. The OS increased from 9.1 months in patients receiving dacarbazine alone to 11.2 months in patients receiving dacarbazine plus ipilimumab (Robert et al, 2011). This study aided bringing ipilimumab as a first in-line treatment for patients with metastatic melanoma.

However, in both phase III trials, immune related adverse events (IRAEs) were observed. The most common IRAE's were skin rash, hepatitis, colitis, hypophysitis and hepatic inflammation. In the first phase III trial, serious (grade 3-5) IRAE's occurred in 10-15% of patients (Hodi et al, 2011; Lipson and Drake, 2011) and 14 deaths resulted in taking ipilimumab (Hodi et al, 2011). This highlights the fact that although ipilimumab clearly improves survival rate, consistent immune monitoring in patients taking ipilimumab is vital (Mansh, 2011).

A recent follow up study of 1861 melanoma patients treated with ipilimumab has emphasized the success of ipilimumab, which reported a 22% 3 year survival rate in all patients. What was most striking from this study was that at the 3 year survival mark, the survival curve started to plateau, with the majority of patients from this point on surviving up to 10 years post treatment. This suggests that patients treated with ipilimumab have long-term durable responses which result in long-term survival (Schadendorf et al, 2015).

1.2.3 PD-1 antibody treatment

The success of immunotherapy has continued with a second generation of immunotherapies that have been developed to target the programmed cell death-1/programmed death-ligand 1 (PD-1/PD-L1) pathway, with two monoclonal anti PD-1 antibodies obtaining FDA approval in 2014. The PD-1 /PD-L1 pathway is another immune checkpoint (similar to the biology behind ipilimumab) and a means by which cancer cells evade the immune system. PD-1 is an inhibitory receptor located on T-cells (Thomson et al, 2006; Hino et al, 2010). There are two ligands for the PD-1 receptor, PD-L1 and PD-L2. When PD-1 binds to either one of its ligands, T-cell activation is inhibited, dampening the immune response (Kier et al, 2008; Okazaki and Honjo, 2007). Many cancer cells have been shown to express PD-L1 and therefore essentially 'hijack' this pathway to evade immune surveillance (Pardoll, 2012).

Antibodies targeting PD-1 and PD-L1 have been developed to block the interaction between the two, enabling restoration of a T-cell anti-tumour response to kill the cancer cells. In 2014 two monoclonal anti PD-1 antibodies were approved by the FDA for the treatment of melanoma; Nivolumab and pembrolizumab. In a phase I trial of nivolumab, 107 melanoma patients were treated with a range of doses of nivolumab every two weeks for a duration of eight weeks. The overall response rate was 31% and the median duration of response was 24 months. (Topailin et al, 2012). In a phase III trial, in which 418 previously untreated melanoma patients negative for a BRAF mutation were recruited to compare nivolumab to dacarbazine, the objective response in the nivolumab arm was 40% compared to 13.9% in the dacarbazine arm. More significantly, the 1 year survival rates for nivolumab treated patients were 72.9% compared with 42.1% for dacarbazine treated patients (Robert et al, 2015). The results of these trials strongly show that nivolumab can improve the response rates, duration of response and OS in melanoma patients. As well as these promising results for melanoma patients, nivolumab and other anti PD-1 and

PD-L1 antibodies have also shown promising results in treating other cancers such as renal, breast and non-small cell lung cancer (Harvey, 2014; Tykodi, 2014; Schapler, 2014; Stagg, 2013).

1.2.4 Small molecule MAPK pathway inhibitors

1.2.5 Vemurafenib

Vemurafenib is a potent small molecule inhibitor of BRAF^{V600E} developed by Plexikon Inc with a 10-fold higher potency for mutated BRAF^{V600E} than wildtype (Tsau et al, 2012). Clinical trials for vemurafenib began in 2006 with an initial Phase I trial referred to as BRAF Inhibitor in Melanoma-1 (BRIM). The BRIM-1 was a multicentre trial involving 55 patients with any cancer type and 32 BRAF^{V600E} melanoma patients. This trial concluded that the recommended maximum tolerated dose (MTD) for the Phase II BRIM-2 trial was 960mg twice daily. Within the BRAF^{V600E} melanoma cohort, there was an 81% partial or complete response rate, indicating vemurafenib had impressive single agent activity (Flaherty et al, 2010).

The Phase II (BRIM-2) multicentre trial targeted BRAF^{V600E} melanoma patients who have had prior treatment with a total of 132 patients enrolling. Ten of these patients had the BRAF^{V600K} mutation and the remaining 122 had the BRAF^{V600E} mutation. The primary end point was overall response rate which proved to be 53%. The median duration of response was 6.8 months and median OS was 15.9 months (Ribas et al, 2011; Sosman et al, 2012).

The overwhelming success of the initial Phase I and II clinical trials led to the initiation of the Phase III trial (BRIM-3). This was a two-armed randomised trial investigating whether vemurafenib would prolong the rate of progression free survival (PFS) compared with dacarbazine. Eligible patients were those with unresectable stage III or IV BRAF^{V600E} positive melanoma who had not had any prior treatment. In total, 675 patients were enrolled for the BRIM-3

trial. The median OS was 13.2 months for the vemurafenib cohort compared to 9.6 months in the dacarbazine cohort. The six month PFS was estimated at 83% and 63% for vemurafenib and dacarbazine treated patients respectively. Throughout each of these trials on vemurafenib, adverse events were noted. Associated adverse events with vemurafenib included the following; arthralgia, rash, fatigue, keratoacanthoma (KA), alopecia and squamous cell carcinoma (SCC) (Chapman et al, 2011).

The FDA approved vemurafenib in August 2011 and it is now used as a first-in line monotherapy for patients with metastatic or unresectable melanoma harbouring the BRAF^{V600E} mutation (Monzon and Dancey, 2012).

1.2.6 MEK inhibitors

Inhibitors targeting another component of the MAPK pathway, MEK 1 and MEK 2 have recently emerged as potential therapeutic treatments for melanoma. However like anti PD-1 antibodies, MEK inhibitors also hold therapeutic value in other cancers including colon, pancreatic and non-small cell lung cancer.

PD98059 and U0126 were the first MEK inhibitors to be reported but exhibited poor pharmacokinetic and pharmacodynamic properties and were not tested in the clinic (Alessi et al, 1995; Dudley et al, 1995; Favata MF et al, 1998). CI-1040 and PD0325901 were the first MEK inhibitors to progress to the clinic (Sebolt-Leopold et al, 1999). Preclinical studies showed both of these MEK inhibitors were able to inhibit downstream ERK in the cell lines tested, determined via western blots. Additional mouse xenograft studies showed that tumour growth was reduced upon treatment with either of these MEK inhibitors (Solit et al, 2006.). However these promising preclinical results did not translate into clinical trials; both were failed due to the toxicity observed in early phase trials (Rinehart et al, 2004; Lorusso et al, 2005).

In May 2013, success with MEK inhibitors was seen with the FDA approval of trametinib, a selective inhibitor of both MEK1 and MEK2 (Gilmartin et al, 2011). In a phase III randomised open-trial, 322 patients were enrolled who harboured either a BRAF^{V600E} or BRAF^{V600K} mutation. Patients were randomly assigned to receive trametinib alone (2mg once daily) or chemotherapy in a 2:1 ratio. The chemotherapy being dacarbazine (1000mg) or paclitaxel (175mg) delivered every 3 weeks intravenously. The primary and secondary end point was PFS and OS respectively. The PFS was 4.8 months in the patients receiving trametinib compared to 1.5 months in patients receiving chemotherapy. The OS at 6 months was 81% for patients receiving trametinib and 67% in patients receiving chemotherapy. However 57 of the 108 patients receiving chemotherapy crossed over to receive trametinib. Common toxicities observed throughout this study were rash, diarrhoea and peripheral edema. Overall this clinical trial demonstrated that trametinib was an effective treatment for melanoma patients harbouring a BRAF^{V600E} or BRAF^{V600K} mutation (Flaherty et al, 2012a).

However, what became apparent from clinical trials with trametinib and other MEK inhibitors was that the response for these inhibitors was strongest in patients that presented with a BRAF mutation^{V600E}. This trend was seen clearly in an early randomised open-label phase II trial of another selective MEK inhibitor, selumetinib. 200 chemotherapy naïve patients with unresectable stage III/IV melanoma were randomly assigned to receive selumetinib (100mg twice daily in 28 day cycles) or temozolomide (200mg/m²/d for 5 days then 23 days off). Although no difference was seen regarding the primary end point of PFS, 5 out of 6 patients who had a partial response to selumetinib harboured a BRAF mutation (V600E, V600K, K601E and K581S) (Kirkwood et al, 2012).

Due to the tumorigenicity of the MAPK pathway in melanoma, MEK inhibitors are an attractive approach in treating melanoma and as a result many more MEK inhibitors are currently undergoing clinical trials. One of

which is MEK162 (Binimetinib, produced by Novartis), a selective inhibitor of MEK1 and MEK2. In a phase II trial the efficacy of MEK162 was studied in melanoma patients with either BRAF (V600E, K601E, V600R, V600K and G606E) or NRAS (Q61R, Q61K and Q61L) mutations. Out of the 41 patients harbouring a BRAF mutation, 8 had a partial response. From the 30 patients harbouring an NRAS mutation, 6 had a partial response. Likewise, the median PFS for the BRAF and NRAS mutant patients was 3.55 and 3.65 months respectively (Ascierto et al, 2013). This study holds significance in the melanoma field not only due to MEK162 having an effect on BRAF mutant melanoma patients, but also due to it being the first reported drug having clear efficacy in NRAS mutant patients. To date, there are no targeting therapies patients with NRAS mutant melanoma and the prognosis is poor. As a result of this study, further clinical trials of MEK162 for treating NRAS mutant melanoma patients are ongoing (Jakob et al, 2012).

1.2.7 Paradoxical ERK activation and vemurafenib resistance phenomena

Despite the clinical efficacy of vemurafenib, the median duration of response in patients is only 6-7 months (Flaherty, 2010b). It is now apparent that selective BRAF inhibitors (SBI's) have opposing roles. They can either inhibit or activate the MAPK pathway depending on the cellular context and genotype (Hatzivassiliou et al, 2010). The three RAF proteins form dimers. Figure 1.7 shows that in melanoma cells with wild-type BRAF, SBI's can inhibit one of the protomers in CRAF-BRAF heterodimers and CRAF-CRAF homodimers, but transactivation of the uninhibited protomer occurs and leads to hyperactivation of the MAPK pathway (Heidorn et al, 2010; Poulikakos et al, 2010; Hatzivassiliou et al, 2010). This paradoxical signalling is enhanced in the presence of oncogenic RAS. Whereas in melanoma cells with the BRAF^{V600E} mutation and non-oncogenic RAS, BRAF functions as a monomer and transactivation does not occur, thus SBI's exert an exclusive inhibitory effect in this context (Poulikakos et al, 2010). This evidence highlights that the genetic profiling of patients' needs to be done with

precision in administration of SBI's to prevent tumourigenesis, not to promote it (Monzon and Dancey, 2012).

Resistance to vemurafenib is currently a key issue researchers within the melanoma field are faced with. There are no second in line treatments for melanoma patients (Monzon and Dancey, 2012), so it is critical to unravel and tackle the mechanisms behind this resistance to develop future therapies. Resistance to SBI's occurs via MAPK-dependent and MAPK-independent mechanisms. MAPK-dependent mechanisms include secondary NRAS mutations, CRAF activation, acquired MEK mutations and up-regulation of COT kinase. MAPK-independent mechanisms include up-regulation of PDGFR β (platelet derived growth factor receptor β) and other RTK'S such as IGF1R (insulin-like growth factor receptor 1), activation of the PI3K pathway and the loss of PTEN (figure 1.8) (Wagle et al, 2011; Nazarian et al, 2010; Johannessen et al, 2010; Villanueva et al, 2010; Paraiso et al, 2010).

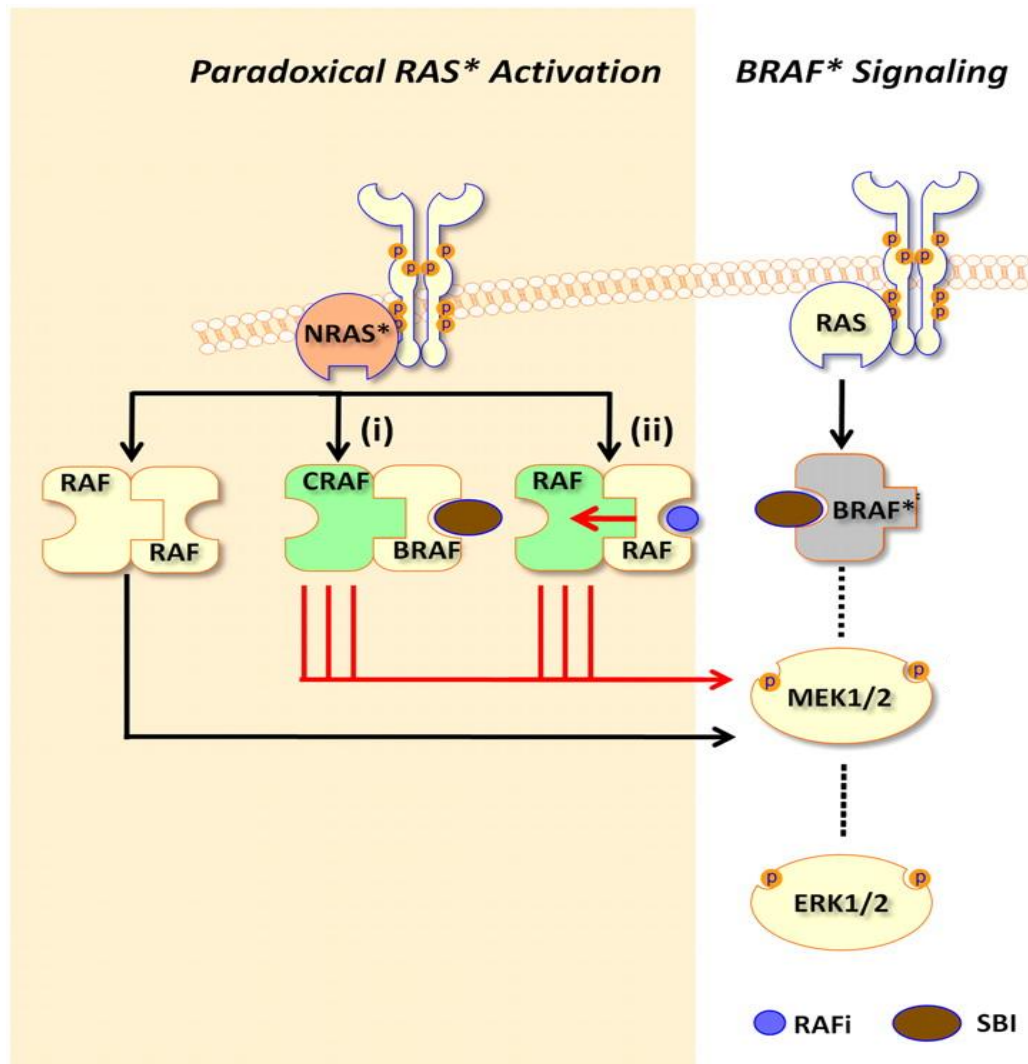


Figure 1.7. Mechanism underlying BRAF inhibition in cells harbouring BRAF^{V600E} mutation and paradoxical signalling of the MAPK pathway caused by SBI's. BRAF* = BRAF^{V600E} (Tsau et al, 2012).

Nazarian and colleagues developed three cell lines with acquired resistance to vemurafenib from melanoma cell lines which harboured the BRAF^{V600E} mutation. One of the cell lines showed strong resistance to PLX4032 and was shown to have acquired an NRAS (Q61K) mutation, which the parental cell line did not have. This acquisition of a NRAS mutation was also confirmed in 2/16 biopsy samples tested. The other two cell lines were revealed to overexpress PDGFR β compared to the parental cell line. This was validated in 4/11 tumour samples from patients compared to the biopsy sample taken prior to treatment (Nazarian et al, 2010).

Villanueva and colleagues approached investigating mechanisms of resistance by evaluating the role of the three RAF isoforms in melanoma cell lines resistant to the BRAF inhibitor SB-590885. Their lab showed that increased expression of ARAF or CRAF in BRAF inhibitor cell lines was able to sustain MAPK signalling and proliferation. They concluded that resistance to BRAF inhibitors causes a dynamic switch of dependence from mutant BRAF^{V600E} to either two of the other wild-type isoforms. Additionally they also showed resistance can occur in a MAPK-independent manner whereby BRAF-inhibitor resistant cell lines were shown to express increased levels of IGF1R by flow cytometry. IGF1R inhibition in these BRAF resistant cell lines showed a decrease in cell viability. Although in this study IGF1R inhibition was shown to suppress AKT activation, IGF1R inhibitors are not very specific. Due to signalling through IGF1R being capable of activating the PI3K/AKT and MAPK pathway, this study has therefore hypothesised that IGF1R signalling can stimulate the PI3K/AKT pathway in BRAF^{V600E} melanomas that have acquired resistance to SBI's (Villanueva et al, 2010; Poulikos and Rosen, 2011).

In a third paper published in 2010, Johannessen and colleagues showed that the two kinases CRAF and COT were able to drive resistance to vemurafenib. In a novel approach, they introduced a cDNA library encoding ~75% of annotated human kinases into a BRAF^{V600E} melanoma cell line that is sensitive to vemurafenib. After the addition of vemurafenib, the kinases CRAF and COT were revealed to have conferred resistance to the inhibitor. This was an interesting finding as it was the first time another kinase has been shown to be able to phosphorylate MEK independent from a RAF kinase. What was also interesting was that COT expression was inversely correlated to BRAF^{V600E} expression implying that BRAF^{V600E} normally antagonised the expression of COT (Johannessen et al, 2010; Alcalá and Flaherty, 2012). Figure 1.7 summarises these findings.

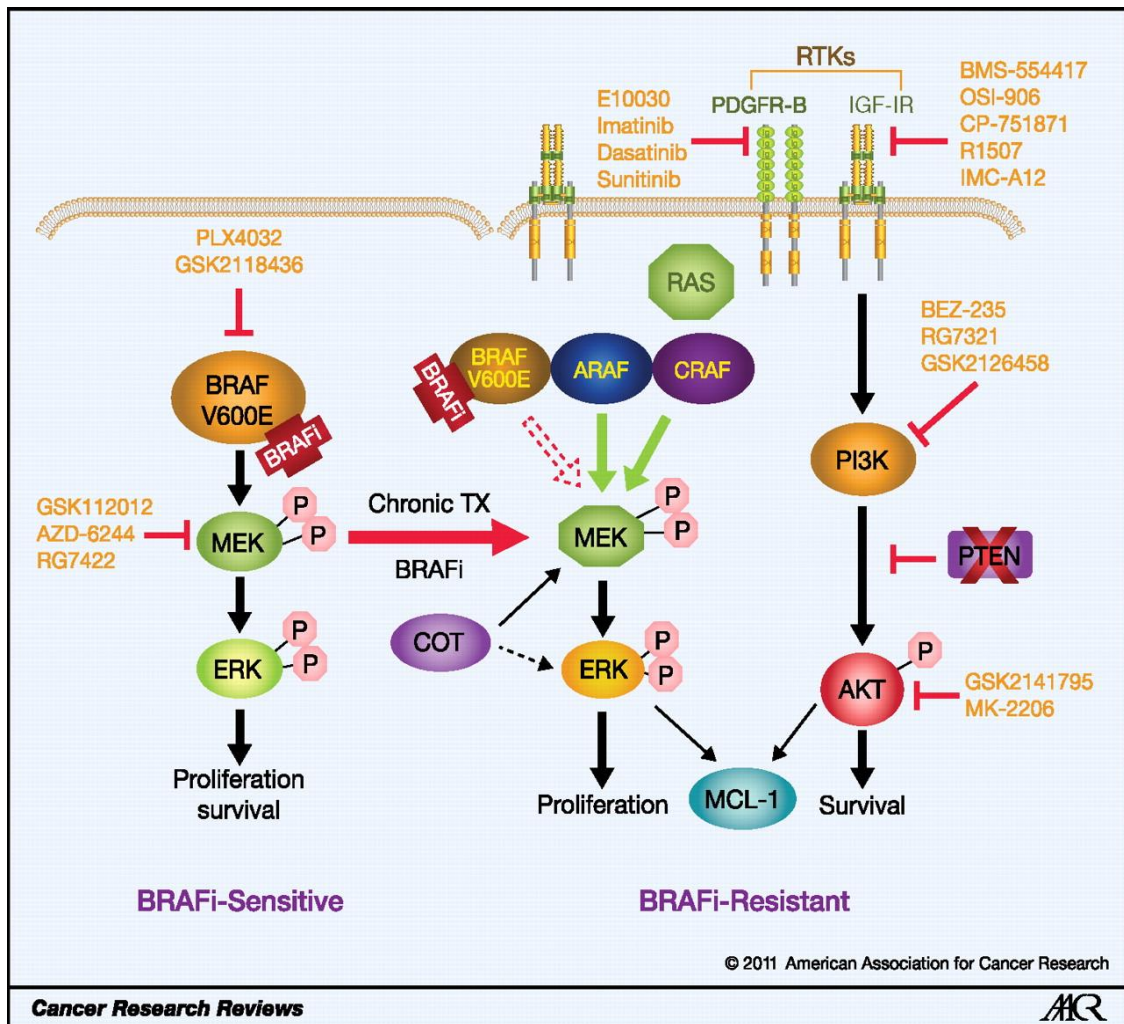


Figure 1.8. Schematic representation of the mechanisms driving BRAF inhibitor resistance. Inhibitors which can be used to block components of the signalling pathways are shown in yellow text (Villanueva et al, 2011).

1.3 Combinatorial therapies and future approaches

It is clearly becoming evident that in treatment of melanoma monotherapy is not the answer. Combinatorial therapy targeting multiple signalling pathways or components within the same pathway is where the future strategies lie to try and delay or override tumour resistance and so provide stronger more durable responses. This is because there is enough evidence suggesting that there is functional redundancy between signalling pathways. A number of drug combinations are currently being investigated in clinical trials with some proving hopeful. Such combinations include combined immunotherapies, BRAF inhibitors in combination with immunotherapies and BRAF inhibitors in combination with MEK inhibitors.

1.3.1 Combined immunotherapy

The combination of the anti CTLA-4 antibody ipilimumab and the anti PD-1 antibody nivolumab is the first immunotherapy combination being explored. In a phase I clinical trial 53 patients received nivolumab and ipilimumab every three weeks for four doses followed by nivolumab alone every three weeks for 4 doses and then again with nivolumab and ipilimumab every 12 weeks for up to 8 doses. This was referred to as concurrent treatment regime. In this cohort of patients there was a 53% overall response (Wolchock et al, 2013).

A subsequent follow up study reported promising results from this initial cohort of 53 patients alongside a new cohort of 41 patients. This new cohort was given the same induction regime as the previous cohort (four doses of nivolumab and ipilimumab every three weeks) but this time followed with nivolumab being delivered at 3mg/kg every 2 weeks for up to 2 years. In both cohorts all of the 94 patients enrolled had either stage III or IV melanoma, with 55% not having any prior treatment. Confirmed results from the first cohort of 53 patients showed that 17% of patients had a complete response. The one and two year overall survival for this cohort was 85% and 79% respectively. Most strikingly 41.5% of these patients had $\geq 80\%$ tumour reduction. The results from this cohort were reiterated in the cohort of 41 patients due to their overall response being 43%. In both cohorts, 62% of patients showed grade 3/4 IRAE's, which are a higher rate than that compared to the IRAE's seen with either immunotherapy alone. However in most patients these IRAE's were manageable or reversible in some cases and the safety profile of this combined immunotherapy was deemed acceptable (Sznol et al, J Clin Oncol 32:5s, 2014 suppl; abstr LBA9003). Success shown in these cohorts has led to a Phase III trial comparing the efficacy of nivolumab and ipilimumab to ipilimumab alone. A total of 945 patients enrolled who had unresectable stage III and IV melanoma and had received no prior treatment. The patients were randomly assigned at a 1:1:1 ratio to either nivolumab alone, ipilimumab alone or ipilimumab and

nivolumab. The primary end points for this study were PFS and OS. However the results for OS have not yet been published, only those for the PFS. The PFS was significantly longer in the patients receiving ipilimumab and nivolumab than either of the drugs alone. The PFS for ipilimumab and nivolumab was 11.5 months and 2.9 months and 6.9 months for ipilimumab and nivolumab alone. An interesting finding from this study was that patients who were positive for PD-L1 had a PFS of 14 months in both the ipilimumab and nivolumab group and nivolumab alone group. However a much more noticeable benefit was seen in the sub-group of patients who were negative for PD-L1 as the PFS for the patients receiving ipilimumab and nivolumab was 11.2 months but for those receiving just nivolumab it was 5.3 months. As reported from other studies, the occurrence of grade 3/4 IRAE's in patients receiving combined immunotherapies is much greater than those receiving either immunotherapy alone. From this study patients receiving ipilimumab and nivolumab, nivolumab alone and ipilimumab alone who experienced grade 3/4 IRAE's was 55%, 16.3% and 27.3% respectively. The most common events were diarrhoea, fatigue and pruritus (Larkin et al, 2015). The results from this study are very promising and encouraging within the field and the awaiting OS results are highly anticipated.

1.3.2 Combined BRAF inhibitors and immunotherapy

On the grounds that BRAF inhibitors give rapid response rates but short term durability and immunotherapies have low responses but elicit more long term durable responses, the combination of the two has been deemed a reasonable therapeutic approach (Ribas and Flaherty, 2011). However clinical trials have shown that for this combination to fulfil its full potential some optimisation in delivery is needed. One such trial had a cohort of 34 enrolled melanoma patients harbouring a BRAF^{V600} mutation. 6 patients were given ipilimumab first then a BRAF inhibitor. All of these 6 patients had stable disease control. The other 28 patients were given a BRAF inhibitor first then ipilimumab. 48% of these patients had rapid disease progression and ultimately death occurred resulting in incomplete ipilimumab treatment. It is

therefore hypothesised that BRAF^{V600} mutant melanoma patients will benefit from receiving ipilimumab prior to a BRAF inhibitor (Ascierto et al, 2012; Ackerman et al, 2012).

In a clinical trial investigating the combination of ipilimumab and vemurafenib, patients that were treatment naïve were given concurrent treatment of vemurafenib and ipilimumab. However, within weeks of patients receiving the first dose of the two drugs in combination, they developed grade 3 elevated levels of aminotransferases and this study was terminated. The outcome of this study was disappointing considering both of these treatment agents were both the only FDA approved agents in treating melanoma at the time this study was conducted (Ribas, 2013).

1.3.3 Combined BRAF inhibitors and MEK inhibitors

The tumorigenicity of the MAPK signalling pathway is at the heart of many melanomas. Dual MAPK inhibition is extensively being researched for two main reasons. Monotherapy with a BRAF inhibitor often results in the emergence of resistance within 6-7 months. The most common mechanism of resistance is re-activation of the MAPK pathway with studies reporting the acquisition of a MEK mutation. Increasing the level of inhibition on the MAPK pathway would raise the threshold required for bypass mechanisms to reactivate the pathway, thus the emergence of resistance is lowered (McArthur, 2015). Therefore it has been rationalised that inhibiting both BRAF and MEK could impede the onset of resistance seen with single agent BRAF inhibitor therapy. Secondly, it is hypothesised that dual BRAF and MEK inhibition could alleviate the commonly observed adverse events associated with BRAF inhibitor monotherapy; such as SSC and KA (Long et al, 2014). In January 2014 the FDA granted accelerated approval to the combination of the BRAF inhibitor dabrafenib and the MEK inhibitor trametinib for the treatment of BRAF V600E OR V600K mutant melanoma patients with unresectable or metastatic melanoma.

A key trial helping to secure this FDA approval was the open-label Phase II trial which enrolled 162 patients harbouring a BRAF mutation (V600E or V600K) who were randomly assigned to receive dabrafenib alone (150mg twice daily) or dabrafenib and trametinib (trametinib at 1 or 2mg twice daily). The response rate in patients given dabrafenib alone was 54% in comparison to 76% in the patients in the combination cohort. Similarly, the duration of response for dabrafenib alone or dabrafenib in combination with trametinib was 5.6 months and 10.5 months respectively. The occurrence of SSC was also reduced, decreasing from 19% in dabrafenib alone patients to 7% in patients receiving the combination indicating that this is a well-tolerated therapeutic option. However common adverse events still presented including pyrexia, chills, fatigue and diarrhoea (Flaherty et al, 2012b).

A recent phase III clinical trial further aided in the road to approval of dabrafenib and trametinib. A total of 423 untreated patients with unresectable or metastatic melanoma harbouring a BRAF mutation (V600E and V600K) were randomly assigned to two groups. One group received dabrafenib (150mg twice daily) with a placebo. The other group received dabrafenib in combination with trametinib (150mg twice daily and 2mg once daily). The primary end point for this study was PFS. The median PFS for dabrafenib alone and in combination with trametinib was 8.8 months and 9.3 months respectively. The overall response rate for dabrafenib alone patients was 51% in comparison to 67% to patients receiving dabrafenib and trametinib. Likewise with the Phase II trial, the occurrence of SCC was less in the dabrafenib and trametinib group than in the dabrafenib group, with a reduction from 9% to 2%. However, the rate and severity of pyrexia was higher in the dabrafenib and trametinib, group compared to the dabrafenib alone group (Long et al, 2014).

Overall, compiling the evidence of these trials and others which are currently ongoing, it is feasible to predict that treating BRAF^{V600} mutant melanoma

patients with a BRAF and MEK inhibitor in combination is a better starting point than the current first in line treatment option, monotherapy of a BRAF inhibitor. This prediction will rely on the success of other ongoing clinical trials.

1.3.4 Triple agent combination

More recently researchers have started to explore the possibilities of using three therapeutic agents in treating melanoma. As previously described, the combination of dabrafenib and trametinib has been clinically proven to be well-tolerated and to improve PFS in melanoma patients. The tolerance of a triple combination such as dabrafenib, trametinib and ipilimumab has not yet been determined. However previous studies have also shown the combination of a BRAF inhibitor with immunotherapy to produce severe hepatotoxicity and successive studies should proceed with caution.

A Phase I clinical trial investigated whether the combination of dabrafenib, trametinib and ipilimumab produced similar hepatotoxicity as seen previously. 10 patients were enrolled who harboured a BRAF^{V600E} or BRAF^{V600K} mutation with unresectable or metastatic melanoma who had received no more than 1 prior treatment. From these patients, 4 received dabrafenib and ipilimumab, 4 received dabrafenib, trametinib and ipilimumab and 2 patients received dabrafenib alone. From the patients receiving the dual combination of dabrafenib and ipilimumab, no grade 3/4 elevated levels of aminotransferases (this is a marker of liver toxicity and can lead to drug-induced liver injury) or dose-limiting toxicities were observed. However from the 4 patients in this cohort, two have stopped the trial due to disease progression, with the remaining two patients ongoing. In the patients receiving the triple agent combination, again, no grade 3/4 elevated levels of aminotransferases were seen. However one patient stopped the trial due to dose limiting toxicities but the remainder are still ongoing. In both cohorts

similar frequent adverse events were presented including chills and fatigue (Puzanov et al, J Clin Oncol 32:5s, 2014 (suppl; abstr 2511).

This current trial is still ongoing and the true efficacy of this triple agent combination is yet to be determined. However due to no grade 3/4 hepatotoxicity being evident in this trial, it could be hypothesised that this toxicity could vary between BRAF inhibitors when in combination with ipilimumab and a 'one rule fits all' approach should not be taken.

1.3.5 Intermittent treatment to overcome BRAF inhibitor resistance

As well as therapeutically targeting components of signalling pathways and combinatorial approaches, the dosing regime of such therapeutic agents is not to be overlooked. Stuart et al (2013) used two primary human xenograft models to investigate two different dosing regimes of vemurafenib and the effect they had regarding resistance. The first dosing regime involved delivering vemurafenib continuously whilst the second regime delivered vemurafenib intermittently (4 weeks on and 2 weeks off). In both regimes vemurafenib was delivered at 15mg/kg^{-1} twice daily. In the mice with continuous delivery of vemurafenib, lethal drug resistance developed within 100 days. In comparison no drug resistance was seen over a 200 day period in the mice treated with vemurafenib intermittently (Thakur et al, 2013). The results from this study can be explained by a proposed model (figure 1.9). Prior to receiving any treatment, the cells within the tumour are mainly drug-sensitive cells with only the rare cell being drug-resistant at this stage. Upon treatment of the BRAF inhibitor, the level of MAPK signalling activity is reduced resulting in regression of the tumour. However when the BRAF inhibitor is delivered continuously, the tumour selects for cells which have high levels of MAPK signalling activity. Such cells are drug resistant and are considered to exhibit a fitness benefit in the presence of the BRAF inhibitor. As a result the population of the drug resistant cells grows. However if the BRAF inhibitor is being delivered intermittently, at the end of each dose the

resistant tumour cells switch to being in a fitness deficit in the absence of the drug and re-population of the drug-sensitive cells occurs. The population of drug sensitive cells again outweighs that of the drug resistant and as a result of these intermittent doses, the emergence of resistance is delayed (Thakur and Stuart, 2013; Holderfield et al, 2014).

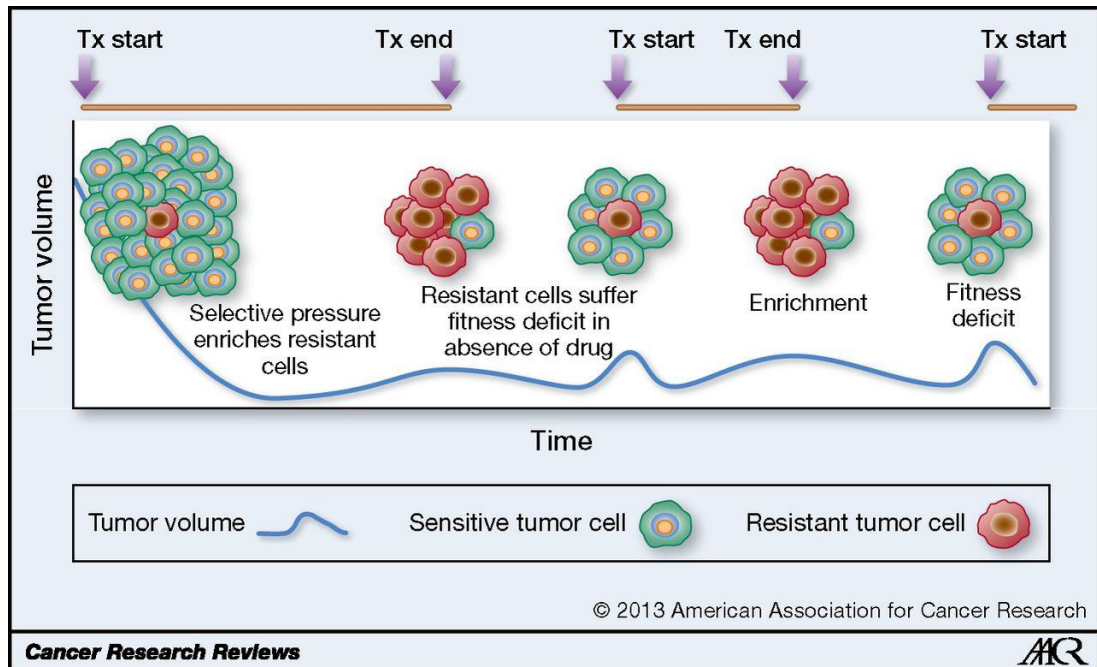


Figure 1.9. The proposed model of the theory behind intermittent drug delivery and the delay in the onset of resistance (Thakur and Stuart, 2013).

Intermittent delivery of a BRAF inhibitor or ‘drug holidays’ can delay the onset of resistance and have only recently started to be seen in the clinic. In a clinical trial, 2 melanoma patients receiving a BRAF inhibitor, presented with a secondary anti-tumour response after the treatment had stopped (Neyns et al, 2012). Many more trials are needed to determine the true significance of this model; however the current data is promising.

1.4 Chemical genetics

1.4.1 Chemical genetic screens

Chemical genetic screens use small molecules, typically less than 2000 Daltons (Da) to assess how they alter the function of genes and to elucidate their role in biological processes. Additionally these screens have the potential to identify novel therapeutic targets for a range of diseases including cancer, aiding in the drug discovery process (Wheeler and Brändli, 2009). Chemical genetic screens are an attractive alternative to mutagenesis screens due to their inexpensive start-up costs, simplicity of the experiments and the ability to control the concentration of the compounds being added. Chemical genetics also allows the addition and removal of compounds at any time, whereas with conventional mutagenesis screens this is not possible (Choi et al, 2014; Wheeler and Brändli, 2009).

There are two approaches to chemical genetic screens, forward and reverse (Cong et al, 2012). Reverse chemical genetics is used when the target, a gene or protein, is known and small molecules are screened to specifically target that protein. If one of the screened compounds has been shown to interact with the known target gene or protein, the phenotype that was produced is studied further to elucidate how that specific gene or target functions in the model organism. Forward chemical genetics takes the opposite approach in which small molecules are screened on cells, tissues or whole embryos for a particular phenotype, but the target of these compounds is unknown. If the compound results in a phenotype of interest being produced, these can be classified as compound 'hits'. These 'hits' are then investigated further to determine what the target is. This approach is also referred to as phenotype-based screens. However, one of the major drawbacks of this latter approach is that the elucidation of the target is often challenging. However, if it becomes known it has the potential of discovering novel genes or proteins or therapeutic targets (Kawasumi and Nghiem, 2007, Spring et al, 2005).

1.4.2 Model organisms for chemical genetic screens

Zebrafish and the amphibian *Xenopus* are the only vertebrate model organisms amenable to chemical genetic screens. This allows compounds to be tested in a whole organism setting rather than an artificial *in vitro* setting as seen in cell-based screens. Zebrafish and *Xenopus* are favourable organisms for the same reasons. Both organisms can generate a large number of embryos and the fertilisation and development of these embryos occurs externally. Thus any dead embryos can be removed and the highest quality embryos can be selected for the screens. Eggs are easily obtainable throughout the year via hormonal injections. Regarding the screen itself, a large quantity of the embryos can be arrayed at one time. Both zebrafish and *Xenopus* embryos are surrounded by a vitelline membrane which is porous enough for the molecules to penetrate through. However *Xenopus* are evolutionarily closer to mammals than zebrafish, which is significant at the genomic level, and thus represent a sound model to study human development and biological processes (Wheeler and Brändli., 2009; Tomlinson et al, 2005; Wheeler and Lui, 2012).

In 2000, the first high-throughput chemical genetic screen was published. In this chemical screen a randomly selected small molecule library consisting of 1100 molecules was screened in zebrafish embryos. Defects in four organ systems were assessed by visual phenotype; central nervous system, cardiovascular system, neural crest and the ear. The results of this study showed that approximately 1% of the small molecules affected one of the specific organs detected for (Peterson et al. 2000). The success of this chemical screen was also translated across in *Xenopus laevis* embryos. In a separate chemical genetic screen, chemicals from the same molecule library and methodology from the Peterson study were used in *Xenopus laevis* embryos. The results from this screen were analogous to that seen in the Peterson study, highlighting that both of these model organism are redundant (Tomlinson et al, 2005).

Subsequent studies have shown success in chemical genetic screens using the *Xenopus laevis* model. One such screen assayed 3000 compounds and their phenotypic effect on the embryos was scored. 40 of these compounds gave rise to an observed phenotype on the embryos. One compound, NSC84093, gave a striking phenotype in which the pigment cells along the dorsal stripe of the embryo were segmented and not in a continuous line as normally seen in the embryos. Also the pigment cells along the ventral side of the tail had failed to form. Structure activity relationship studies (SARS) plus other tests carried out on NCS84093 revealed this compound to be an 8-quinol derivative or more specifically, a matrix metalloproteinase (MMP) inhibitor. Further experiments went on to investigate two potential targets of NSC84093, MMP-2 and MMP-14. Morpholino knockdown of these two MMP's in the embryos partially re-produced the pigment cell migration phenotype observed with NSC84093. This study conclusively demonstrated that MMP's play a role in melanophore migration in *Xenopus* embryos (Tomlinson et al, 2009).

1.5 Leflunomide

Another 'hit' from the screen that caused a pigment migration phenotype NSC210627. This and other compounds that showed interesting phenotypes in the *Xenopus* screen were added to a chemical genetic screen in zebrafish to identify small molecules which suppressed neural crest development. 2000 compounds were screened to identify those which inhibited the levels of *crestin*. Crestin is a specific pan-neural crest marker specific to zebrafish during embryogenesis. Therefore any compounds that reduced the levels of crestin could also potentially be inhibiting the neural crest development and NSC210627 scored significantly in this assay. Using the chemoinformatic algorithm DiscoveryGate, it was revealed that NSC210627 was structurally similar to brequinar, an inhibitor of dihydroorotate dehydrogenase (DHODH). Furthermore, NSC210627 was shown to also inhibit DHODH activity *in vitro*. Leflunomide, also an inhibitor of DHODH mimicked the effect of NSC210627, even though it is structurally different to NSC210627. Leflunomide is an FDA

approved drug for the treatment of rheumatoid arthritis (White et al. 2011) and on this basis was used in the subsequent experiments.

Further work investigating how leflunomide inhibits neural crest development revealed it exerts its effects by inhibiting transcriptional elongation of genes necessary for neural crest development and also melanoma growth. Genes such as *sox10* and *dct* which are necessary for normal neural crest and melanocyte development respectively exhibited reduced expression. The effect leflunomide has on *Xenopus* and zebrafish embryos is phenotypically similar to the suppressors of Ty 5 and 6 (*spt5/spt6*) mutant in zebrafish embryos. *Spt5/spt6* have been shown to be involved in transcriptional elongation (Keegan et al. 2002). The gene expression profiles of leflunomide treated embryos and the *spt5^{sk8}* mutant are very similar at 24 hours post fertilisation. Of the 223 genes identified to be downregulated by leflunomide, 183 of these were also downregulated in the *spt5^{sk8}* with downregulation of *sox10*, microphthalmia-associated transcription factor (*mitf*) and *crestin* (White et al, 2011). MITF is the master regulator of melanogenesis whereby it is involved in melanocyte induction, terminal differentiation, development and function (Hornyak et al, 2001; Levy et al, 2006). However in 10-20% cases of melanoma MITF has been shown to be amplified and thus drives melanocyte-derived cells into malignant melanoma cells. This is an example of how a melanocyte specific transcription factor (or melanocyte-specific modulator) involved in the development of normal melanocytes can become a lineage addicted oncogene in melanoma when mutated (Garraway et al, 2005; Haq and Fisher, 2011; Sommer, 2011; Hartman and Czyz, 2015).

Due to melanoma being a cancer arising from melanocytes, derivatives of the neural crest cells, the effect of leflunomide on melanoma growth was investigated. The metabolite of leflunomide, A771726, caused a dose-dependent decrease in the number of viable cells in BRAF^{V600E} mutant cell lines (figure 1.10). The effect of A771726 on the number of viable cells in these BRAF^{V600E} mutant cell lines was synergistically enhanced when it was

combined with the BRAF inhibitor PLX4032. This observation was then investigated *in vivo* using xenografts of A375 cells transplanted into nude mice. At 12 days post treatment, the combination of leflunomide and PLX4032 caused almost complete abrogation of tumour growth compared to mice treated with leflunomide or PLX4032 alone (figure 1.10) (White et al. 2011).

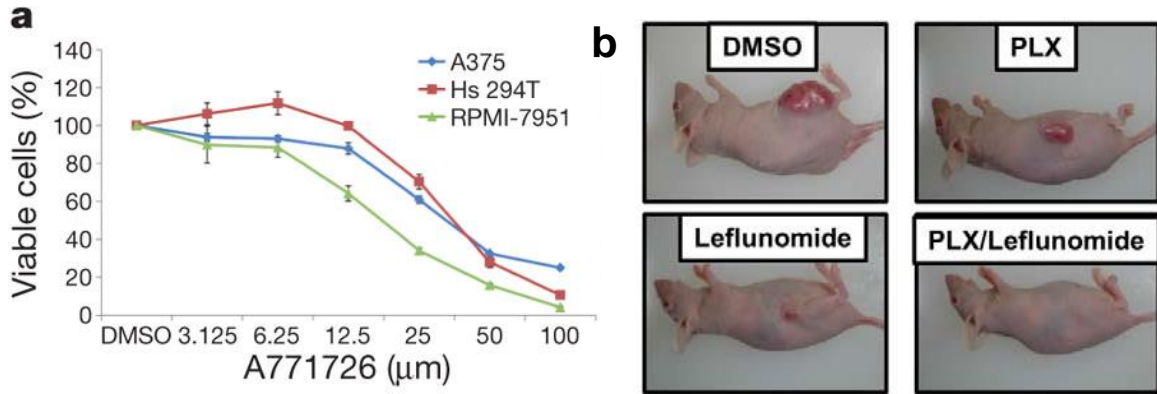


Figure.1.10. The effect of A771723 on melanoma cell viability and mouse xenograft. A) The effect on cell viability in BRAF mutant cell lines treated with A771723. B) A375 xenografts in nude mice at day 12 post treatment. (White et al, 2011).

Aims

For this thesis the three separate aims are represented as individual chapters. The first aim was to carry out a chemical genetic screen of the National Cancer Institute (NCI) diversity set II compound library on *Xenopus laevis* embryos. From this screen specific phenotypes were scored with the goal of identifying compounds with novel therapeutic potential in treating melanoma.

The second aim was to follow up from the success of a previous chemical genetic screen carried out in the lab which identified leflunomide as showing therapeutic potential in treating melanoma. Leflunomide is an FDA approved drug used in the treatment of rheumatoid arthritis. However, how leflunomide exerts its therapeutic effects in treating melanoma is unknown and thus was investigated in this part of the thesis.

Finally, the possibility of using leflunomide in combinatorial studies in treating melanoma was also considered. Here, the combination of leflunomide and the MEK inhibitor selumetinib was investigated both *in vitro* and *in vivo* experiments.

Chapter 2: Materials and methods

2.1 Frequently used solutions

1 x Phosphate buffered saline (PBS): 137mM NaCl, 2.7mM KCl, 10mM Na₂HPO₄ adjusted to pH 7.4

PBST: PBS with 0.1% Tween-20

4% Paraformaldehyde (PFA): 500ml of 1 x PBS was heated to approximately 60°C. A few crystals of NaOH were added, which helps to dissolve the PFA. 20g of PFA was added and dissolved with the aid of a magnetic stirrer and adjusted to pH7.4. Once dissolved and left to cool, the 4% PFA was aliquoted and stored at -20°C.

0.1% Gelatin: 0.5g Gelatin in 500ml dH₂O

Tris-Acetate-EDTA (TAE) buffer: 40mM Tris, 1mM EDTA, 1% Acetic acid

10X Tris-buffered saline 0.1% Tween-20 (TBST): 24g and 88g of Tris base and NaCl was dissolved in 900ml distilled water respectively. The solution was adjusted to pH 7.6. 10ml of Tween-20 was added and the solution was made up to 1 litre with distilled water

High sodium dodecyl sulphate (SDS) content lysis buffer: 65mM sucrose, 60mM Tris-HCL, 3% SDS, adjusted to pH 6.8

Sample buffer: 4% SDS, 10% 2-mercaptoethanol, 20% glycerol, 0.004% bromophenol blue, 0.125M Tris HCL adjusted to pH 6.8

10X Running buffer: For 1L, 30g Tris base, 144g glycine, 100ml SDS, 900ml distilled water adjusted to pH 8.3

1X Running buffer: For 1L. 100ml 10X running buffer and 900ml distilled water at pH8.3

10X Transfer buffer: For 1L, 30g Tris base, 144g Glycine and 1000ml distilled water adjusted to pH8.3. Kept at 4°C

1X Transfer buffer: For 1 L, 100ml 10X transfer buffer, 200ml Methanol and 700ml distilled water. Kept at 4°C

Bovine serum albumin (BSA): 1% BSA in 1xMMR

1X Marc's Modified Ringers MMR: 100mM NaCl, 2mM KCl, 1mM MgCl₂, 2mM CaCl₂, 5mM HEPES, adjusted to pH7.5

0.1XMMR: 10mM NaCl, 0.2mM KCl, 0.1mM MgCl₂, 0.2mM CaCl₂, 0.5mM HEPES, adjusted to pH7.5

0.05XMMR: 0.5mM NaCl, 0.1mM KCl, 0.05mM MgCl₂, 0.1mM CaCl₂, 0.25mM HEPES, adjusted to pH7.5

Human Chorionic Gonadotrophin (HCG): 100U/ml of HCG was prepared in PBS and stored at 4°C

Pregnant mare's serum gonadotrophin (PMSG): 1000U/ml of PMSG was prepared in PBS and stored at 4°C

X.laevis testes buffer: 10% 1xMMR and 80% FBS (Fetal Bovine Serum)

2% cysteine: For 100ml add 2g L-cysteine to 100ml distilled water and adjust to pH 8

2.2 Cell lines and cell culture

The human melanoma M202, M285, M375, M296, A375, M229, SKmel28 and SKmel5 cell lines were a kind gift from Antoni Ribas (University of California, Los Angeles). Primary human melanocytes adult (HEMa-LP) were obtained from Gibco. Human embryonic kidney cells (HEK-293) and rhabdomyosarcoma cells (RD-1) were obtained from the Biomedical Research Centre (University of East Anglia, UK).

Human melanoma cells were cultured in RPMI-1640 medium (1X) (HyClone) supplemented with 10% heat inactivated FBS (Gibco), 1% L-glutamine (Gibco) and 1% penicillin and streptomycin (Gibco). HEMa-LP cells were cultured in Medium-254 (Gibco) with the addition of PMA- Free Human Melanocyte Growth Supplement-2 (HMGS-2) (Gibco). HEK-293 cells were cultured in Dulbecco's modified Eagle medium (DMEM) + GlutMAX (Gibco) supplemented with 10% FBS, 1% L-glutamine and penicillin and streptomycin. RD-1 cells were cultured in Dulbecco's modified Eagle medium (DMEM) + GlutMAX (Gibco) supplemented with 10% FBS and penicillin and streptomycin.

All cells were maintained at 37°C in a 5% CO₂ air-humidified incubator and were routinely screened for mycoplasma.

2.3 Mycoplasma PCR

Media samples were taken from cells which had been in culture for approximately 48 hours. Samples were heated at 100°C for 5 minutes then centrifuged for 1 minute at 13g. The PCR recipe per sample was 10µl BIOMIX Red (BIOLINE), 0.5µl forward primer, 0.5µl reverse primer, 1µl MgCl₂, 6.5µl Sigma water and 1.5µl sample (total 20µl). Two additional PCR reaction mixes were made up with 1.5µl Sigma water and 1.5µl Mycoplasma DNA, serving as negative and positive controls respectively.

The reaction conditions were 98 °C for 30 seconds, 40 cycles of 98 ° for 10 seconds, 52 °C for 20 seconds and 72 °C for 30 seconds. The cycle ended with 72 °C for 2 minutes.

Mycoplasma primer sequences

Myco 1

5' GGG AGC AAA CAG GAT TAG ATA CCC T 3'

Myco 2

5' TGC ACC ATC TGT CAC TCT GTT AAC CTC 3'

Analysis of the PCR reaction was performed by running a 1.5% agarose gel electrophoresis and visualised via ethidium bromide under UV light. Any positive samples should give a band at ~270bp.

2.4 Drugs and Compounds

Leflunomide (Sigma-Aldrich) was dissolved in Dimethyl sulphoxide (DMSO) Hybri-Max (Sigma-Aldrich) and stored at 4°C at stocks of 10mM.

AZD6244 ((selumetinib)(SelleckChem)) was dissolved in DMSO and stored at -20°C at stocks of 2mM. When aliquots of the stock were in use they were stored at 4°C for two weeks.

2.5 Cell viability assays

96-well clear bottom plates coated with poly-L-lysine (PLL) (Sigma-Aldrich) were used to seed cells on day 1 in 100µl of culture medium. Seeding densities for each cell line are shown in table 2.1.

Table 2.1. The seeding densities for each cell line used for the cell viability assays.

Cell Line	Seeding density
M202	12,000
M285	9,000
M375	20,000
M296	22,000
A375	2,000
M229	20,000
SKmel28	10,000
SKmel5	7,500
Melanocytes	22,000
HEK-293	15,000
RD-1	7,500

Cells were left for 24 hours to equilibrate. On day 2, cells were treated with either a range of Leflunomide concentrations (1.5625 μ M-100 μ M) or selumetinib (ranging from 0.015625 μ M to 1 μ M), or vehicle for 72 hours. Cytochalasin D (Sigma Aldrich) was used as a positive control. All conditions were repeated in triplicate.

Cell viability was determined on day 5 using the CellTiter-Glo Luminescence assay (Promega). 50 μ l of culture medium from each well was removed and replaced with 50 μ l of CellTiter-Glo as so a 1:1 ratio was added. Each plate was gently rocked at room temperature for 15-30 minutes. Luminescence from the plate was read on a BMG LabTech Omega Series plate reader (data analysed using OMEGA software). A summary of this experimental design can be seen in figure 2.1.

The mean cell viability was calculated as a percentage of the mean vehicle control. Three independent experiments were performed for each cell line. IC₅₀'s were generated using Prism Graphpad software (GraphPad Software, Inc) and calculated using a nonlinear regression model.

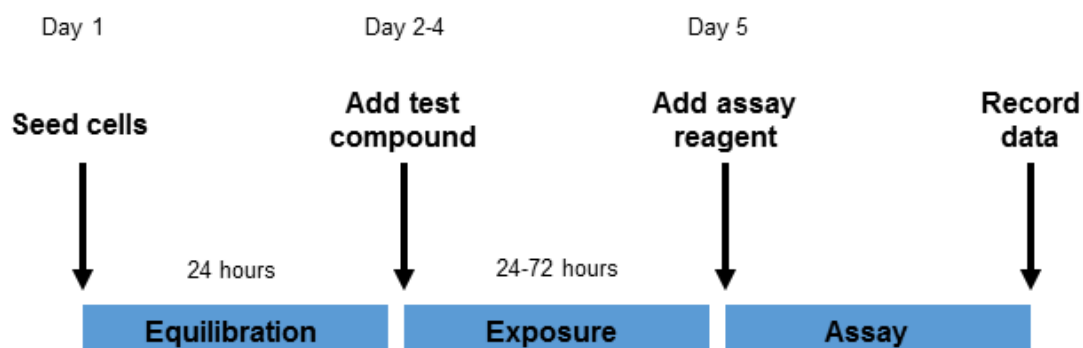


Figure 2.1. Experimental design of how the cell viability assays were carried out.

2.6 BrdU proliferation assay

A375 melanoma cells were seeded in 12 well plates at a density of 10,000 cells per 2ml of medium per well and grown on gelatine coated coverslips (day 1). On day 2 leflunomide was added to cells at 12.5, 25 and 50 μ M alongside a vehicle control for 72 hours. After 72 hours (day 5), Cells were pulsed for 2 hours with 5-Bromo-2'-Deoxyuridine (BrdU) (Sigma-Aldrich) at a final working concentration of 10 μ M at 37°C, 5% CO₂.

Cells were washed in PBS and fixed in 4% PFA for 20 minutes at room temperature. After 3 5 minute PBS washes, cells were permeabilised in 2N-HCL + 0.5% Triton X-100 for 10 minutes. Cells were washed extensively in PBS and blocked for 1 hour and a half in 10% goat serum. Next, primary BrdU antibody diluted 1:100 in 1% goat serum in PBS was applied and incubated overnight at 4°C. Cells were washed 3 times for 5 minutes in PBS.

Subsequently, Alexa Fluor 488 anti-mouse secondary antibody diluted 1:1000 with 1% goat serum in PBS was added for 1 hour at room temperature in the dark. Cells were extensively washed in PBS and counterstained with DAPI (1:10,000 dilution). Again, cells were extensively washed and mounted onto slides using a drop of hydromount (Company), placing a large coverslip on top of the cells.

Cells were examined under a Zeiss AxioPlan 2ie widefield microscope with AxioCam HRm CCD camera and photographed at four random fields. The number of DAPI positive and BrdU positive cells were counted and analysed using Image J software (Company). Three independent experiments were carried out.

2.7 Cell cycle analysis

A375 melanoma cells were seeded in 24-well plates at a density of 4,600 cells per 2ml of medium per well. After 24 hours, the cells were treated with vehicle, 25, 50 and 100 μ M of Leflunomide. After 72 hours, the cells were trypsinised and pelleted along with the culture medium. Cells were washed in PBS and fixed in ice cold absolute ethanol and left on ice for 2 hours or in the freezer overnight. Cells were equilibrated to room temperature and washed in PBS. Cells were then stained with 200 μ l PI/RNase A solution (Cell Signalling) and incubated at 37 $^{\circ}$ C for 30 minutes in the dark. Cells were analysed on the BD AccuriTM C6 flow cytometer and the data was analysed using the BD AccuriTM C6 Software and FlowJo. Three independent experiments were carried out.

2.8 Annexin V apoptosis assay

Apoptosis was assessed using an Annexin V Apoptosis detection kit FITC (eBioscience). Cells were seeded in 24-well plates at a density of 4,600 cells per 2ml of medium per well. After 24 hours the cells were treated with

vehicle, 25, 50 and 100 μ M of Leflunomide. After 72 hours cells were trypsinised, washed in PBS and pelleted along with the culture medium. Cells were resuspended in 1ml 1X binding buffer. 5 μ l of fluorochrome-conjugated Annexin V was added to 100 μ l of the cell suspension and was subject to 20 minute incubation at room temperature. Cells were pelleted, washed in 1X binding buffer and resuspended in 200 μ l 1X binding buffer with the addition of 5 μ l propidium iodide staining solution.

Cells were analysed on the BD AccuriTM C6 flow cytometer within the hour and the data was analysed using the BD AccuriTM C6 Software. Three independent were carried out and a two-way ANOVA was carried for statistical analysis.

2.9 JC1 mitochondrial membrane ($\Delta(\psi)$) potential assay

A375 melanoma cells were seeded in 12 well plates at a density of 10,000 cells per 1ml of medium per well. After 24 hours, the cells were treated with vehicle, 25, 50 and 100 μ M of Leflunomide. After 72 hours, the cells were incubated with 2 μ M JC1 (Life technologies) for 45 minutes at 37 $^{\circ}$ C, 5% CO₂. The cells were trypsinised and pelleted along with the culture media. Cells were washed in PBS and resuspended in 200 μ l of fresh PBS and analysed on the BD AccuriTM C6 flow cytometer. Samples were exposed to 488nm excitation, with JC1 green monomer fluorescence detected at 530nm in the FL1 channel and JC1 red aggregates fluorescence detected at 590nm in the FL2 channel. Data was analysed using the BD AccuriTM C6 Software. Three independent experiments were carried out.

2.10 Mitotracker green

A375 melanoma cells were seeded in 12 well plates at a density of 10,000 cells per 1ml of medium per well. After 24 hours, the cells were treated with

vehicle, 25, 50 and 100 μM of Leflunomide. After 72 hours, the cells were incubated with 25nm Mitotracker green (Invitrogen) for 45 minutes at 37°C, 5% CO_2 . Cells were trypsinised and pelleted along with the culture medium. Cells were washed in PBS and resuspended in 200 μl of fresh PBS.

Cells were analysed on the BD Accuri™ C6 flow cytometer with green fluorescence detected in the FL1 channel. Data was analysed using the BD Accuri™ C6 Software. Three independent experiments were carried out and a one-way ANOVA was carried out for statistical analysis.

2.11 Combinatorial cell viability assays

96-well clear bottom plates were used to seed cells on day 1 in 100 μl of culture medium, with the seeding density for each cell line shown in Table 2.1. Cells were left for 24 hours to equilibrate. On day 2, cells were treated with 12.5, 25 and 50 μM leflunomide and 0.025, 0.05 and 0.1 μM selumetinib alone and in combination for 72 hours (day 5). The combination of leflunomide and selumetinib was added to the cells at the same time. Additional experiments pre-treated the cells with either leflunomide or selumetinib for 24 hours (day 2) with the second drug introduced after the 24 hours (day 3). Cytochalasin D (Sigma Aldrich) was used as a positive control. All conditions were repeated in triplicate.

Cell viability was determined on day 5 using the CellTiter-Glo Luminescence assay (Promega). 50 μl of culture medium from each well was removed and replaced with 50 μl of CellTiter-Glo as so a 1:1 ratio was added. Each plate was gently rocked at room temperature for 15-30 minutes. Luminescence from the plate was read on a BMG LabTech Omega Series plate reader (data analysed using OMEGA software). A summary of this experimental design can be seen in figure 2.2.

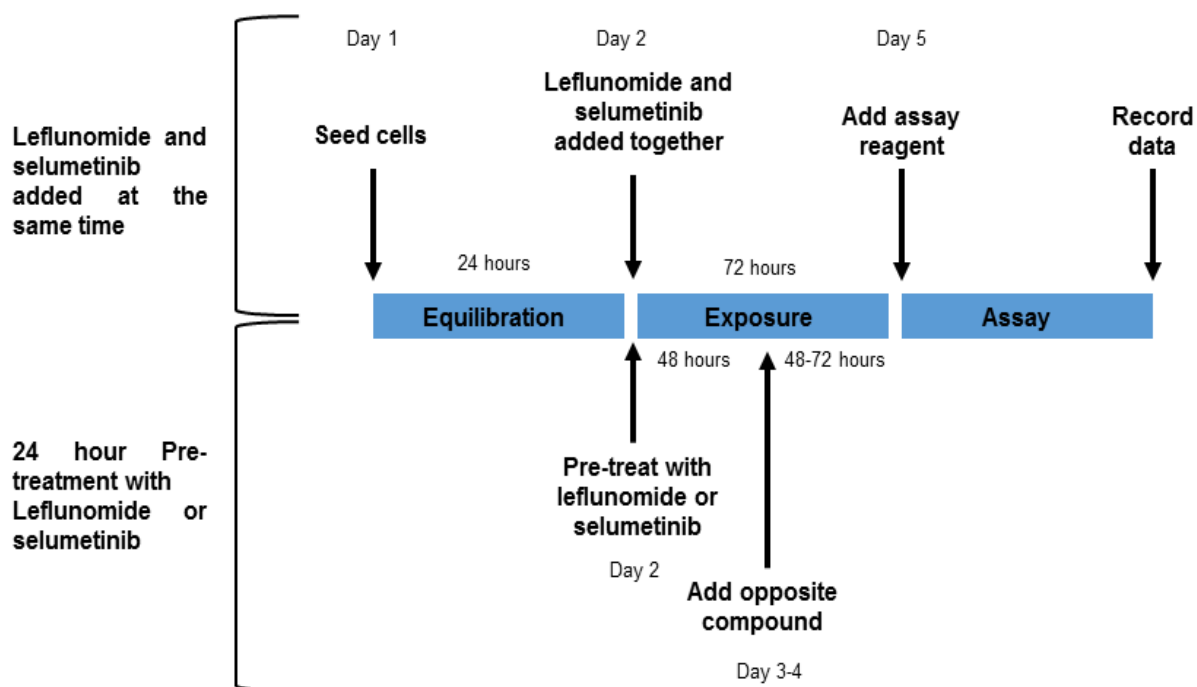


Figure 2.2. Experimental design of the combinatorial cell viability assays whereby leflunomide and selumetinib were added either at the same time or 24 hour pre-treatment.

Luminescence from the plate was read on a BMG LabTech Omega Series plate reader (data analysed using OMEGA software). The mean cell viability was calculated as a percentage of the mean vehicle control. Three independent experiments were performed for each cell line tested.

2.12 Calculation of drug synergy

Drug synergy was calculated using CalcuSyn (Biosoft) software using the median effects methods as described by T-C Chou and P Talalay.

2.13 Western blots

A375 melanoma cells were seeded and treated for 72 hours in varying drug conditions to detect for different proteins as shown in table 2.2.

Table 2.2. The different drug conditions A375 melanoma cells were subjected to for detection of specific proteins by western blot.

Drug treatments for detection of pERK and tERK	Drug treatments for detection of Mcl-1, BIM, PARP and PUMA
Vehicle	Vehicle
0.1µM selumetinib	50µM leflunomide
1µM selumetinib	0.05µM selumetinib
	0.1µM selumetinib
	50µM leflunomide and 0.05µM selumetinib
	50µM leflunomide and 0.1µM selumetinib

Cells were washed in PBS and lysed in 100µl of high SDS content lysis buffer and passed through a thin gauge needle. Samples were homogenised for 2 minutes at 50Hz and spun down for 10 minutes at 12,000g. Protein quantification of each sample was determined via the DC BIO-RAD protein assay. Samples were prepared at 10µg and equal volume of sample buffer was added to each. Samples were then denatured at 70°C for 10 minutes and spun down.

The proteins in the lysates were separated by SDS-PAGE by preparing a 10% resolving gel and 5% stacking gel, with the components shown in table 2.3.

Table 2.3. Composition of the resolving and stacking gels.

	10% Resolving gel	5% Stacking gel
Stock	Final concentration	
30% Acrylamide	10%	5%
1.5M Tris pH 8.8 (Resolving)	375mM	126mM
Tris pH 6.8 (Stacking)		
10% SDS	0.10%	0.10%
10% APS	0.10%	0.10%
TEMED	0.10%	0.10%
dH ₂ O	n/a	n/a

The resolving gel was prepared first in the gel assembly cassette, with isopropanol added on top to prevent oxygen interfering with the polymerisation of the gel. Once set, excess isopropanol was removed and the stacking gel placed into the cassette along with a gel comb. Once set, the gel comb was removed and the cassette placed into a gel tank with 1X running buffer. Samples were loaded into the wells and the gel was run at 100V for 1-2 hours stopping the run when the dye front had reached the bottom of the gel.

Next, the protein from the SDS-PAGE gel was transferred onto polyvinylidene difluoride (PVDF) membrane. PVDF membrane was cut to the correct size to fit the transfer cassette and prepared by soaking in methanol for 5 minutes then soaked in cold 1X transfer buffer. Whatmann paper cut to the correct size and sponges were also soaked in cold 1X transfer buffer. The gel was carefully removed from the glass plates and assembled into the transfer tank as shown below in figure 2.3.

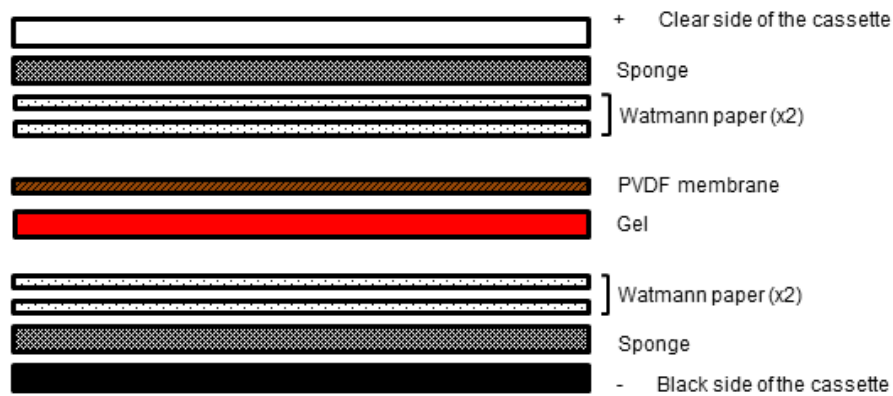


Figure 2.3. Illustration showing how to assemble a transfer cassette.

The transfer cassette was then assembled into the tank with 1X transfer buffer along with an ice block and runs at 115V for 1 hour 15 minutes. Following the transfer, the PVDF membrane was soaked in Ponceau S stain to check for the presence of proteins and a successful transfer. The membrane was then thoroughly washed in distilled water to be then placed in blocking solution for 2 hours at room temperature with gentle rocking. The blocking solution varied for each antibody as shown in table 2.4.

Incubation with the primary antibody was done overnight at 4°C on a rotation rocker with the antibody dilutions shown in table 2.4. The next day, the membrane was placed in TBST for 4 10 minute washes at room temperature.

Table 2.4. Primary and secondary antibodies used in western blots on A375 melanoma cells (blocking solution, dilution factor and supplier also shown).

Primary antibody	Blocking solution	Dilution	Secondary antibody*
Rabbit polyclonal phospho ERK (Cell signalling technology)			Both anti-rabbit IgG HRP linked secondary antibody (Jackson ImmunoResearch)
Rabbit polyclonal phospho-p44/42 MAPK (ERK1/2) (Cell signalling technology)		1:1000	
Mouse monoclonal HSC-70 (Santa-cruz Biotechnology)	All blocked in 5% dry non-fat milk in TBST		Anti-mouse IgG HRP linked secondary antibody (Jackson ImmunoResearch)
Rabbit polyclonal Mcl-1 (Santa-cruz Biotechnology)		1:500	
Rabbit polyclonal anti-BIM (Merck-Millipore)			All anti-rabbit IgG HRP linked secondary antibody (Cell signalling technology)
Rabbit polyclonal PARP (Cell signalling technology)		1:1000	
Rabbit polyclonal PUMA (Cell signalling technology)	Blocked in 5% BSA in TBST		

*(All secondary antibodies were diluted 1:2000).

Incubation with the secondary antibody was done in the dark for 1 hour at room temperature on a rotation rocker. Again the membrane was washed in TBST in the dark for 6 5 minute washes. Detection of the proteins on the PVDF membrane was achieved by using the PierceTM ECL western blotting substrate kit. ECL detection reagents 1 and 2 were added in a 1:1 ratio and enough reaction mixture was added

onto the membrane to cover it and incubated for 5 minutes. Excess ECL reaction mixture was removed and the membrane placed in-between a clear plastic sheet ready for imaging.

2.14 Preliminary mouse study

Severe combined immunodeficient (SCID) mice were purchased from Charles River and were acclimatised for 2 weeks. 1×10^6 cells in 0.1ml of A375, M229, SKMEL5, M285 and M375 cells were injected intraperitoneally into the mice. In the subsequent preliminary experiment 3×10^6 cells in 0.1ml of M285 and M375 cells were injected. When a visible palpable tumour was observed the mice were culled. All procedures were performed under Home Office approved protocols and university guidelines.

2.15 Mouse xenograft study

A total of 3×10^6 M375 melanoma cells were injected intraperitoneally into 40 SCID mice (purchased from Charles River). After approximately 4 weeks when the tumours were palpable, the mice were randomised into 4 arms. The 4 arms were; vehicle alone, leflunomide alone, selumetinib alone and leflunomide and selumetinib in combination. There were 10 mice in each arm. The drug regime was administered for 12 days. Leflunomide was administered by intraperitoneal injection daily at 7.5mg/kg. Selumetinib was administered by oral gavage twice daily at 30mg/kg for the first two days and was then delivered once daily thereafter. The tumour volume was measured every three days with callipers. At the end of the experiment, the mice were culled and the excised tumours were weighed. All procedures were performed under Home Office approved protocols and university guidelines.

2.16 Testes isolation

A male *X. laevis* was euthanized by placing the male into a 500ml beaker with 0.5g 1.6% ethyl 3-aminobenzoate methane sulfonate in 300ml water. The beaker was covered in tinfoil and placed at 4°C for 1 hour. The testes were surgically removed and stored for up to a week at 4°C in testes buffer. The *X. laevis* carcass was disposed of by incineration.

2.17 Generation of *X.laevis* eggs and *in vitro* fertilisation

Adult female *X.laevis* were primed with 100 units of pregnant mare serum gonadotrophin (PMSG) 4 days before eggs were required and were isolated during this period. 12-18 hours before eggs were required, adult female *X.laevis* were induced subcutaneously with 500 units of human chorionic gonadotrophin (HCG) and kept at 18°C. Over a clean petri dish, eggs were obtained by physically squeezing the abdomens of the female every hour over a 6 hour period. A portion of the dissected testes is pulped with 1ml of 1 x MMR and evenly distributed over the embryos and left for 5 minutes at 18°C. Embryos were then immersed in 0.1 x MMR for 20 minutes at 18°C.

2.18 De-jellying of the embryo

Xenopus embryos are enveloped in a transparent jelly coat which needs to be removed post fertilisation. 0.1 x MMR was poured off the embryos and replaced with 2% L-Cysteine pH 8 for approximately 7 minutes. Concurrently the embryos were swirled to gradually remove the jelly coat. Embryos were subsequently washed in 1 x MMR and 0.1 x MMR and transferred to a BSA coated petri dish immersed in 0.1 x MMR with 0.1 % gentamycin. The embryos were kept to develop to the required stage according to Niewkoop and Faber 1967.

2.19 Embryo fixing

Embryos were fixed once they reached their required stage. Embryos were fixed in MEMFA (3.7% formaldehyde, 1 x MEM salts and DEPC H₂O) overnight at 4°C, washed in PBS 3 times and stored in 100% methanol.

2.20 Compounds used in chemical genetic screen

The NCI Diversity Set II compound library was used in this chemical genetic screen. The library was obtained from the synthesis and chemistry branch, development therapeutics program, division of cancer treatment and diagnosis, national cancer institute, USA. The library consisted of 1363 compounds. The library was received in a 96-well plate format with each well containing one compound. Each compound was at a stock concentration of 10mM dissolved in 100µl of DMSO. Any compounds of interest later identified were ordered in as solids and made up to 10mM stocks dissolved in DMSO stored at -20°C.

2.21 Chemical genetic screen using *X.laevis*

Each NCI compound was screened at 20 and 40µM in 96-well plates (as previously determined in the lab). The compounds were initially arrayed at double the required concentration into the wells at a volume of 150µl. Next, five stage 15 embryos in 150µl of 0.1xMMR supplemented with 0.1% gentamycin were placed into each well, making it to be the desired concentration in the wells. Each plate was sealed with a permeable plate seal and embryos were left to develop to stage 38 at 18°C. Once at stage 38, the compound solution in each of the wells was replaced with MEMFA to fix the embryos. After 2 hours at room temperature the MEMFA was removed and replaced with PBST.

2.22 Observing the embryos

To observe and score the phenotypes of the embryos, the five embryos from each well were observed in turn under a Zeiss Stemi5V6 microscope. Images were captured using a 01-MP3.3-RTV-CLR-10 camera mounted and processed with the Q capture software. All images were taken with the anterior of the embryo to the left and the posterior to the right.

2.23 Analysis of the chemical screen

The performance of the chemical genetic screen was analysed based on the following classification of phenotypes; total and partial loss pigment, edema, blistering, general morphology, melanophore morphology, melanophore migration and eye development. Each well of every 96-well plate was assayed twice blind visually. Analysis of any phenotype observed was recorded for the 5 embryos in that particular well.

2.24 Validation of compounds

Each positive NCI compound 'hit' identified from the chemical screen was validated again at 20 and 40 μ M but in 48-well plates. The compounds were again initially arrayed at double the required concentration into the wells at a volume of 500 μ l. Subsequently, ten stage 15 embryos in 500 μ l of 0.1xMMR supplemented with 0.1% gentamycin were placed into each well, making it to be the desired concentration in the wells. Each plate was sealed with a permeable plate seal and embryos were left to develop to stage 38 at 18°C. Once at stage 38, the compound solution in each of the wells was replaced with MEMFA to fix the embryos. After 2 hours at room temperature the MEMFA was removed and replaced with PBST. Embryos were observed and analysed as described above. Any repeatable phenotypes from a given compound were recorded.

2.25 Cell viability assays on NCI 'hit' compounds

Cell viability assays were carried (exactly as described in 2.6 and shown in figure 2.1) using some of the NCI compounds. The concentrations used for each NCI compound ranged from 1.5625 μ M-100 μ M. The cell lines used for these assays were A375 melanoma cells, HEK293 cells and RD1 cells with the seeding densities previously shown in table 2.1.

Chapter 3

Chemical genetic screen of the NCI diversity set II library in *X.laevis* embryos succeeded by a cell-based screen

3.1 Introduction

Work by the Wheeler lab had previously shown *Xenopus* to be a good model to do chemical genetic screens (Tomlinson et al, 2005, 2009). The chemical genetic screening of the NCI diversity set I library in *X.laevis* embryos in our lab had been proven to be successful. This screen illustrated how abnormal pigment phenotypes caused by screened compounds can efficiently lead to the identification of interesting compounds and novel therapeutic agents in the treatment of melanoma (Tomlinson et al. 2009a and b; White et al. 2011).

It was therefore felt that the potential was there to identify more interesting compounds. Myself and colleague Adam Hendry used the same chemical genetic screen method used by Tomlinson et al (2009) to carry out a chemical genetic screen of the NCI diversity II library, the sequel to the NCI diversity set I library. The compounds within this library are all structurally dissimilar to each other having the potential to cover a broad range of possible therapeutic targets. There is a 10% overlap between the NCI diversity set I and II library which enabled the possibility of internal positive controls being identified.

Myself and Adam initially carried out a chemical genetic screen in *X.laevis* embryos of the NCI diversity set II library, which consisted of 1363 compounds. From this screen a total of 72 compounds were identified as compounds which gave an abnormal phenotype which was reproducible. These 72 compounds were then screened in a cell viability assay in three cell lines; A375 melanoma cells, HEK293 and RD1 cells. The aim of this additional cell-based screen was to determine if any of the IC50's calculated

for the compounds were statistically significantly lower in the A375 melanoma cell line than in comparison to the two non-melanoma cell lines. From the 72 compounds, 13 compounds fulfilled this criterion. Therefore the results from both screens of the compounds have led to the identification of 13 compounds which hold the potential of being possible therapeutic agents for treating melanoma.

3.2 Results

3.2.1 Phenotypic scoring criteria of the chemical genetic screen

The compounds in the library were screened at 20 μ M and 40 μ M with five embryos in each well. To help with the understanding of the results to follow, figure 3.1 shows an *X.laevis* embryo annotated with some associated terminology when describing some of the phenotypes the compounds gave rise to.

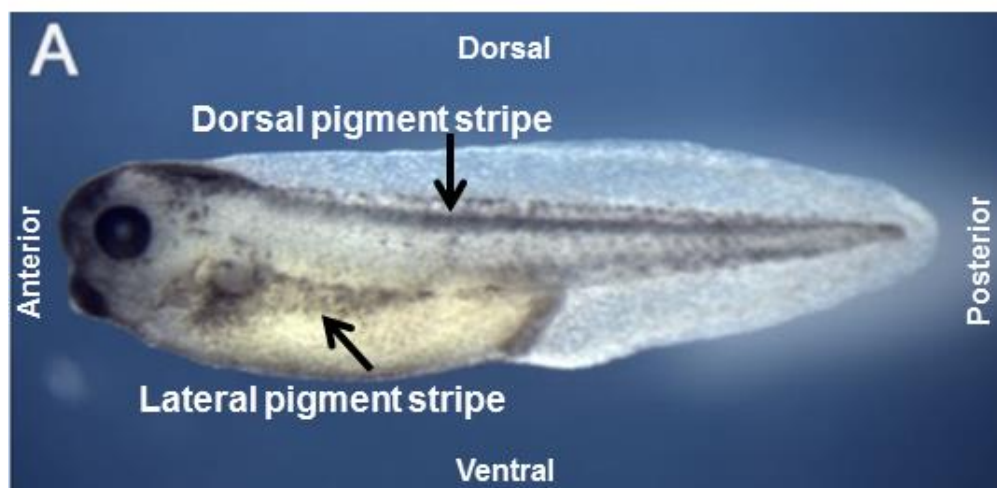


Figure 3.1. Annotation of an *X.laevis* embryo showing the anterior of the embryo to the left and the posterior to the right. The two main areas of the embryo in which pigmentation (localisation of the melanophores) are seen, are indicated by the black arrows.

To reduce experimental bias of this screen, the phenotypes of the embryos produced by the compounds were scored twice blind by myself and Adam Hendry. There was eight phenotypes which we scored for; total pigment loss, partial pigment loss, abnormal melanophore migration, abnormal melanophore migration, edema, blistering, abnormal general morphology and abnormal eye development. An example for each phenotypic class is shown in figure 3.2A. Total pigment loss referred to the loss of pigment in both the dorsal and lateral pigment stripes of the embryo including loss of pigment in the retinol pigment epithelium (RPE) (figure 3.2Aii). Partial pigment loss was where there was a noticeable reduction in pigment in the dorsal and/or lateral pigment stripe, but pigment cells were still present (figure 3.2Aiii). Abnormal melanophore migration was scored if the melanophores had not migrated correctly along the dorsal and lateral pigment stripes or produced an abnormal pigmentation patterning (figure 3.2Aiv). Abnormal melanophore morphology was classified if a compound caused the melanophores to produce morphology other than the normal dendritic morphology seen in control embryos (figure 3.2Av). Edema was scored when fluid retention around the area of the developing heart was presented (figure 3.1Aviii). Abnormal general morphology was recorded if the embryo's overall general morphology did not mimic that of the control embryos (3.2Avi). Abnormal eye development referred to if any of the developing eye features appeared to not be forming correctly compared to the control embryos eye (figure 3.2Avii). Finally, blistering was scored for if a build-up of fluid was seen on any part of the embryo (figure 3.2Aix). This is generally associated with toxicity.

The strength of the phenotype observed which a compound gave rise to was scored on a scale of 1-3. The score of 1 was given when the phenotype presented was very obvious to the eye and there was no ambiguity in the phenotype. A score of 3 was given when the phenotype was present but only subtly. In many cases throughout this screening, the majority of the compounds presented with more than one phenotype, as shown later.

3.2.2 Summary of results of the chemical genetic screen of the NCI diversity set II library on *X.laevis* embryos.

From the 1363 compounds screened, 72 compounds were identified as 'hit's in that they produced a phenotype. This data is shown in figure 3.2B, which shows the percentage breakdown of the phenotypes observed. As previously mentioned many of the compounds produced more than one phenotype. The phenotype that was the most prominent was the category in which the compound was allocated to, which is represented in figure 3.2B. Overall the pigmentation phenotype was the most observed at 38% (total and partial). The other phenotypes involved with pigmentation, melanophore migration and melanophore morphology were also frequently observed at 13% and 10% respectively. Abnormal general morphology was also well represented from the screen with 17% of compounds being classified with this phenotype. Abnormal eye development was also commonly scored for with 14%. Edema and blistering were amongst the categories which held the least proportion of compounds with 1% and 7% respectively.

Figure 3.2C on the other hand shows the percentage each time a phenotype was observed, taking into account the multiple phenotypes a compound gave rise to. The data presented on this graph is regardless of the strength scoring system that was in place (scores of 1-3). An example of this phenomenon can be seen in figure 3.2Aix. This embryo has a very clear blistering phenotype and thus would have been categorised for this phenotype in regards to figure 3.2B. However you can also see this embryo has a total pigment loss phenotype and in regards to figure 3.2C both the blistering and total pigment loss phenotype was recorded for this compound. Overall, the pigmentation phenotypes (total and partial) were again the most observed phenotype contributing to 38% of 'active' compounds. Abnormal general morphology and eye development were the second highest phenotypes observed with 22% and 20% respectively. Next melanophore migration with 16% and melanophore morphology with 7% were overall still highly observed phenotypes from the 'hit' compounds.

Finally, the phenotypes less commonly produced by the compounds were again edema and blistering with 2% and 4% respectively. This highlights that these 'hit' compounds could be affecting more than one potential target, resulting in multiple phenotypes being observed.

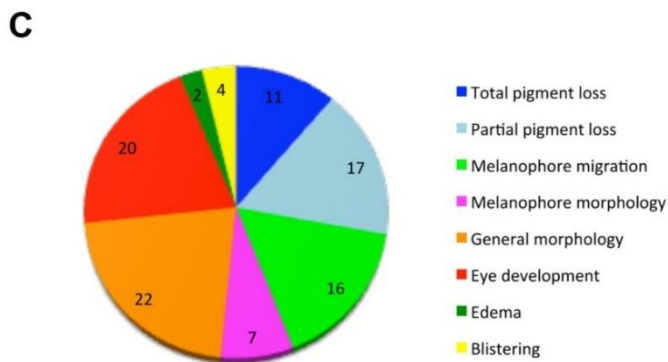
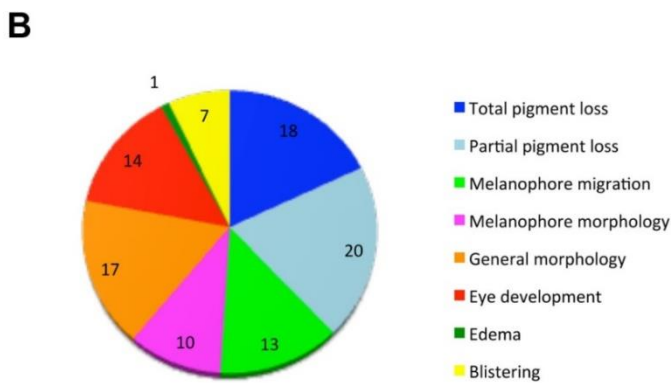
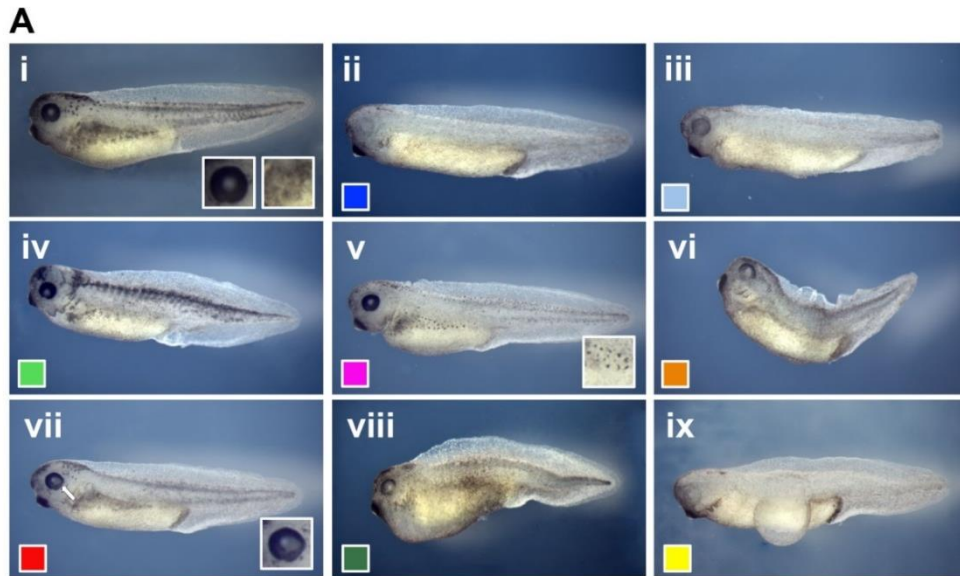


Figure 3.2. Summary of the phenotypes produced from the ‘hit’ compounds in the chemical genetic screen of the NCI diversity set II library. A. represents an example of each phenotype that was scored for as follows; i DMSO vehicle control, ii total pigment loss, iii partial pigment loss, iv abnormal melanophore migration, v abnormal melanophore morphology, vi abnormal general morphology, vii abnormal eye development, viii edema and ix blistering. B shows the percentage in which each ‘hit’ compound was categorised into (n=72). C represents the percentage of the overall amount of times each phenotype was observed (n=161). All embryos are shown with the anterior to the left and posterior to the right.

3.2.3 Compounds categorised into the total pigment loss phenotype

A total of 13 compounds were categorised as compounds producing a total pigment loss phenotype; NCI 9358, NCI 20618, NCI 20619, NCI 99657, NCI 99660, NCI 131982, NCI 131986, NCI 164965, NCI 515893, NCI 12588, NCI 135810, NCI 205913 and NCI 319034 (figure 3.3). However these 13 compounds can be further split into two groups. Those which appeared to almost completely cause a loss of pigment in both the dorsal and lateral stripe, reducing pigment in the head region and in the retinal pigment epithelium. Compounds NCI 9358, NCI 20618, NCI 20619, NCI 99657, NCI 99660, NCI 131982, NCI 131986, NCI 164985 and NC 515893 (figures 3.3 B,D,E,F,G,H,I,K, and N) fit into the group of compounds which achieved this phenotype. Secondly, those which appeared to almost cause a loss of pigment in both the dorsal and lateral stripe; some pigment remains in the head region, but only very subtly. The compounds which fit into this sub-category are NCI 12588 NCI 135810, NCI 205913 and NCI 319034 (figures 3.3 C,J,L and M).

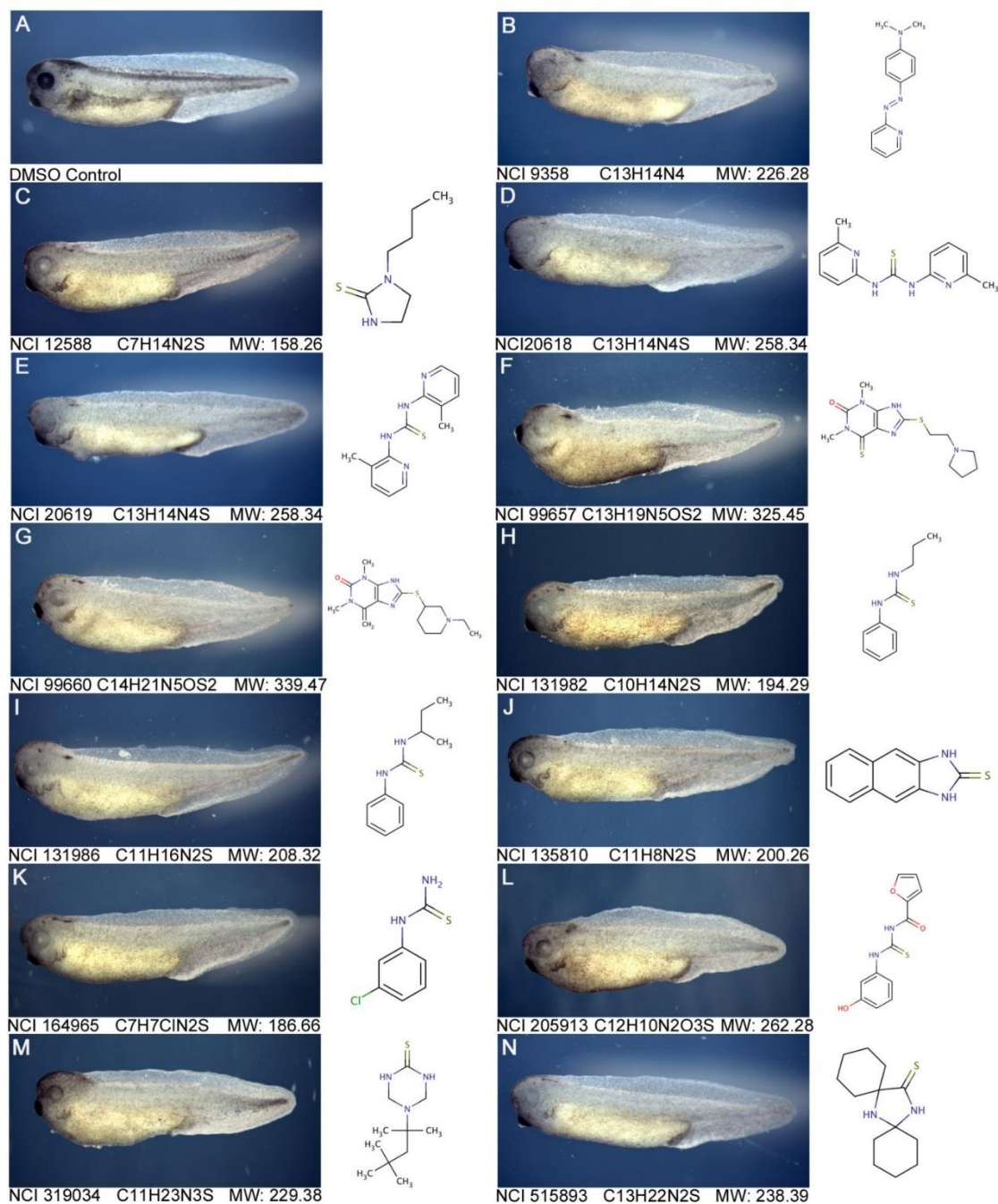


Figure 3.3. NCI compounds that caused a total loss of pigment in *X.laevis* embryos. Each NCI compound is shown by its representative phenotype produced at 40 μ M. The compound structure of the NCI compound is shown to the right of the embryo. The NCI compound name, compound formula and molecular weight (MW) are also shown. A, DMSO control, B, NCI 9358, C, NCI 12588, D, 20618, E, NCI 20619, F, NCI 99657, G, NCI 99660, H, NCI 131982, I, NCI 131986, J, NCI 135810, K, NCI 164965, L, NCI 205913, M, NCI 319034, N, NCI 515893. All embryos are at stage 38 with the anterior of the embryo facing to the left and the posterior to the right.

3.2.4 Compounds categorised into the partial pigment phenotype

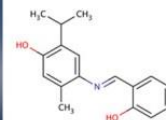
The phenotype of a partial loss of pigment was produced by a total of 15 'hit' compounds; NCI 30712, NCI 42028, NCI 45536, NCI 45545, NCI 59620, NCI 62609, NCI 62611, NCI 87084, NCI 104993, NCI 106581, NCI 111848, NCI 117741, NCI 153792, NCI 154718 AND NCI 319471 (figure 3.4). These compounds all produced a reduction in the dorsal and lateral pigment stripes of the embryos but the pigment in the head region and in most cases, that of the retinal pigment epithelium was still visible. Whilst compounds NCI 104993 and NCI 154718 both produced a partial pigment phenotype, they also presented with a decrease in pigmentation in the RPE (figures 3.4J and 3.4O) when compared to the DMSO control (figure 3.4A). Therefore NCI 104993 and NCI 154718 also seem to generate an abnormal eye development phenotype. An additional 'hit' compound which also produced an abnormal eye development was NCI 319471 (figure 3.4P) where the developing eye appeared larger in size than the DMSO control.



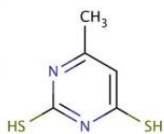
DMSO Control



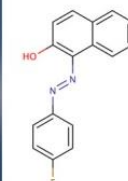
NCI 30712 C₁₇H₁₉NO₂ MW: 269.34



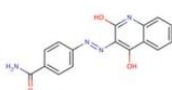
NCI 42028 C₅H₆N₂S₂ MW: 158.23



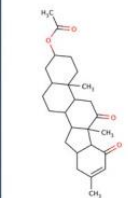
NCI 45536 C₁₆H₁₁FN₂O MW: 266.27



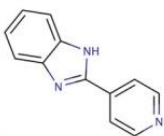
NCI 45545 C₁₆H₁₂N₄O₃ MW: 308.30



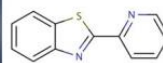
NCI 59620 C₂₆H₃₆O₄ MW: 412.57



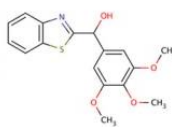
NCI 62609 C₁₂H₉N₃ MW: 195.22



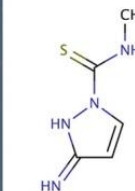
NCI 62611 C₁₂H₈N₂S MW: 212.27



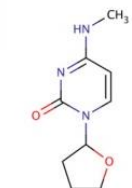
NCI 87084 C₁₇H₁₇NO₄S MW: 331.39



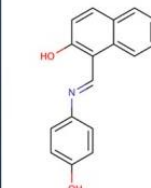
NCI 104993 C₄H₇N₅S MW: 157.19



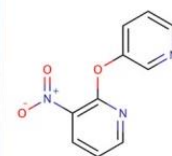
NCI 106581 C₉H₁₃N₃O₂ MW: 195.22



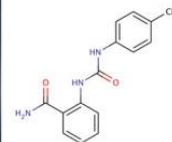
NCI 111848 C₁₇H₁₃NO₂ MW: 263.30



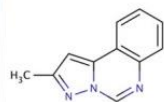
NCI 117741 C₁₀H₇N₃O₃ MW: 217.18



NCI 153792 C₁₅H₁₅N₃O₂ MW: 269.30



NCI 154718 C₁₁H₉N₃ MW: 183.21



NCI 319471 C₁₂H₁₆N₂O₂S MW: 252.33

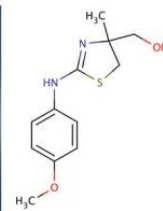


Figure 3.4. NCI compounds that caused a partial loss of pigment in *X.laevis* embryos. Each NCI compound is shown by its representative phenotype produced at 40 μ M. The compound structure of the NCI compound is shown to the right of the embryo. The NCI compound name, compound formula and molecular weight (MW) are also shown. A, DMSO control, B, NCI 30712, C, NCI 42028, D, 45536, E, NCI 45545, F, NCI 59620, G, NCI 62609, H, NCI 62611, I, NCI 87084, J, NCI 104993, K, NCI 106581, L, NCI 111848, M, NCI 117741, N, NCI 153792, O, NCI 154718, P, NCI 319471. All embryos are at stage 38 with the anterior of the embryo facing to the left and the posterior to the right

3.2.5 Compounds categorised into the abnormal melanophore morphology phenotype.

Seven 'hit' compounds were capable of altering the normal morphology of the melanophores of the embryo compared to the DMSO control embryo; NCI 4292, NCI 117987, NCI 133002, NCI 204262, NCI 275971, NCI 34871 and NCI 138398 (figure 3.5). Two distinct different melanophore morphologies were detected. NCI 34871 and NCI 138398 (figure 3.5C and 3.5F) altered the normal dendritic morphology of the melanophores as seen in the DMSO control embryo (figure 3.5A) to enlarged flattened melanophores. In comparison NCI 4292, NCI 117987, NCI 133002, NCI 204262 and NCI 275971 (figures 3.5B, D, E, G and H) all give rise melanophores which appeared much more rounded and smaller compared to the DMSO control embryos. NCI 275971 (figure 3.5H) also presented with a noticeable abnormal eye development phenotype in which the eye appeared much smaller in anatomical size compared to the DMSO control embryo (figure 3.5A).

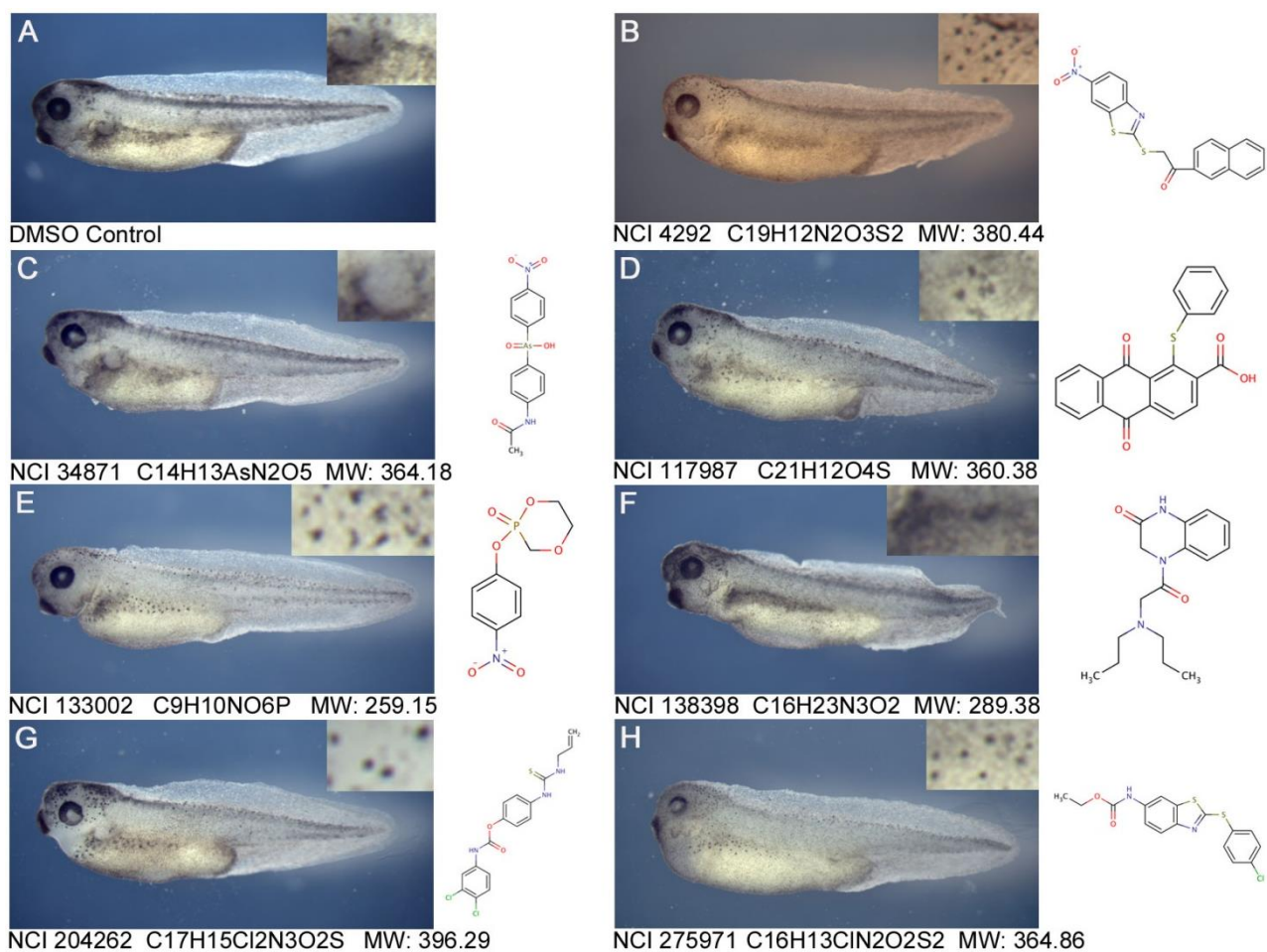


Figure 3.5. NCI compounds that caused abnormal melanophore morphology in *X.laevis* embryos. Each NCI compound is shown by its representative phenotype produced at 40 μ M. The compound structure of the NCI compound is shown to the right of the embryo. The NCI compound name, compound formula and molecular weight (MW) are also shown. A, DMSO control, B, NCI 4292, C, NCI 34871, D, 117987, E, NCI 133002, F, NCI 138398, G, NCI 204232, H, NCI 275971. All embryos are at stage 38 with the anterior of the embryo facing to the left and the posterior to the right.

3.2.6 Compounds categorised into the abnormal melanophore migration phenotype

A total of 9 'hit' compounds produced an abnormal melanophore migration phenotype; NCI 11624, NCI 13156, NCI 13653, NCI 36525, NCI 92794, NCI 125197, NCI 139021, NCI 150982 and NCI 246415 (figure 3.6). Abnormal melanophore migration was defined as compounds preventing the correct migration of the melanophores along both the dorsal and lateral pigment stripes. The most striking abnormal melanophore migration pattern was seen in 3 'hit' compounds which produced a segmented pigmentation pattern along the dorsal pigment stripe, NCI 13156, NCI 139021 and NCI 150982 (figures 3.6 C, H and I). This pattern was distinguishably produced by NCI 13156 (figure 3.6C). It was also apparent that NCI 13156 prevented melanophores from fully migrating to the lateral pigment stripe. Thus this compound had a very prominent effect on melanophore migration. Other 'hit' compounds also prevented the migration of the melanophores to the lateral pigment stripe. NCI 92794 and NCI 150982 are examples of 'hit compounds which did this (figures 3.6 F and I). NCI 92794 and NCI 246415 (figures 3.6 F and J) both also presented with edema phenotypes.

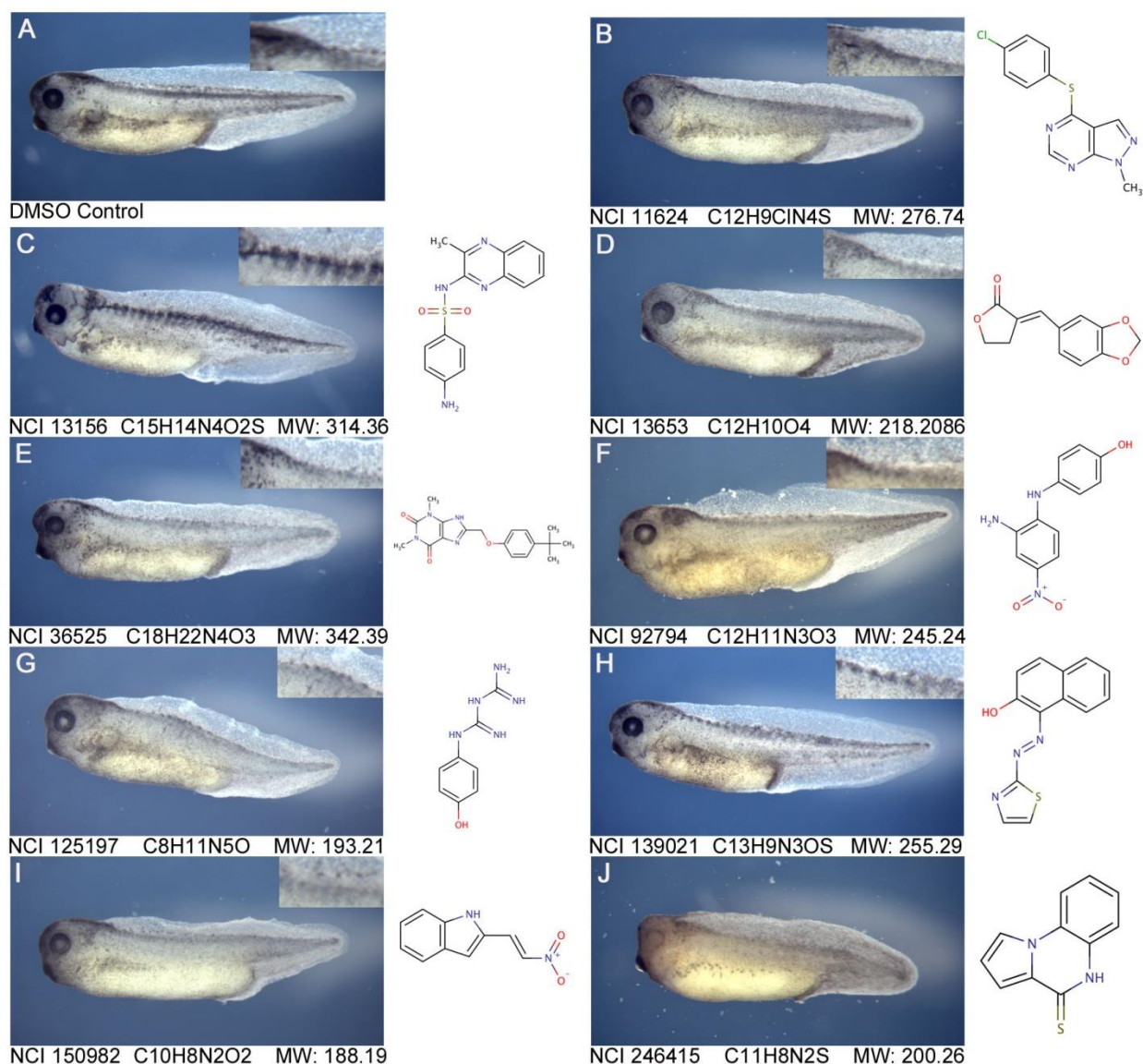


Figure 3.6. NCI compounds that caused abnormal melanophore migration in *X.laevis* embryos. Each NCI compound is shown by its representative phenotype produced at 40 μ M. The compound structure of the NCI compound is shown to the right of the embryo. The NCI compound name, compound formula and molecular weight (MW) are also shown. A, DMSO control, B, NCI 11624, C, NCI 13156, D, 13653, E, NCI 36525, F, NCI 92794, G, NCI 125197, H, NCI 139021. I, NCI 150982, J, NCI 246415. All embryos are at stage 38 with the anterior of the embryo facing to the left and the posterior to the right.

3.2.7 Compounds classified into the abnormal general morphology phenotype

A total of 12 'hit' compounds produced an abnormal general morphology phenotype; NCI 21683, NCI 30930, NCI 31762, NCI 43013, NCI 79253, NCI 85326, NCI 88916, NCI 151262, NCI 377389, NCI 402590, NCI 645987 and NCI 667251 (figure 3.7). It is to notice that all of these compounds, bar one (NCI 31762, figure 3.7 D), also promoted either a total or partial loss of pigmentation phenotype. NCI 43013, NCI 79253, NCI 85326, NCI 88916 and NCI 402590 (figures 3.7 E, F, G, H and K) all produced the same abnormal general morphology phenotype in comparison the DMSO control embryo (figure 3.7A). These compounds caused the body of the embryo to kink or become inverted upwards. Another striking abnormal general morphology observed was caused by the four 'hit' compounds NCI 377384, NCI 402590, NCI 645987 and NCI 607251 (figures 3.7 J, K, L and M). These compounds caused the body of the embryo to become more elongated than normal compared to the DMSO control (figure 3.7A).

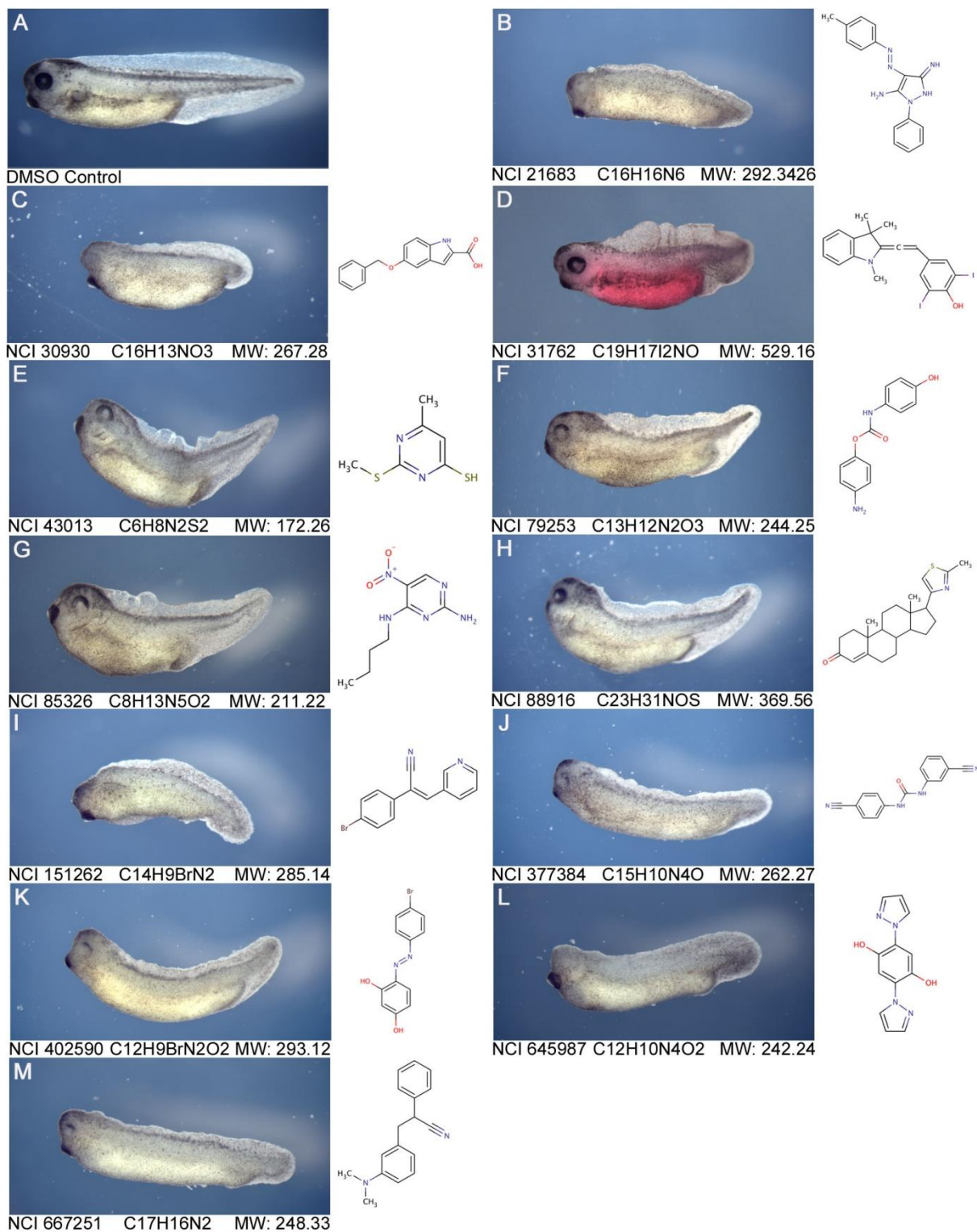


Figure 3.7. NCI compounds that caused abnormal general morphology in *X.laevis* embryos. Each NCI compound is shown by its representative phenotype produced at 40µM. The compound structure of the NCI compound is shown to the right of the embryo. The NCI compound name, compound formula and molecular weight (MW) are also shown. A, DMSO control, B, NCI 21683, C, NCI 30930, D, NCI 31762, E, NCI 43013, F, NCI 79253, G, NCI 85326, H, NCI 88916, I, NCI 151262, J, NCI 377384, K, NCI 402590, L, NCI 645987, M, NCI 667251. All embryos are at stage 38 with the anterior of the embryo facing to the left and the posterior to the right.

3.2.8 Compounds classified into the abnormal eye development phenotype

From the 72 compounds, 10 gave rise to an abnormal eye development phenotype (figure 3.8). Eight of these compounds caused an abnormal development of the RPE, NCI 5907, NCI 19219, NCI 45572, NCI 66020, NCI 130872, NCI 211490, NCI 340852 and NCI 378719 (figures 3.8 C, D, F, G, H, I, J and K). A unique abnormal eye development phenotype was observed with NCI 3001 (figure 3.8 B) in which the lens appeared to be displaced from its normal developing location when compared to the DMSO control (figure 3.8A).

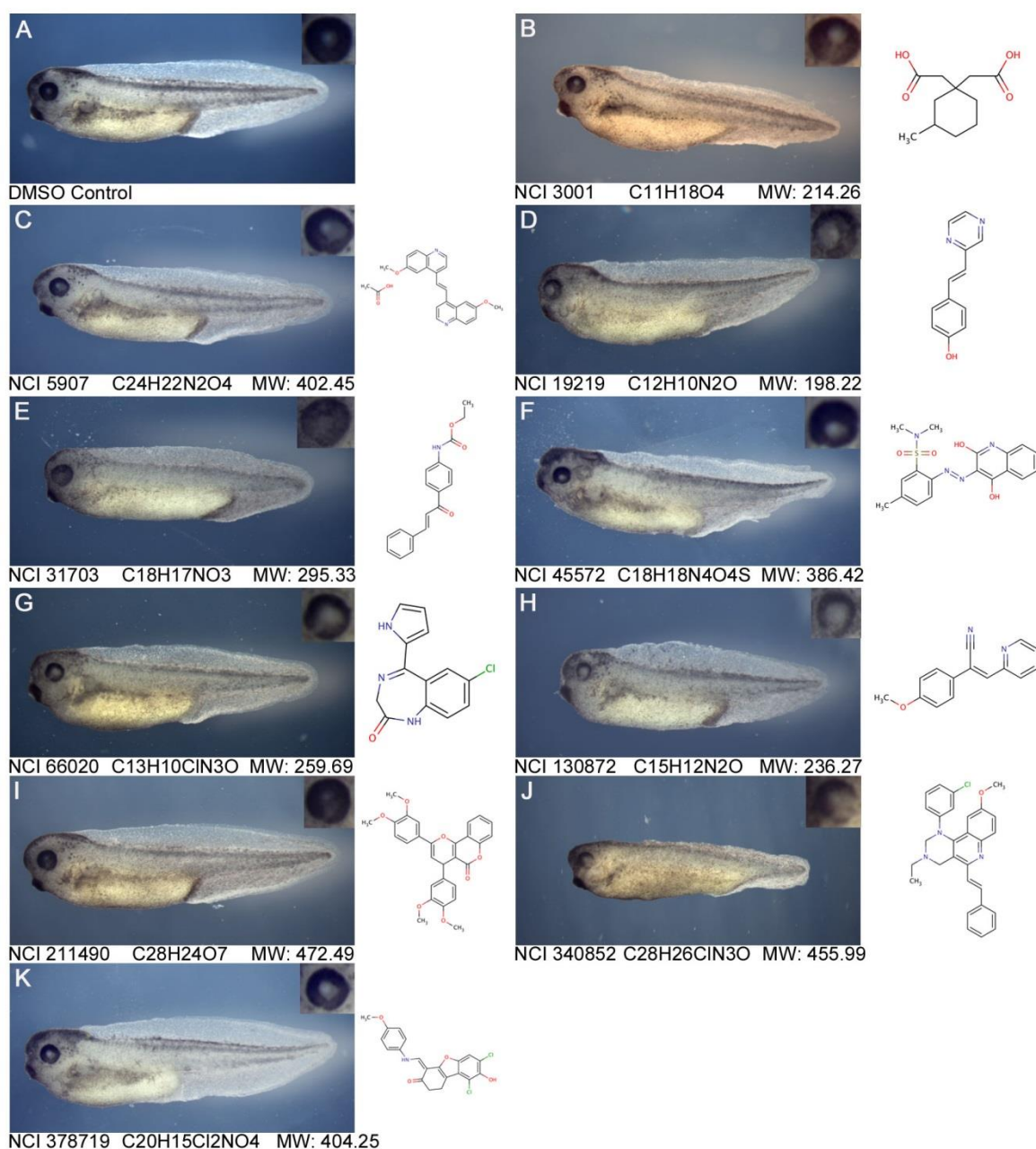


Figure 3.8. NCI compounds that caused abnormal eye development in *X. laevis* embryos. Each NCI compound is shown by its representative phenotype produced at 40 μ M. The compound structure of the NCI compound is shown to the right of the embryo. The NCI compound name, compound formula and molecular weight (MW) are also shown. A, DMSO control, B, NCI 3001, C, NCI 5907, D, 19219, E, NCI 31703, F, NCI 45572, G, NCI 66020, H, NCI 130872, I, NCI 211490, J, NCI 340852, K, NCI 378719. All embryos are at stage 38 with the anterior of the embryo facing to the left and the posterior to the right.

3.2.9 Compounds categorised into the edema phenotype

Only one 'hit' compound from all of the 72 compounds produced a strong edema phenotype, NCI 205832 (figure 3.9B). This compound clearly shows extensive fluid retention in the area of the developing heart. Due to the excessive fluid retention it is possible that the abnormal general morphology and partial pigment loss phenotypes also seen are due to the edema.

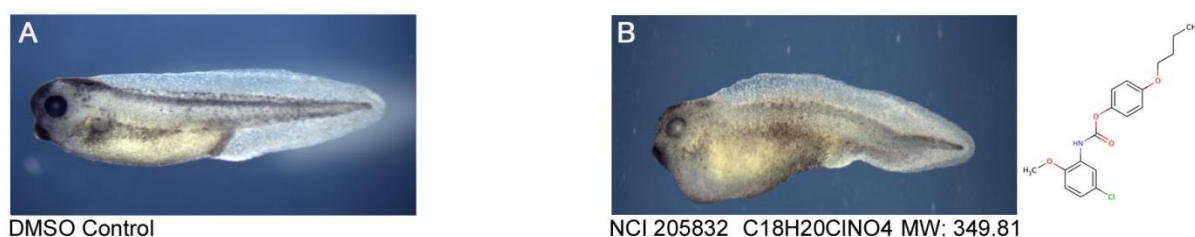


Figure 3.9. NCI compound that caused edema in *X.laevis* embryos. Each NCI compound is shown by its representative phenotype produced at 40 μ M. The compound structure of the NCI compound is shown to the right of the embryo. The NCI compound name, compound formula and molecular weight (MW) are also shown. A, DMSO control, B, NCI 205832. All embryos are at stage 38 with the anterior of the embryo facing to the left and the posterior to the right.

3.2.10 Compounds classified into the blistering phenotype

5 compounds of the 72 compounds identified in the screen produced a blistering phenotype, NCI 14380, NCI 68971, NCI 246415, NCI 308847 and NCI 343557 (figure 3.10). The blistering phenotypes observed were consistent and localised to the same anatomical position. NCI 246415 (figure 3.10D) also presented with a total pigment loss phenotype. A melanophore morphology phenotype was seen clearly with NCI 308847 and NCI 68971 (figure 3.1C and E) in which the melanophores appeared more rounded and compact compared to the DMSO control (figure 3.10 A).

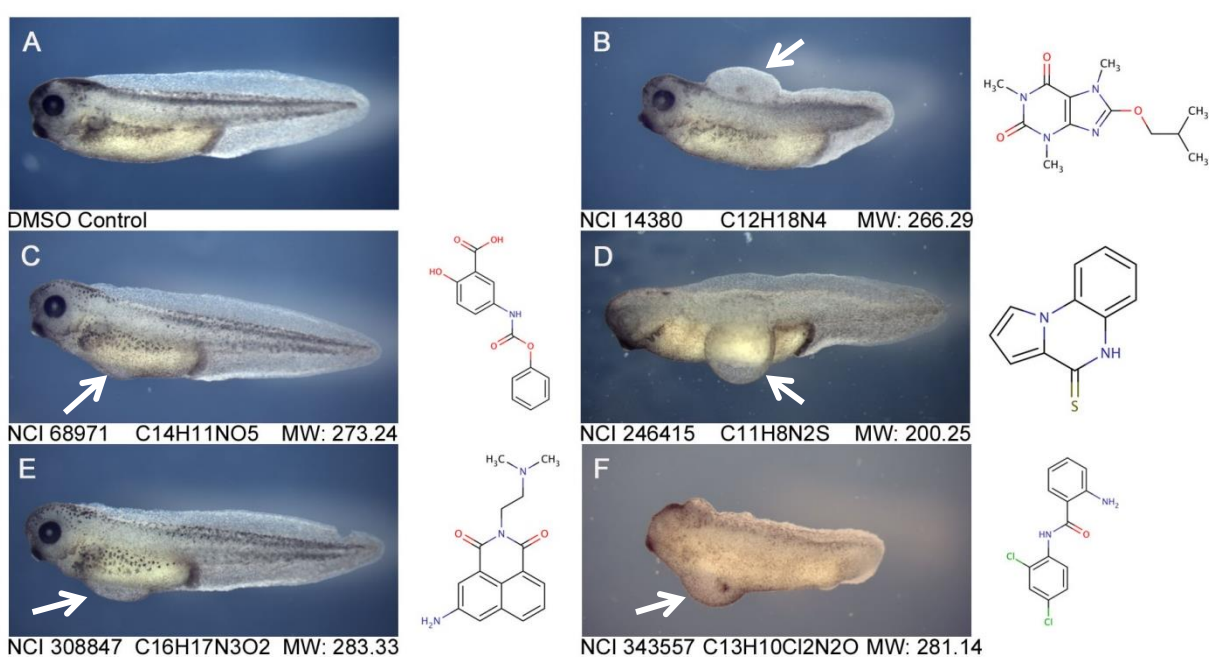


Figure 3.10. NCI compounds that caused blistering in *X. laevis* embryos. Each NCI compound is shown by its representative phenotype produced at 40 μ M. The compound structure of the NCI compound is shown to the right of the embryo. The NCI compound name, compound formula and molecular weight (MW) are also shown. A, DMSO control, B, NCI 14380, C, NCI 68971, D, 246415, E, NCI 308847, F, NCI 343557. All embryos are at stage 38 with the anterior of the embryo facing to the left and the posterior to the right.

3.2.11 Dose-response assays on the 72 'hit' compounds

All of the 72 'hit' compounds were subjected to a dose response assay to determine if the phenotype was reproducible at different concentrations other than the 20 and 40 μ M already tested. Twenty embryos per well were arrayed at the following range of compound concentrations; 0.1, 1, 10, 25, 50 and 100 μ M. The majority of compounds gave reproducible phenotypes across the concentration range. Two examples are shown in Table 3.1, NCI 133002 and NCI 111848. NCI 111848 was categorised into the partial pigment phenotype and this phenotype was still present at all of the concentrations tested. However at 0.1-10 μ M, additional melanophore morphology and migration phenotypes became present, but were not present from 25-100 μ M. Another example of a 'hit' compound which maintained its phenotype was NCI 133002. NCI 133002 was categorised into the abnormal melanophore morphology phenotype and at concentrations ranging from 25-100 μ M this phenotype was still seen. However at 100 μ M the presence of an abnormal melanophore migration phenotype appeared.

Table 3.1. Dose response data for NCI 133002 and NCI 111848. 20 embryos were arrayed into each well at the indicated range of concentrations. The data is shown as a percentage of embryos which presented with each phenotype (1=100%). M=abnormal general morphology, S=stunted growth, P= pigmentation loss, MM=abnormal melanophore morphology, MG=abnormal melanophore migration, E= Edema, ED=abnormal eye development, B=blistering, PD=percentage death.

		Concentration	M	S	P	MM	MG	E	ED	B	PD
		(μ M)									
NCI 133002		0.1	0	0	0	0	0	0	0	0	0
		1	0	0	0	0	0	0	0	0	0
		10	0	0	0	0	0	0	0	0	0
		25	0	0	0	1	0	0	0	0	0
		50	0	0	0	1	0	0	0	0	0
		100	0	0	0	1	1	0	0	0	0
<hr/>											
NCI 111848		0.1	0	0	1	1	1	0	0	0	0
		1	0	0	1	1	1	0	0	0	0
		10	0	0	1	1	1	0	0	0	0
		25	0	0	1	0	0	0	0	0	0
		50	0	0	1	0	0	0	0	0	0
		100	0	0	1	0	0	0	0	0	0

3.2.12 Cell-based cell viability screen on the 72 'hit' compounds

The 72 'hit' compounds were then subject to a cell-based screen whereby the cell viability of the 72 compounds was initially tested in the A375 melanoma cell line. From this preliminary screen, 40 of the compounds did not decrease the cell viability at the highest concentration of 100 μ M and were not followed up any further. The 32 compounds which did reduce cell viability in the A375 cell line were then further tested in the RD1 and HEK293 cell lines. The preferential outcome from this next cell viability screen is compounds which reduce the cell viability in the A375 melanoma cell line but to a lesser extent or not all in the RD1 and HEK293 cell lines. To determine this outcome, dose response graphs for each compound with the averaged viability data for the three cell lines per graph were constructed. Representative IC₅₀'s were generated for each cell line. Thirteen out of the 32 compounds produced IC₅₀'s which were significantly lower in the A375 cells compared to the RD1 and HEK293 cell lines.

Figure 3.11 A and B show two examples of 'hit' compounds that exhibited identical potency in all three cell lines when cell viability was assessed (table 3.2) (NCI 13653 and NCI 20619). NCI 3001, NCI 19219, NCI 43013, NCI 45536, NCI 79253, NCI 92794, NCI 111848, NCI 131982, NCI 131986, NCI 133002, NCI 138398, NCI 153792 and NCI 319471 are the remaining 13 compounds that exhibited lower IC₅₀'s in the A375 cell line compared to the RD1 and HEK293 cell lines (figures 3.11 C-0 and table 3.2).

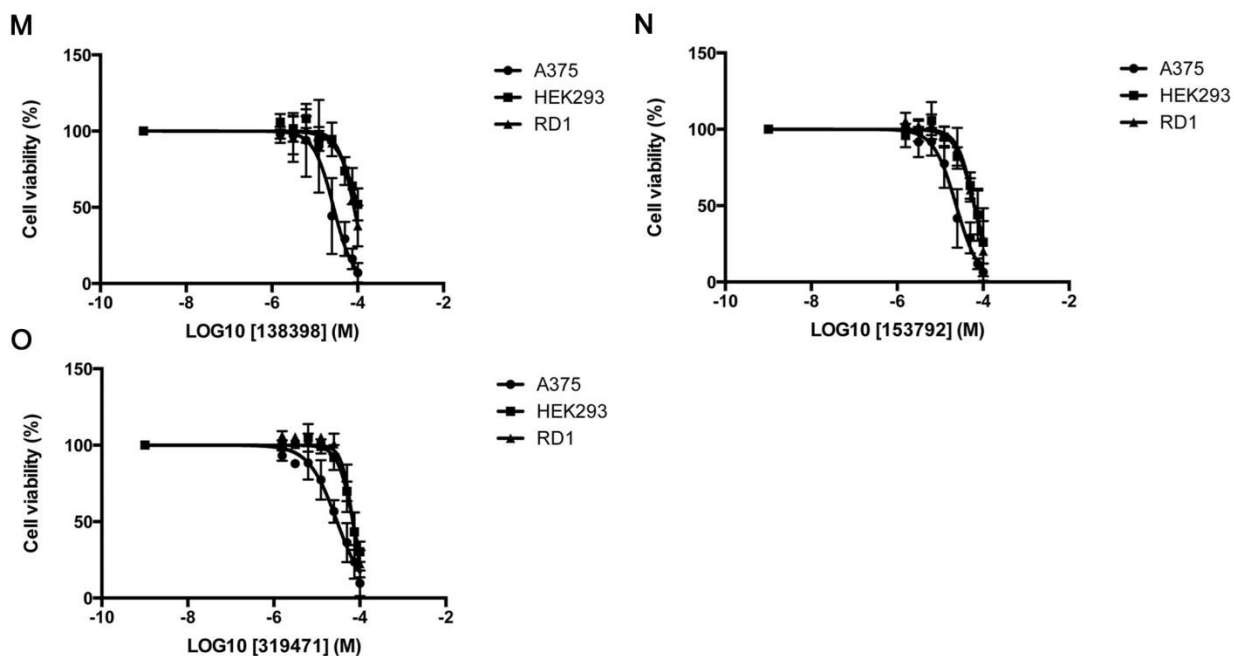


Figure 3.11. Dose response curves of NCI compounds showing effect on cell viability for the A375, RD1 and HEK293 cell lines. A, NCI 13653 and B, NCI 20619 are examples of compounds which do not lower the cell viability in the A375 greater than the RD1 and HEK293 cell lines. C, NCI 3001, D, NCI 19219, E, NCI 43013, F, NCI 45536, G, NCI 79253, H, NCI 92794, I, NCI 111848, J, NCI 131982, K, NCI 131986, L, NCI 133002, M, NCI 138398, N, NCI 153792, O, NCI 319471 are the 13 compounds which reduce the cell viability greater than the RD1 and HEK293 cell line. Data is presented as the mean \pm SEM of three independent experiments each performed in cell culture triplicate.

Table 3.2. The generated IC₅₀'s for 32 of the NCI compounds for the A375, RD1 and HEK293 cell lines. The IC₅₀'s highlighted in blue represent the 13 compounds which have lower IC₅₀'s compared to the RD1 and HEK293 cell lines.

	A375	HEK293	RD1
3001	1.487E-05	1.191E-04	6.828E-05
13653	2.504E-05	4.397E-05	5.074E-05
19219	1.152E-05	7.070E-05	6.685E-05
20619	1.137E-05	1.429E-05	2.258E-05
30712	4.397E-06	3.311E-06	9.185E-06
34871	2.724E-05	1.916E-05	1.081E-05
36525	9.710E-06	6.538E-06	2.646E-05
43013	3.947E-05	1.146E-04	7.887E-05
45536	1.616E-05	3.640E-05	3.423E-05
59620	3.975E-05	1.273E-05	2.881E-05
79253	2.996E-05	5.976E-05	4.509E-05
87084	1.115E-05	1.105E-05	2.895E-05
88916	3.630E-06	2.764E-06	1.248E-05
92794	8.391E-06	2.190E-05	2.829E-05
99660	4.357E-05	6.735E-05	3.860E-05
111848	5.431E-06	2.706E-05	3.128E-05
117987	1.911E-05	2.395E-05	1.703E-05
125197	7.423E-05	1.244E-04	7.737E-05
130872	2.788E-05	2.199E-05	3.402E-05
131982	1.904E-05	6.320E-05	4.424E-05
131986	1.505E-05	3.494E-05	4.020E-05
133002	4.502E-05	8.511E-05	7.336E-05
138398	2.738E-05	1.029E-04	8.174E-05
151262	2.340E-05	1.591E-05	3.512E-05
153792	2.365E-05	6.322E-05	6.194E-05
205832	1.533E-05	4.757E-05	2.506E-05
205913	3.791E-05	5.273E-05	5.731E-05
246415	2.588E-05	6.767E-05	3.826E-05
275971	4.539E-06	1.920E-05	7.897E-06
319471	2.958E-05	6.924E-05	6.866E-05
343557	1.855E-05	1.753E-05	2.952E-05
378719	3.652E-06	~ 1.238e-005	1.012E-05

3.2.13 Statistical analysis of the IC₅₀'s generated between the A375, RD1 and HEK293 cell lines

To determine if the differences between the IC₅₀'s for the 13 compounds which had lower IC₅₀'s for the A375 cell line than the RD1 and HEK293 cell lines were statistically significant, a student T-test was carried out. However statistical analysis was not performed on the IC₅₀'s generated from the dose response graphs in figure 3.11. This decision was based upon the fact that for each of the three cell viability replicates, each concentration was performed in triplicate. The triplicate data for each concentration was then averaged and normalised to the DMSO control. The data points on the graphs in figure 3.11 are therefore the average of three different experiments and the decision to not do statistical analysis on data that had been averaged twice was made. Instead IC₅₀'s were generated by making dose response graphs with each replicate for each cell line on. The three IC₅₀'s produced for each cell line were then averaged and this data was used for statistical analysis.

However it proved difficult in some cases to generate a level top plateau in the dose-response graphs for some of the replicates for the NCI compounds. To resolve this problem, a very small dose of the concentration of compound, $1 \times 10^{-9} \text{M}$, was tested alongside a DMSO control in the cell viability assay in all three cell lines. Only a selection of NCI compounds were tested for this experiment and for all tested, there was no significant difference in the cell viability between this low concentration and the corresponding vehicle control (figure 3.12). Thus this data point was added onto the subsequent graphs and is also seen on those in figure 3.11.

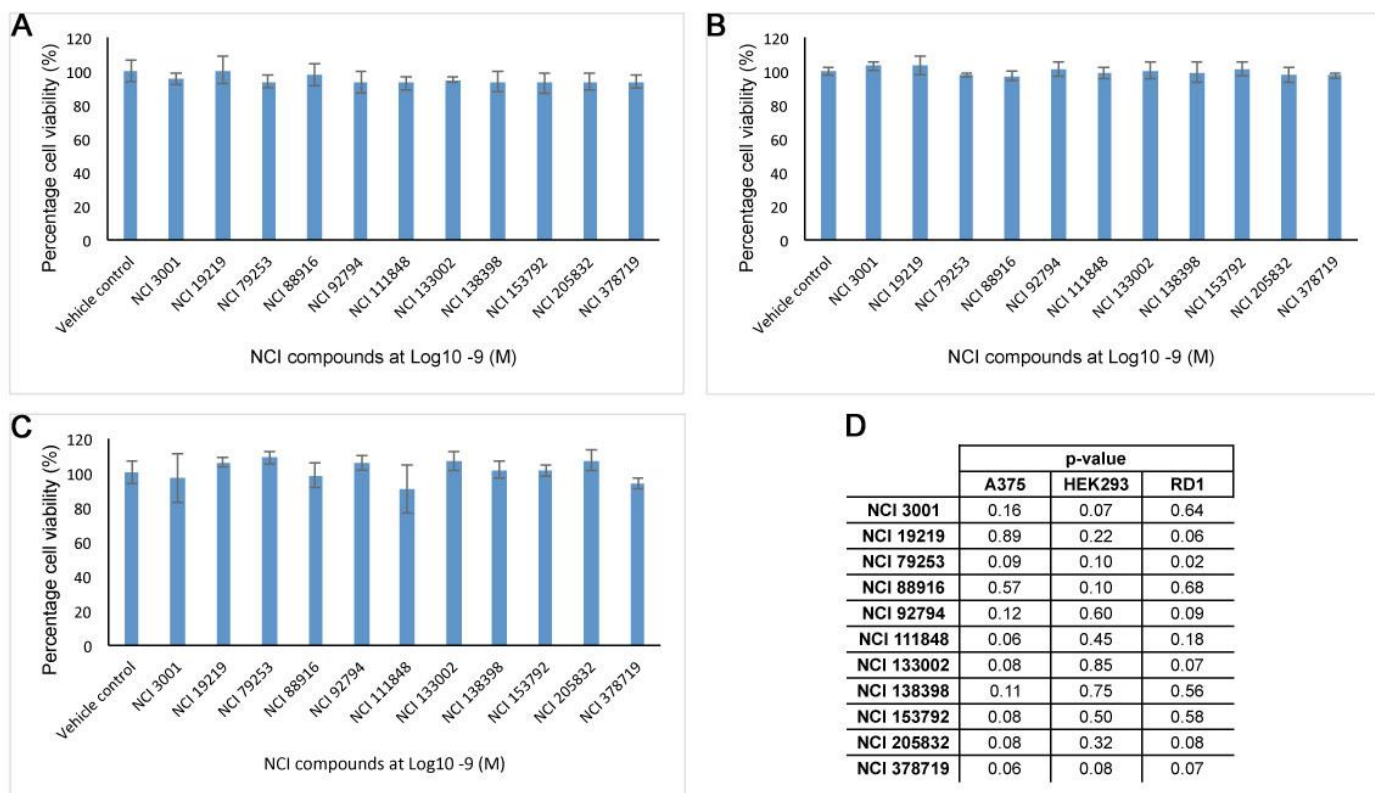
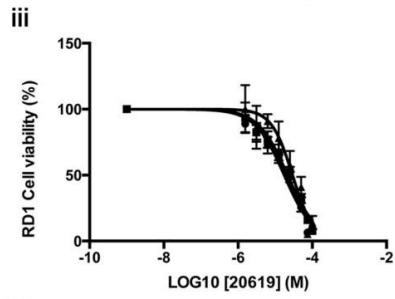
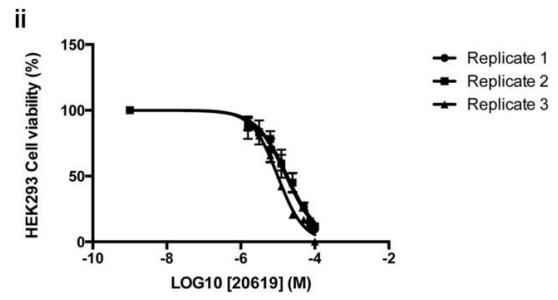
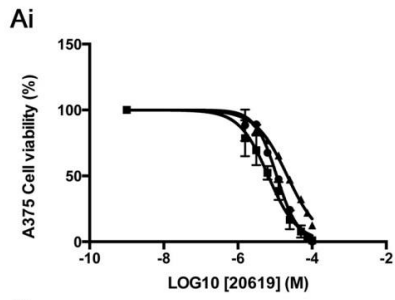


Figure 3.12. Statistical analysis of 11 of the NCI compounds comparing the cell viability for DMSO control and the $1 \times 10^{-9} \text{M}$ for each of the compounds. A shows the cell viability for the NCI compounds and DMSO control in the A375 cell line. B shows the cell viability for the NCI compounds and DMSO control in the HEK293 cell line. C shows the cell viability for the NCI compounds and DMSO control in the RD1 cell line. D shows the p values for the NCI compounds tested. For all cell lines $n=6$. Statistical analysis was a student t-test ($p \leq 0.05$).

The generation of IC_{50} 's with the new data point added was now successful. An example of this can be seen with NCI 43013 (figure 3.13 C). Figures 3.13 i, ii and iii are the resulting dose response graphs for the three replicates for the A375, HEK293 and RD1 cell lines respectively. The corresponding IC_{50} 's are shown in figure iv. From the statistical analysis of a student t-test, the IC_{50} 's for the A375 cell line was statistically significantly lower than both the RD1 and HEK293 cell lines with p values of 0.009 and 0.007 respectively (figure 3.13 Cv). Figure 3.13 A on the other hand shows the compound NCI 20619 as an example of a compound in which the IC_{50} 's were not statistically significantly lower in the A375 cell line compared to the RD1 or HEK293 cells. For some compounds the IC_{50} of the A375 cell line was only statistically significant lower compared to one of the two cell lines. This was the case for NCI 36525 shown in figure 3.13 B. The IC_{50} was statistically lower in the A375 cell line compared to the RD1 (p value 0.007). Whereas the A375 cell line was not statistically lower when compared to the HEK293 cell line (p value 0.192).

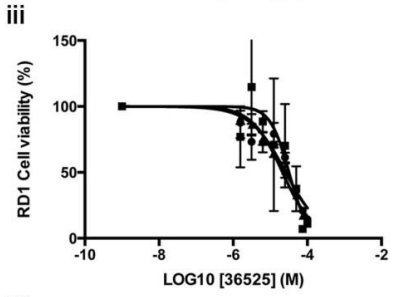
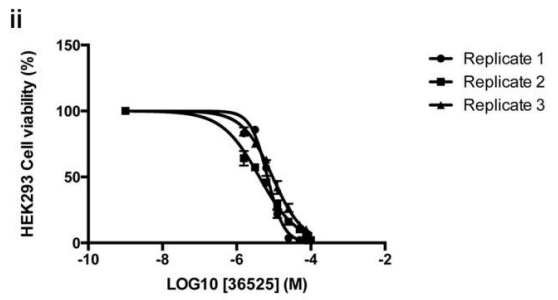
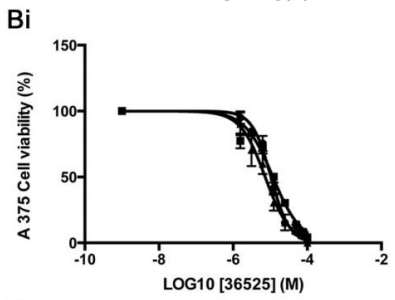


iv

NCI 20619	IC50		
	A375	HEK293	RD1
Replicate 1	1.11E-05	1.68E-05	1.76E-05
Replicate 2	6.57E-06	1.81E-05	2.15E-05
Replicate 3	2.15E-05	2.10E-05	2.94E-05

v

p-value	A375 VS HEK293	A375 VS RD1	HEK293 VS RD1
		0.294	0.158

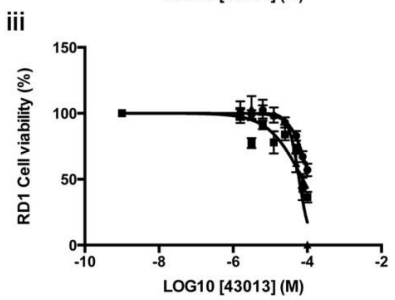
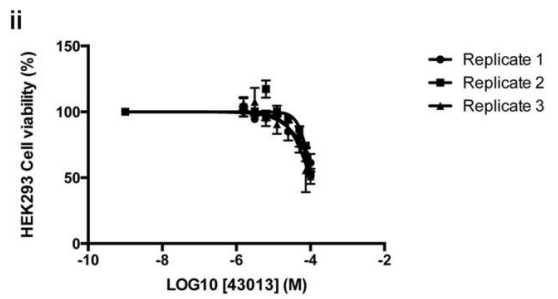
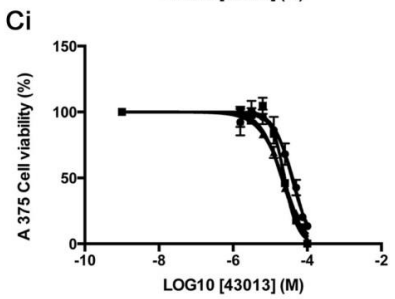


iv

NCI 36525	IC50		
	A375	HEK293	RD1
Replicate 1	1.05E-05	6.77E-06	2.61E-05
Replicate 2	1.18E-05	4.09E-06	3.19E-05
Replicate 3	7.32E-06	9.30E-06	2.15E-05

v

p-value	A375 VS HEK293	A375 VS RD1	HEK293 VS RD1
		0.192	0.007



iv

NCI 43013	IC50		
	A375	HEK293	RD1
Replicate 1	3.84E-05	1.57E-04	1.16E-04
Replicate 2	2.03E-05	1.07E-04	7.56E-05
Replicate 3	2.47E-05	1.00E-04	6.03E-05

v

p-value	A375 VS HEK293	A375 VS RD1	HEK293 VS RD1
		0.007	0.009

Figure 3.13. Data used for the statistical analysis for the comparison of the IC₅₀'s for the A375, RD1 and HEK293 cell lines. A, data for NCI 20619, B, NCI 36525 and C ,43013. For each NCI compound shown here, i represents the cell viability graph for the replicates of the A375 cell line. The cell viability graphs for the replicates of the HEK293 and RD1 cell lines are shown in ii and iii respectively. The generated IC50's for each replicate for each cell line are shown in iv and the subsequent statistical analysis are shown in v. Statistical analysis was a student t-test (p≤0.05).

3.3 Discussion

Overall, the chemical genetic screen of the NCI diversity set II compound library was a success. From the 1363 compounds screened a total of 72 compounds gave rise to a phenotype that was reproducible. This equates to a 5% 'hit' rate. Comparing this to the previous screen of the NCI diversity set I library in which a 2% 'hit' rate was observed (Tomlinson et al. 2005), this present screen has improved the 'hit' rate by 3%. This enhanced efficacy of the screen could be due to a number of reasons. The major difference between the two screenings is that one individual screened the NCI diversity set I library, whereas two individuals screened the NCI diversity set II library. The work involved in carrying out such screens is very labour intensive and time-consuming. With this work-load spread across two individuals, coupled with the fact that all of the compounds were scored twice blind by myself and my colleague Adam Hendry, the possibility of false-negative and/or false-positives from appearing was lowered. However, as with the previous screening of the NCI diversity set I library, all of the compounds were screened at both 20 and 40µM too help eliminate any false negative and/or false positives (Tomlinson et al, 2009).

As previously mentioned, there is a 10% overlap of the compounds in the NCI diversity set I library that were also present in the NCI diversity set II library. One of these compounds was identified, NCI 30712, which produced

a similar phenotype to that previously observed. This confirmed our confidence in these chemical genetic screens and the technique in identifying phenotypes and ultimately using *X.laevis* as a model organism. Chemical genetic screens carried out in other research laboratories have also reiterated the efficacy of the screens performed in our lab. In the Patton lab a recent screen was carried out on small compounds known to cause specific pigmentation phenotypes in zebrafish. This screen identified leflunomide as causing a reduction in the number of melanocytes in the zebrafish (Colanesi et al, 2012). Leflunomide is a compound which was previously identified in a screen in our lab (White et al. 2011) and the fact that this was also identified in a screen with zebrafish also highlights the interchangeability of *X.laevis* and zebrafish for these screens. Leflunomide is further characterised in the subsequent chapters of this thesis.

The most commonly observed phenotypes in this screen were those related to abnormal pigmentation. Collectively, total pigment loss, partial pigment loss, abnormal melanophore migration and abnormal melanophore morphology accounted for 51% of all the reported phenotypes. Due to these phenotypes having an apparent effect on the melanophores in *X.laevis*, it can be hypothesised that these compounds are similar with the pigment cells in the skin of humans called melanocytes. Melanocytes are the pre-cursor cells to melanoma, the most deadly form of skin cancer. Compounds which reduce the number of melanophores or prevent the migration of such cells could potentially be therapeutic targets in the treatment of melanoma. However in cases where a total loss of pigment was observed, this lack of pigment could be either due to the absence of melanin synthesis (whereby the pigment cells are present, but are not visible due to the lack of melanin), or there could genuinely be a lack of pigment cells being produced (possibly due to a lack of differentiation or from cell death). A simple experiment which could answer this question and could be carried out on all the 72 'hit' compounds is by carrying out a mushroom tyrosinase assay. Tyrosinase is an enzyme involved in the synthesis of melanin (Wang and Hebert. 2006). If any of these compounds were inhibitors of tyrosinase, one might see a loss

of melanin, indicating melanin synthesis was being affected. Inhibitors of tyrosinase are very well characterised to date, however if some of the compounds were shown to not inhibit tyrosinase activity, these compounds could be targeting novel pathways or targets which are less characterised.

For the majority of the 72 'hit' compounds screened more than one phenotype was observed for each compound. As just mentioned, 51% of the phenotypes were pigmentation related however 20% and 22% of the observed phenotypes were abnormal eye development and abnormal general morphology respectively. It is debatable if the latter two phenotypes are purely down to general toxicity of the compound (but still tolerable doses), in particular the abnormal general morphology phenotype. For example, as the compounds are arrayed onto early staged embryos and left to develop to stage 38, if a compound was toxic to the embryo, we would expect to see malformed development of the embryos (such as stunted growth and inverted kinks in the embryo). Nonetheless, the compounds which gave rise to the pigmentation phenotypes may ultimately be of interest in regards to therapeutically treating melanoma.

The incorporation of the cell-based cell viability screen for the 72 'hit' compounds also proved successful and supports the data from the chemical screen. The identification of a compound with a potential novel therapeutic target from cell-based screens is an established approach for investigating this further. For example the NCI60 is an in vitro cell line screening project in which researchers can have a compound (s) of interest tested on a bank of 60 human cancer cell lines with their cell viability being determined at an initial dose of 10 μ M and. If the test compounds significantly reduce the cell viability at this single dose, the compound is then subject to the same assay but at 5 different concentrations (Shoemaker. 2006). Utilising this principle, we screened the 72 'hit' compounds against the A375 melanoma cell line over range of concentrations to determine cell viability. Two non-melanoma cell lines were also screened (RD1 and HEK293) and as a result 13

compounds were identified as exhibiting statistically lower IC₅₀'s in the A375 cell line compared to both the RD1 and HEK293 cell lines. Of these 13 compounds 7 gave rise to total or partial pigment loss phenotypes, 5 produced abnormal melanophore migration and 1 produced abnormal melanophore morphology. Remarkably, all of the phenotypes are considered as pigmentation phenotypes. Therefore this cell-based screening appears to have identified compounds which have activity against biological processes that are related to melanogenesis.

Further experiments exploring the function of these 13 compounds in melanoma cells are planned. The 13 compounds will each be subject to proliferation, cell cycle and apoptosis assays. This will determine why there is a decrease in cell viability in the A375 melanoma cell line tested. Additional cell viability assays on other melanoma cell lines will also be carried out to identify if the potential therapeutic value in the treatment of melanoma stands true for these compounds. From the collective results from all of these assays, it is hoped that some of the 13 compounds will be disregarded, narrowing the number of compounds further to just a select few. If this proves to be successful, then these select few compounds will be tested for their therapeutic value *in vivo* in a mouse xenograft study.

Overall the chemical genetic screen of the NCI diversity set II library was a success, with the 1363 compounds being reduced to just 72 'hit' compounds with reproducible phenotypes in the *X.laevis* embryos. Seventy two compounds were then further reduced to just 13 following the cell-based viability screen. The IC₅₀'s for the 13 compounds were all statistically significantly lower in the A375 cell line compared to the RD1 and HEK293 cell lines, suggesting these compounds have potential therapeutic value in treating melanoma. However the biological activity and thus the targets of these compounds is currently unknown, which is one of the major disadvantages of these forward chemical genetic screens. A collaboration with Dr Andreas Bender has shown that using *in silico* chemoinformatical

algorithms to predict the targets for these compound using the compound chemical structure and phenotype given in the *X.aevis* embryos is a possible means to circumvent this issue, with promising preliminary data (Liggi et al, 2013 and Drakakis et al, 2014).

Chapter 4

Characterising the function of leflunomide as an effective melanoma drug

4.1 Introduction

Leflunomide is an inhibitor of the enzyme dihydroorotate DHODH. DHODH is the rate limiting enzyme in the *de novo* pyrimidine synthesis pathway. The *de novo* pyrimidine synthesis pathway consists of six enzymatic reactions which generates ribonucleotide uridine monophosphate (rUMP). DHODH is located in the inner mitochondrial membrane of the mitochondria and catalyses the conversion of dihydroorotate to orotate, the fourth step of this pathway (figure 4.1). Inhibition of DHODH prevents the synthesis of pyrimidines which has a knock on effect on the synthesis of pyrimidine derivatives, such as the nucleotide bases cytosine (C) and thymine (T). This ultimately decreases the pool of nucleotides available to make new DNA (as well as RNA). Treatment with leflunomide inhibits DHODH, which causes a reduction in the levels of rUMP in cells. One of the G1 checkpoints in the cell cycle is to detect the levels of rUMP. Upon this detection of low levels of rUMP, the nuclear transcription factor p53 is activated. This activation of p53 causes the levels of p21 to increase. p21 is an effector of the G1 checkpoint in the cell cycle by inhibiting the activity of the complex cyclin E/cdk2. Inhibiting the activity of this complex results in the dephosphorylation of the Rb and consequently maintains the sequestration of the transcription factor E2F. Thus this causes the cells to arrest in G1 and inhibits cellular proliferation (Fox et al, 1998).

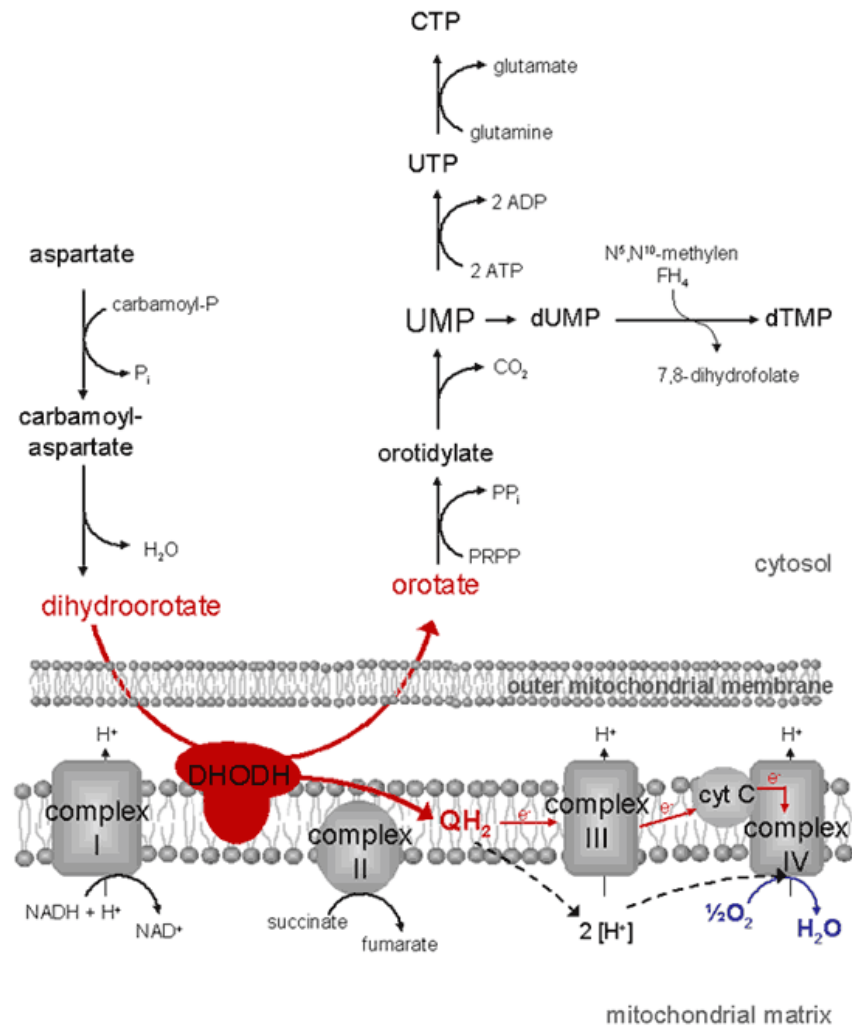


Figure 4.1. A schematic diagram of the *de novo* pyrimidine synthesis pathway of rUMP. The first step in this pathway is the synthesis of carbamoyl phosphate catalysed by carbamoyl phosphate synthetase II. Second is the formation of carbamoyl aspartate via the condensation of carbomyl phosphate with aspartate, catalysed by aspartate transcarbamylase. The third step involves the formation of the pyrimidine ring, forming dihydroorotate catalysed by dihydroorotase. The fourth step oxidises dihydroorotate to orotate catalysed by DHODH (shown in red). The next step involves orotate reacting with 5-phospho-alpha-d-ribose-1-phosphate (PRPP) to form orotidine-5-monophosphate (OMP or orotidylate) catalysed by orotate phosphoribosyl transferase. The final step is the removal of a carboxyl group from OMP to form uridine monophosphate (UMP) catalysed by decarboxylase. Note that DHODH is the only enzyme in this pathway located in the mitochondria; the remainder are all cytosolic enzymes (Metabolic database, 2015; Fox et al, 1999).

From a chemical genetic screen carried out on *X.laevis* embryos the drug leflunomide (a FDA approved drug used for treatment of rheumatoid arthritis), was shown to have potential therapeutic value in treating melanoma. This study showed that leflunomide reduced cell viability in three melanoma cell lines harbouring the BRAF^{V600E} mutation (White et al, 2011). It is not known if leflunomide affects melanoma cells that do not harbour the BRAF^{V600E} mutation. It is also not known in detail how leflunomide mechanistically exerts its effects in melanoma.

In this chapter a panel of eight human melanoma cell lines were obtained to further characterise the potential effects of leflunomide as a melanoma drug. Half of these melanoma cell lines harboured the BRAF^{V600E} mutation and half were wildtype for BRAF. Cell viability assays were initially carried out on all eight of the melanoma cells lines. Leflunomide caused a dose dependent decrease in the number of viable cells. To determine how leflunomide caused this effect additional assays were only carried out on the A375 melanoma cell line testing the following concentrations of leflunomide; 25, 50 and 100µM. Additional assays that were carried out included cell proliferation, cell cycle analysis and cell death assays.

4.2 Results

4.2.1 Cell viability assays

Initially cell viability assays were carried out using CellTiter 96[®] Aqueous one solution reagent (MTS). However when performed with CellTiter-Glo one solution reagent, an enhanced reduction in cell viability was observed. At 100 μ M leflunomide the average cell viability in A375 melanoma cells was 48.43% when determined by MTS reagent. In comparison when determined with Celltiter-Glo, the average cell viability was reduced to 28% (figure 4.2.). With this noticeable enhanced reduction in cell viability given with the CellTiter-Glo, all subsequent cell viability assays were carried out using this reagent.

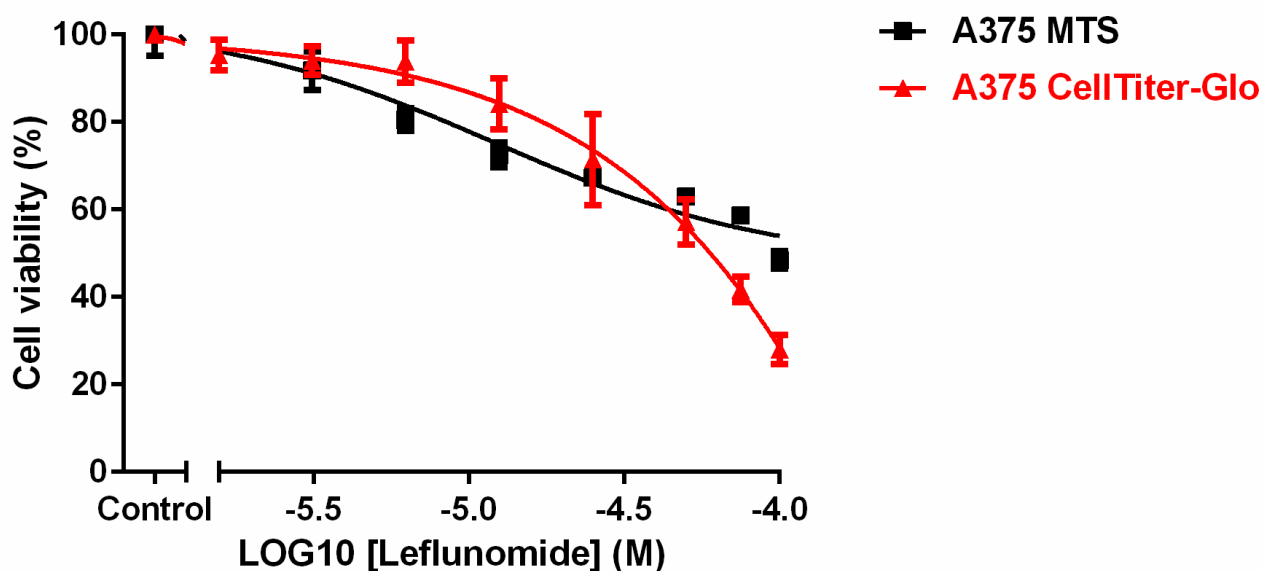


Figure 4.2. Cell viability data for the A375 melanoma cell line in response to a range of leflunomide concentrations analysed by two different reagents. Cell viability was measured by either MTS reagent (data shown in black) or with CellTiter-Glo reagent (data shown in red). Data is presented as the mean \pm SEM of three independent experiments each performed with cell culture triplicates.

Cell viability assays were carried out on a bank of eight human melanoma cell lines (table 4.1), testing the effect of leflunomide. A375, M229, SKmel28 and SKmel5 are melanoma cell lines harbouring the BRAF^{V600E} mutation. Whereas M202, M285, M375 and M296 are melanoma cell lines wild-type for BRAF.

Table 4.1 The eight human melanoma cell lines used and their status for the BRAF^{V600E} mutation. Their statuses for other common mutations seen in melanoma are also listed.

Melanoma cell line	BRAF status	N-RAS status	PTEN status	PI3K status	MITF amplification	CDKN2A status
M202	wt	Q61L	Intact	wt	No	Homo deletion
M285	wt	wt	Intact	wt	No	No
M375	wt	wt	Intact	wt	No	No
M296	wt	Q61L	Intact	wt	No	No
A375	Homo V600E	wt	Intact	wt	No	n/a
M229	Homo V600E	wt	Het Deletion	wt	Yes	No
SKmel28	Homo V600E	wt	Het Deletion	wt	Yes	Het Deletion
SKmel5	Het V600E	wt	Intact	wt	No	n/a

These results (figure 4.3) revealed that leflunomide reduced the cell viability in all eight melanoma cell lines in a dose dependent manner, but to varying degrees. For example, the M202 cell line (shown in blue) was the most sensitive with cell viability being reduced to 25.22% at 100µM leflunomide. In comparison the SKmel28 cell line (shown in khaki) was the least sensitive, with cell viability being reduced to just 62.20% at 100µM leflunomide.

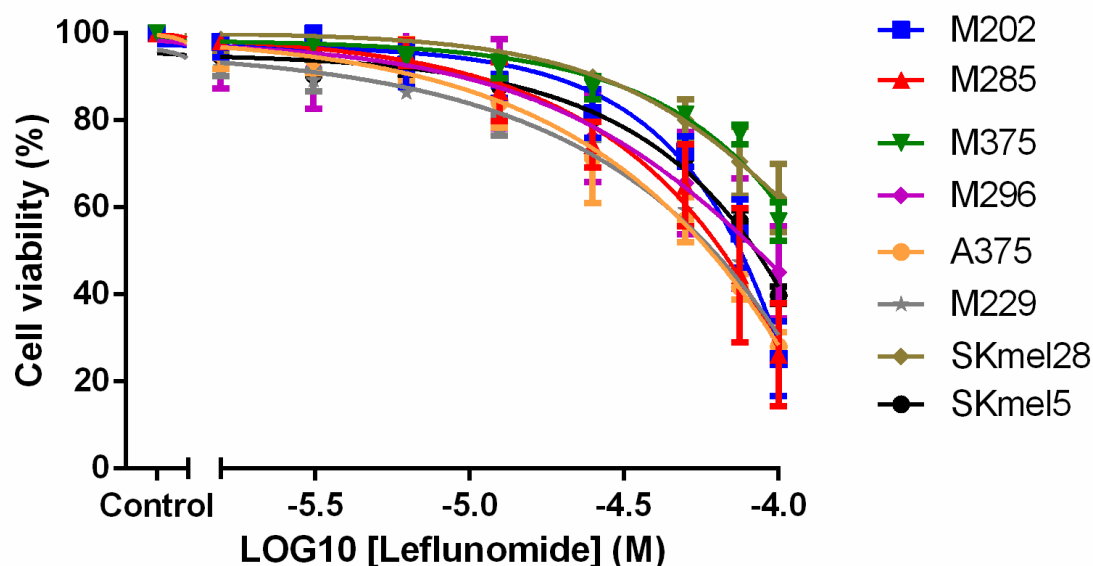


Figure 4.3. Leflunomide causes a dose-dependent decrease in cell viability in eight human melanoma cell lines. Wildtype cell lines; M202 (blue), M285 (red), M375 (green) and M296 (purple). BRAF^{V600E} mutant cell lines; A375 (orange), M229 (grey), SKmel28 (khaki) and SKmel5 (black). Cell viability was determined by using CellTiter-Glo reagent and all values are represented as a percentage (%) relative to the vehicle control. Data is presented as the mean \pm SEM of three independent experiments each performed with cell culture triplicates.

IC₅₀'s can be defined as the concentration of a drug or compound that inhibits cellular response by 50% (Neubig et al, 2003). IC₅₀'s for all eight melanoma cell lines were calculated in response to leflunomide (table 4.2). The IC₅₀'s produced ranged from 57.46 μ M to 166.88 μ M, again highlighting that leflunomide caused a varied response amongst the eight melanoma cell lines tested.

Table 4.2. IC₅₀ values for the eight melanoma cell lines, HEK293, RD1 cells and melanocytes in response to leflunomide

Cell line	IC ₅₀ (μM)
M202	68.13
M285	61.51
M375	64.12
M296	111.75
A375	57.46
M229	58.20
SKmel28	166.88
SKmel5	122.53
Melanocytes	147.73
HEK293	48.12
RD1	84.21

It is also evident that leflunomide primarily caused an effect on cell viability at the higher doses the cells were exposed to on all eight melanoma cell lines tested. In the A375 cells (shown in orange) lower concentrations of leflunomide from 0-25μM resulted in a decrease in cell viability from 100 to 84.15%. However at the higher concentrations of leflunomide, 25-100μM, a dramatic decrease in cell viability from 84.15 to 28% was seen. The M285 cell line responded similarly to leflunomide (shown in red). At 0-25μM leflunomide there was a decrease in cell viability from 100% to 86.60%. Whereas at 25-100μM leflunomide, the viability of M285 cells decreased from 86.60% to 26.22%.

The cell viability data for all four of the wildtype cell lines were grouped together and averaged. The same was done for the four cell lines harbouring the BRAF^{V600E} mutation. These two data sets were then plotted on a graph (figure 4.4). These results showed that leflunomide affected the viability of the wildtype BRAF cell lines to a similar level as it did the cell lines mutant for BRAF. For example at 100µM leflunomide, the average cell viability for wildtype BRAF cells was 36.46%, compared with 36.68% for mutant BRAF cells.

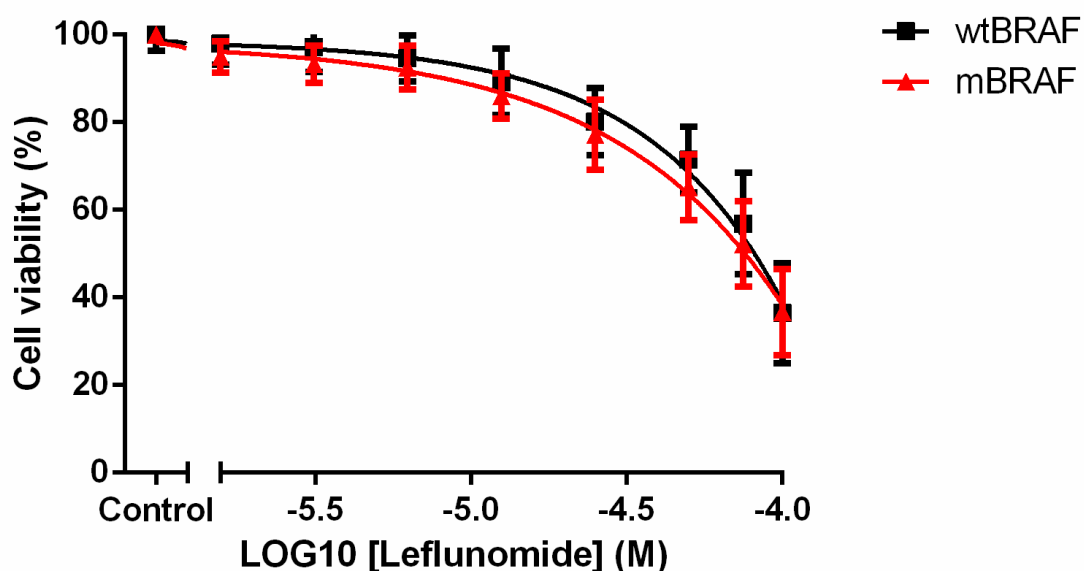


Figure 4.4. Leflunomide reduces cell viability at a similar rate in wildtype BRAF melanoma cells and BRAF^{V600E} mutant cell lines. The data from the four wildtype cell line was averaged and is shown above in black. The same was done for the four BRAF^{V600E} mutant cells and is shown above in red. Cell viability was determined by using CellTiter-Glo reagent and all values are represented as a percentage (%) relative to the vehicle control. Data is presented as the mean \pm SEM of twelve independent experiments each performed with cell culture triplicates.

Alongside the bank of melanoma cell lines, two non-melanoma cell lines and primary melanocytes were treated with leflunomide and their cell viability determined. The two non-melanoma cell lines used were HEK293 (human epithelial kidney) and RD1 (rhabdomyosarcoma) cells. It can be clearly seen

that leflunomide also decreased cell viability in a dose-dependent manner in both the HEK293 and RD1 cells as well as the melanocytes (figure 4.5). The HEK293 cells were more sensitive to leflunomide than the melanoma cell line most sensitive to leflunomide, the M202 cells. The cell viability at 100 μ M leflunomide was reduced to 16.025% in the HEK293 cells compared with 25.22% of the M202 cell line. The IC₅₀'s of these three cell lines were also calculated and can be seen in table 4.2. However what was striking was that the IC₅₀'s for all of the cell lines tested were within 3-fold of each other.

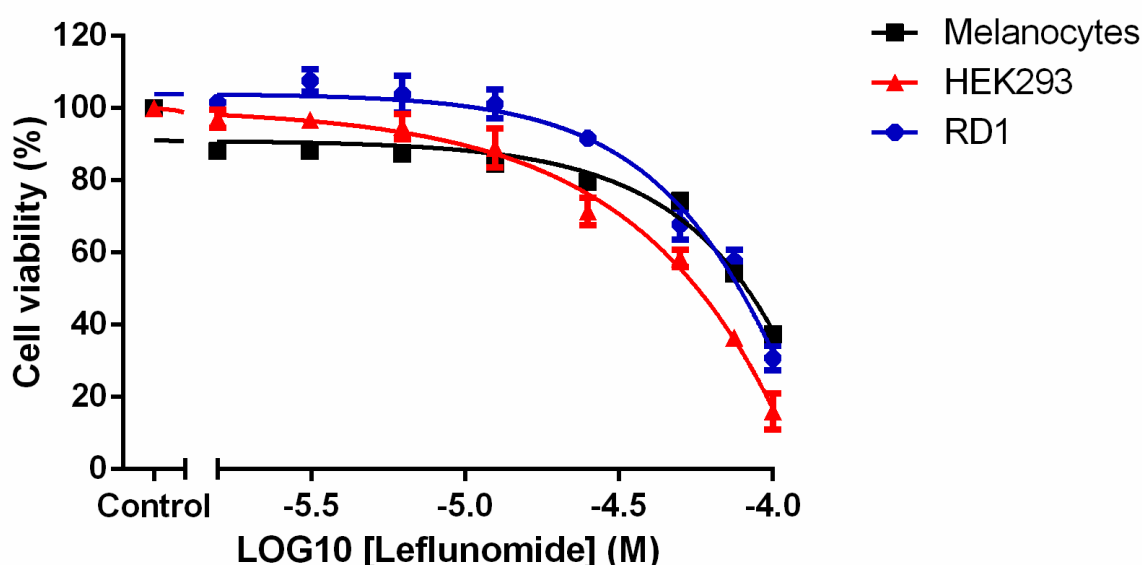


Figure 4.5. Leflunomide causes a dose-dependent decrease in cell viability in melanocytes, HEK293 and RD1 cells. Melanocytes are shown above in black, HEK293 cells in red and RD1 cells in blue. Cell viability was determined by using CellTiter-Glo reagent and all values are represented as a percentage (%) relative to the vehicle control. Data is presented as the mean \pm SEM of three independent experiments each performed with cell culture triplicates.

4.2.2 Visualisation of leflunomide treated A375 cells

In a 12-well plate where A375 cells were treated for 72 hours with DMSO, 25, 50 and 100 μ M leflunomide, cells were examined under a Zeiss Axiovert inverted microscope. Figure 4.6A-D show images taken at 10x magnification and figure 4.6E-I show images taken at 40x magnification. As shown

previously in figure 4.2, the viability of A375 cells (shown in orange) decreased in a dose-dependent manner upon treatment with leflunomide. Figure 4.6A-D clearly shows the number of cells decreased with increasing concentrations of leflunomide visually in the microscopic field of view. As an estimate, the cells treated with DMSO after 72 hours appeared to be 80-90% confluent (figure 4.6A). Upon treatment with 25, 50 and 100 μ M leflunomide the cells were 80%, 50-60% and 20-30% confluent respectively (figures 4.6B-D).

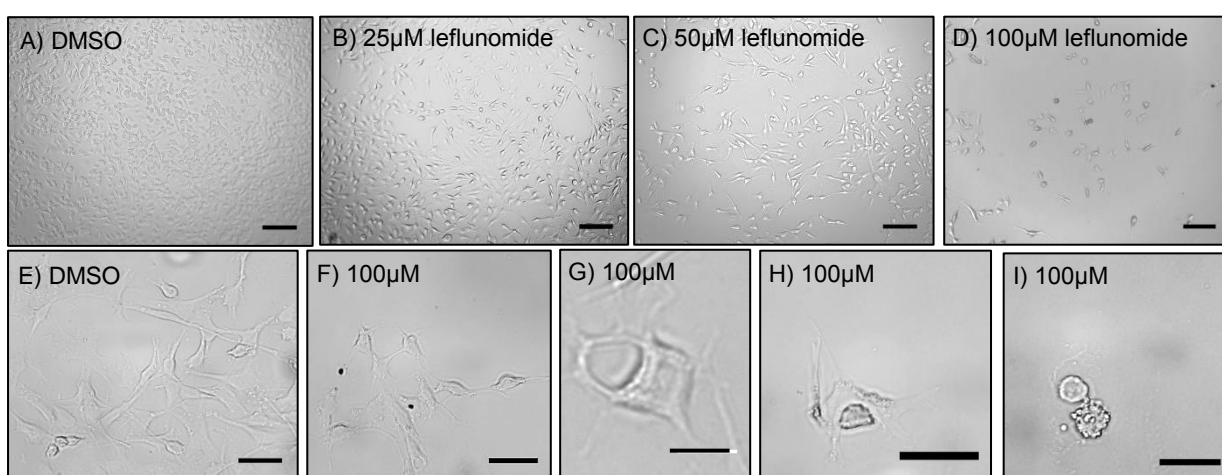


Figure 4.6. Phenotypic images of A375 cells treated with leflunomide for 72 hours. Images A-D were taken at 10x magnification whilst images E-I were taken at 40x magnification. All images were taken under a Zeiss Axiovert inverted microscope.

Whilst observing the cells under the microscope it became apparent that a few cellular phenotypes were present only in the 100 μ M leflunomide treated cells. Under DMSO conditions (figure 4.6E), the A375 cells acquired an elongated morphology with a couple of protrusions. At 100 μ M leflunomide the appearance of tiny black dots (figure 4.6F) and vacuoles (figure 4.6G) within the cells became noticeable. Figure 4.6H depicts a healthier cell eating an unhealthy cell by phagocytosis. Finally, condensed, rounded cells with blebbing were frequently observed as shown in figure 4.6I.

4.2.3 BrdU proliferation assay

To determine why there was a reduction in cell viability upon treatment with leflunomide, cell proliferation assays were initially carried out. Staining A375 cells with BrdU and counterstaining with DAPI determined cell proliferation. A375 cells were treated with DMSO, 25, 50 and 100 μ M leflunomide for 72 hours and the staining protocol for BrdU was carried out. Figure 4.7 shows the results from the cell proliferation assay, which shows the number of BrdU positive cells in each of the treatment conditions. Figure 4.7 reveal a clear dose-dependent decrease in the number of proliferating cells with increasing concentrations of leflunomide. The results from three independent experiments were averaged and the number of proliferating cells in the DMSO control was set at 100%. Upon treatment with 25 μ M leflunomide, the percentage of proliferating cells declined by almost half to 54.50%, equally whilst 50 μ M leflunomide also reduced the number of proliferating cells by half to 24.34%. Finally upon treatment with 100 μ M leflunomide this number reduced to just 5.41%. Therefore leflunomide caused a dose-dependent decrease in the number of proliferating A375 cells.

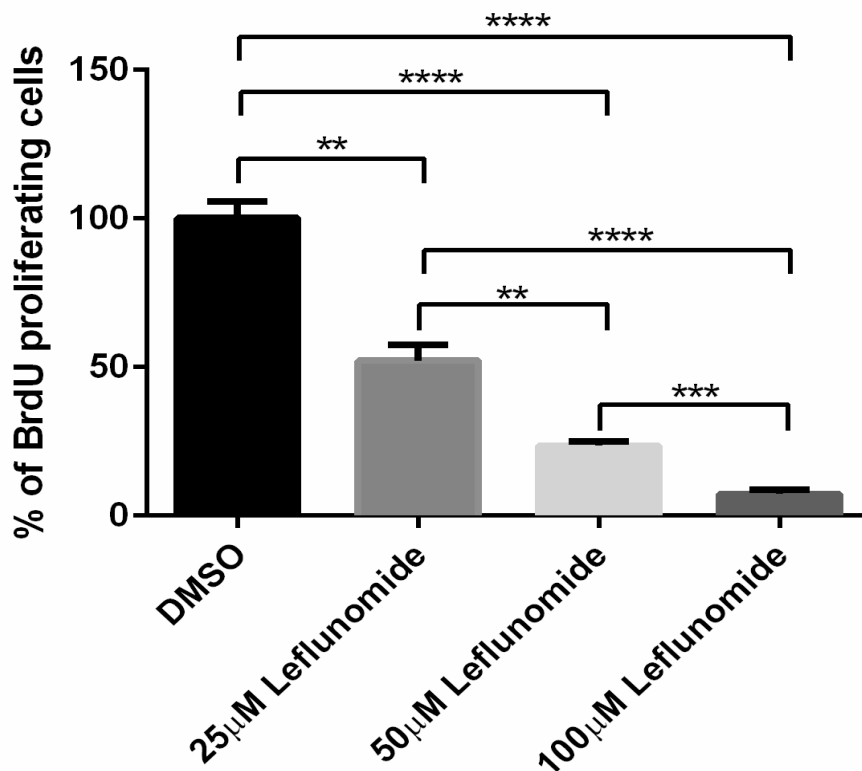


Figure 4.7. Percentage of BrdU positive A375 cells after 72 hours treatment with leflunomide. Data is presented as the mean \pm SEM of the three independent experiments each performed with cell culture triplicates. Asterisks indicate the degree of statistical difference determined by one-way ANOVA with Turkey's post-hoc test. * $P \leq 0.05$, ** $P \leq 0.01$, *** $P \leq 0.001$ and **** $P \leq 0.0001$.

4.2.4 Cell cycle analysis

To determine if leflunomide was affecting a particular stage of the cell cycle, cell cycle analysis was performed using propidium iodide to stain for cellular DNA content. PI binds to cellular DNA and the amount of fluorescence detected is proportional to the amount of DNA present. A375 cells were stained with PI following a 72-hour treatment with DMSO control, 25, 50 or 100 μ m leflunomide. To begin with, forward scatter (FSC) vs side-scatter (SSC) plots were made to gate only for singlet cells that were subject for further analysis.

Figure 4.8 shows representative DNA histogram plots from one of three experiments conducted. PI fluorescence has a peak emission of 617nm and was detected in the FL2 channel, representing the amount of DNA. The intensity of PI fluorescence is shown along the x-axis, whereas the y-axis is the cell count.

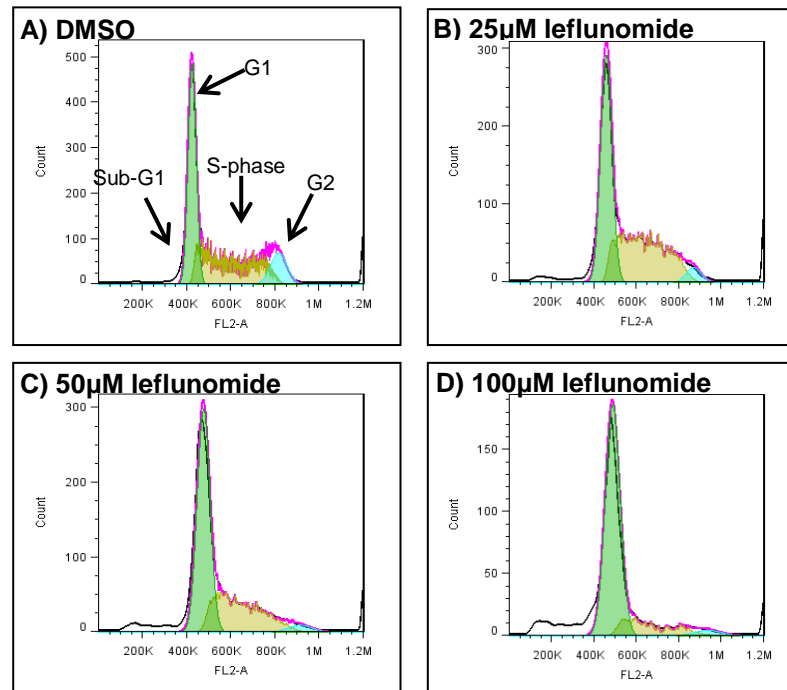


Figure 4.8. Representative DNA histogram plots of the cell cycle analysis performed on A375 cells treated for 72 hours with leflunomide. A shows DMSO treated cells and the arrows on the plot indicate the different phases of the cell cycle. B, C and D show cells treated with 25, 50 and 100 μM leflunomide respectively.

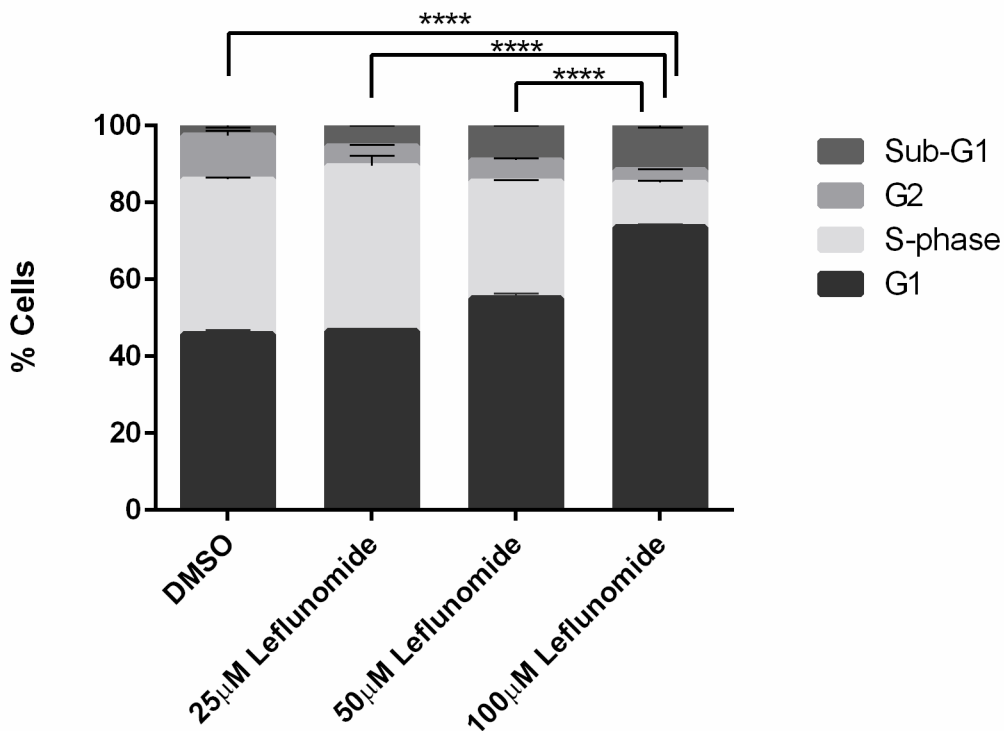


Figure 4.9. Cell cycle phase distribution for A375 cells treated for 72 hours with leflunomide. Data is presented as the mean \pm SEM of three independent experiments each performed with cell culture triplicates. Asterisks indicate the degree of statistical difference comparing each % of G1 population of cells for each condition to 100 μ M leflunomide determined by two-way ANOVA with Turkey's post-hoc test. * $P \leq 0.05$, ** $P \leq 0.01$, *** $P \leq 0.001$ and **** $P \leq 0.0001$.

The first peak on the plots in green represents the G1 phase of the cell cycle. Next, the second plateau in yellow shows cells that are cycling through the S phase. The next smaller peak in blue represents cells going through the G2 phase of the cell cycle. Additionally, there is a small white plateau prior to the G1 peak called the sub-G1 phase. This population of cells signifies cells undergoing apoptosis or cell death. Figure 4.8 clearly shows the DNA histogram plots in which each of the four cell cycle stages is populated by cells. However from these histograms you do not know the percentage of cells in each of the phases. To quantitatively calculate this, FlowJo software was used to analyse each data set. Each data set was plotted with an algorithm to fit a Gaussian curve producing the quantitative results. Figure

4.9 and table 4.3 reveal the averaged results for all three independent experiments.

Table 4.3. Quantification of the percentage of cells in each phase of the cell cycle

	DMSO	25µM Lef	50µM Lef	100µM Lef
G1	45.71	46.56	55.05	73.56
S-Phase	40.26	42.93	30.41	11.60
G2	11.43	5.17	5.49	3.20
Sub-G1	2.60	5.36	9.12	11.84

The first phase of the cell cycle, G1, shown in dark grey in figure 4.9 increased in a dose-dependent manner. From the DMSO control 45.71% of cells are actively cycling through G1, which increased to 46.56%, 55.05% and 73.56% upon treatment with 25, 50 and 100µM leflunomide respectively. In contrast the number of cells in S-phase (pale grey) decreased from 40.26% in DMSO control cells to (42.93% in 25µM leflunomide treated cells), 30.41% in 50µM leflunomide treated cells and 11.60% at 100 µM leflunomide. From these two results alone it is evident that with increasing concentrations of leflunomide, the cells are becoming arrested in the G1 phase of the cell cycle and as a consequence the number of cells in S phase decrease. The percentage of cells in G2 at 25µM was reduced by 50% compared to the DMSO control. However the percentage of cells in G2 for 50 and 100µM leflunomide does not alter drastically compared to the 25µM leflunomide. The percentage of cells in G2 in DMSO control cells was 11.43% changing to 5.17%, 5.49% and 3.20% upon treatment with increasing concentrations of leflunomide.

Interestingly the percentage of cells populated in sub-G1 gradually increased in a dose-dependent manner. In DMSO treated cells 2.60% cells were in sub-G1. This increased to 5.36%, 9.12% and 11.84% upon treatment with 25, 50 and 100 μ M leflunomide respectively, indicating that there was an increase in the number of dead cells undergoing apoptosis.

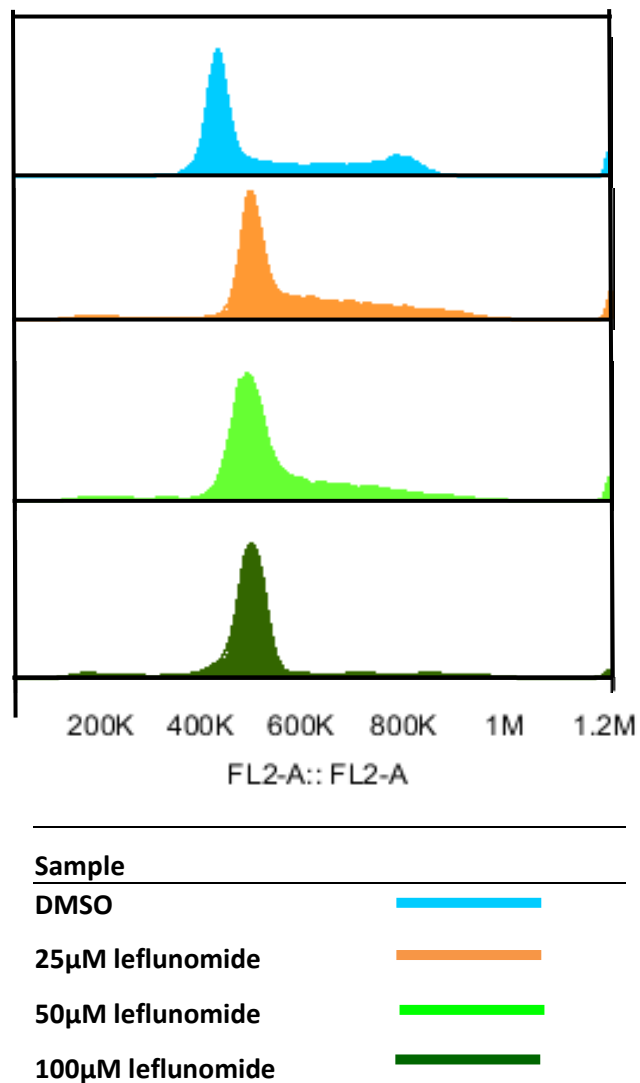


Figure 4.10. Representative data showing the distribution of cells in each phase of the cell cycle.

An additional way of showing the cell cycle analysis data (compared to that in figure 4.7) is shown above in figure 4.10. This figure shows a simple representation of the PI fluorescence detected in the FL-2 channel (x-axis). From this figure you can see that first peak (G1 phase), gradually increases in size with increasing concentrations of leflunomide. Also with increasing concentrations you can see that the second peak/plateau (S-phase) noticeably decreases. Again, this highlights that the A375 cells are arresting in G1-phase, which subsequently causes a decrease of cells in S-phase.

4.2.5 Annexin V assay

A375 cells were stained using the Annexin V FITC Apoptosis detection kit post treatment with DMSO, 25, 50 or 100 μ M leflunomide for 72 hours. To begin with, forward scatter (FSC) vs side-scatter (SSC) plots were made to gate the desired population of cells for subsequent analysis. Annexin V FITC fluorescence has a peak emission of 525nm and was detected in the FL1 channel (the x-axis on plots shown in figure 4.11). PI fluorescence has a peak emission of 617nm and is detected in the FL3 channel (the y-axis on the plots shown in figure 4.11).

Figure 4.11 shows the representative pseudo colour plot from one of the three experiments conducted. Each plot is split into four quadrants, which denotes different stages of apoptosis. The first quadrant depicted as Q4 in figure 4.11 indicates the population of cells that are viable and healthy and are negative for both annexin V and PI staining (Annexin⁻/PI⁻). The second quadrant shown in figure 4.11 as Q3 depicts cells stained positive for only annexin V (Annexin⁺/PI⁻), therefore indicative of early apoptosis. The next quadrant shown as Q2 represents cells stained positive for annexin V and PI (Annexin⁺/PI⁺), which is evidence of cells undergoing late apoptosis/necrosis. Finally the fourth quadrant, Q1, show cells that have stained positive for only PI (Annexin⁻/PI⁺) which signifies cells that are directly necrotic. If cells shift through quadrant Q4 to Q3 ending in Q2, this

suggests that cells are undergoing cell death via the conventional apoptotic route.

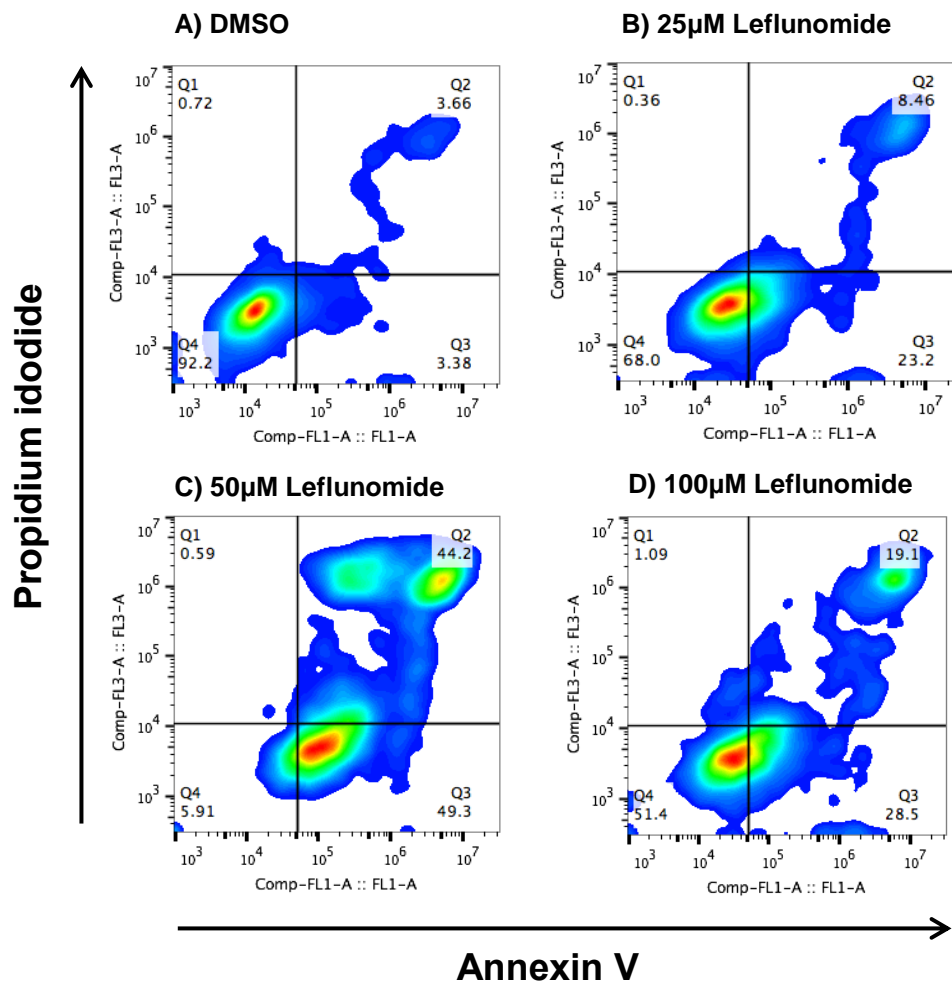


Figure 4.11. Representative pseudo plots of cell death analysis determined by flow cytometry. A375 cells were treated with DMSO, 25, 50 and 100µM leflunomide for 72 hours and stained with annexin v and PI. The numbers indicate the percentage of cells present in each quadrant.

In DMSO control samples (figure 4.11 A) the majority of the cells were viable (92.2%). When cells were treated for 72 hours with 25µM leflunomide, the number of viable cells decreased to 68% and there was an increase in the number of early apoptotic cells from 3.38% to 23.2%. A slight increase was also seen in the late apoptotic/necrotic quadrant from 3.66% to 8.46% (figure 4.11 B). The most noticeable effect of apoptosis was observed when cells were treated for 72 hours with 50µM leflunomide (figure 4.11 C). Compared

to 25 μ M leflunomide, the number of viable cells dramatically decreased from 68% (figure 4.11 B) to 5.91%. There was also an increase in the number of cells in the early apoptotic quadrant from 23.2% up to 49.3%. More strikingly there was an increase from 8.46% to 44.2% in the late apoptotic/necrotic quadrant. However at 100 μ M leflunomide unpredicted results were observed. Following on from what was seen at 50 μ M leflunomide, the number of viable cells increased from 5.91% back up to 51.4% (figure 4.11 D). Interestingly the number of early apoptotic cells decreased from 49.3% to 28.5%. Similarly, there was a decrease in late apoptotic/necrotic cells from 44.2% to 19.1%. Nevertheless, under all conditions the number of cells in the Q1 quadrant (directly necrotic) was relatively constant. DMSO, 25 μ M, 50 μ M and 100 μ M leflunomide treated cells gave rise to 0.72%, 0.36%, 0.59% and 1.09% respectively in this quadrant.

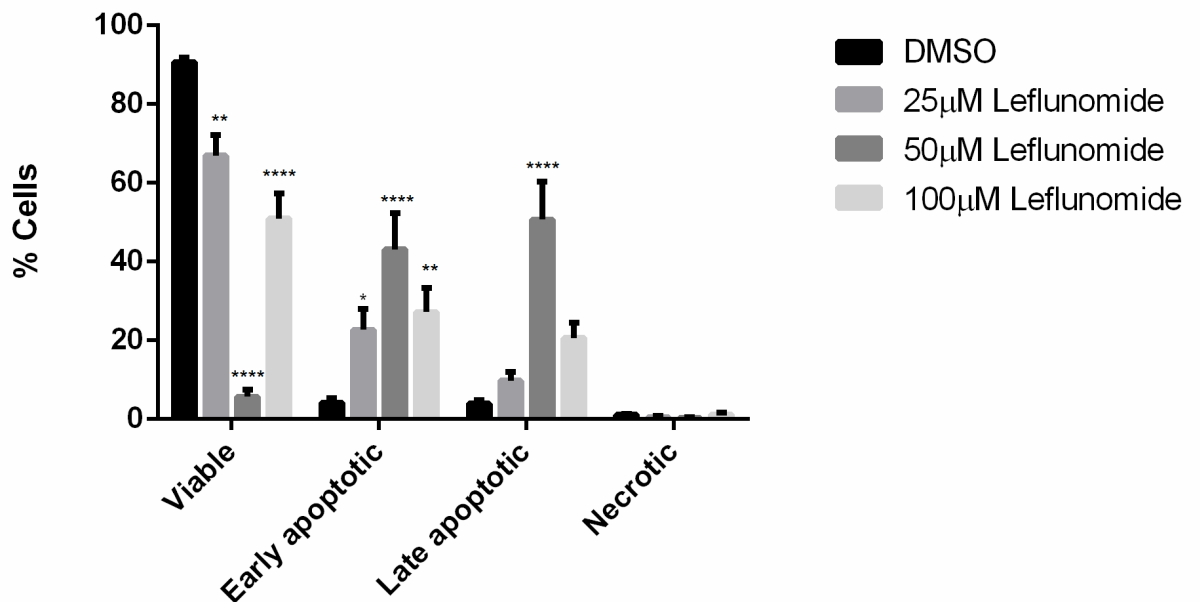


Figure 4.12. Graph quantifying the percentage of A375 cells that are viable, early apoptotic, late apoptotic and necrotic after 72 hours of treatment with leflunomide. Data is presented as the mean \pm SEM of three independent experiments each performed with cell culture triplicate. Asterisks indicate the degree of statistical difference comparing each leflunomide condition to the DMSO control determined by two-way ANOVA with Turkey's post-hoc test. * $P \leq 0.05$, ** $P \leq 0.01$, *** $P \leq 0.001$ and **** $P \leq 0.0001$.

Figure 4.12 shows the results from all three experiments performed exhibiting the same trends as just described in figure 4.11. Taking into account the first three bars corresponding to DMSO, 25 and 50 leflunomide in this order, you can see that there is a significant dose-dependent decrease in the number of viable cells. 100 μ M leflunomide noticeably does not follow this trend and significantly increased. Similarly with the early apoptotic cells there is a dose-dependent increase in the number of cells undergoing early apoptosis. However 100 μ M leflunomide treated cells caused a significant decrease in the number of early apoptotic cells. This same trend can be seen for the number of cells undergoing late apoptosis/necrosis just more prominently. However, for all four conditions the number of cells that were directly necrotic was constantly low throughout.

These results indicate a dose-dependent effect on apoptosis upon treatment of 25 and 50 μ M leflunomide. Strikingly, at 100 μ M there appeared to be a decrease in the number of apoptotic cells and a shift back to an increase in the number of viable cells. This contradicts what was seen from the cell viability data in figure 4.3. Figure 4.3 showed that the cell viability decreased in a dose-dependent manner, with 100 μ M leflunomide causing the maximum effect. Here (figure 4.11 and 4.12), 100 μ M leflunomide appeared to have an opposing effect whereby it increased the number of viable cells. Similarly, the data in figure 4.9 and table 4.3 showed that the sub-G1 population of cells increased in a dose-dependent manner, with 100 μ M leflunomide having the maximum effect. Again, this data in figure 4.11 and 4.12 disputes this due to 100 μ M leflunomide showing there is more viable cells.

When running each sample on the flow cytometer, the total number of events recorded was set to 5000. Each event refers to one unit of data, equivalent to one cell. The time taken for each sample to run until this limit was reached was recorded. The time it took for each sample to run to this limit can be indicative of whether the sample had many or few cells present. For example if a sample had many cells, the time it took to run through the fluid stream to

the laser beam to reach the events limit would be relatively fast. In contrast, a sample that had fewer cells, it would have taken a longer time for the data to be acquired and thus a higher volume of the sample would be used to reach the events limit.

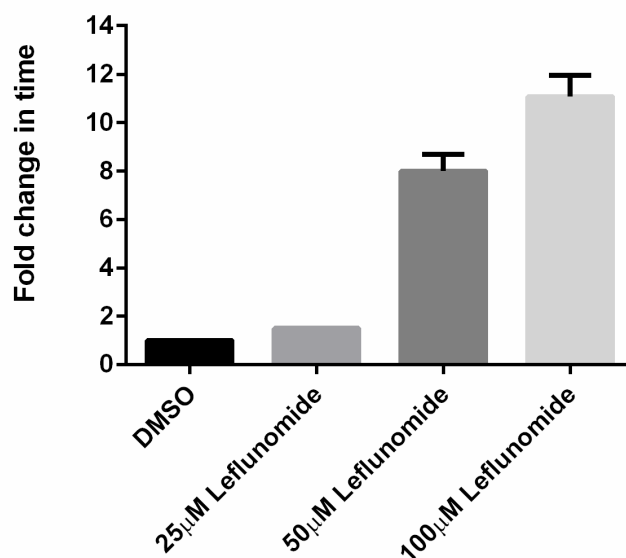


Figure 4.13. Increasing concentrations of leflunomide cause a dose-dependent increase in the time taken to capture 5000 cells compared to the DMSO control. Data is presented as the mean \pm SEM of three independent experiments each performed with cell culture triplicate.

Each leflunomide treatment was compared against the DMSO control and the fold change relative to the DMSO control was measured. These results (figure 4.13) revealed that there was a dose-dependent increase in the fold change in time it took for the sample to be read. There was no difference in fold change comparing 25µM leflunomide to the DMSO control. However there was an 8-fold and 11-fold increase in the 50µM and 100µM leflunomide samples respectively. This considerable fold increase could suggest that these samples had fewer cells than the DMSO and 25µM leflunomide samples. This corresponds to an observation made previously in the cell viability data. It was noted that the reduction in cell viability was primarily caused at higher concentrations of leflunomide (figure 4.3). Therefore this

increase in fold change in both the 50 and 100 μ M leflunomide samples (compared to DMSO), which indicates these samples hold fewer cells, could also confirm the decrease in cell viability observed at these higher concentrations.

4.2.6 JC-1 mitochondrial membrane ($\Delta(\psi)$) potential assay

Due to the ambiguity of some of the results obtained from the annexin V assay, JC1 mitochondrial membrane potential assay was performed as another means to look at apoptosis. JC-1 is a dye that is commonly used to detect changes in mitochondrial membrane potential, an indicator of healthy or apoptotic cells. In a healthy cell, there is a high mitochondrial membrane potential and JC-1 forms aggregates that fluoresce red. In the opposite scenario, unhealthy cells have a low mitochondrial membrane potential and the JC-1 is in the monomeric form which fluoresces green. Therefore as the mitochondrial membrane potential decreases, there is a shift from red to green fluorescence. This shift is solely dependent on mitochondrial membrane potential and other factors such as mitochondrial size or shape do not play a role. Using the FL-1 channel to detect green fluorescence and the FL-2 channel to detect red fluorescence, any change in mitochondrial membrane potential can be detected.

Figure 4.14 shows representative plots from one of the three experiments conducted, whereby A375 cells were treated with DMSO, 25, 50 or 100 μ M leflunomide for 72 hours. FSC vs SSC plots were initially made to gate around the desired population of cells to be used for subsequent analysis. This population of cells was then plotted with the FL-1 channel (green JC-1) along the x-axis and the FL-2 channel (red JC-1) on the y-axis, like the ones shown in figure 4.14 below. With increasing concentrations of leflunomide the main population of cells appeared to increase up the FL-2 y-axis, which suggests an increase in red fluorescence and an increase in mitochondrial membrane potential, thus healthy cells. However there is only a subtle

increase along the FL-1 channel with increasing concentrations of leflunomide. This slight increase is mainly observed at 100 μ M leflunomide (figure 4.14 D) indicating that the mitochondrial membrane potential is not substantially decreased and thus cells are in a healthy state.

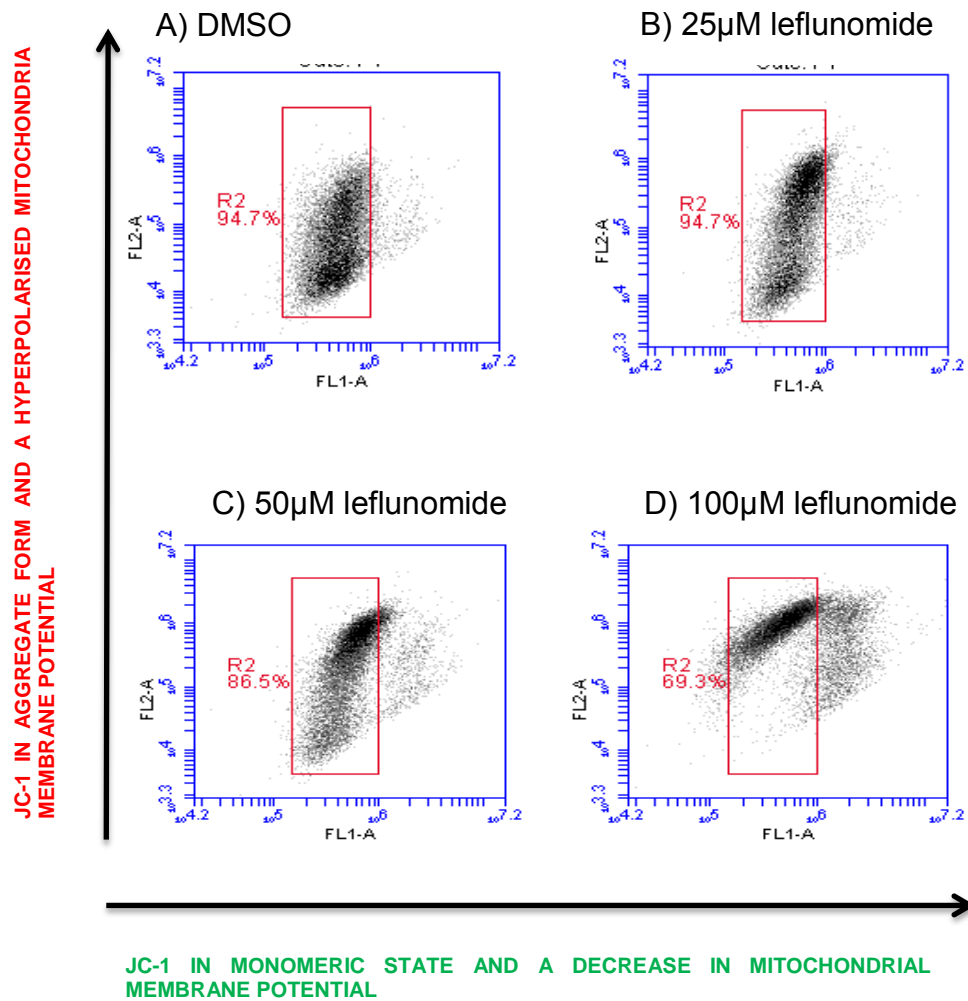


Figure 4.14. Representative JC-1 plots measuring mitochondrial membrane potential determined by flow cytometry. A375 cells were treated with DMSO, 25, 50 and 100 μ M leflunomide for 72 hours and stained with JC-1.

From the representative plots seen in figure 4.15, it was not clear to see the actual change in values from the amount of fluorescence detected in the FL-1 and FL-2 channels. The average FL-1 and FL-2 fluorescence for all three experiments carried out for each treatment condition was plotted on a graph (figure 4.15) to try and observe this change more clearly and quantitatively.

Figure 4.15 clearly shows that with increasing concentrations of leflunomide the green fluorescence is relatively stable, with only a slight noticeable increase at 100 μ M leflunomide. What is more visible is the increase of the intensity of red fluorescence, which occurs in a dose-dependent manner. From DMSO control treated cells the intensity increased from 105,306.06 up to 918,009.72 in the 100 μ M leflunomide treated cells. This data suggests that upon treatment of leflunomide the mitochondrial membrane potential is actually becoming hyperpolarised. Also, with no obvious shift from red fluorescence to green, this data also indicates that the population of cells are remaining healthy from the general consensus for JC-1 dyes.

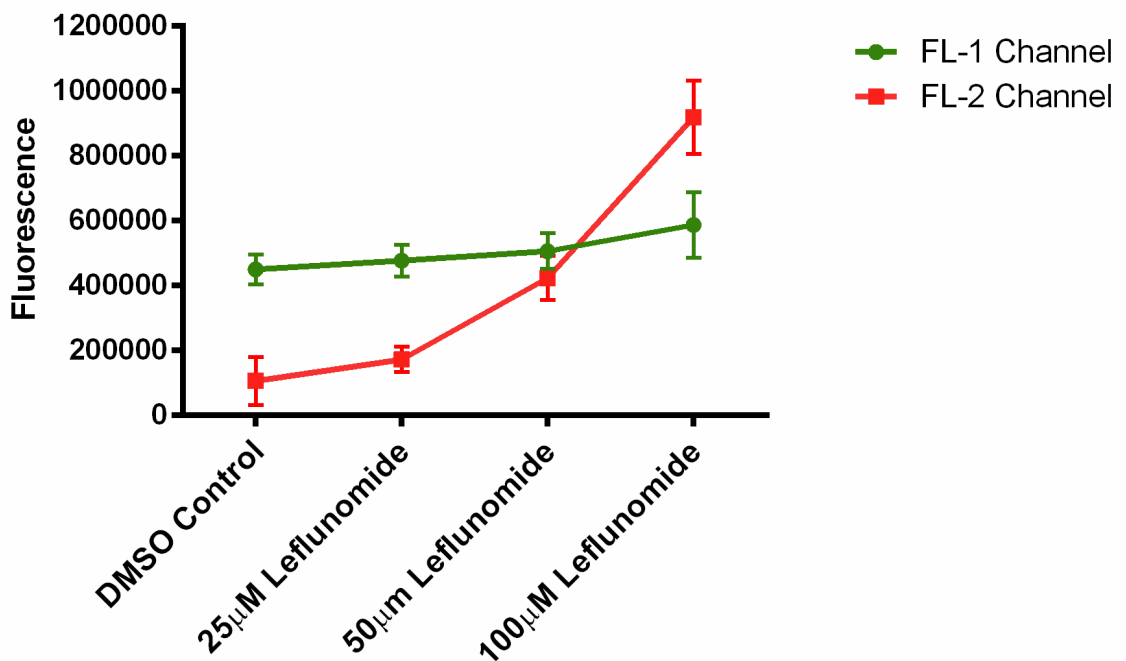


Figure 4.15. Graph quantifying the intensity of red and green fluorescence of JC-1 dye, determined by flow cytometry. A375 cells were treated with DMSO, 25, 50 and 100 μ M leflunomide for 72 hours. Data is presented as the mean \pm SEM of three independent experiments each performed with cell culture triplicate.

4.2.7 Mitotracker Green staining

The puzzling result from the JC-1 led to a more detailed investigation of the effect of leflunomide on the mitochondria. Mitotracker green dye, which contains a thiol-reactive chloromethyl moiety, was used as a probe to label the mitochondria. Cells in culture were incubated with the mitotracker green dye which passively diffuses across the plasma membrane and accumulates in active mitochondria. Mitotracker green dye transitions from a non fluorescent dye in an aqueous solution into a fluorescent dye upon accumulation into the lipid environment of active mitochondria. The amount of green fluorescence detected in the active mitochondria is irrespective of mitochondrial membrane potential. However an increase in green fluorescence detected could be indicative of an increase in abundance or mitochondria or a change in morphology, such as swelling of the mitochondria.

Using mitotracker green dye, again, A375 cells were treated with DMSO, 25, 50 and 100 μ M leflunomide for 72 hours and stained for 30 minutes with mitotracker green. The intensity of the green fluorescence was detected in the FL-1 channel using flow cytometry. Figure 4.16 shows a representative data read out from one of the three independent experiments carried out. Along the x-axis is the intensity of the green fluorescence detected (FL-1) and along the y-axis is the cell count. It can be clearly seen in Figure 4.16 that the intensity of green fluorescence for DMSO (shown in black), 25 (shown in green) and 50 μ M leflunomide (shown in red) are relatively similar, especially between the 25 and 50 μ M leflunomide samples. At 100 μ M leflunomide however (shown in magenta), there was a substantial increase in the intensity of green fluorescence.

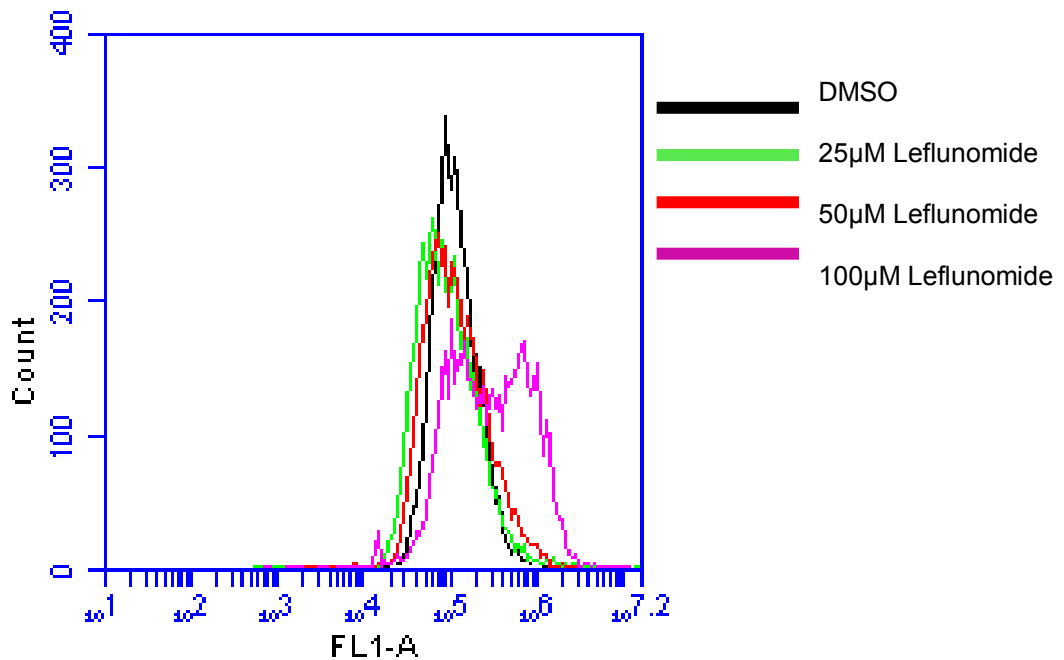


Figure 4.16. Representative data plot showing the intensity of green fluorescence for DMSO, 25, 50 and 100 μ M leflunomide treated A375 cells. DMSO treated cells are shown in black, 25, 50 and 100 μ M leflunomide treated cells are shown in green, red and magenta respectively.

Quantifying the data from all three independent experiments, again, shows the trend whereby there was only a substantial increase in green fluorescence at 100 μ M leflunomide. Figure 4.17 clearly shows this increase in green fluorescence as shown by the fold change compared to the DMSO control. There was not much difference in the fold change in 25 and 50 μ M leflunomide compared to the DMSO control. However there was a 3-fold increase in the amount of green fluorescence at 100 μ M leflunomide when compared to the DMSO control. Statistical analysis comparing 100 μ M leflunomide to all the samples shows that this fold change is statistically significant

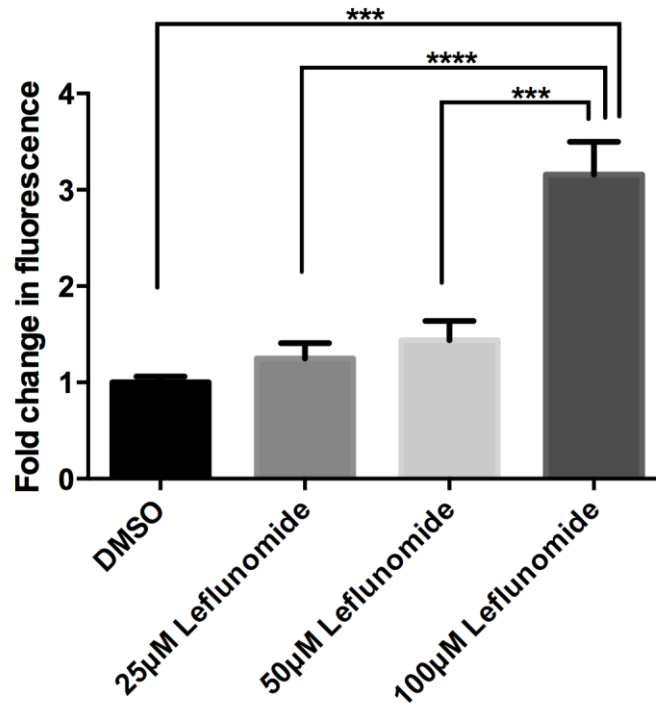


Figure 4.17. Quantification of the fold change of the intensity of green fluorescence between 25, 50 and 100µM leflunomide treated A375 cells and DMSO control cells. Data is presented as the mean \pm SEM of three independent experiments each performed with cell culture triplicate. Asterisks indicate the degree of statistical difference comparing each leflunomide condition to the DMSO control determined by one-way ANOVA with Turkey's post-hoc test. *** $P \leq 0.001$ and **** $P \leq 0.0001$.

Each leflunomide treated sample was compared to DMSO to determine if there was any fold change difference in time that it took for the samples to reach the 5000 events limit set. Figure 4.18 clearly shows a similar relationship that was seen in figure 4.13 with the annexin V data. Comparing the 25 and 50µM leflunomide treated samples to the DMSO control, there was a 4-fold increase in time. In contrast there was a remarkable 12-fold increase in the 100µM leflunomide treated cells compared to the DMSO control.

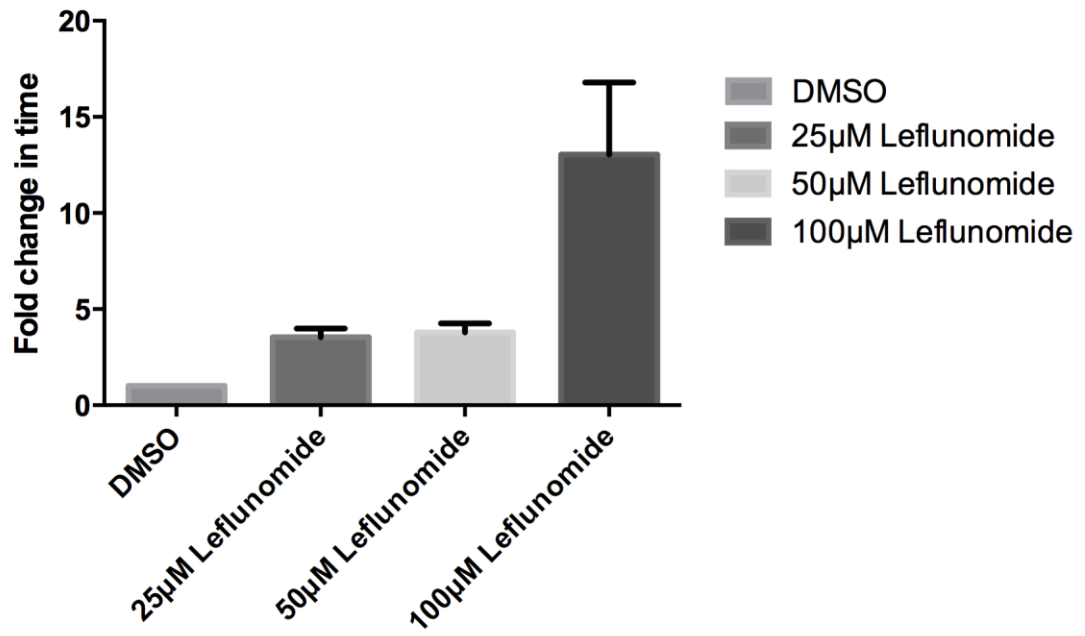


Figure 4.18. Increasing concentrations of leflunomide cause an increase in the fold change in time compared to the DMSO control. Data is presented as the mean \pm SEM of three independent experiments each performed with cell culture triplicate.

4.3: Discussion

Leflunomide is an immunosuppressive drug which was approved by the FDA in 1998 for the treatment of rheumatoid arthritis (RA). However leflunomide has recently been identified as having therapeutic value in treating melanoma in a mouse xenograft model (White et al. 2011). The aim of this chapter of the thesis was to further characterise the function of leflunomide in treating melanoma.

Studies have previously shown that leflunomide reduced the cell viability in three melanoma cell lines harbouring the BRAF^{V600E} mutation (White et al. 2011), but the effect of leflunomide on melanoma cells with wild-type BRAF was not tested. Therefore this was the starting point for this set of experiments. A bank of eight melanoma lines was obtained, four of which harboured the BRAF^{V600E} mutation with the remaining four being wild-type. Cell viability assays showed there was a dose-dependent decrease in all eight of these cell lines upon treatment of leflunomide. When the four BRAF^{V600E} mutant cell lines were grouped together and averaged at 100µM leflunomide, the cell viability was reduced to 36.68%. The viability of the grouped and averaged wild-type cell lines was reduced at a similar level with viability being reduced to 36.46% at the same concentration. This indicates that leflunomide has the potential to treat melanoma patients who do not harbour the BRAF^{V600E} mutation, thus proving a potential treatment for a broader spectrum of patients. This is a promising finding considering that a lot of current treatments are aimed at BRAF^{V600E} harbouring patients, which automatically excludes approximately 50% of patients who do not harbour this mutation.

From these cell viability assays it was observed that the effect on cell viability was predominately seen only at the higher doses of leflunomide. This is in line with other studies which have also shown from *in vitro* experiments that effects with leflunomide were only seen at high concentrations of

leflunomide. For example, a study testing the effect of leflunomide on the growth of neuroblastoma cell lines determined by the CCK-8 assay, revealed that the preferred concentration of leflunomide to inhibit cell growth was 100 μ M (Zhu et al. 2013). Although this study used a different type of cell line, the indication of the concentration at which leflunomide exerts its effect is within the same parameters.

The effect leflunomide had on cell viability on two non-melanoma cell lines, HEK293 and RD1 cells, was also tested. Remarkably out of all the melanoma and non-melanoma cell lines tested, the HEK293 was the most sensitive to leflunomide. In comparison with the most sensitive melanoma cell line (M202), viability was reduced to 16.025% in the HEK293 cells compared to 25.22% for the M202 cell line. The viability of the RD1 cell line was also reduced in a dose-dependent manner upon leflunomide treatment. From this data, it is fair to say leflunomide equally affects the viability of non-melanoma cells and melanoma cells. However in one study it has been reported that there was a less potent effect of leflunomide on the cell viability on the three non-melanoma cell lines they tested (White et al. 2011). Nonetheless, the results from this study are not to be discarded. Taking into account that leflunomide is an already FDA approved drug for the treatment of RA and studies since then have also shown therapeutic effects for other cancers and diseases such as neuroblastoma and multiple myeloma (Zhu et al. 2013; Baumann et al. 2009), it is not out of place in the literature that leflunomide also reduced the viability of the non-melanoma cell lines (RD1 and HEK293) tested here. Moreover given leflunomide mechanisms of action of inhibiting DHODH, one would expect the effect to be universal across all cell lines and not specific to just one.

A question was then posed, what is the reason for this reduction in cell viability? Cell proliferation, cell cycle analysis and cell death assays were initially carried out to try and answer this question. The number of proliferating cells decreased in a dose-dependent manner upon the

treatment with leflunomide, determined by BrdU staining. Additionally upon treatment with leflunomide, the cells underwent a G1 arrest, showing that the cells were not proceeding through to DNA replication (S-phase). The decrease in proliferating cells and the cells arresting in G1 are partially linked together and the same reasoning can be used to explain both of these results.

Leflunomide is an inhibitor of DHODH, the rate limiting enzyme in the de novo pyrimidine synthesis pathway. The enzyme DHODH is located in the inner mitochondrial membrane of the mitochondria. As previously described treatment with leflunomide inhibits DHODH, causes a reduction in the levels of rUMP in cells. One of the G1 checkpoints in the cell cycle is to detect the levels of rUMP. Upon this detection of low levels of rUMP, the nuclear transcription factor p53 is activated. This activation of p53 causes the levels of p21 to increase. p21 is an effector of the G1 checkpoint in the cell cycle by inhibiting the activity of the complexes cyclin D/ cdk and cyclin E/cdk. Inhibiting the activity of these complexes results in the dephosphorylation of the retinoblastoma protein (Rb) and consequently maintains the sequestration of the transcription factor E2F. Thus this causes the cells to arrest in G1 and this could explain the G1 cell cycle arrest observed in the A375 melanoma cells in this thesis. It could also explain the decrease in proliferation in the A375 melanoma cells as the cells are not entering the DNA replication phase (S-phase) to enable cells to divide and produce new cells. The decrease in the pool of pyrimidines and ultimately the nucleotide bases C and T will also have an effect on the lack of new DNA being made and thus a decrease in cell proliferation seen here. Studies have reported that in cells arrested in G1, the levels of p53 and p21 increase upon treatment of leflunomide (Breedveld and Dayer, 2000; Siesmasko et al, 1996; Cherwinski et al, 1995; Lang et al 1995; Wahl et al, 1997; Linke et al, 1996; Linke et al, 1997; Lane, 1992; Herrmann et al 2000). Determining the levels of p53 and p21 in leflunomide treated melanoma cells would be a good experiment to carry out in the future.

The detection of apoptosis was carried out by annexin V and PI staining on the melanoma cells. Upon treatment with 25 μ M or 50 μ M of leflunomide, the melanoma cells were undergoing a clear dose-dependent increase of apoptosis. However at 100 μ M leflunomide the majority of cells were viable. This result at 100 μ M leflunomide contradicts what was seen from the cell viability data in which there was a dose-dependent decrease in viable cells, with 100 μ M causing the highest percentage decrease in the number of viable cells. Also from the cell cycle experiments, there was an increase in the sub-G1 population of cells which is indicative of apoptotic cells. The percentage of cells in the sub-G1 population steadily raised from 2.86% in the DMSO treated cells up to 12.74% in the 100 μ M leflunomide treated cells. So how is it possible that an increase in viable cells was observed at 100 μ M leflunomide when detecting for apoptosis?

The most likely explanation for this could be that when the most pronounced G1 arrest was observed at 100 μ M leflunomide, at this high concentration, leflunomide is exhibiting a cytoprotective effect. With leflunomide's main mechanism of action being inhibiting pyrimidine synthesis, cells in S phase (making new DNA) will be more sensitive to the effects of leflunomide as the demand for pyrimidines is high. Hence the dose-dependent increase in apoptosis observed. On the other hand at 100 μ M leflunomide in which the cells are predominately in G1 arrest, there is a reduced demand for pyrimidines as the cells at this phase are not making new DNA. Therefore at 100 μ M there is less toxicity associated with DHODH inhibition, signifying the decrease in apoptosis and increase in the percentage of cells seen in this thesis. Another study reporting this cytoprotective effect at high concentrations of a drug investigated the effects of paclitaxel in HCT116 cells. At 10nM of paclitaxel mitotic arrest was observed at 4 and 8 hours which returned back to basal levels by 24 hours. Cell death was observed at 10nM paclitaxel from 16 hours onwards. However at 100nm paclitaxel, mitotic arrest was sustained for over 48 hours above the basal level and the onset of cell death was noticeably delayed and inhibited (Gilley et al, 2012). Interestingly an additional study investigated the cytotoxic effects of the

DHODH inhibitor teriflunomide (TFN) in normal human epidermal keratinocytes (NHEK). It was reported that after 96 hours exposure to TFN NHEK arrested in G1 with no evidence of cell death. This study concluded that p53 had a role in the cytoprotective effect against long term exposure to TFN observed (Hail et al, 2012).

Another explanation for this could be because the remaining cells being analysed at 100 μ M leflunomide on the flow cytometer were the only intact cells at this time point post treatment. At this high concentration of leflunomide, the majority of cells that would have undergone apoptosis are likely to be very weak and fragile or may even have burst, and it is no longer possible to detect them for apoptosis using this assay. Therefore the cells which are being detected are the percentage of cells remaining that are still viable. Given that from the cell viability data leflunomide only reduced the viability at 100 μ M to 28%, this reasoning that the cells being analysed at this concentration are the remaining viable ones is the most likely reason for this ambiguous result. But it should also be noted that it has been reported that leflunomide can also target tyrosine kinases at higher concentrations. Specifically which tyrosine kinases are inhibited is not yet fully known. However studies have reported two tyrosine kinases related to the proto-oncogene tyrosine-protein kinase Src family and Jak1 and Jak3 tyrosine kinases to be those inhibited by leflunomide (Xu et al, 1995). Inhibition of tyrosine kinases involves signal transduction pathways which effect cellular proliferation, apoptosis, angiogenesis and invasion, all fundamental processes involved in the progression of cancer. However in all reported cases of inhibited tyrosine kinases, it is agreed within the literature that this effect is a secondary action of leflunomide and not the primary one of DHODH inhibition.

In order to try and clarify the ambiguous result seen at 100 μ M leflunomide when investigating cell death, another marker to detect apoptosis was used,

JC-1. JC-1 detects changes in the mitochondrial membrane potential and as an aggregate fluoresces red in healthy cells with a high mitochondrial membrane potential. On the other hand, JC-1 as a monomer fluoresces green which indicates cells with a decrease in mitochondrial membrane potential including those undergoing apoptosis. Upon treatment of a drug which induces apoptosis a shift from red to green fluorescence will occur. The results from the JC-1 assay using leflunomide treated A375 melanoma cells did not produce this clear shift in red to green fluorescence as expected. Instead no noticeable increase in green fluorescence (indicating apoptotic cells) was detected at any of the concentrations of leflunomide tested. Instead the opposite was seen at 100 μ M leflunomide in which there was an increase in red fluorescence which would indicate hyperpolarisation of the mitochondrial membrane and indicated the cells were healthy. The same reasoning can be used here which was used to explain the ambiguous annexin V result, which was also at 100 μ M leflunomide. This being the cells which are analysed on the flow cytometer at this concentration are the remaining cells which are viable, thus the increase in red fluorescence and the indication that the cells are healthy.

However from this experiment, the result still remains inconclusive due to technical reasons and some optimisation of the protocol is still needed which could also clarify these findings. An optimisation that could be carried out is to leave the cells incubating with JC-1 for a longer period of time. Additionally a time course experiment could also be carried out. It could be possible that the time point tested in this thesis (72 hours) may have missed the detection of a change in mitochondrial membrane potential which may be occurring at earlier time points. Thus a time course would determine this and allow the change in mitochondrial membrane potential to be seen over time.

Due to an apparent effect occurring on the mitochondria, the mitochondria were stained with mitotracker green to stain for the mitochondria. The analysis from this revealed a 3-fold increase in the intensity of green

fluorescence at 100 μ M compared to the DMSO control as well as 25 and 50 μ M leflunomide. It cannot be elucidated from staining with this dye whether this increase in fluorescence is due to mitochondrial swelling or an increase in mitochondria. Therefore further experiments are required to decipher this increase in fluorescence which would include live imaging of the cells post staining. Looking at the live cells would enable identification of any potential mitochondrial swelling or increase in mitochondria. However it is to note that any effect seen with the mitotracker green dye is irrespective of mitochondrial membrane polarisation.

All of the unexpected results that did not follow the trend of results seen appear to occur at 100 μ M leflunomide. It could be proposed that leflunomide has a bi-phasic mode of action whereby leflunomide is affecting specific targets between a certain concentration range with a different set of targets being targeted at the higher concentrations of leflunomide. Although explanations for the results in this chapter have just been discussed, several other possible theories could also be feasible. Regarding the cell death aspect from this thesis, for example, from the annexin V/PI staining showed the occurrence of apoptosis at 25 and 50 μ M leflunomide. However at 100 μ M leflunomide there appeared to be a shift back to an increase in the number viable cells. Although the reasoning for this result has been explained, collectively the results for 100 μ M leflunomide from the annexin V/PI apoptosis assay, JC-1 mitochondrial membrane potential and the mitotracker green staining, it is possible that an unconventional method of cell death could be occurring at this higher concentration of leflunomide (100 μ M). This could indicate a tyrosine kinase target of leflunomide which has yet to be identified. This highlights that the tyrosine kinases in which leflunomide targets at high concentrations and how they exert their effects, has yet to be explored to its full potential. Oncosis is a possible other mode of cell death which could be taking place. Indicative of oncosis is swelling of the nucleus, cytoplasm and mitochondria, cytoplasm vacuolisation and failure of the plasma membrane ion channels, including the calcium (Ca^{2+}) and sodium (Na) ion channels (Trump et al, 1997). To either reject or accept this

hypothesis, further experiments for this could include staining of the nucleus with a nuclear dye such as DAPI or Hoescht. Experiments determining if the normal influx or efflux of the Ca^{2+} and Na channels are being altered could also be carried out. If these ion channels prove to be affected, this could potentially explain the JC-1 result (seen in figures 4.13 and 4.14) and obscuring the polarisation of the mitochondrial membrane potential. Another possible hypothesis is that mitotoxicity could also be occurring and future experiments could also look into this avenue.

Chapter 5

Investigating the possibility of using leflunomide in combination with selumetinib to treat melanoma

5.1 Introduction

In the previous chapter it was shown that leflunomide has the potential to be an anti-cancer drug in treating melanoma. In recent years it has become more accepted that combinatorial therapy is a better approach in treating melanoma. Within the field, there is substantial clinical data supporting MEK inhibitors being used for the treatment of melanoma. Taking this into account, the possibility of using leflunomide in combination with the MEK inhibitor, selumetinib was investigated. The rationale being that BRAF^{V600E} mutant melanomas are addicted to MEK for proliferation and survival. Therefore inhibition of MEK might reduce survival signalling and sensitises cells to the cytotoxic effects leflunomide. However G1 arrest may reduce sensitivity to leflunomide.

Cell viability assays were carried out on the bank of eight melanoma cell lines treated with selumetinib. Combinatorial cell viability assays using leflunomide and selumetinib were also carried out on all eight melanoma cell lines. Synergy between these two drugs at the concentrations tested was determined by the Chou and Talalay combination index method. Pre-treatment for 24 hours with either leflunomide or selumetinib was also investigated in this chapter to elucidate if this altered the synergy between to two drugs. At the end of this chapter a mouse xenograft study on the M375 melanoma cell line is presented determining the efficacy of leflunomide and selumetinib *in vivo* as a potential drug combination in treating melanoma.

5.2 Results

5.2.1 Selumetinib cell viability assays

Initially, cell viability assays were carried out using CellTiter-Glo on all eight of the melanoma cell lines as shown in table 4.1. The MEK inhibitor selumetinib is a highly potent drug, thus a much lower concentration range than previous experiments using leflunomide was used. Figure 5.1 shows a dose-dependent decrease in the number of viable cells upon 72 hours treatment with selumetinib in all eight of the melanoma cell lines. However, this decrease in cell viability appeared to start to plateau off at the higher concentrations of selumetinib. Again there was a broad range of variation in the level of sensitivity to selumetinib than in the results to leflunomide. For example the most sensitive melanoma cell line to selumetinib according to the IC_{50} 's was M375 (shown in green), with an IC_{50} of $0.10\mu\text{M}$. In comparison, the least sensitive melanoma cell line was SKmel5 (shown in black) with an IC_{50} of $1.01\mu\text{M}$.

The IC_{50} 's for selumetinib-induced growth inhibition for all eight melanoma cell lines was calculated (table 5.1). Similarly the IC_{50} 's produced differed amongst the cell lines ranging from $0.19286\mu\text{M}$ to $1.01\mu\text{M}$. Again, this emphasizes that selumetinib produces a varied response in the eight melanoma cell lines tested.

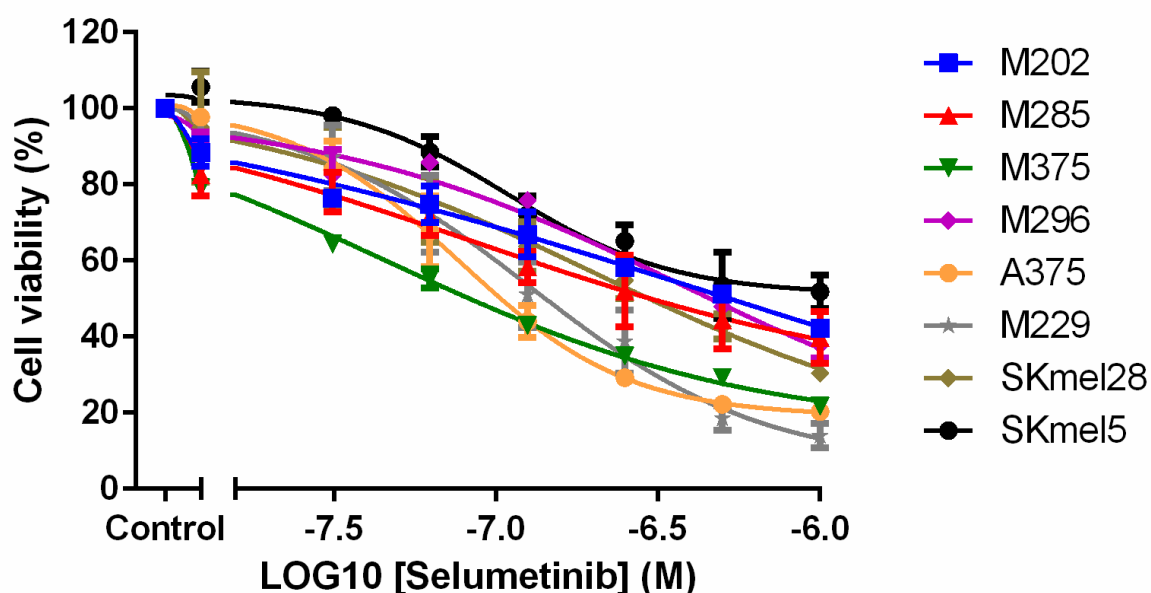


Figure 5.1. Selumetinib caused a dose-dependent decrease in cell viability in eight human melanoma cell lines. Melanoma cell lines include M202 (blue), M285 (red), M375 (green) and M296 (purple), A375 (orange), M229 (grey), SKmel28 (khaki) and SKmel5 (black). Cell viability was determined by using CellTiter-Glo reagent and all values are represented as a percentage (%) relative to the vehicle control. Data is presented as the mean \pm SEM of three independent experiments each performed with cell culture triplicate.

Table 5.1. IC_{50} values for eight melanoma cell lines, HEK293, RD1 cells and melanocytes in response to selumetinib

Cell line	IC_{50} (μ M)	BRAF status	NRAS status
M202	0.50	wt	Q61L
M285	0.50	wt	wt
M375	0.10	wt	wt
M296	0.47	wt	Q61L
A375	0.19	Homo V600E	wt
M229	0.20	Homo V600E	wt
SKmel28	0.43	Homo V600E	wt
SKmel5	1.01	Het V600E	wt
Melanocytes	n/a	-	-
HEK293	n/a	-	-
RD1	1.05	-	-

Alongside the melanoma cells, the two non-melanoma cell lines used previously and melanocytes were also treated with selumetinib and their cell viability determined (figure 5.2). Interestingly, all three of these cell lines were less sensitive to selumetinib compared to the eight melanoma cell lines. The RD1 cell line was the most sensitive with cell viability being reduced to 55% at 1 μ M selumetinib. This sensitivity was very close to the least sensitive melanoma cell line, SKmel5 where its cell viability was reduced to just 51.80% at the same concentration. The IC₅₀ value for RD1 was 1.0461 μ M, which again is similar to the IC₅₀ produced for SKmel5 (1.01 μ M). This highlights the fact that these two cell lines were the least sensitive to selumetinib in comparison to the other IC₅₀'s produced. Equally, the HEK293 cell line and melanocytes were very insensitive to selumetinib and such that 50% growth inhibition was not even reached.

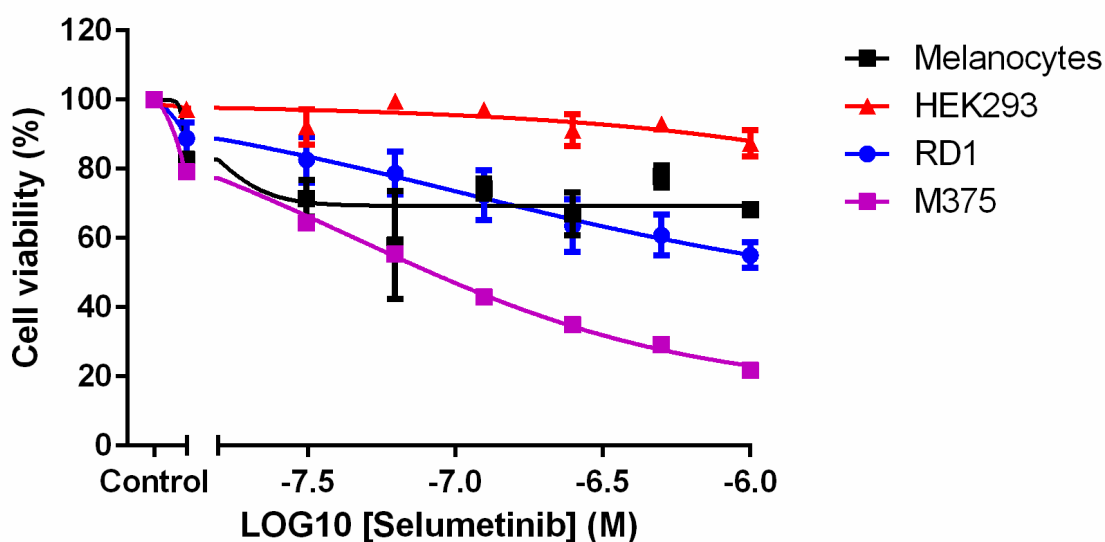


Figure 5.2. Selumetinib had little effect on cell viability of the melanocytes (shown in black), HEK293 (shown in red), RD1 (shown in blue) and M375 (shown in purple) cell lines. Cell viability was determined by using CellTiter-Glo reagent and all values are represented as a percentage (%) relative to the vehicle control. Data is presented as the mean \pm SEM of three independent experiments each performed with cell culture triplicate.

5.2.2 Western blot detection of phospho ERK and total ERK

To confirm selumetinib, a MEK inhibitor, was active and acting 'on target' western blots were performed to detect the levels of phospho ERK; since ERK is a direct substrate of MEK a decrease in phospho-ERK would be anticipated in selumetinib treated cells. It can be clearly seen in figure 5.3 that both the A375 and M202 melanoma cell line tested the amount of pERK protein decreases in a dose-dependent manner. This confirms that selumetinib is effectively inhibiting its target. HSC70 was used as a loading control.

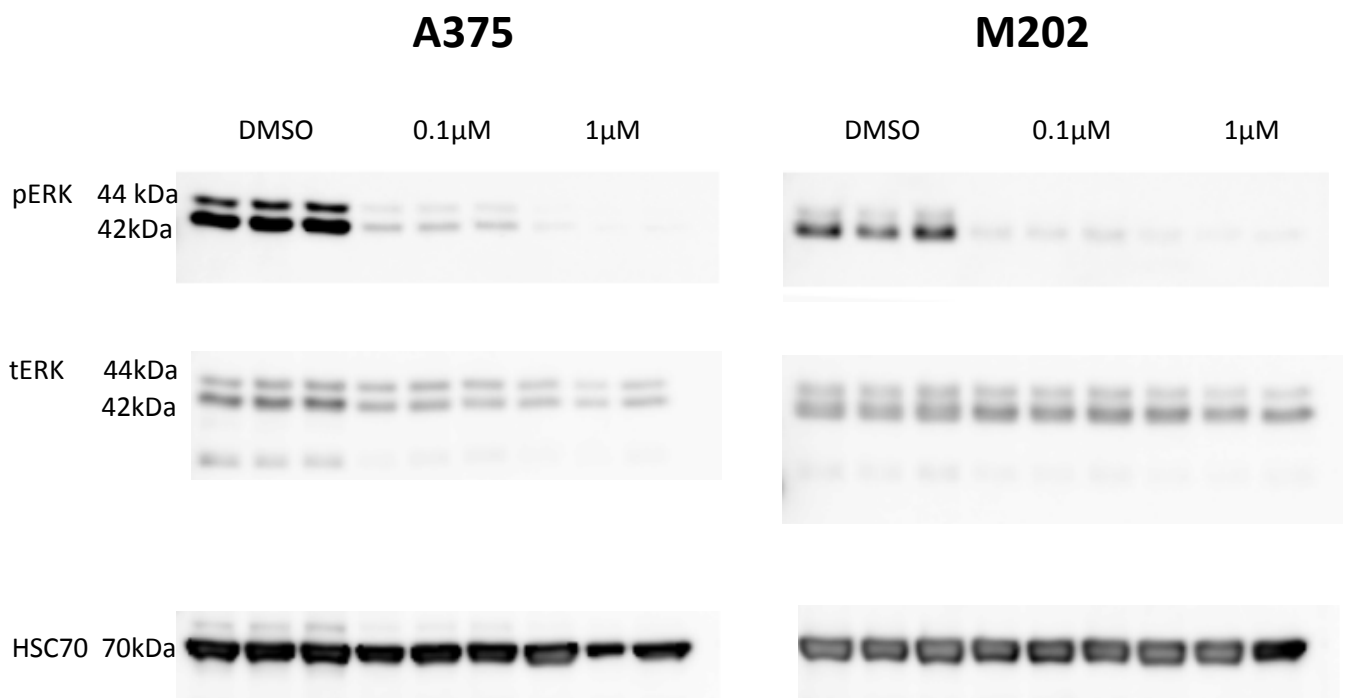


Figure 5.3. Western blot analysis confirming the decrease in phospho-ERK upon treatment with 0.1 or 1 μM selumetinib in A375 and M202 melanoma cell lines. The molecular weights are shown on the left. Results for pERK and tERK are from a single experiment representative of three independent experiments.

5.2.3 Leflunomide and selumetinib combinatorial cell viability assays

The preceding results, carried out on a panel of eight melanoma cell lines, showed both leflunomide and selumetinib were effective at reducing cell viability (figure 4.2 and 5.2). Prompted by these results, experiments were designed to determine if the combination of leflunomide and selumetinib reduced cell viability further than each drug alone. Combinatorial cell viability assays were carried out on all eight of the melanoma cell lines. For these cell viability assays, lower concentrations of each drug were used. The concentrations of leflunomide used were 12.5, 25 and 50 μ M. For selumetinib the concentrations used were 0.025, 0.05 and 0.1 μ M.

For each cell line and in the results to follow in figures 5.4 to 5.11, there are two cell viability graphs. The first graph shows the selumetinib concentrations along the x axis and the second graph has leflunomide along the x axis. This was done in order to complete statistical analysis comparing the drug combinations to each drug alone. Thus, the statistics shown on these graphs showed the statistics determining if the drug combinations were significantly better than either drug alone. No statistical analysis was carried out comparing the different drug combinations with each other.

Figures 5.4-5.11 clearly shows that all of the eight melanoma cell lines responded to the combinations of leflunomide and selumetinib, but again to varying degrees. However, one cell line stands out as the least sensitive to any of the drug combinations, the SKmel28 (figure 5.10). This may not be too surprising given it was the least sensitive cell line to leflunomide (figure 4.2 and table 4.2), and was one of the least sensitive to selumetinib (figure 5.1 and table 5.1).

To determine which cell line was the most sensitive from these cell viability experiments was hard to elucidate. One could define the most sensitive cell

line as either the cell line in which the viability was reduced the most at a given combination of leflunomide and selumetinib. Or one could define it as the cell line which produced the most defined separation of cell viability with increasing concentrations of the combination of leflunomide and selumetinib.

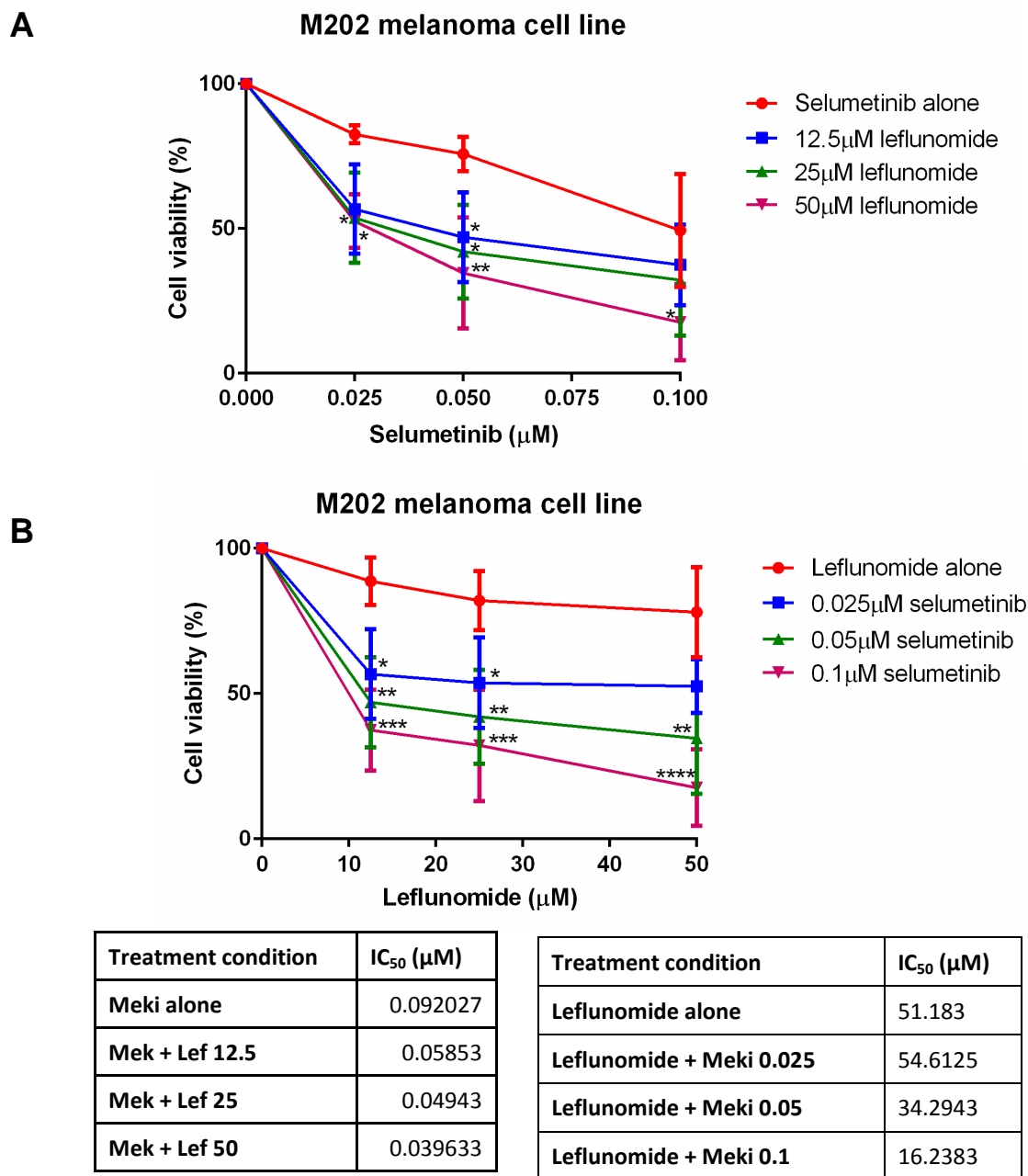
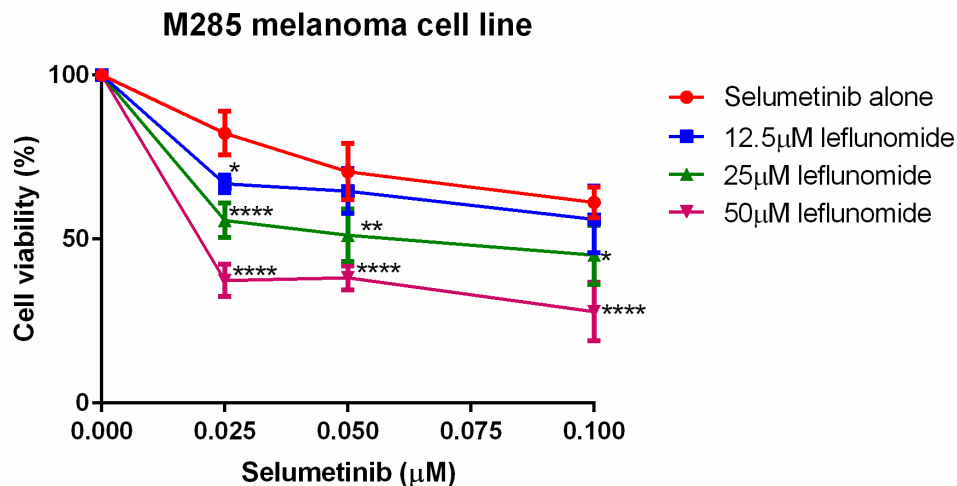
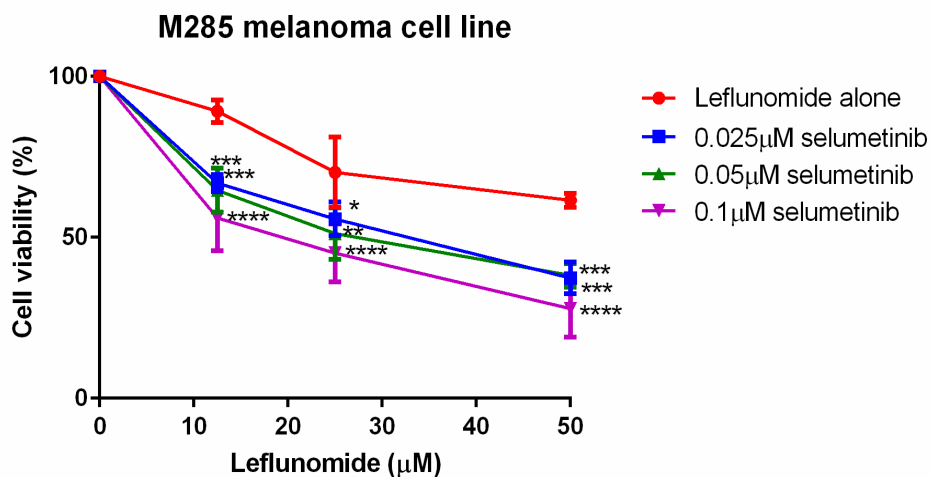


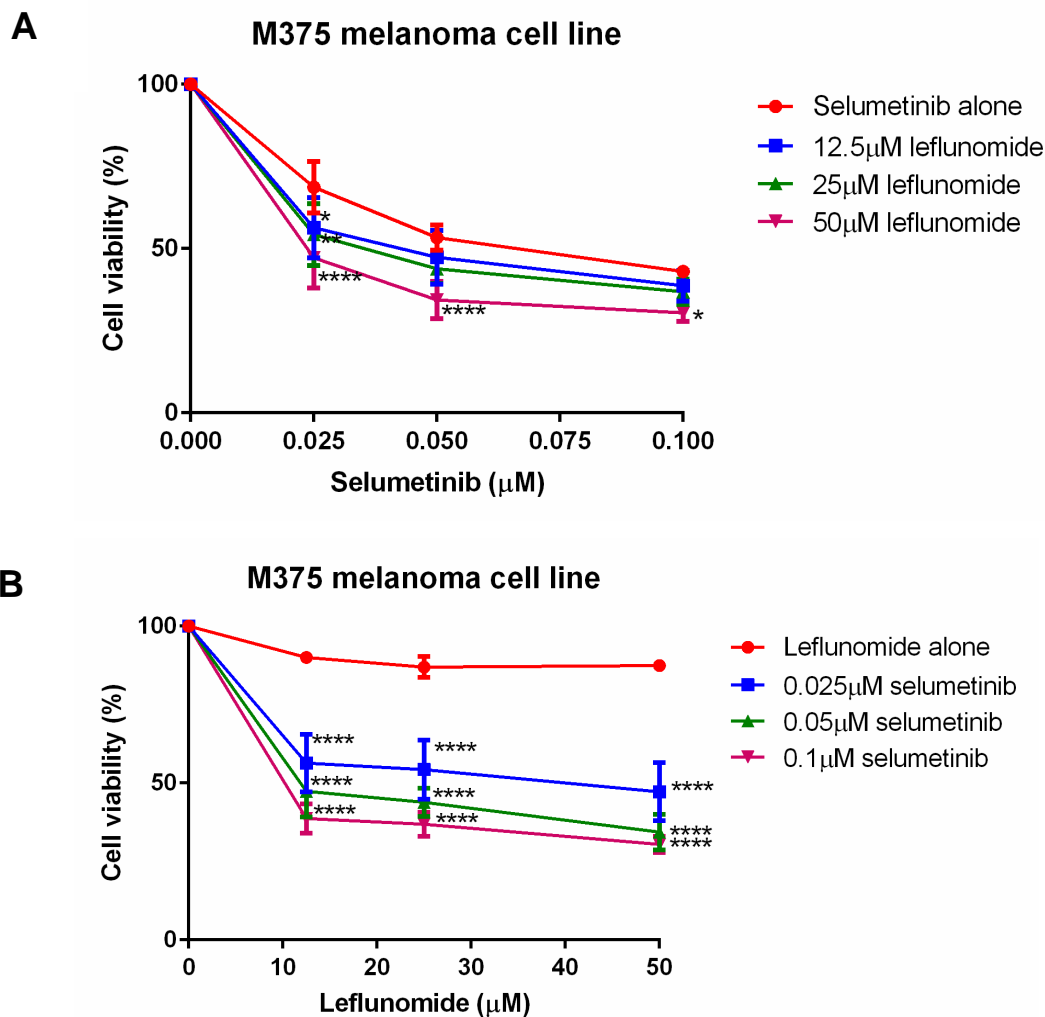
Figure 5.4. The combination of leflunomide and selumetinib reduces cell viability in the M202 cell line. Graph A shows the concentrations of selumetinib along the x-axis. The statistical analysis on this graph compares the combinations of drugs to selumetinib alone. Graph B shows the concentrations of leflunomide along the x-axis. The statistical analysis on this graph compares the drug combinations to leflunomide alone. The IC₅₀'s are for each graph are also shown. Cell viability was determined by using CellTiter-Glo reagent and all values are represented as a percentage (%) relative to the vehicle control. Data is presented as the mean ± SEM of three independent experiments each performed with cell culture triplicate. Asterisks indicate the degree of statistical difference comparing each leflunomide and selumetinib condition to leflunomide alone (graph A) or selumetinib alone (graph B). Statistical analysis was determined by two-way ANOVA with Turkey's post-hoc test. *P≤0.05, **P≤0.01, ***P≤0.001 and ****P≤0.0001.

A**B**

Treatment condition	IC ₅₀ (μM)
Meki alone	0.165867
Mek + Lef 12.5	0.175397
Mek + Lef 25	0.06337
Mek + Lef 50	0.02238

Treatment condition	IC ₅₀ (μM)
Leflunomide alone	72.3867
Leflunomide + Meki 0.025	29.57
Leflunomide + Meki 0.05	26.9967
Leflunomide + Meki 0.1	17.7733

Figure 5.5. The combination of leflunomide and selumetinib reduced cell viability in the M285 cell line. Graph A shows the concentrations of selumetinib along the x-axis. The statistical analysis on this graph compared the combinations of drugs to selumetinib alone. Graph B shows the concentrations of leflunomide along the x-axis. The statistical analysis on this graph compared the drug combinations to leflunomide alone. IC₅₀'s for each graph are also shown. Cell viability was determined by using CellTiter-Glo reagent and all values are represented as a percentage (%) relative to the vehicle control. Data is presented as the mean \pm SEM of three independent experiments each performed with cell culture triplicate. Asterisks indicate the degree of statistical difference comparing each leflunomide and selumetinib condition to leflunomide alone (graph A) or selumetinib alone (graph B). Statistical analysis was determined by two-way ANOVA with Turkey's post-hoc test. *P \leq 0.05, **P \leq 0.01, ***P \leq 0.001 and ****P \leq 0.0001.

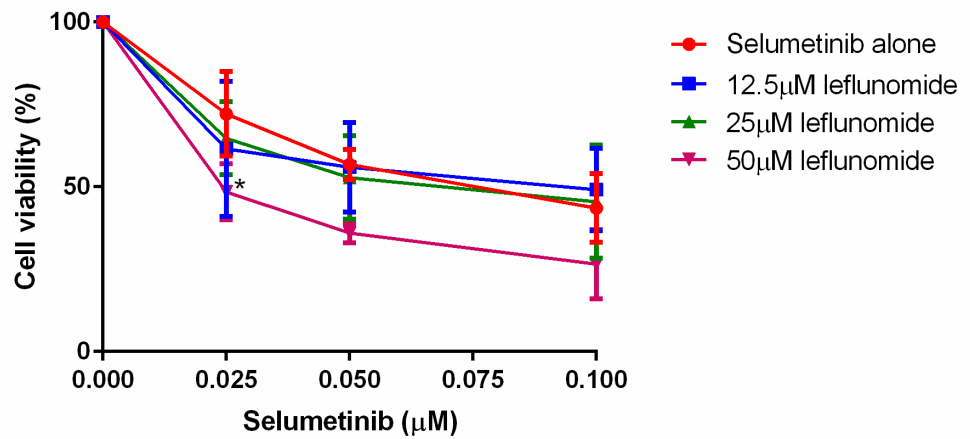


Treatment condition	IC ₅₀ (μM)
Meki alone	0.064
Mek + Lef 12.5	0.046912
Mek + Lef 25	0.039495
Mek + Lef 50	0.026858

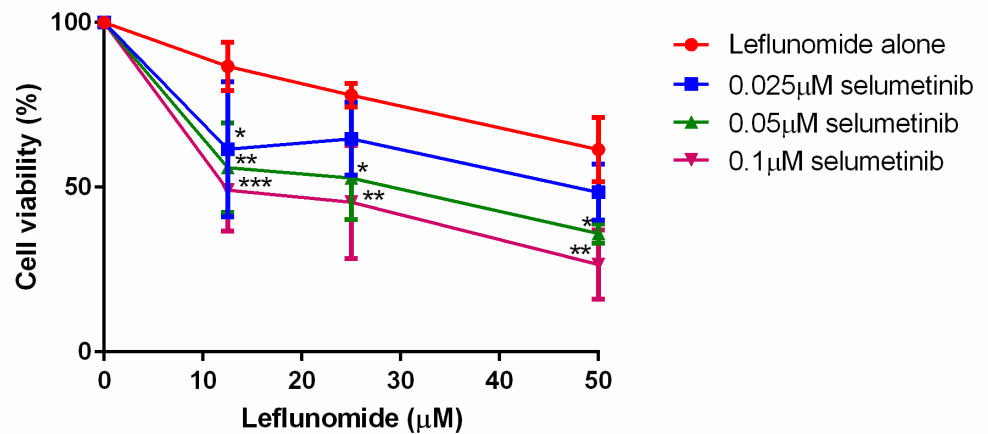
Treatment condition	IC ₅₀ (μM)
Leflunomide alone	n/a
Leflunomide + Meki 0.025	36.14
Leflunomide + Meki 0.05	13.028
Leflunomide + Meki 0.1	6.02175

Figure 5.6. The combination of leflunomide and selumetinib reduced cell viability in the M375 cell line. Graph A shows the concentrations of selumetinib along the x-axis. The statistical analysis on this graph compared the combinations of drugs to selumetinib alone. Graph B shows the concentrations of leflunomide along the x-axis. The statistical analysis on this graph compared the drug combinations to leflunomide alone. The IC₅₀'s for each graph are also shown. Cell viability was determined by using CellTiter-Glo reagent and all values are represented as a percentage (%) relative to the vehicle control. Data is presented as the mean ± SEM of three independent experiments each performed with cell culture triplicate. Asterisks indicate the degree of statistical difference comparing each leflunomide and selumetinib condition to leflunomide alone (graph A) or selumetinib alone (graph B). Statistical analysis was determined by two-way ANOVA with Turkey's post-hoc test. *P≤0.05, **P≤0.01, ***P≤0.001 and ****P≤0.0001.

A M296 melanoma cell line



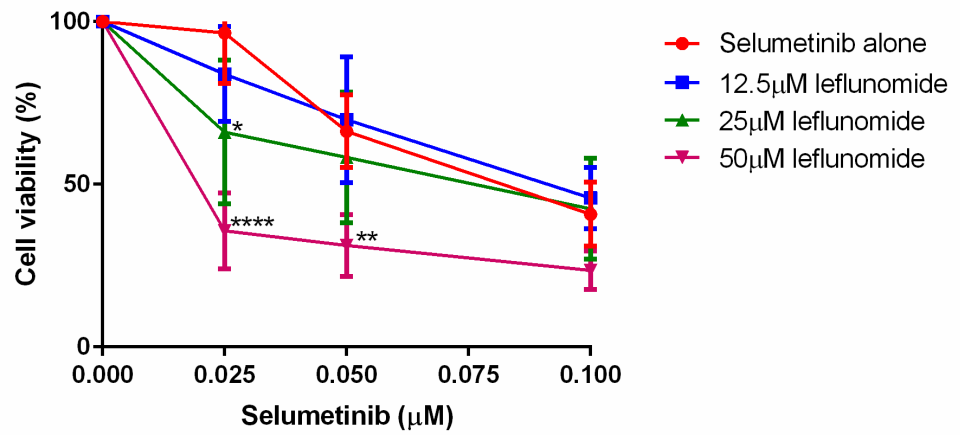
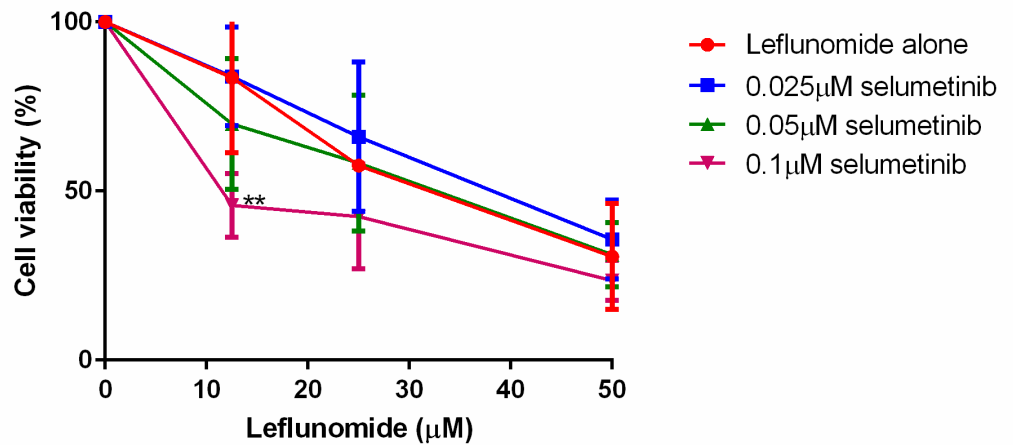
B M296 melanoma cell line



Treatment condition	IC ₅₀ (μM)
Meki alone	0.073586
Mek + Lef 12.5	0.0845
Mek + Lef 25	0.10596
Mek + Lef 50	0.02805

Treatment condition	IC ₅₀ (μM)
Leflunomide alone	109.936
Leflunomide + Meki 0.025	42.56
Leflunomide + Meki 0.05	21.3153
Leflunomide + Meki 0.1	17.3686

Figure 5.7 The combination of leflunomide and selumetinib reduced cell viability in the M296 cell line. Graph A shows the concentrations of selumetinib along the x-axis. The statistical analysis on this graph compared the combinations of drugs to selumetinib alone. Graph B shows the concentrations of leflunomide along the x-axis. The statistical analysis on this graph compared the drug combinations to leflunomide alone. The IC₅₀'s for each graph are also shown. Cell viability was determined by using CellTiter-Glo reagent and all values are represented as a percentage (%) relative to the vehicle control. Data is presented as the mean ± SEM of three independent experiments each performed with cell culture triplicate. Asterisks indicate the degree of statistical difference comparing each leflunomide and selumetinib condition to leflunomide alone (graph A) or selumetinib alone (graph B). Statistical analysis was determined by two-way ANOVA with Turkey's post-hoc test. *P≤0.05, **P≤0.01, ***P≤0.001 and ****P≤0.0001.

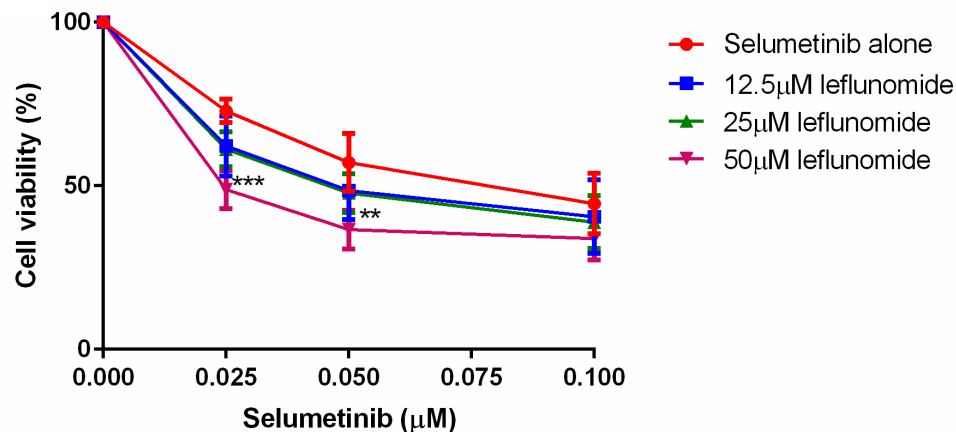
A**A375 melanoma cell line****B****A375 melanoma cell line**

Treatment condition	IC ₅₀ (μM)
Meki alone	0.085327
Mek + Lef 12.5	0.083253
Mek + Lef 25	0.070023
Mek + Lef 50	0.019527

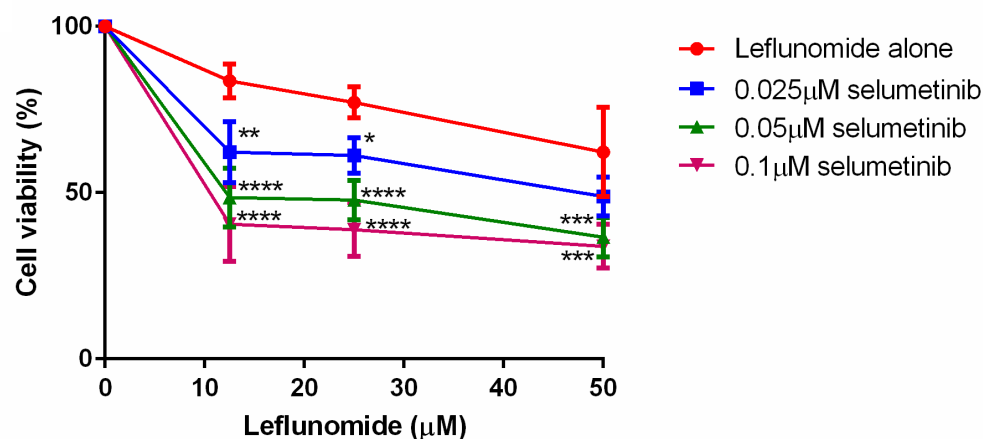
Treatment condition	IC ₅₀ (μM)
Leflunomide alone	31.8067
Leflunomide + Meki 0.025	34.85
Leflunomide + Meki 0.05	27.53
Leflunomide + Meki 0.1	13.0997

Figure 5.8. The combination of leflunomide and selumetinib reduced cell viability in the A375 cell line. Graph A shows the concentrations of selumetinib along the x-axis. The statistical analysis on this graph compared the combinations of drugs to selumetinib alone. Graph B shows the concentrations of leflunomide along the x-axis. The statistical analysis on this graph compared the drug combinations to leflunomide alone. The IC₅₀'s for each graph are also shown. Cell viability was determined by using CellTiter-Glo reagent and all values are represented as a percentage (%) relative to the vehicle control. Data is presented as the mean ± SEM of three independent experiments each performed with cell culture triplicate. Asterisks indicate the degree of statistical difference comparing each leflunomide and selumetinib condition to leflunomide alone (graph A) or selumetinib alone (graph B). Statistical analysis was determined by two-way ANOVA with Turkey's post-hoc test. *P≤0.05, **P≤0.01, ***P≤0.001 and ****P≤0.0001.

A M229 melanoma cell line



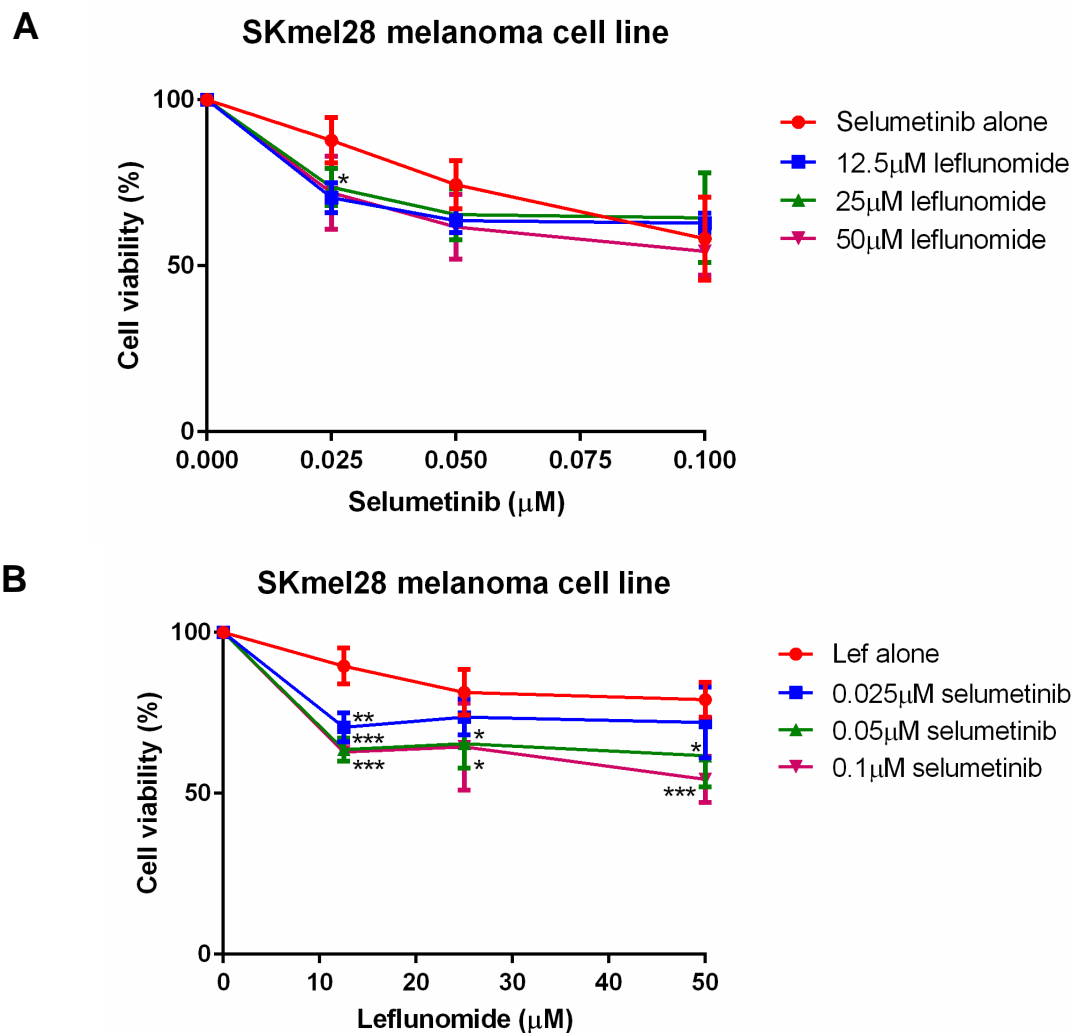
B M229 melanoma cell line



Treatment condition	IC ₅₀ (μM)
Meki alone	0.082073
Mek + Lef 12.5	0.058577
Mek + Lef 25	0.050353
Mek + Lef 50	0.030117

Treatment condition	IC ₅₀ (μM)
Leflunomide alone	89.115
Leflunomide + Meki 0.025	53.16
Leflunomide + Meki 0.05	15.525
Leflunomide + Meki 0.1	8.773667

Figure 5.9. The combination of leflunomide and selumetinib reduced cell viability in the M229 cell line. Graph A shows the concentrations of selumetinib along the x-axis. The statistical analysis on this graph compared the combinations of drugs to selumetinib alone. Graph B shows the concentrations of leflunomide along the x-axis. The statistical analysis on this graph compared the drug combinations to leflunomide alone. The IC₅₀'s for each graph are also shown. Cell viability was determined by using CellTiter-Glo reagent and all values are represented as a percentage (%) relative to the vehicle control. Data is presented as the mean ± SEM of three independent experiments each performed with cell culture triplicate. Asterisks indicate the degree of statistical difference comparing each leflunomide and selumetinib condition to leflunomide alone (graph A) or selumetinib alone (graph B). Statistical analysis was determined by two-way ANOVA with Turkey's post-hoc test. *P≤0.05, **P≤0.01, ***P≤0.001 and ****P≤0.0001.

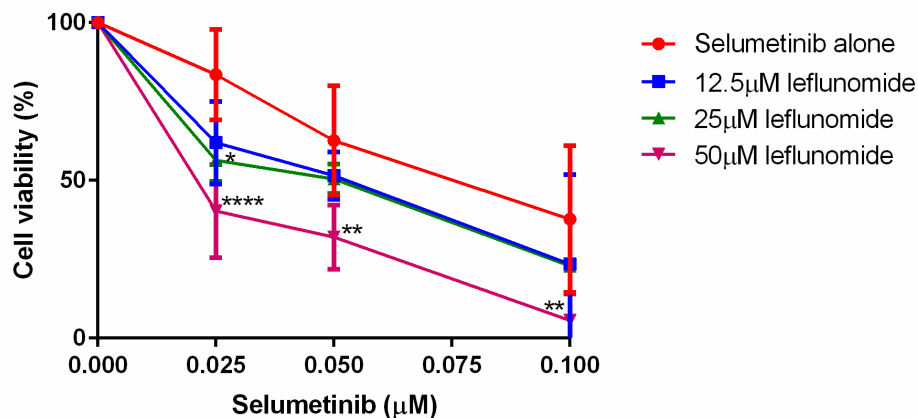


Treatment condition	IC ₅₀ (μM)
Meki alone	0.1684
Mek + Lef 12.5	0.1875
Mek + Lef 25	0.585
Mek + Lef 50	0.112

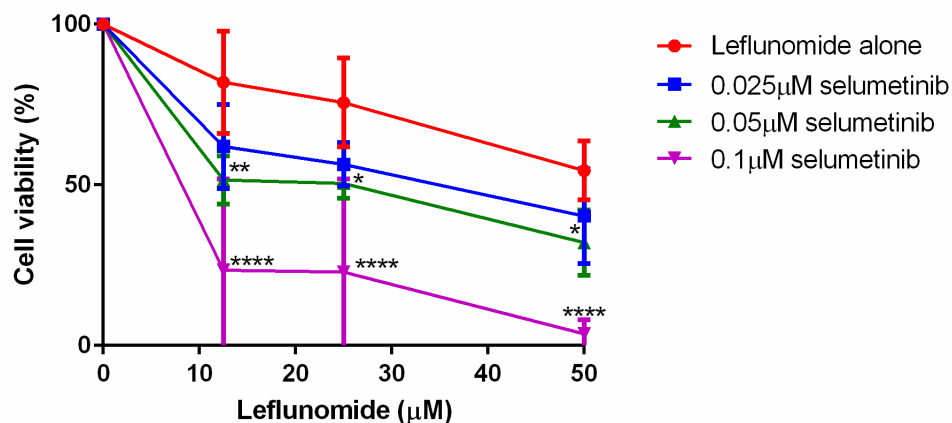
Treatment condition	IC ₅₀ (μM)
Leflunomide alone	n/a
Leflunomide + Meki 0.025	n/a
Leflunomide + Meki 0.05	n/a
Leflunomide + Meki 0.1	n/a

Figure 5.10. The combination of leflunomide and selumetinib reduced cell viability in the SKmel28 cell line. Graph A shows the concentrations of selumetinib along the x-axis. The statistical analysis on this graph compared the combinations of drugs to selumetinib alone. Graph B shows the concentrations of leflunomide along the x-axis. The statistical analysis on this graph compared the drug combinations to leflunomide alone. The IC₅₀'s for each graph are also shown. Cell viability was determined by using CellTiter-Glo reagent and all values are represented as a percentage (%) relative to the vehicle control. Data is presented as the mean ± SEM of three independent experiments each performed with cell culture triplicate. Asterisks indicate the degree of statistical difference comparing each leflunomide and selumetinib condition to leflunomide alone (graph A) or selumetinib alone (graph B). Statistical analysis was determined by two-way ANOVA with Turkey's post-hoc test. *P≤0.05, **P≤0.01, ***P≤0.001 and ****P≤0.0001.

A SKmel5 melanoma cell line



B SKmel5 melanoma cell line



Treatment condition	IC ₅₀ (μM)
Mek alone	0.088842
Mek + Lef 12.5	0.052304
Mek + Lef 25	0.048602
Mek + Lef 50	0.022102

Treatment condition	IC ₅₀ (μM)
Leflunomide alone	62.152
Leflunomide + Meki 0.025	31.5225
Leflunomide + Meki 0.05	18.852
Leflunomide + Meki 0.1	8.2473

Figure 5.11. The combination of leflunomide and selumetinib reduced cell viability in the SKmel5 cell line. Graph A shows the concentrations of selumetinib along the x-axis. The statistical analysis on this graph compared the combinations of drugs to selumetinib alone. Graph B shows the concentrations of leflunomide along the x-axis. The statistical analysis on this graph compared the drug combinations to leflunomide alone. The IC₅₀'s for each graph are also shown. Cell viability was determined by using CellTiter-Glo reagent and all values are represented as a percentage (%) relative to the vehicle control. Data is presented as the mean ± SEM of three independent experiments each performed with cell culture triplicate. Asterisks indicate the degree of statistical difference comparing each leflunomide and selumetinib condition to leflunomide alone (graph A) or selumetinib alone (graph B). Statistical analysis was determined by two-way ANOVA with Turkey's post-hoc test. *P≤0.05, **P≤0.01, ***P≤0.001 and ****P≤0.0001.

Taking the first definition into account, the two cell lines which were the most sensitive to the given combination of 50 μ M leflunomide and 0.1 μ M selumetinib were the SKmel5 and M202 cell lines (figures 5.11 and 5.4). At this given concentration combination, the cell viability of the SKmel5 cell line was reduced to just 3.578%. Whereas when cells were treated with 50 μ M leflunomide and 0.1 μ M selumetinib alone, the cell viability was reduced to 54% and 37.2% respectively (figure 5.11). Similarly with the M202 cell line, cell viability was reduced to 20.96% when treated with 50 μ M leflunomide and 0.1 μ M selumetinib. However viability was reduced to 78.07% and 48.6% when treated with 50 μ M leflunomide and 0.1 μ M selumetinib alone respectively (figure 5.4).

Considering the second definition of the most sensitive cell lines in which clearly defined separation of cell viability with increasing concentrations of the combination of leflunomide and selumetinib can be seen, the M375 and M229 cell lines were amongst these which responded the best (figures 5.6 and 5.9). The second graph on figure 5.6 clearly shows for the M375 melanoma cell line, cells treated with leflunomide alone are shown in red. The combination of leflunomide with selumetinib at 0.025, 0.05 and 0.1 μ M are shown in blue, green and purple respectively. As the concentrations of selumetinib and leflunomide increased a clear separation of the reduction in cell viability was seen. This trend was also seen for the M229 cell line in figure 5.9. These two cell lines along with the M285 cell line (figure 4.5) were the three best cell lines statistically, in which the combinations of leflunomide and selumetinib were more statistically significant than leflunomide alone. The most significant from the three was the M375 cell line which had p values of ≤ 0.0001 across the board of all the possible combinations of leflunomide and selumetinib.

From figures 5.4-5.11, it is clear that the most statistically significant combination of leflunomide and selumetinib appeared to be at 50 μ M

leflunomide and 0.1 μ M selumetinib. This is seen clearly in the M285 cell line in figure 5.5. Therefore this specific combination of leflunomide and selumetinib indicates that these concentrations could be within the optimal working concentration range for this combination.

5.2.4. Calculation of drug synergy between leflunomide and selumetinib

As a whole, it can be said that these drug-combination cell viability experiments were successful. But the fundamental factor in the success of drug combinatorial approaches is whether the two drugs are acting synergistically or not. One approach of determining drug synergy is by calculating the combination index (CI) values for multiple drug combinations. Software which enables such analysis is the CalcuSyn software based on the T-C Chou and P Talalay method (Chou and Talalay, 1984). Using this software, the cell viability data from the leflunomide and selumetinib experiments was used to generate the CI values for each separate combination of leflunomide and selumetinib (non-constant ratio). This was done for all eight of the melanoma cell lines.

Figure 5.12 represents how to interpret the CI values produced. If a CI value of 1 is given, that drug combination is said to be acting additively (shown in orange). If a CI value higher than 1 is produced, that drug combination is said to acting antagonistically (shown in red). If a CI value of less than 1 is given, that drug combination is said to working synergistically (shown in green). Regarding antagonistic and synergistic values produced, there is scale to the strength of these values. For example, the closer the CI value is to 0, the stronger the synergism. On the other hand, the further away the CI value from 1, the stronger the antagonism.

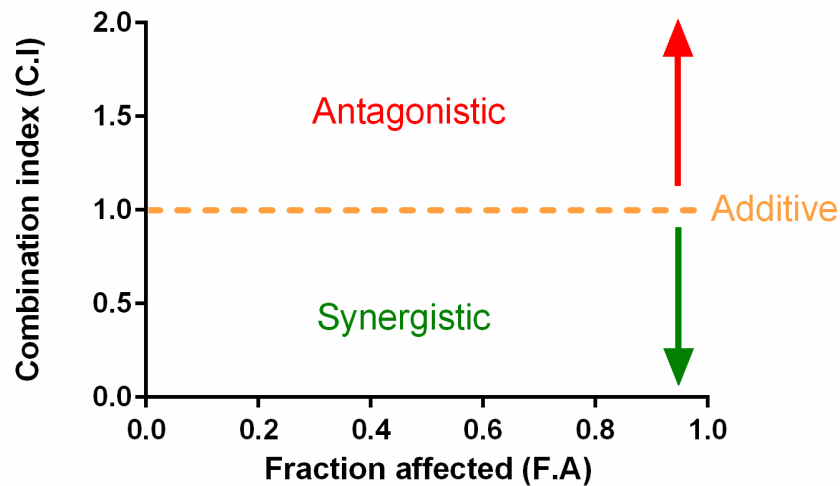
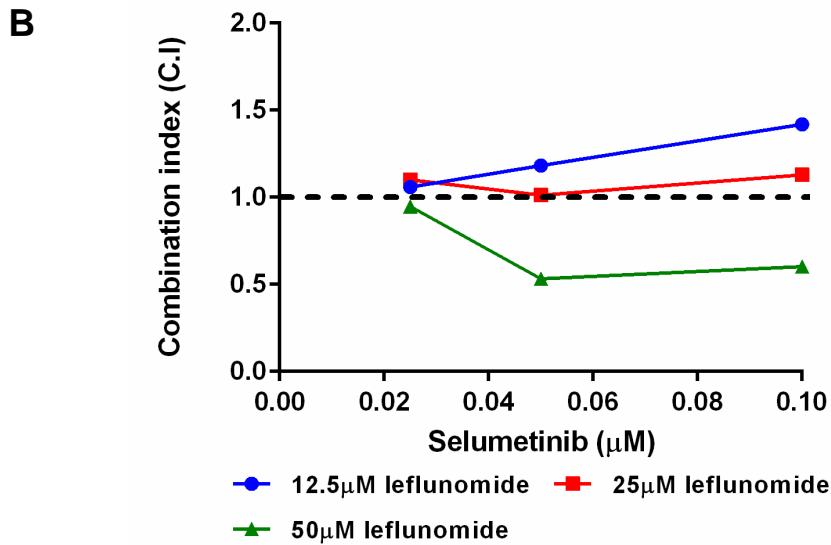
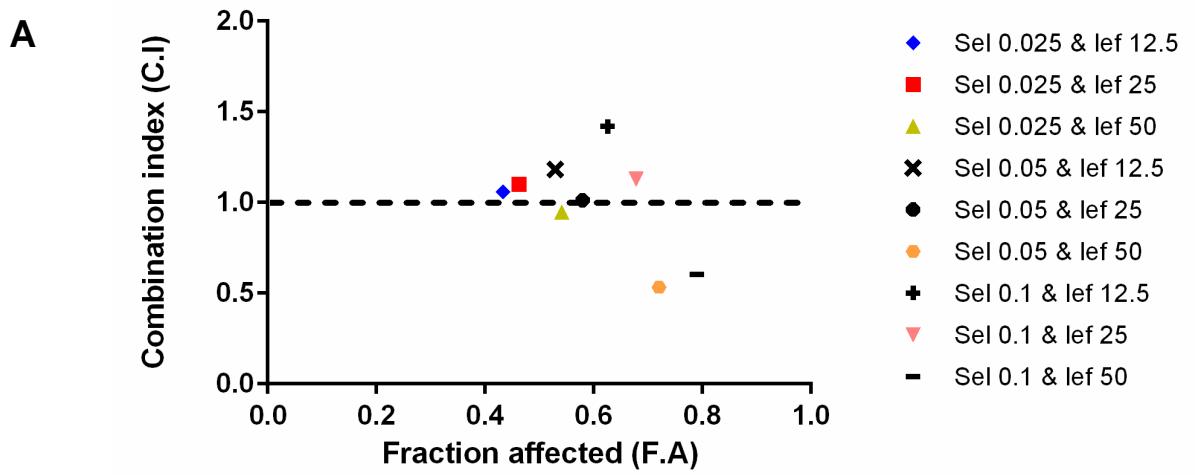


Figure 5.12. A representative graph highlighting how the combination index values are to be interpreted.

For each cell line, two graphs were plotted to represent the synergism data (figures 5.13 to 5.20). The first graph has the same appearance of the graph previously shown in figure 5.12. Along the x-axis is the fraction affected (FA) which corresponds to the cell viability data inputted (i.e. what fraction of the cells were affected/how much of the cell viability was being reduced by this combination of leflunomide and selumetinib). Along the y axis is the CI values. A dotted line was placed across the CI value of 1 to make it easier to see if a particular combination of leflunomide or selumetinib was synergistic or not. The second graph utilises the same CI value data with the CI values again shown along the y axis, but along the x axis is the concentration of selumetinib with the data sets on the graph corresponding to the leflunomide concentrations. This graph was plotted to see if there was any dose dependency of leflunomide or selumetinib on the CI values produced. Under both sets of graphs is a summary table showing the each combination of leflunomide and selumetinib and the CI value given coloured in purple indicating antagonism, orange indicating an additive effect and green indicating synergism.

From the synergism analysis, an initial surprising result was observed with the A375 melanoma cell line (figure 5.17). All of the leflunomide and selumetinib drug combinations produced antagonistic CI values. Given the sound cell viability results seen in figure 5.8 and coupled with the fact that the A375 cells normally respond very well to selumetinib and other MEK inhibitors it was an unexpected result that no synergy was observed with selumetinib and leflunomide. Comparing the A375 and SKmel28 cell viability data (figures 5.8 and 5.10) the A375 cell line was more sensitive to leflunomide and selumetinib and had a greater reduction in cell viability than SKmel28. From this data one could have predicted that the A375 cell line could have produced stronger CI values but in fact SKmel28 gave better CI values (figure 5.19). For all of the leflunomide concentrations in combination with 0.025 and 0.05 μ M selumetinib the CI values were either synergistic or additive. However the CI values at 12.5 μ M leflunomide and 0.025 and 0.05 μ M selumetinib gave the strongest of these synergistic values. These data perhaps highlights that when judging drug synergism, cell viability data should not be the only data to consider.

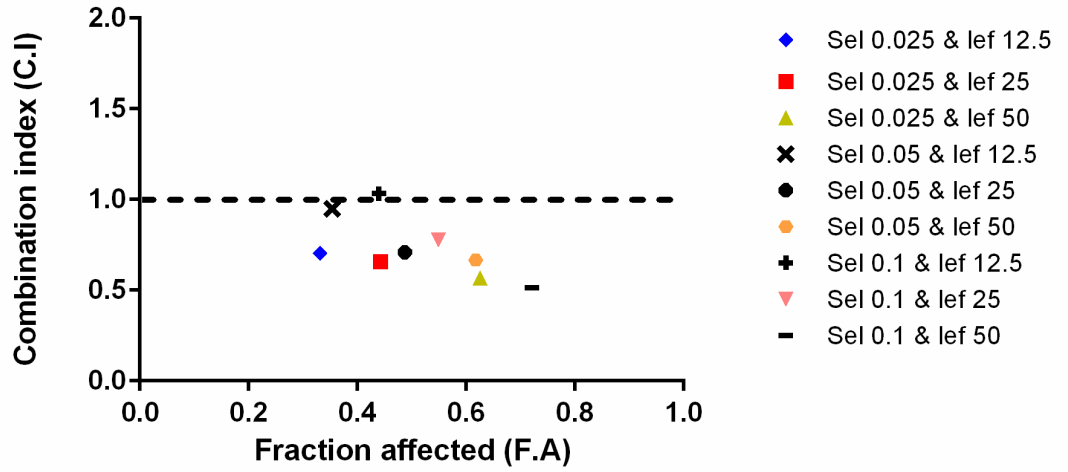


C

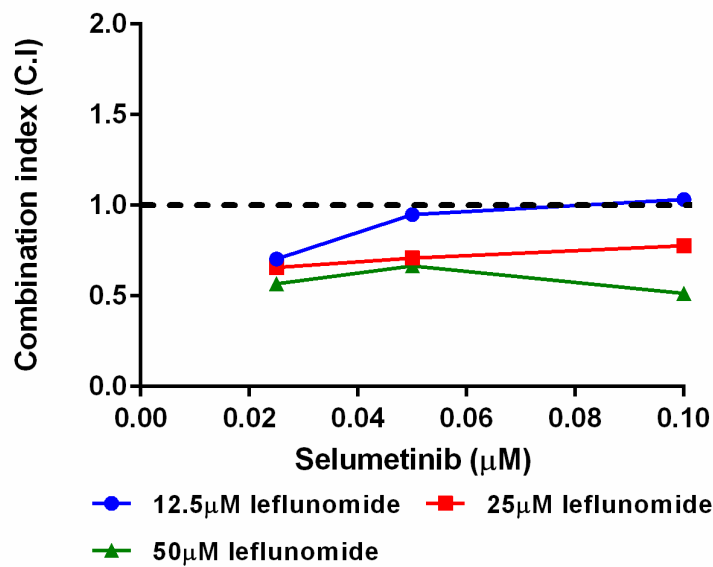
M202 melanoma cell line		
Selumetinib (μM)	Leflunomide (μM)	Combination index
0.025	12.5	1.059
0.05	12.5	1.182
0.1	12.5	1.42
0.025	25	1.1
0.05	25	1.013
0.1	25	1.13
0.025	50	0.947
0.05	50	0.532
0.1	50	0.603

Figure 5.13. Combination index values for M202 melanoma cell line with leflunomide and selumetinib in combination at increasing concentrations. In the table, purple indicates antagonism, orange indicated additive and green indicates synergism.

A



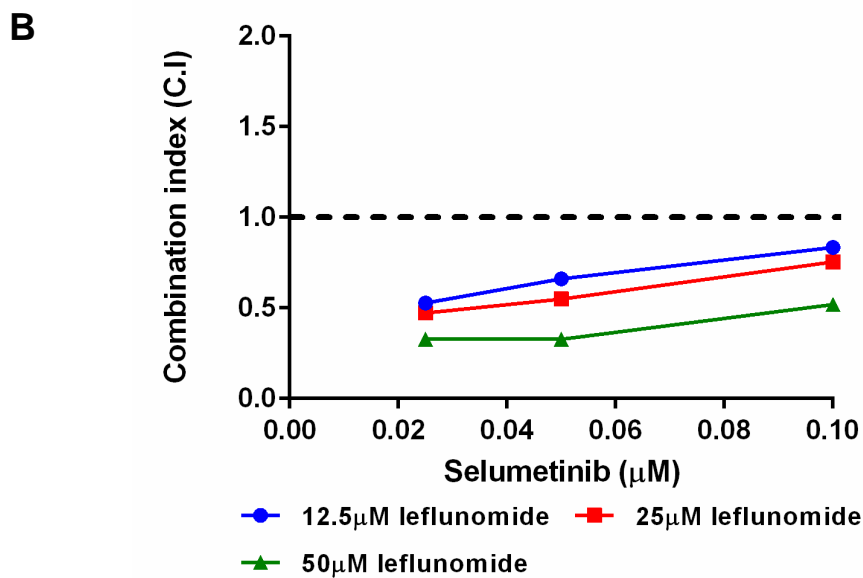
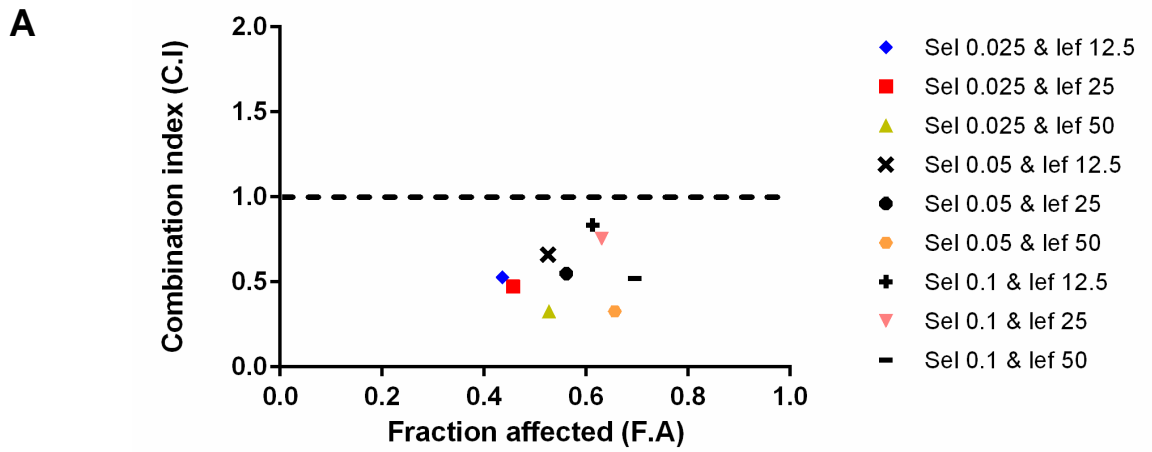
B



C

M285 melanoma cell line		
Selumetinib (μM)	Leflunomide (μM)	Combination index
0.025	12.5	0.704
0.05	12.5	0.95
0.1	12.5	1.033
0.025	25	0.657
0.05	25	0.709
0.1	25	0.777
0.025	50	0.568
0.05	50	0.665
0.1	50	0.515

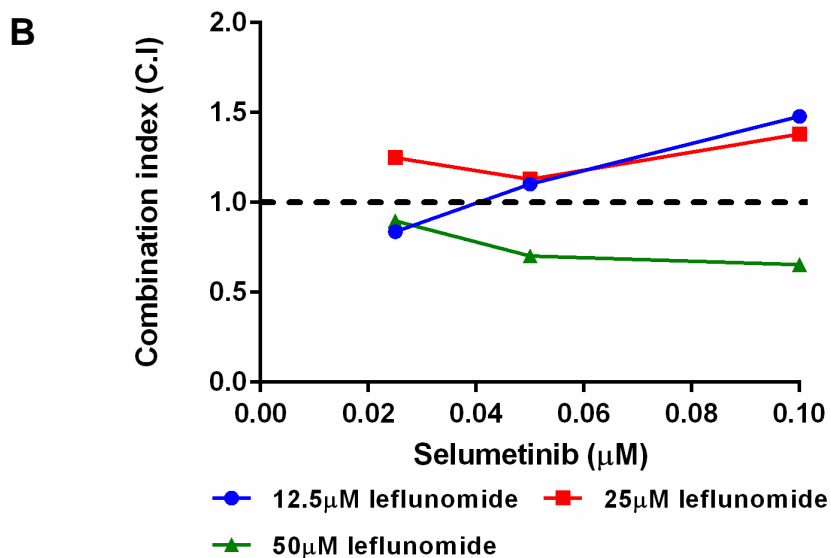
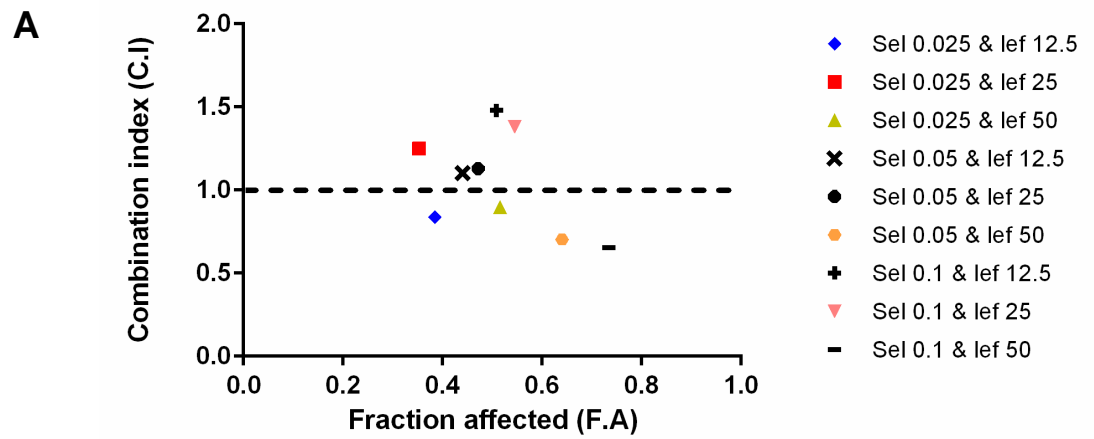
Figure 5.14. Combination index values for M285 melanoma cell line with leflunomide and selumetinib in combination at increasing concentrations. In the table, purple indicates antagonism, orange indicated additive and green indicates synergism.



C

M375 melanoma cell line		
Selumetinib (μM)	Leflunomide (μM)	Combination index
0.025	12.5	0.528
0.05	12.5	0.661
0.1	12.5	0.834
0.025	25	0.473
0.05	25	0.549
0.1	25	0.754
0.025	50	0.328
0.05	50	0.327
0.1	50	0.519

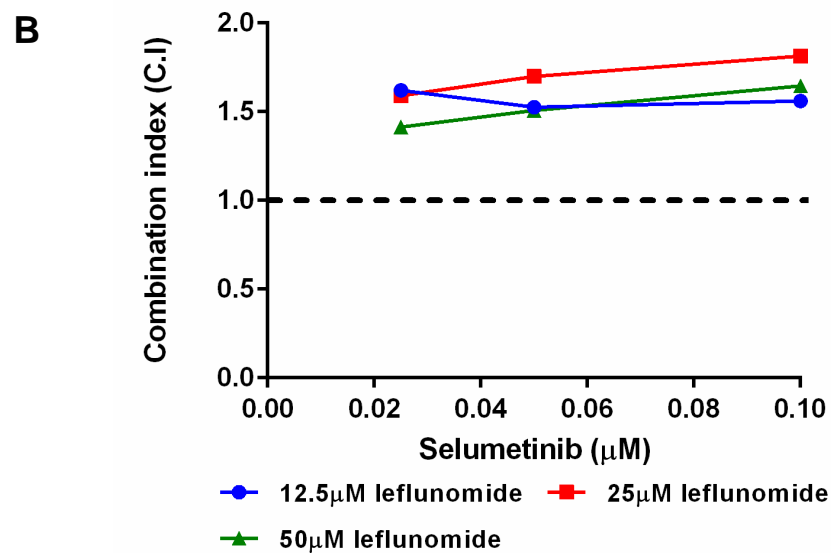
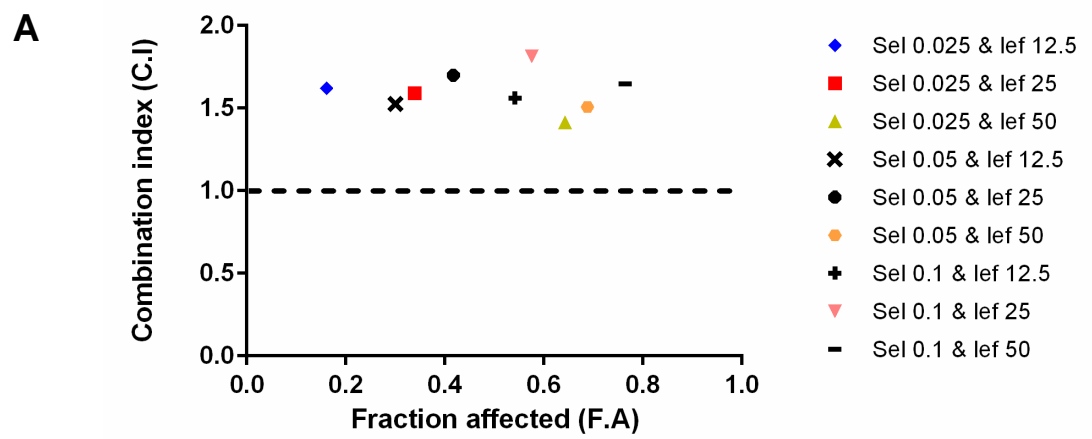
Figure 5.15. Combination index values for M375 melanoma cell line with leflunomide and selumetinib in combination at increasing concentrations. In the table, purple indicates antagonism, orange indicated additive and green indicates synergism.



C

M296 melanoma cell line		
Selumetinib (μM)	Leflunomide (μM)	Combination index
0.025	12.5	0.837
0.05	12.5	1.103
0.1	12.5	1.479
0.025	25	1.249
0.05	25	1.13
0.1	25	1.381
0.025	50	0.897
0.05	50	0.703
0.1	50	0.655

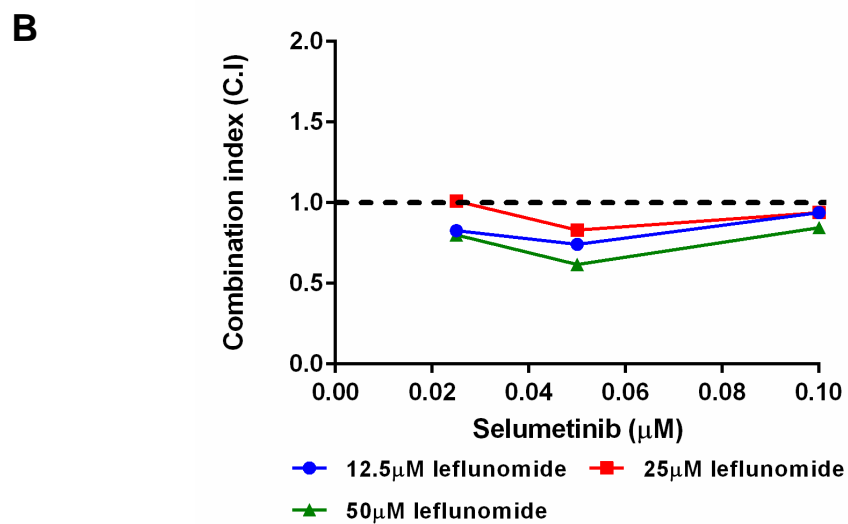
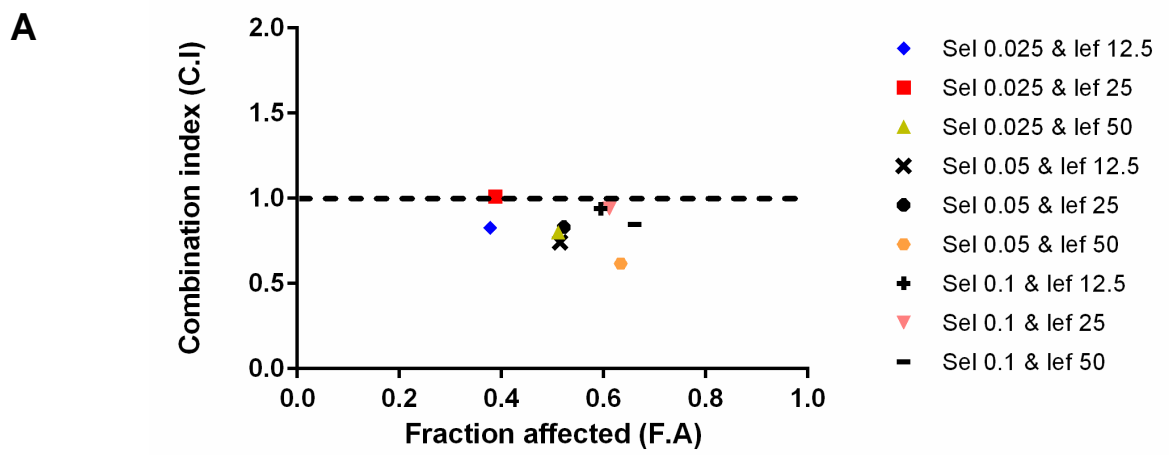
Figure 5.16. Combination index values for M296 melanoma cell line with leflunomide and selumetinib in combination at increasing concentrations. In the table, purple indicates antagonism, orange indicated additive and green indicates synergism.



C

A375 melanoma cell line		
Selumetinib (μM)	Leflunomide (μM)	Combination index
0.025	12.5	1.621
0.05	12.5	1.526
0.1	12.5	1.561
0.025	25	1.59
0.05	25	1.699
0.1	25	1.814
0.025	50	1.414
0.05	50	1.507
0.1	50	1.646

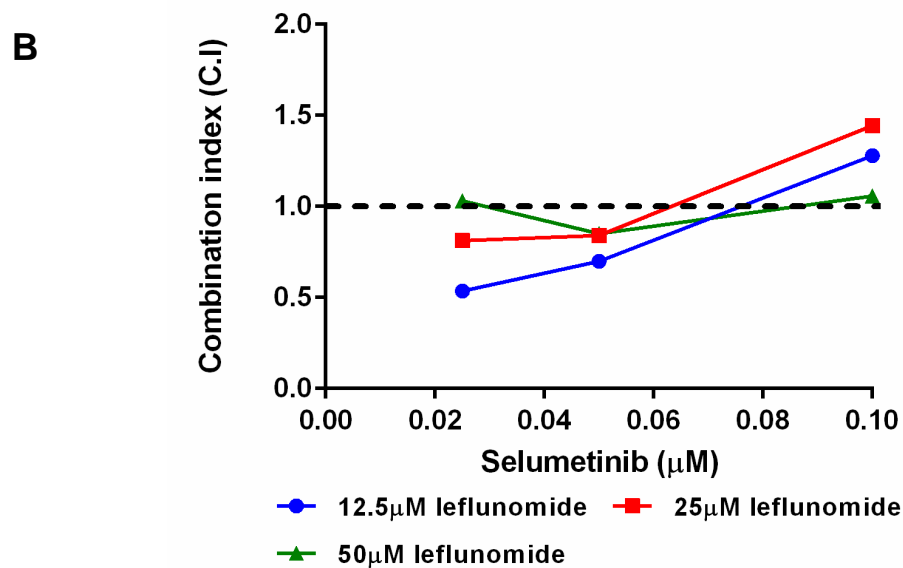
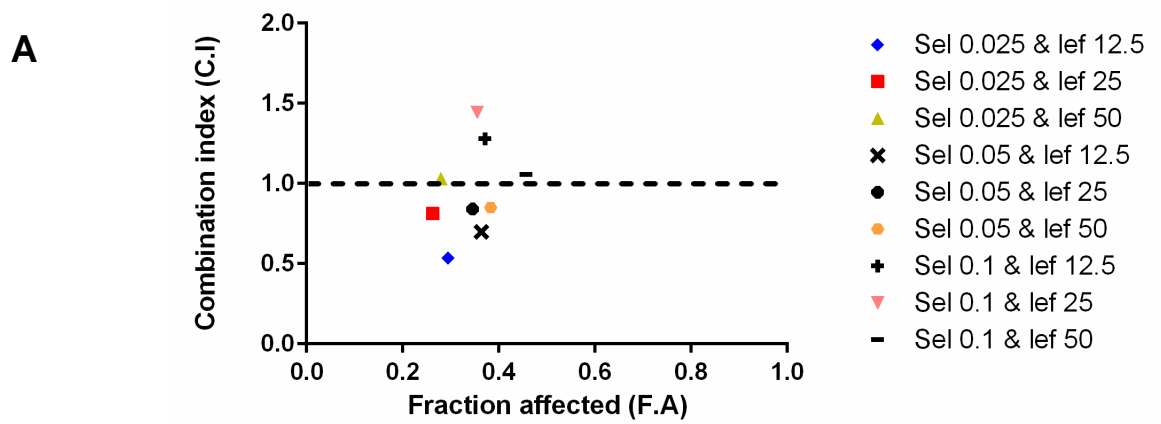
Figure 5.17. Combination index values for A375 melanoma cell line with leflunomide and selumetinib in combination at increasing concentrations. In the table, purple indicates antagonism, orange indicated additive and green indicates synergism.



C

M229 melanoma cell line		
Selumetinib (μM)	Leflunomide (μM)	Combination index
0.025	12.5	0.827
0.05	12.5	0.743
0.1	12.5	0.939
0.025	25	1.011
0.05	25	0.831
0.1	25	0.94
0.025	50	0.801
0.05	50	0.617
0.1	50	0.846

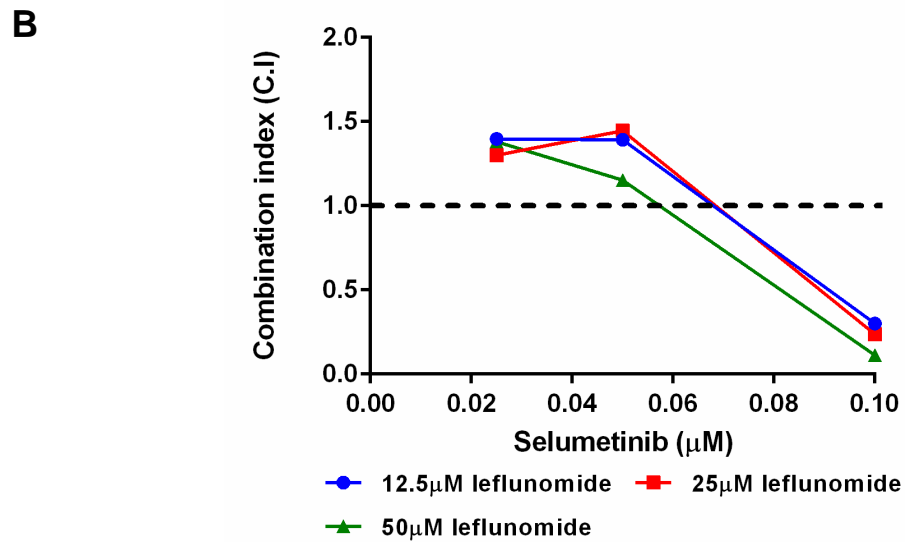
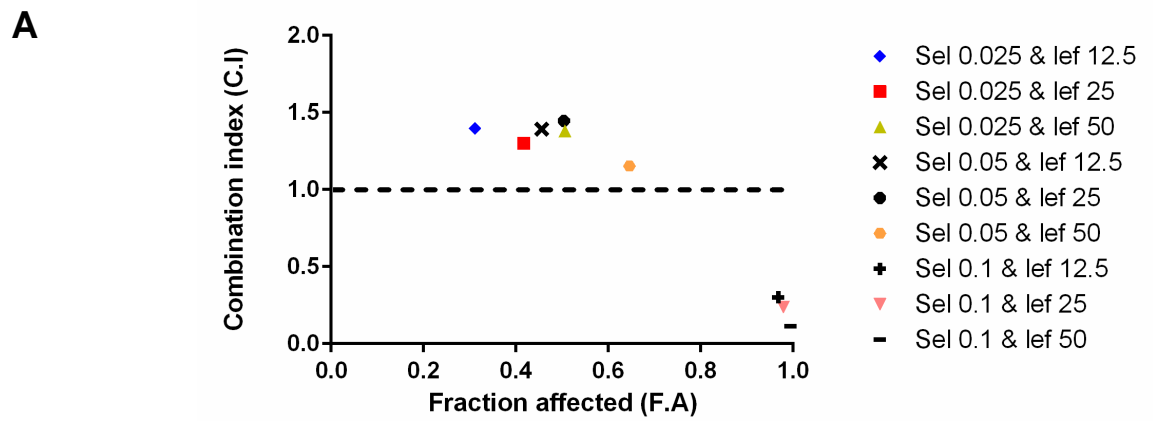
Figure 5.18. Combination index values for M229 melanoma cell line with leflunomide and selumetinib in combination at increasing concentrations. In the table, purple indicates antagonism, orange indicated additive and green indicates synergism.



C

SKmel28 melanoma cell line		
Selumetinib (μM)	Leflunomide (μM)	Combination index
0.025	12.5	0.536
0.05	12.5	0.699
0.1	12.5	1.279
0.025	25	0.812
0.05	25	0.841
0.1	25	1.444
0.025	50	1.031
0.05	50	0.85
0.1	50	1.058

Figure 5.19. Combination index values for SKmel28 melanoma cell line with leflunomide and selumetinib in combination at increasing concentrations. In the table, purple indicates antagonism, orange indicated additive and green indicates synergism.



C

SKmel5 melanoma cell line		
Selumetinib (μM)	Leflunomide (μM)	Combination index
0.025	12.5	1.397
0.05	12.5	1.393
0.1	12.5	0.3
0.025	25	1.301
0.05	25	1.445
0.1	25	0.237
0.025	50	1.381
0.05	50	1.152
0.1	50	0.112

Figure 5.20. Combination index values for SKmel5 melanoma cell line with leflunomide and selumetinib in combination at increasing concentrations. In the table, purple indicates antagonism, orange indicated additive and green indicates synergism.

Table 5.2. Summary of the combination index values for all eight melanoma cell lines

Melanoma cell line	Leflunomide 12.5µM			Leflunomide 25µM			Leflunomide 50µM		
	MEKi 0.025µM	MEKi 0.05µM	MEKi 0.1µM	MEKi 0.025µM	MEKi 0.05µM	MEKi 0.1µM	MEKi 0.025µM	MEKi 0.05µM	MEKi 0.1µM
A375	1.621	1.526	1.561	1.59	1.699	1.814	1.414	1.507	1.646
M375	0.528	0.661	0.834	0.473	0.549	0.754	0.328	0.327	0.519
M296	0.837	1.103	1.479	1.249	1.13	1.381	0.897	0.703	0.655
M202	1.059	1.182	1.42	1.1	1.013	1.13	0.947	0.532	0.603
M229	0.827	0.743	0.939	1.011	0.831	0.94	0.801	0.617	0.846
M285	0.704	0.95	1.033	0.657	0.709	0.777	0.568	0.665	0.515
SKMEL28	0.536	0.699	1.279	0.812	0.841	1.444	1.031	0.85	1.058
SKMEL 5	1.397	1.393	0.3	1.301	1.445	0.237	1.381	1.152	0.112

A cell line which gave promising CI values was the M375 cell line (figure 5.15). This cell line produced all synergistic CI values for all of the combinations of leflunomide and selumetinib. The second graph in figure 5.15 clearly shows this cell line exhibited a clear trend in that the CI values got stronger as the concentrations of leflunomide increased. It is also apparent that the CI values were enhanced when leflunomide was in combination with 0.025 μ M selumetinib. For example at 12.5 μ M leflunomide and 0.025 μ M selumetinib, the CI value was 0.528. This CI value increased in synergism to a value of 0.473 when cells were treated with 0.025 μ M selumetinib and 25 μ M leflunomide. Again, this CI became even stronger at 0.025 μ M selumetinib with 50 μ M leflunomide with a value of 0.327.

A cell line which displayed a completely unique trend was the SKmel5 cell line (figure 5.20). Out of all the CI values produced, this cell line gave the strongest synergistic CI values, but only when leflunomide was in combination with 0.1 μ M selumetinib (figure 5.20). At 0.1 μ M selumetinib and 12.5 μ M leflunomide the CI value produced was 0.3, which became more synergistic at 0.237 when the leflunomide concentration increased to 25 μ M. At 0.1 μ M selumetinib and 50 μ M leflunomide a remarkable CI value of 0.112 was given, the strongest synergistic CI value observed from this entire analysis. However the remainder of the leflunomide and selumetinib combinations for this cell line gave antagonistic CI values.

A summary of the CI values can be seen in table 5.2. What is prominent is that the majority of the synergistic values were obtained at the highest concentration of leflunomide, 50 μ M. However the effect of the concentration of selumetinib is not as clear cut. For example at 0.025 μ M selumetinib and 50 μ M leflunomide, the strongest synergistic CI value was observed with the M375 cell line. In comparison this same combination gave rise to an antagonistic CI value in the SKmel5 cell. It is also worth noting that the M285 and M229 also both gave all synergistic CI values for all of the leflunomide

and selumetinib concentrations bar one combination each. Overall, the M285 cell line gave stronger synergistic CI values in comparison to the M229 cell line. The strongest CI value for M285 and M229 was 0.515 at 50 μ M leflunomide and 0.1 μ M selumetinib and 0.617 at 50 μ M leflunomide and 0.05 μ M selumetinib respectively. The difference in trends observed across the eight melanoma cell lines would imply that the effect of the different combination of leflunomide and selumetinib and the resulting CI value differs for each cell line.

5.2.5. Pre-treatment of the melanoma cells for 24 hours with leflunomide or selumetinib cell viability assays

Previous experiments showed the synergy calculated in which leflunomide and selumetinib drug combinations were added at the same time. However, could this synergy alter if the cells were pre-treated for 24 hours with leflunomide or selumetinib? Results from clinical trials testing the combined effect of immunotherapy and a BRAF inhibitor have implied that this combination is more efficacious administering ipilimumab prior to a BRAF inhibitor to patients. This speculated the idea whether 24 hour pre-treatment with leflunomide or selumetinib would alter the efficacy of these two drugs in terms of the outcome from synergy analysis. For example, given that MEK inhibitors are known to cause cells to arrest in G1 of the cell cycle could 24 hour pre-treatment with selumetinib sensitise the cells more to the cytotoxic effects observed with leflunomide? Therefore would this alter the strength in synergism observed?

The next set of experiments were carried out on four of the eight melanoma cell lines; A375, M229, M285 and M375. The cell viability data will be presented first, with the subsequent synergy analysis after. The cell viability data will only be touched upon as the synergy analysis is the main focus of these experiments.

The cell viability data for the A375 cell line (figures 5.21 and 5.22) showed no major differences in pre-treating the cells for 24 hours with leflunomide or selumetinib. If any difference is to be noted, it would be that pre-treating with selumetinib fractionally reduced cell viability more. For example, the combination of 50 μ M leflunomide and 0.1 μ M selumetinib the cell viability was reduced to 42.76% and 36% when cells were pre-treated with leflunomide and selumetinib respectively. But to emphasize this difference was very marginal. A similar trend was observed in the M229 cell line (figures 5.23 and 5.24). At 50 μ M leflunomide and 0.1 μ M selumetinib the cell viability was reduced to 54% and 51% when cells were pre-treated with leflunomide and selumetinib respectively. At this highest concentration of the combination of drugs, there is no obvious difference. However, at 25 μ M leflunomide and 0.1 μ M selumetinib, the cell viability reduced from 73% to 60.39% which was a more noticeable difference.

A cell line which showed a clear difference in pre-treating for 24 hours with either leflunomide or selumetinib was the M375 cell line. This cell line exhibited a greater reduction in cell viability when pre-treated with selumetinib in comparison to pre-treated with leflunomide (figures 5.25 and 5.26). For all three of the combinations of leflunomide and selumetinib tested the reduction in cell viability was greater when pre-treated with selumetinib than leflunomide. At 12.5 μ M leflunomide and 0.1 μ M selumetinib, the cell viability decreased from 60.99% to 50.28% when pre-treated with leflunomide and selumetinib respectively. Similarly at 50 μ M leflunomide and 0.1 μ M selumetinib, pre-treated cells with leflunomide caused a 44.71% reduction in cell viability. Whereas cells pre-treated with selumetinib caused a 29.76% reduction in cell viability.

The M285 cell line however responded to the pre-treatments different to all of the other three cell lines. The M285 cell line was more sensitive to the leflunomide pre-treatment than selumetinib (figures 5.27 and 5.28). At 25 μ M

leflunomide and 0.1 μ M selumetinib viability reduced to 49.15% in leflunomide pre-treated cells. In comparison the viability in selumetinib pre-treated cells reduced to just 63.54%. Equally, at 50 μ M leflunomide and 0.1 μ M selumetinib the cell viability reduced to 27% and 52.05% in leflunomide and selumetinib pre-treated cells respectively.

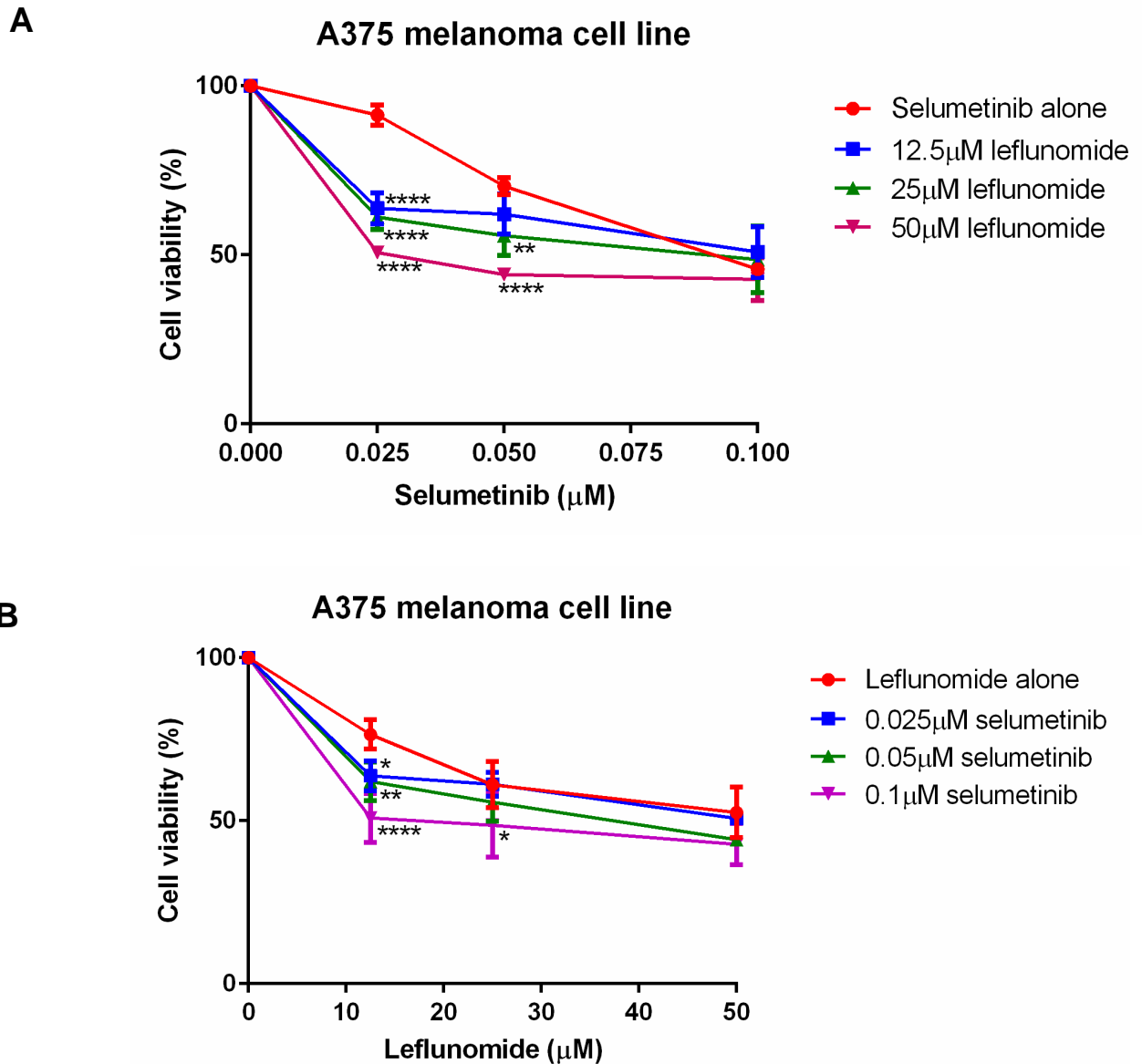


Figure 5.21. Sensitivity of the A375 melanoma cell line with pre-treatment for 24 hours with leflunomide, prior to the addition of selumetinib. Graph A displays selumetinib concentrations along the x-axis. Statistical analysis on this graph compares the drug combinations to selumetinib alone. Graph B shows the concentrations of leflunomide along the x-axis. The statistical analysis on this graph compares the drug combinations to leflunomide alone. Cell viability was determined by using CellTiter-Glo reagent and all values are represented as a percentage (%) relative to the vehicle control. Data is presented as the mean \pm SEM of three independent experiments each performed with cell culture triplicate. Asterisks indicate the degree of statistical difference comparing each leflunomide and selumetinib condition to leflunomide alone (graph A) or selumetinib alone (graph B). Statistical analysis was determined by two-way ANOVA with Turkey's post-hoc test. * $P \leq 0.05$, ** $P \leq 0.01$, *** $P \leq 0.001$ and **** $P \leq 0.0001$.

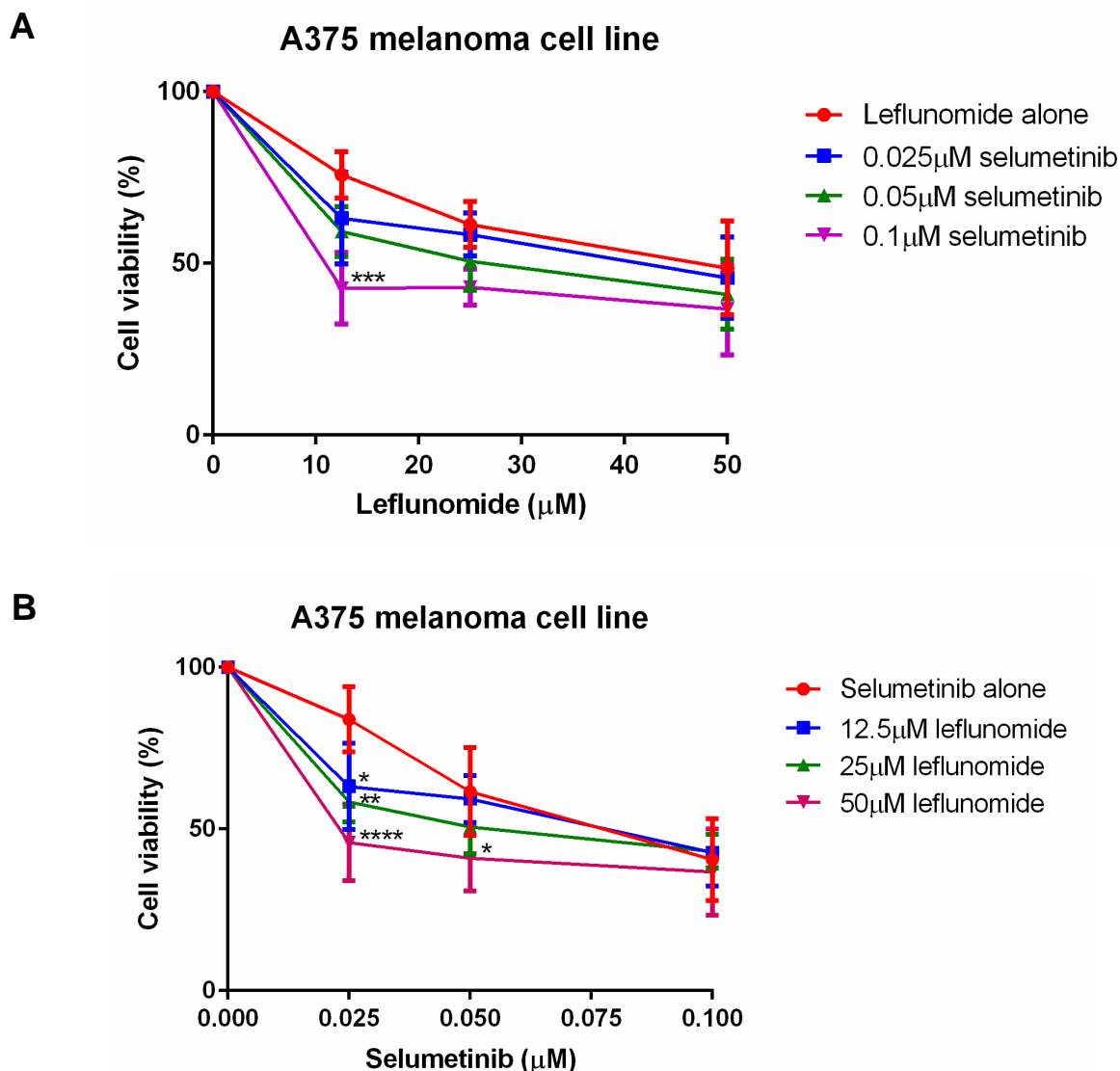


Figure 5.22. Sensitivity of the A375 melanoma cell line with pre-treatment for 24 hours with selumetinib, prior to the addition of leflunomide. Graph A displays selumetinib concentrations along the x-axis. Statistical analysis on this graph compares the drug combinations to selumetinib alone. Graph B shows the concentrations of leflunomide along the x-axis. The statistical analysis on this graph compares the drug combinations to leflunomide alone. Cell viability was determined by using CellTiter-Glo reagent and all values are represented as a percentage (%) relative to the vehicle control. Data is presented as the mean \pm SEM of three independent experiments each performed with cell culture triplicate. Asterisks indicate the degree of statistical difference comparing each leflunomide and selumetinib condition to leflunomide alone (graph A) or selumetinib alone (graph B). Statistical analysis was determined by two-way ANOVA with Turkey's post-hoc test. * $P \leq 0.05$, ** $P \leq 0.01$, *** $P \leq 0.001$ and **** $P \leq 0.0001$.

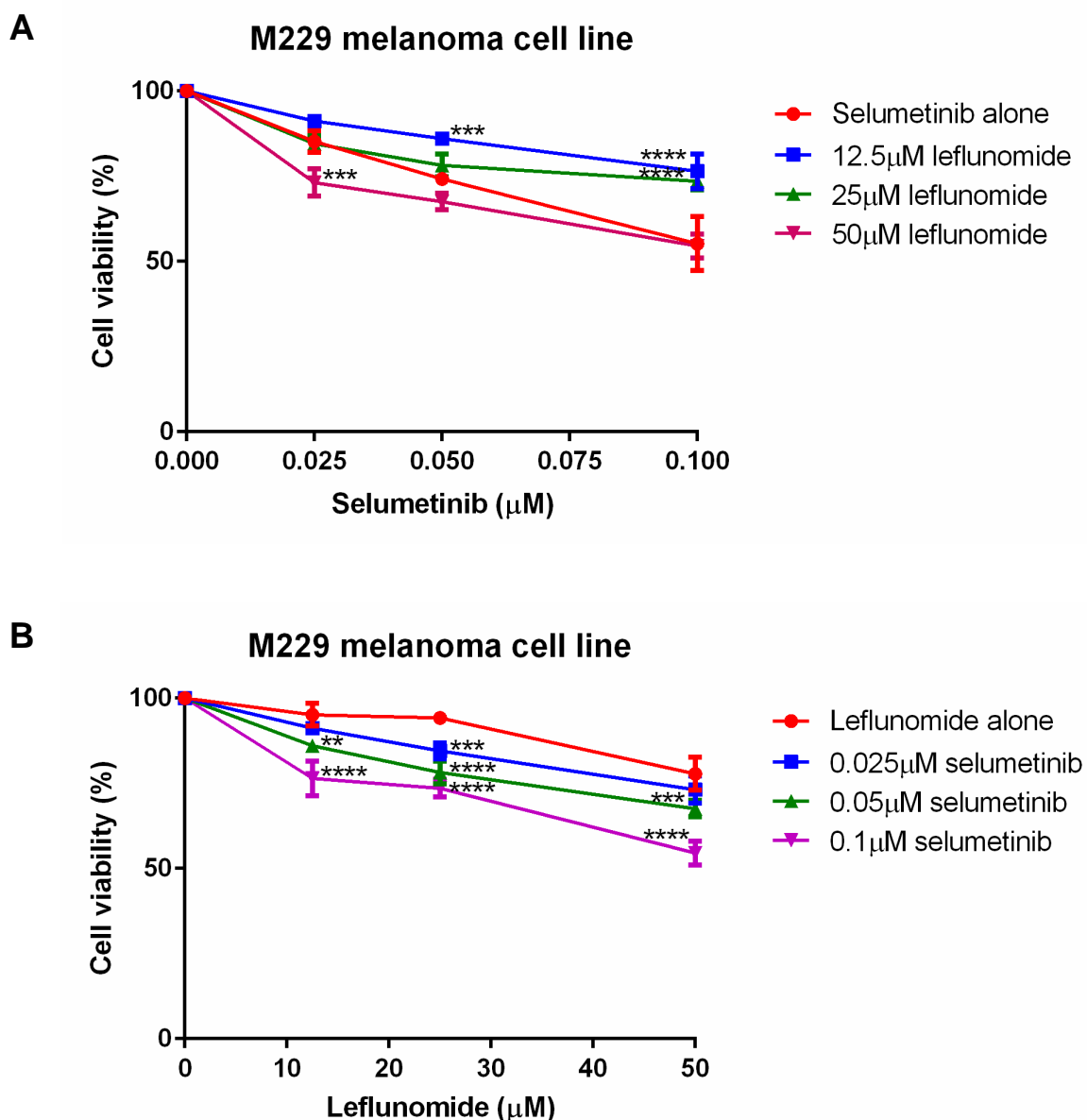


Figure 5.23. Sensitivity of the M229 melanoma cell line with pre-treatment for 24 hours with leflunomide, prior to the addition of selumetinib. Graph A displays selumetinib concentrations along the x-axis. Statistical analysis on this graph compares the drug combinations to selumetinib alone. Graph B shows the concentrations of leflunomide along the x-axis. The statistical analysis on this graph compares the drug combinations to leflunomide alone. Cell viability was determined by using CellTiter-Glo reagent and all values are represented as a percentage (%) relative to the vehicle control. Data is presented as the mean \pm SEM of three independent experiments each performed with cell culture triplicate. Asterisks indicate the degree of statistical difference comparing each leflunomide and selumetinib condition to leflunomide alone (graph A) or selumetinib alone (graph B). Statistical analysis was determined by two-way ANOVA with Turkey's post-hoc test. * $P \leq 0.05$, ** $P \leq 0.01$, *** $P \leq 0.001$ and **** $P \leq 0.0001$.

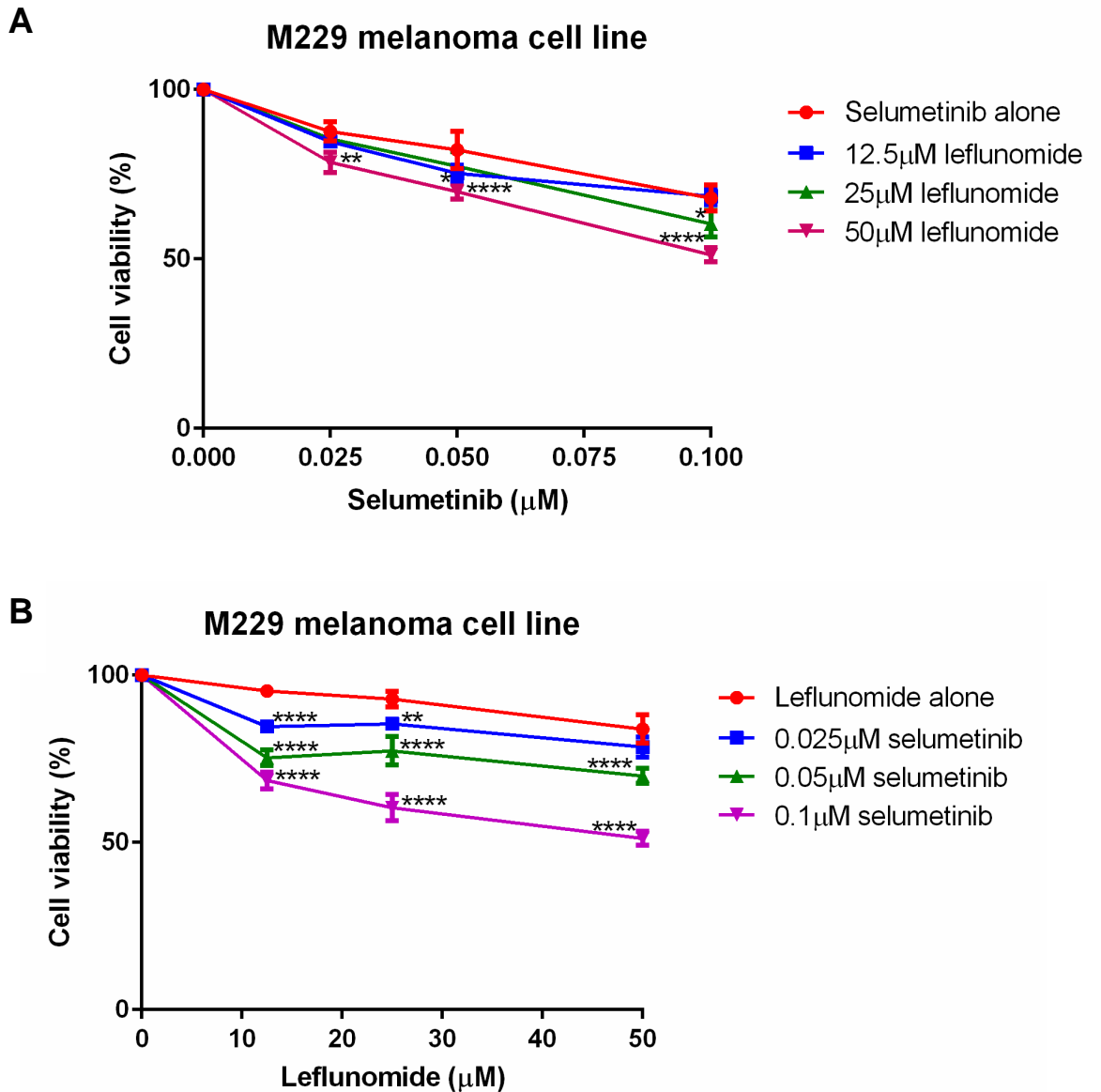


Figure 5.24. Sensitivity of the M229 melanoma cell line with pre-treatment for 24 hours with selumetinib, prior to the addition of leflunomide. Graph A displays selumetinib concentrations along the x-axis. Statistical analysis on this graph compares the drug combinations to selumetinib alone. Graph B shows the concentrations of leflunomide along the x-axis. The statistical analysis on this graph compares the drug combinations to leflunomide alone. Cell viability was determined by using CellTiter-Glo reagent and all values are represented as a percentage (%) relative to the vehicle control. Data is presented as the mean \pm SEM of three independent experiments each performed with cell culture triplicate. Asterisks indicate the degree of statistical difference comparing each leflunomide and selumetinib condition to leflunomide alone (graph A) or selumetinib alone (graph B). Statistical analysis was determined by two-way ANOVA with Turkey's post-hoc test. * $P \leq 0.05$, ** $P \leq 0.01$, *** $P \leq 0.001$ and **** $P \leq 0.0001$.

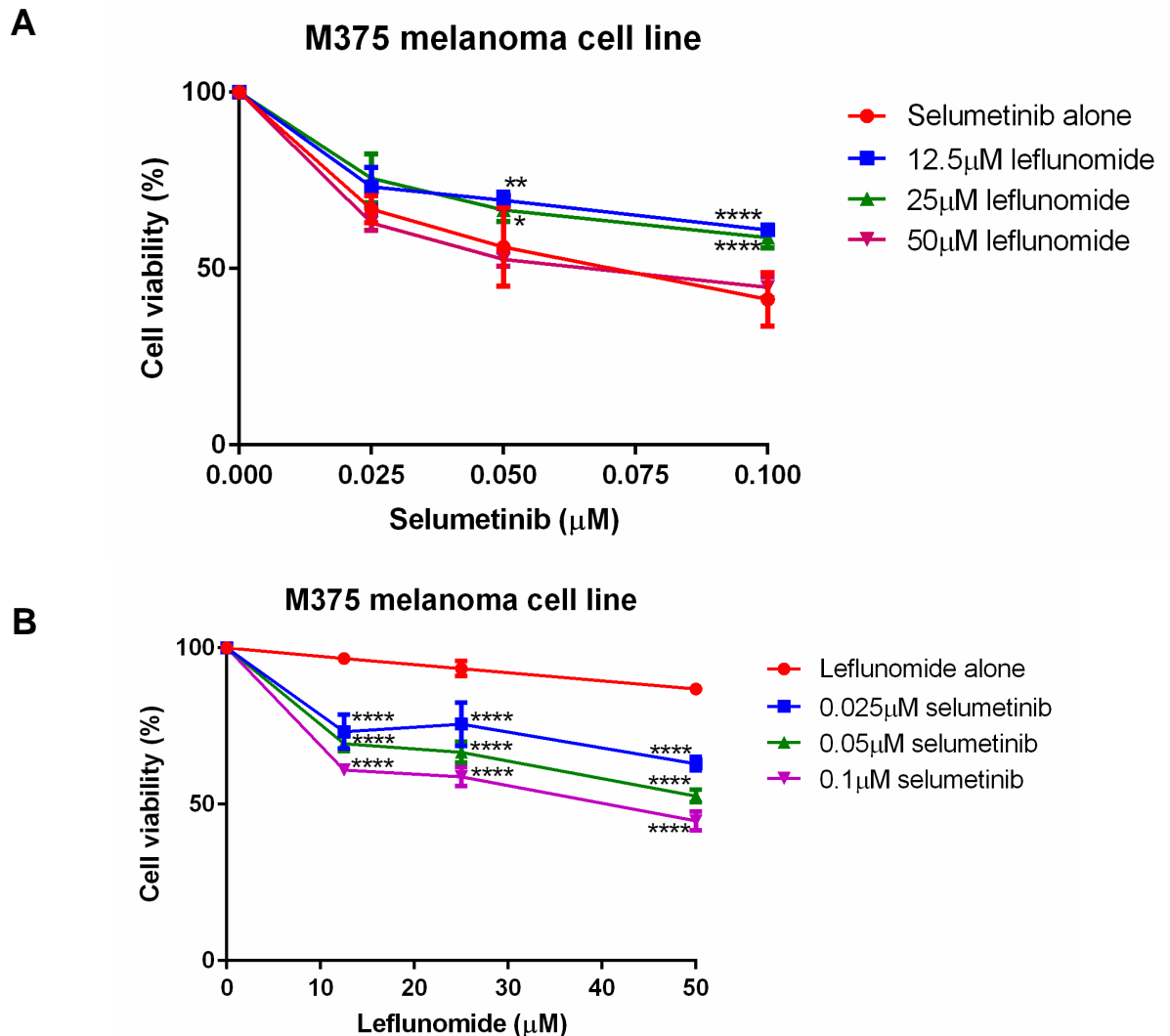


Figure 5.25. Sensitivity of the M375 melanoma cell line with pre-treatment for 24 hours with leflunomide, prior to the addition of selumetinib. Graph A displays selumetinib concentrations along the x-axis. Statistical analysis on this graph compares the drug combinations to selumetinib alone. Graph B shows the concentrations of leflunomide along the x-axis. The statistical analysis on this graph compares the drug combinations to leflunomide alone. Cell viability was determined by using CellTiter-Glo reagent and all values are represented as a percentage (%) relative to the vehicle control. Data is presented as the mean \pm SEM of three independent experiments each performed with cell culture triplicate Asterisks indicate the degree of statistical difference comparing each leflunomide and selumetinib condition to leflunomide alone (graph A) or selumetinib alone (graph B). Statistical analysis was determined by two-way ANOVA with Turkey's post-hoc test. * $P \leq 0.05$, ** $P \leq 0.01$, *** $P \leq 0.001$ and **** $P \leq 0.0001$.

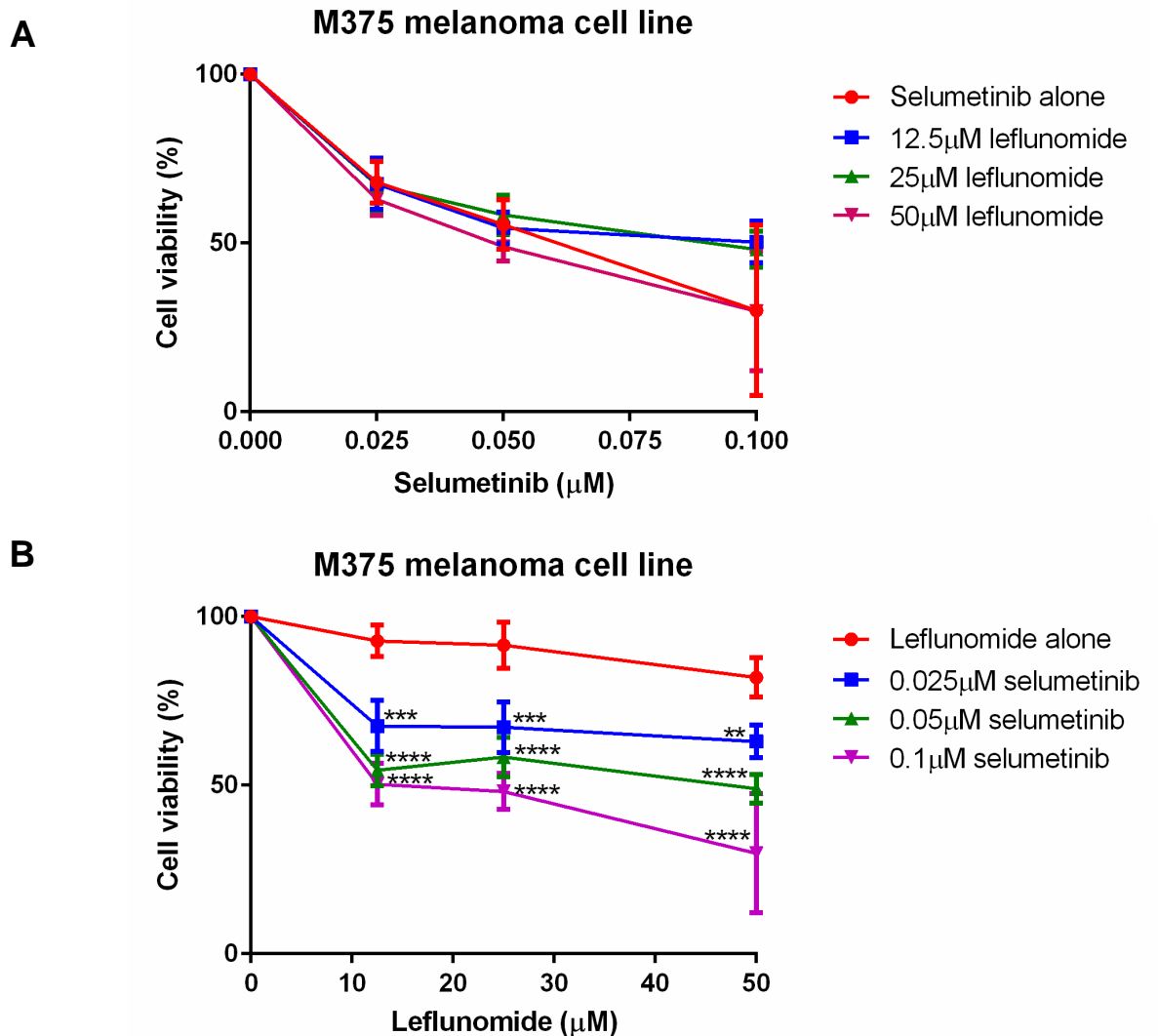


Figure 5.26. Sensitivity of the M375 melanoma cell line with pre-treatment for 24 hours with selumetinib, prior to the addition of leflunomide. Graph A displays selumetinib concentrations along the x-axis. Statistical analysis on this graph compares the drug combinations to selumetinib alone. Graph B shows the concentrations of leflunomide along the x-axis. The statistical analysis on this graph compares the drug combinations to leflunomide alone. Cell viability was determined by using CellTiter-Glo reagent and all values are represented as a percentage (%) relative to the vehicle control. Data is presented as the mean \pm SEM of three independent experiments each performed with cell culture triplicate. Asterisks indicate the degree of statistical difference comparing each leflunomide and selumetinib condition to leflunomide alone (graph A) or selumetinib alone (graph B). Statistical analysis was determined by two-way ANOVA with Turkey's post-hoc test. * $P \leq 0.05$, ** $P \leq 0.01$, *** $P \leq 0.001$ and **** $P \leq 0.0001$.

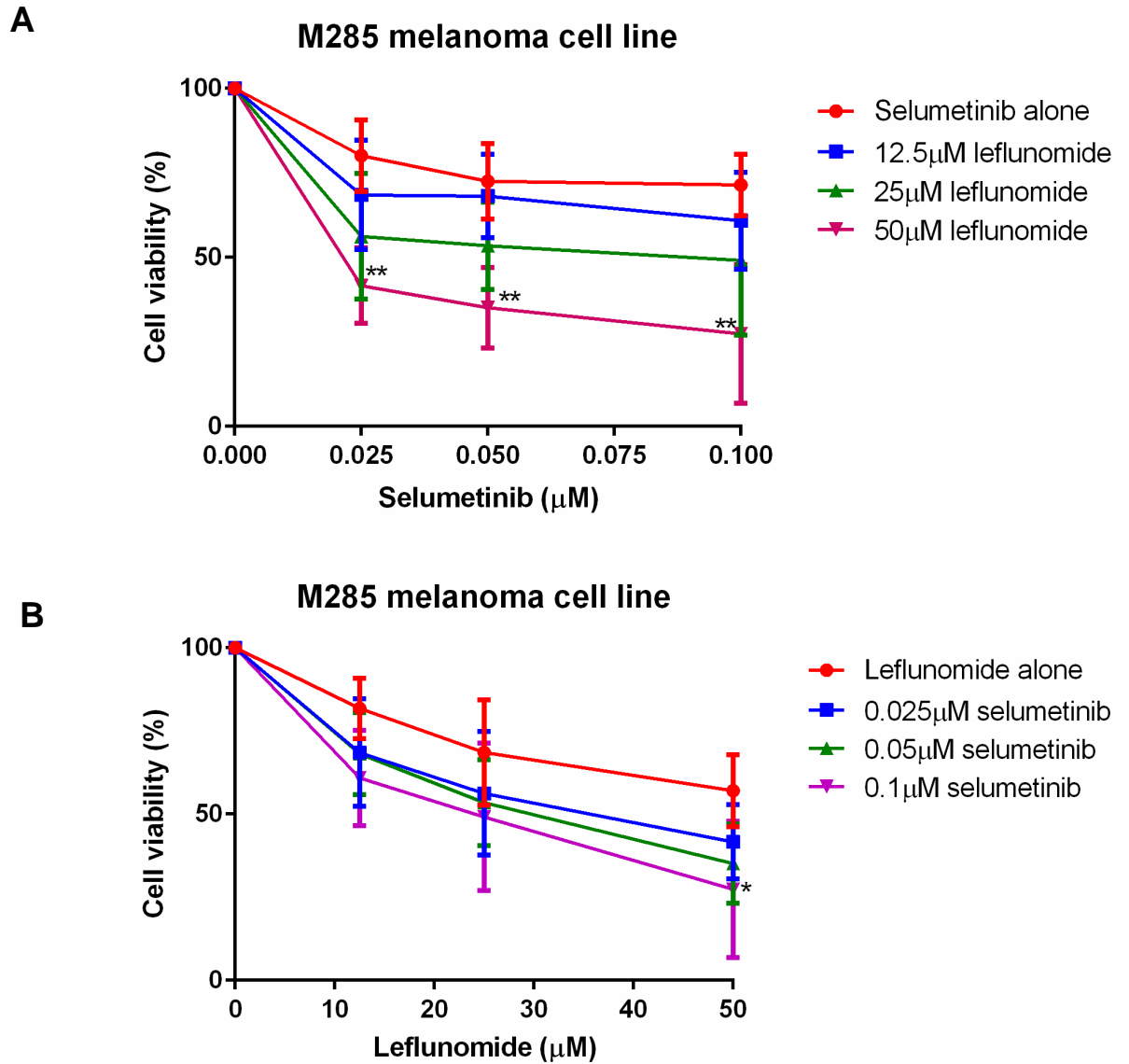


Figure 5.27. Sensitivity of the M285 melanoma cell line with pre-treatment for 24 hours with leflunomide, prior to the addition of selumetinib. Graph A displays selumetinib concentrations along the x-axis. Statistical analysis on this graph compares the drug combinations to selumetinib alone. Graph B shows the concentrations of leflunomide along the x-axis. The statistical analysis on this graph compares the drug combinations to leflunomide alone. Cell viability was determined by using CellTiter-Glo reagent and all values are represented as a percentage (%) relative to the vehicle control. Data is presented as the mean \pm SEM of three independent experiments each performed with cell culture triplicate. Asterisks indicate the degree of statistical difference comparing each leflunomide and selumetinib condition to leflunomide alone (graph A) or selumetinib alone (graph B). Statistical analysis was determined by two-way ANOVA with Turkey's post-hoc test. * $P \leq 0.05$, ** $P \leq 0.01$, *** $P \leq 0.001$ and **** $P \leq 0.0001$.

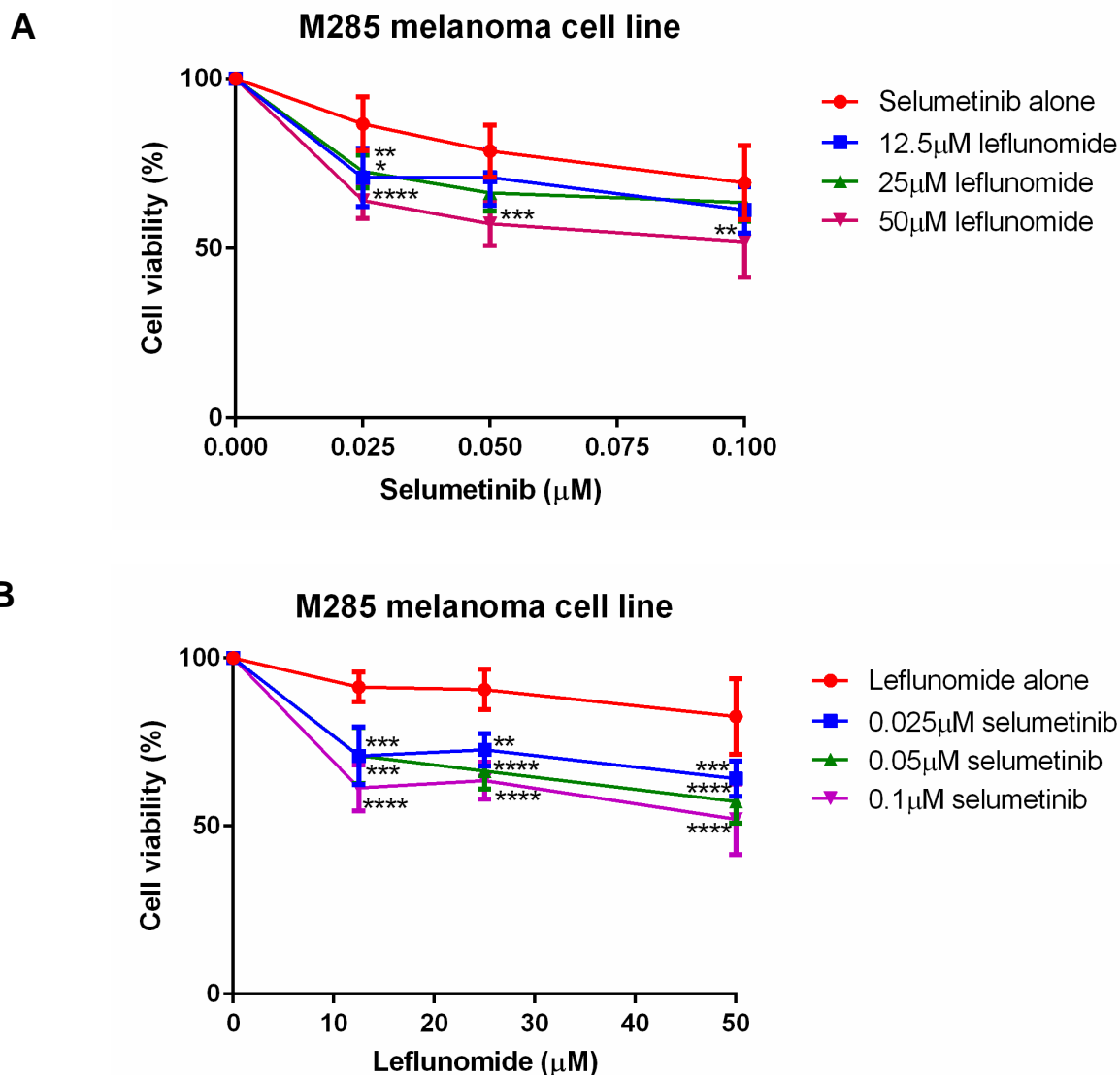


Figure 5.28. Sensitivity of the M285 melanoma cell line with pre-treatment for 24 hours with selumetinib, prior to the addition of leflunomide. Graph A displays selumetinib concentrations along the x-axis. Statistical analysis on this graph compares the drug combinations to selumetinib alone. Graph B shows the concentrations of leflunomide along the x-axis. The statistical analysis on this graph compares the drug combinations to leflunomide alone. Cell viability was determined by using CellTiter-Glo reagent and all values are represented as a percentage (%) relative to the vehicle control. Data is presented as the mean \pm SEM of three independent experiments each performed with cell culture triplicate. Asterisks indicate the degree of statistical difference comparing each leflunomide and selumetinib condition to leflunomide alone (graph A) or selumetinib alone (graph B). Statistical analysis was determined by two-way ANOVA with Turkey's post-hoc test. * $P \leq 0.05$, ** $P \leq 0.01$, *** $P \leq 0.001$ and **** $P \leq 0.0001$.

5.2.6. Pre-treatment of the melanoma cells for 24 hours with leflunomide or selumetinib and calculation of drug synergy

The main goal of these sets of experiments was to determine if the synergy altered with either leflunomide or selumetinib pre-treatment. Synergy analysis was carried out, with the results clearly seen in figures 5.29 to 5.36. For the A375 cell line (figures 5.29 and 5.30), all but two drug combinations remained antagonistic. At 12.5 μ M leflunomide and 0.025 μ M selumetinib for both leflunomide and selumetinib pre-treatments, now produced synergistic values. However these CI values of 0.88363 and 0.9167 for leflunomide and selumetinib respectively, are still closer to 1 than 0, thus are classed as not strong synergy values and are close to becoming additive. Comparing leflunomide and selumetinib pre-treatments all bar two drug combinations, the selumetinib pre-treatment produced better CI values, even if they were still antagonistic.

Regarding the M229 cell line (figures 5.31 and 5.32) leflunomide pre-treatment produced all antagonistic CI values. In comparison, selumetinib pre-treatment produced a mixture of synergistic and antagonistic CI values. However three of the synergistic combination index values produced were not as strong as when leflunomide and selumetinib were added to the cells at the same time. For example at 50 μ M leflunomide and 0.05 μ M selumetinib the CI for when the two drugs were added at the same time was 0.617. However, when the cells were pre-treated with selumetinib the CI increased to 0.92337.

For the M375 melanoma cell line, it is evident that all bar one drug combinations in the leflunomide pre-treated cells now produced antagonistic CI values. These CI values are markedly worse compared with when leflunomide and selumetinib were added at the same time. For example, when added together 12.5 μ M leflunomide and 0.1 μ M selumetinib produced a CI value of 0.834 which dramatically increased to 2.83633. Although

selumetinib pre-treatment did not produce as many antagonistic CI values as leflunomide pre-treatment, ultimately none improved the synergy values.

On the other hand, M285 cell line responded very well to both the leflunomide and selumetinib pre-treatments and as a result, enhanced all of the CI values. The most noticeable enhancements were seen with 50 μ M leflunomide. For example at 50 μ M leflunomide and 0.05 μ M selumetinib the CI was 0.665 when added at the same. When the cells were pre-treated with leflunomide or selumetinib, the CI value decreased to 0.38382 and 0.34852 respectively. This decrease in a CI value indicates stronger synergism.

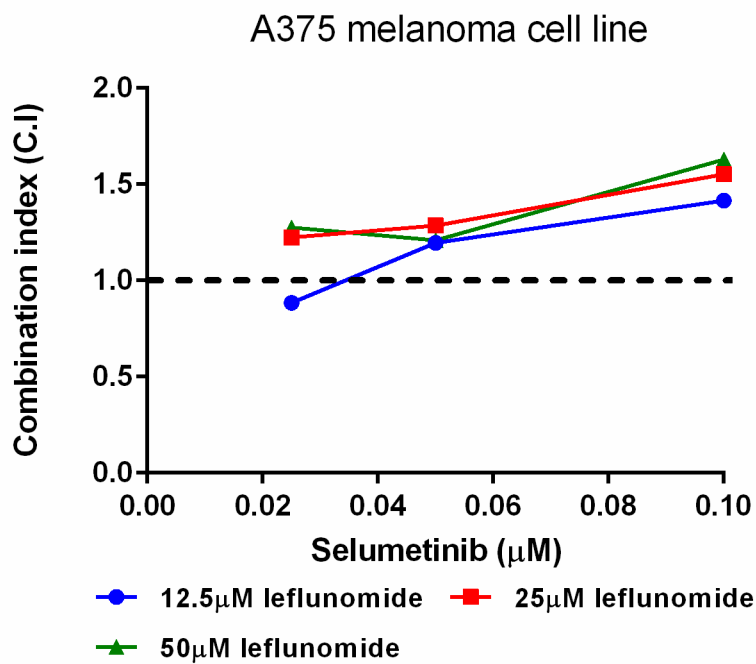
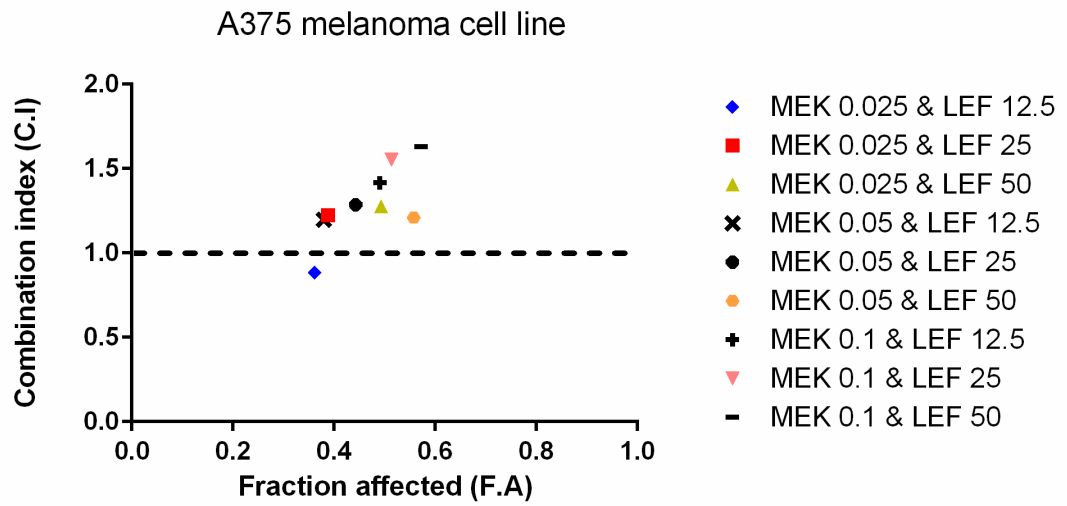
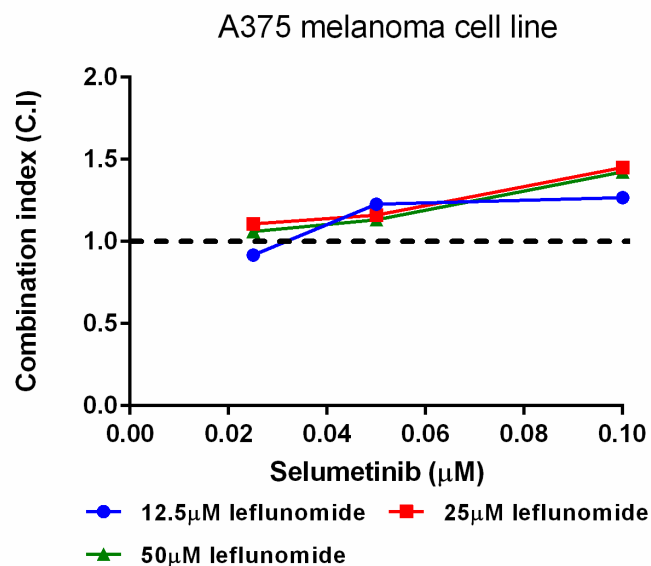
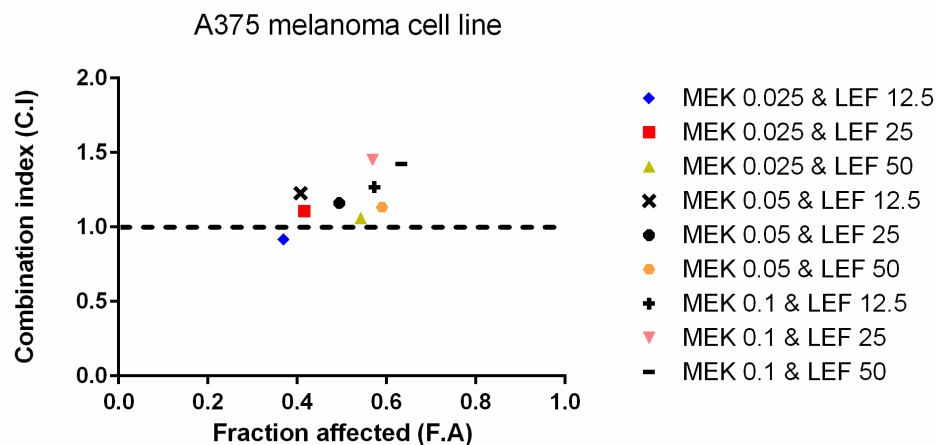


Figure 5.29. Combination index values for the A375 melanoma cell line with pre-treatment for 24 hours with leflunomide, prior to the addition of selumetinib.



A375 melanoma cell line				
		Combination index		
Selumetinib (μM)	Leflunomide (μM)	Leflunomide and selumetinib at the same time	Leflunomide 24 hour pre treatment	Selumetinib 24 hour pre treatment
0.025	12.5	1.621	0.88363	0.9167
0.05	12.5	1.526	1.19666	1.22762
0.1	12.5	1.561	1.41595	1.26827
0.025	25	1.59	1.22344	1.10714
0.05	25	1.699	1.28659	1.16125
0.1	25	1.814	1.55264	1.45044
0.025	50	1.414	1.27643	1.06051
0.05	50	1.507	1.20974	1.13169
0.1	50	1.646	1.6285	1.42372

Figure 5.30. Combination index values for the A375 melanoma cell line with pre-treatment for 24 hours with selumetinib, prior to the addition of leflunomide. In the summary table, purple indicates antagonism, orange indicated additive and green indicates synergism.

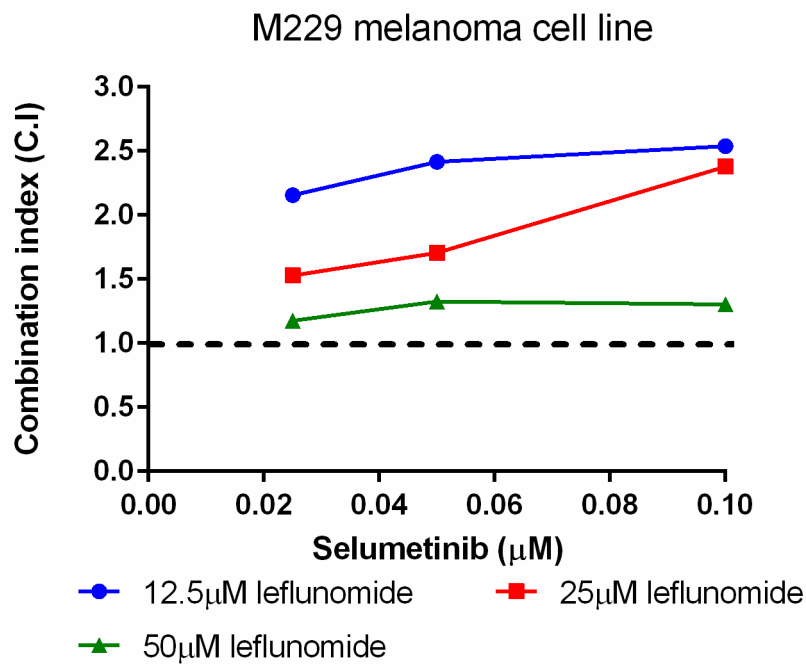
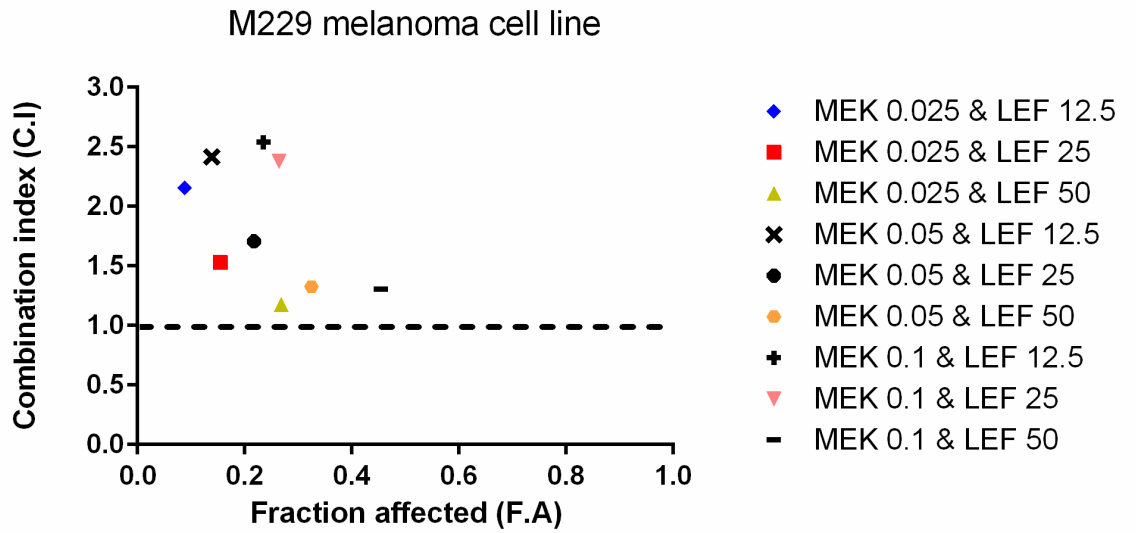
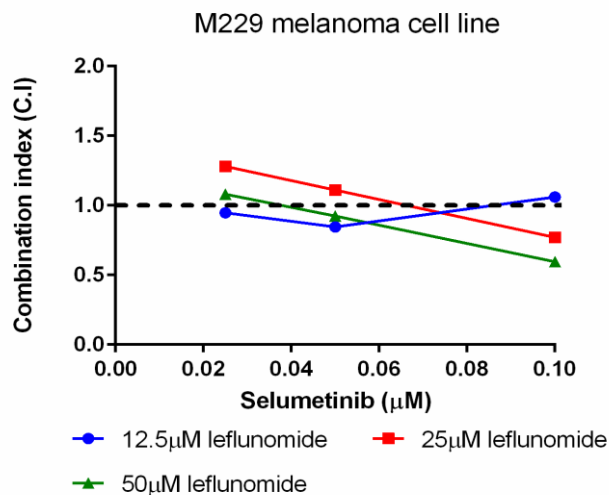
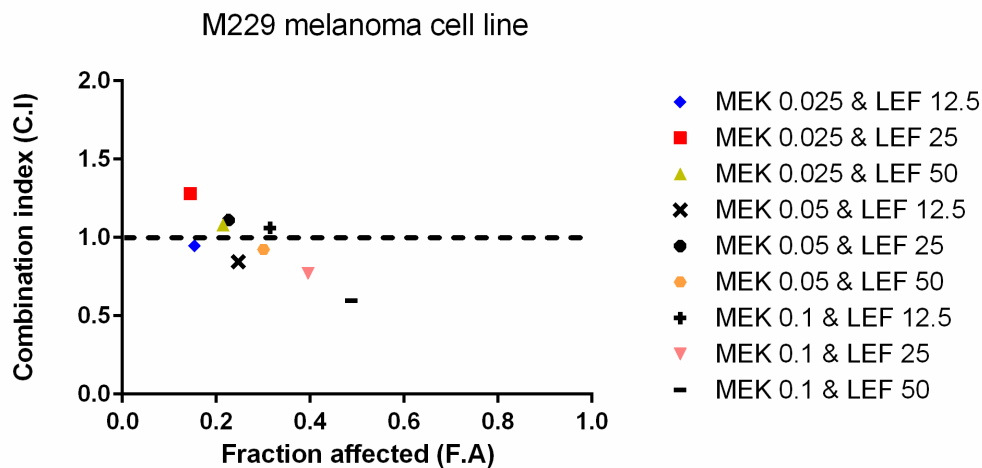


Figure 5.31. Combination index values for the M229 melanoma cell line with pre-treatment for 24 hours with leflunomide, prior to the addition of selumetinib.



M229 melanoma cell line				
Selumetinib (μM)	Leflunomide (μM)	Combination index		
		Leflunomide and selumetinib at the same time	Leflunomide 24 hour pre treatment	Selumetinib 24 hour pre treatment
0.025	12.5	0.827	2.1567	0.94701
0.05	12.5	0.743	2.41606	0.84505
0.1	12.5	0.939	2.53868	1.06029
0.025	25	1.011	1.52786	1.28151
0.05	25	0.831	1.70506	1.11133
0.1	25	0.94	2.37912	0.77127
0.025	50	0.801	1.17593	1.08006
0.05	50	0.617	1.32693	0.92337
0.1	50	0.846	1.30465	0.59609

Figure 5.32. Combination index values for the M229 melanoma cell line with pre-treatment for 24 hours with selumetinib, prior to the addition of leflunomide. In the summary table, purple indicates antagonism, orange indicated additive and green indicates synergism.

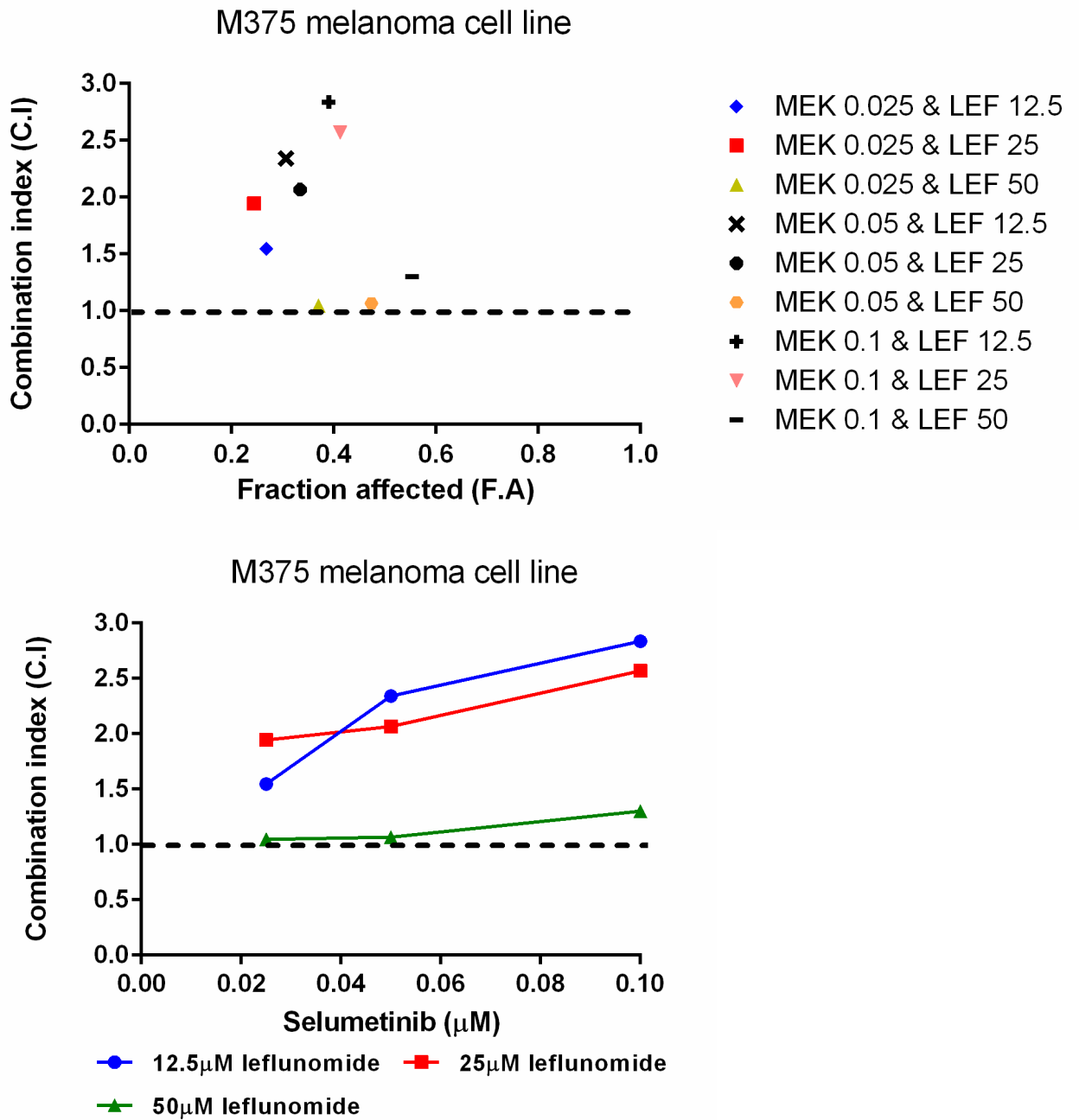
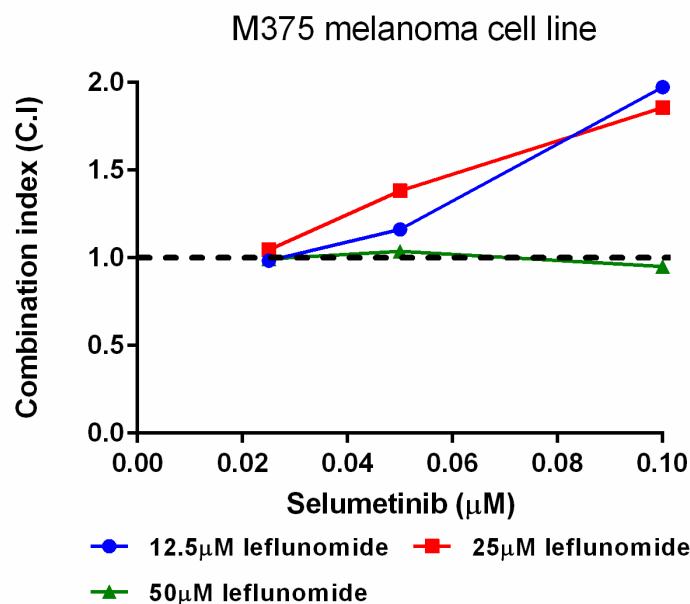
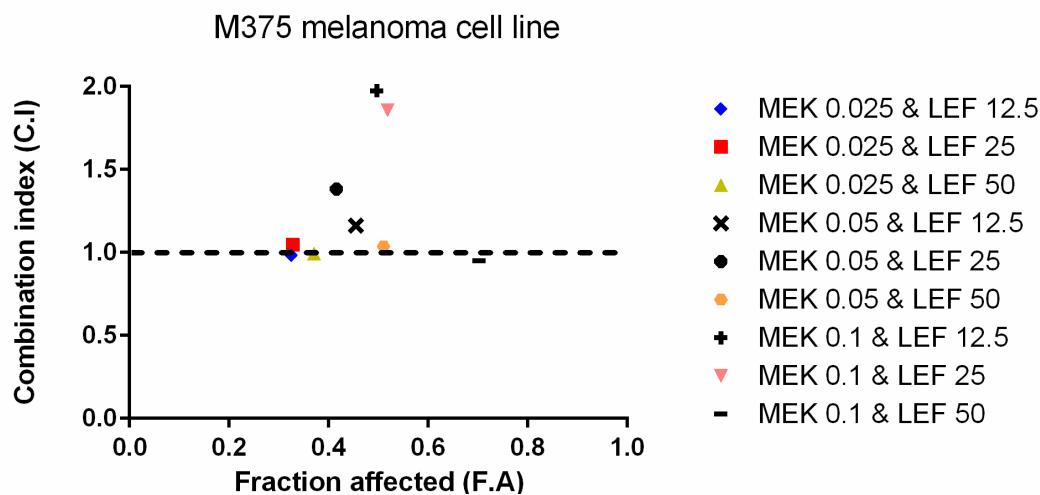


Figure 5.33. Combination index values for the M375 melanoma cell line with pre-treatment for 24 hours with leflunomide, prior to the addition of selumetinib.



M375 melanoma cell line				
Selumetinib (μM)	Leflunomide (μM)	Combination index		
		Leflunomide and selumetinib at the same time	Leflunomide 24 hour pre treatment	Selumetinib 24 hour pre treatment
0.025	12.5	0.528	1.54708	0.98374
0.05	12.5	0.661	2.34111	1.16188
0.1	12.5	0.834	2.83633	1.9737
0.025	25	0.473	1.94343	1.04623
0.05	25	0.549	2.06715	1.38204
0.1	25	0.754	2.56872	1.85773
0.025	50	0.328	1.04531	0.99408
0.05	50	0.327	1.06653	1.03813
0.1	50	0.519	1.3012	0.95124

Figure 5.34. Combination index values for the M375 melanoma cell line with pre-treatment for 24 hours with selumetinib, prior to the addition of leflunomide. In the summary table, purple indicates antagonism, orange indicated additive and green indicates synergism.

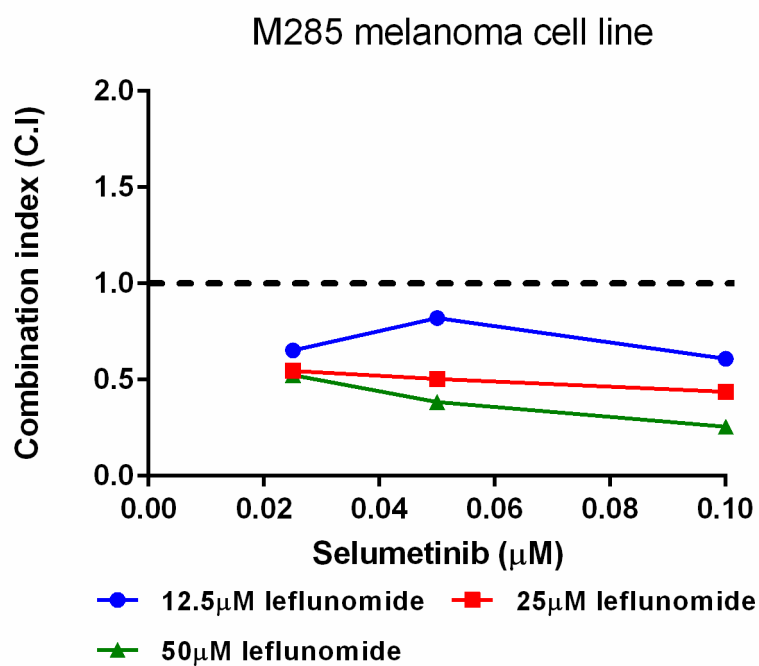
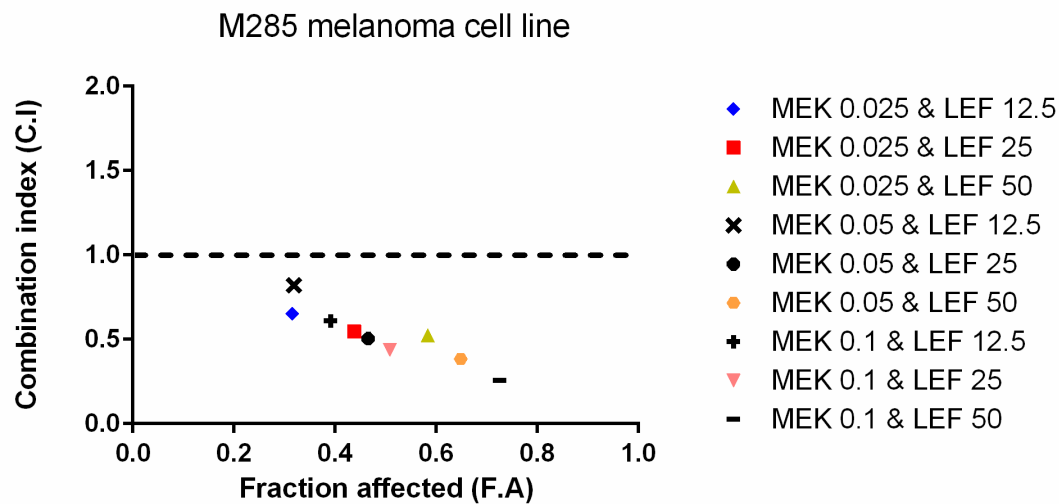
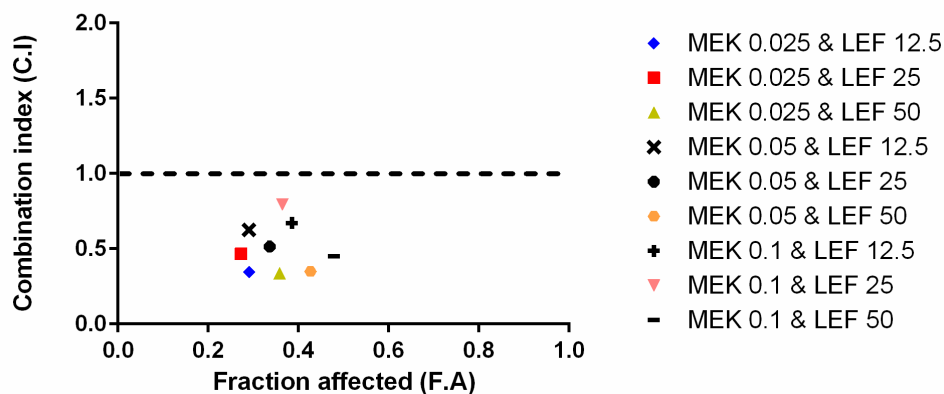
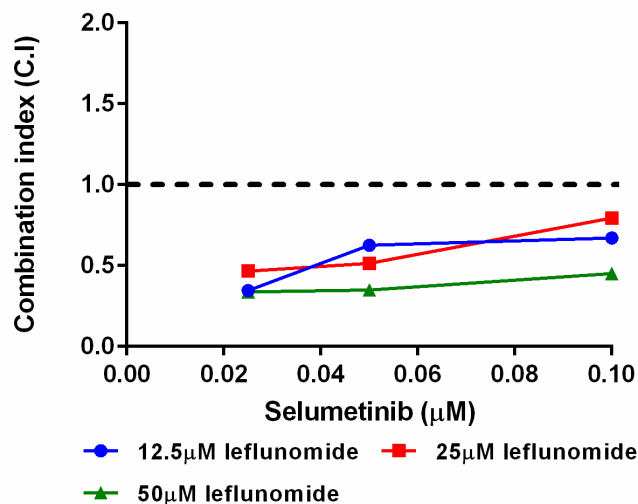


Figure 5.35. Combination index values for the M285 melanoma cell line with pre-treatment for 24 hours with leflunomide, prior to the addition of selumetinib.

M285 melanoma cell line



M285 melanoma cell line



M285 melanoma cell line					
		Combination index			
Selumetinib (μM)	Leflunomide (μM)	Leflunomide and selumetinib at the same time	Leflunomide 24 hour pre treatment	Selumetinib 24 hour pre treatment	
0.025	12.5	0.704	0.65261	0.34513	
0.05	12.5	0.95	0.82107	0.62615	
0.1	12.5	1.033	0.60839	0.6709	
0.025	25	0.657	0.54502	0.46565	
0.05	25	0.709	0.50348	0.51353	
0.1	25	0.777	0.43781	0.79389	
0.025	50	0.568	0.52379	0.33812	
0.05	50	0.665	0.38382	0.34852	
0.1	50	0.515	0.25503	0.45099	

Figure 5.36. Combination index values for the M285 melanoma cell line with pre-treatment for 24 hours with selumetinib, prior to the addition of leflunomide. In the summary table, purple indicates antagonism, orange indicated additive and green indicates synergism.

5.2.7 Western blots detecting apoptotic markers in leflunomide and selumetinib treated cells.

Inhibitors that target the MAPK pathway typically have a cytostatic effect; in which a G1 cell cycle arrest is observed with little apoptosis. This is the case with selumetinib and therefore any apoptosis observed with the combination of leflunomide and selumetinib must be due to leflunomide. This prompted the next set of experiments to investigate what leflunomide is functionally targeting to push this cytostatic threshold over to a more cytotoxic one. Three pro-apoptotic markers (poly (ADP-ribose) polymerase (PARP), BCL2-interacting mediator of cell death (BIM) and p53 up-regulated modulator of apoptosis (Puma)) and one anti-apoptotic marker (myeloid cell leukemia 1 (Mcl-1)) were chosen. As the cell death proteins which leflunomide might be targeting with respect to melanoma are unknown, BCL2 proteins thought to be regulated by the MAPK pathway were selected. In addition these BCL2 proteins were also chosen due to them being part of different cell death pathways (e.g. caspase-dependent apoptosis, p53-mediated apoptosis and DNA damage-induced apoptosis). This provides a broad insight into the potential ways leflunomide could induce cell death. For example, BIM and PUMA have been reported to bind and inhibit several main anti-apoptotic proteins; whereas other BCL2 proteins tend to inhibit a few anti-apoptotic proteins. This will aid in elucidating whether a single cell death pathway is being targeted or whether multiple cell death pathways are being targeted in parallel to each other. The western blots were conducted on A375 melanoma cell samples and it is to be highlighted that these experiments are very preliminary.

Puma is a pro-apoptotic marker and the antibody for this protein detected two bands, one at 23 kDa and another non-specific band at 18 kDa. Focussing on the 23 kDa band in figure 5.37, there was a clear decrease in the amount of protein present in all of the given treatments compared to the DMSO control. This is an ambiguous finding; given that Puma is a pro-apoptotic protein, one might expect the levels of protein to have increased

upon treatment with leflunomide and/or selumetinib. The levels of BIM appeared to increase upon treatment with leflunomide and selumetinib however it is noted that this western blot is not of the best quality. On the other hand a convincing result was observed when detecting for the levels of PARP. Again PARP is a pro apoptotic marker and it can be clearly seen in figure 5 that in both combinations of leflunomide and selumetinib (the last two lanes) cleavage of PARP is present, but hardly in any of the other samples. This cleavage of PARP is indicative of cells undergoing apoptosis.

The blot for the anti-apoptotic marker Mcl-1 is again not of the best quality. Nonetheless you can see that the levels of Mcl-1 remain relatively stable in all of the samples but a possible decrease in the levels of Mcl-1 can be seen at 50 μ M leflunomide in combination with both 0.05 and 0.1 μ M selumetinib.

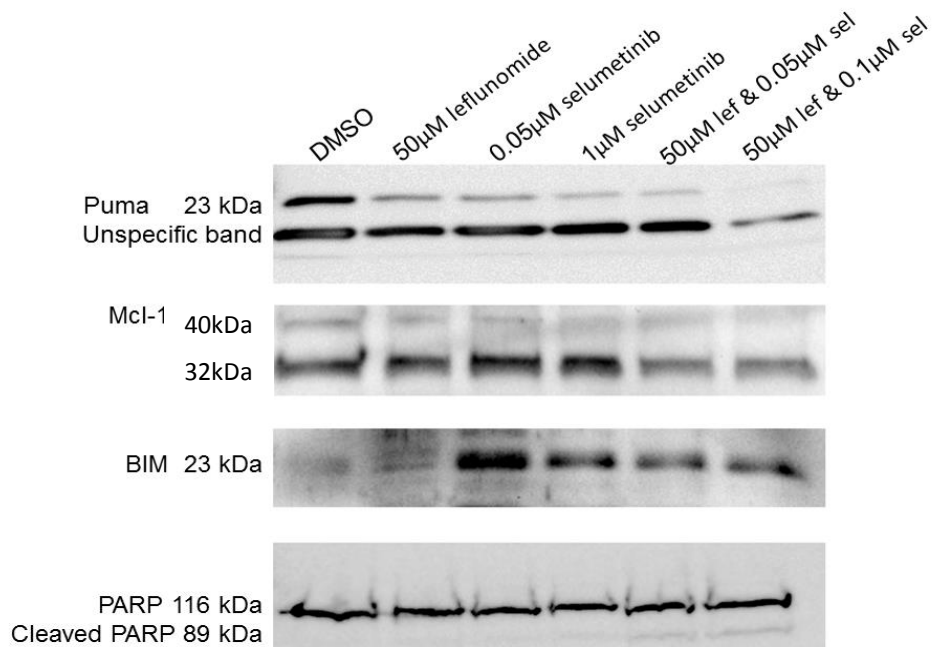


Figure 5.37. Western blot analysis detecting the presence for anti and pro apoptotic markers in A375 melanoma cells. Puma, BIM and PARP are the pro-apoptotic markers and Mcl-1 is the anti-apoptotic marker. Cells were subject to treatment with leflunomide and selumetinib alone and in combination together at the indicated concentrations. 10 μ g of protein was loaded onto each lane. The molecular weights are shown on the left. Results for Puma, Mcl, BIM and PARP are from a single experiment representative of two, one, one and two independent experiments respectively.

5.2.8 Pilot mouse study

To determine if the combination of leflunomide and selumetinib also works *in vivo*, a mouse xenograft study a mouse xenograft study was undertaken. The calculated CI values of the cell viability assays in which leflunomide and selumetinib were added in combination at the same time (figures 5.13 to 5.20) was the starting point for planning the mouse xenograft study. The four melanoma cell lines which had the 'best' or strongest synergistic combination index values were all considered as potential cell lines for the xenograft study. The M375 cell line was considered due to all the combination index values being synergistic. The M229 and M285 were considered as they both gave all synergistic combination index values bar one additive and one antagonistic value respectively. Finally, the SKmel5 cell line was considered due to it producing the strongest synergistic values, even though these were only produced when leflunomide was in combination with 0.1 μ M selumetinib.

Having picked the four potential melanoma cell lines, a literature search was carried out to see if any of these cell lines have been previously used in a mouse xenograft study. Unfortunately, the literature search did not provide much more information as some of these cell lines did not appear to have been used in a xenograft study before. With this lack of information a pilot mouse study was carried out to test whether these four melanoma cell lines could give rise to a palpable tumour. The aim of this experiment was to determine which cell line to go forward with for the xenograft study.

The M375, M285, M229 and SKmel5 melanoma cell lines were each injected into an individual SCID mouse at 1×10^6 cells. As it was not known how long these cell lines would take to form a palpable tumour, if at all, we used the A375 cell line to act as a positive control. The A375 cell line is the most commonly used cell line in melanoma studies and takes approximately 8 days to form a palpable tumour in xenograft studies. This also was injected into an individual SCID mouse at 1×10^6 cells. After the mice were injected

with each of the cell lines, they were monitored until a visible palpable tumour could be seen. Due to this being a pilot study, the mice were not monitored on a fixed schedule, but the maximum they were left unobserved was 4 days.

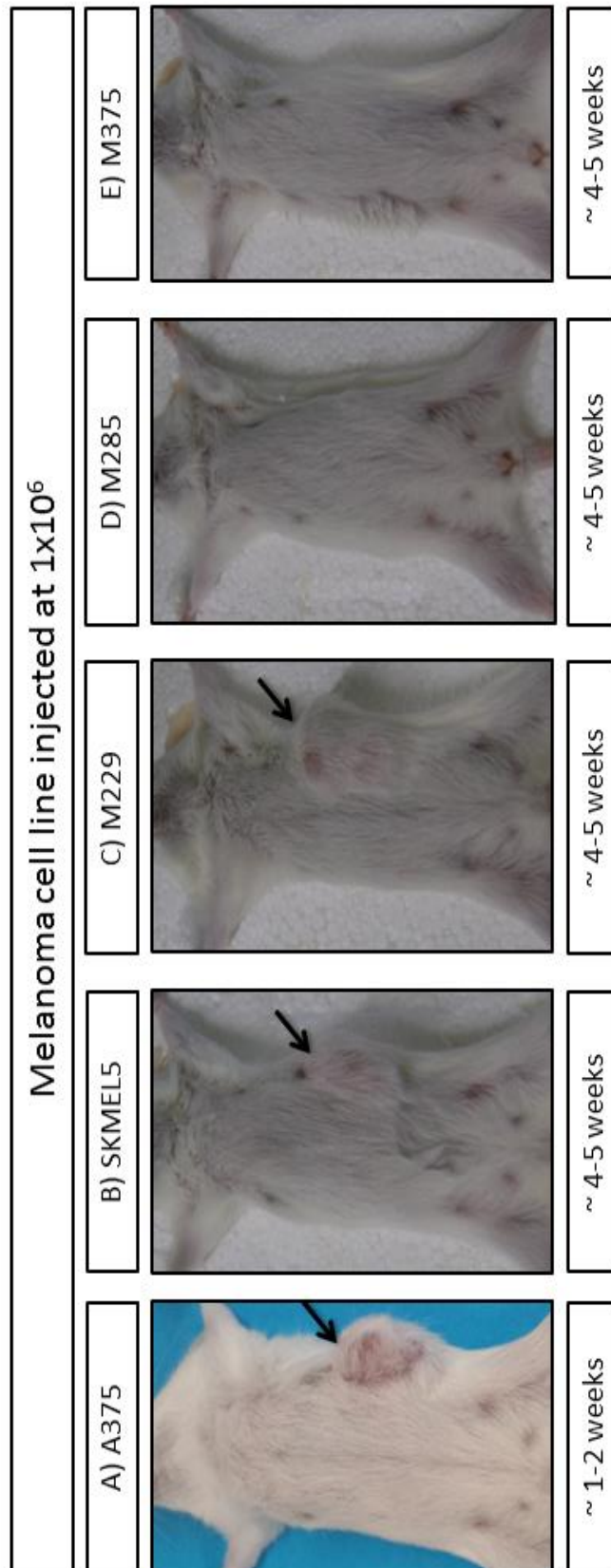


Figure 5.38. Results of the pilot study showing tumours for the A375, SKmel5 and M229 cell lines, but not for the M285 and M375 melanoma cell lines. Black arrows indicate the location of the tumours.

The A375 cell line was the first to form a palpable tumour, which took somewhere between 1-2 weeks to grow (figure 5.38). The next two cell lines to form palpable tumours were M229 and SKmel5, which both took approximately 4-5 weeks (figure 4.38). Neither the M375 nor M285 cell line had any sign of a palpable tumour after 4-5 weeks (figure 5.38). Due to both of these latter 2 cell lines providing the most promising synergistic data from the cell viability experiments, they were preferred to pursue in the xenograft study. As neither had yet to produce a palpable tumour after 4-5 weeks, the experiment was stopped and was repeated in a subsequent study using a larger number of injected cells.

The repeated pilot study for the M375 and M285 cell lines was carried out exactly the same, except more cells were injected into the SCID mice. In this experiment the M375 and M285 cells were injected at 3×10^6 cells, with the hypothesis that injecting more cells would give a higher probability of the formation of a palpable tumour. This hypothesis proved true, with both cell lines producing a palpable tumour but at different times. The M285 cell line was the first to produce a palpable tumour in approximately 5 weeks (figure 5.39). After approximately 7 weeks, the M375 cell line gave rise to a palpable tumour (figure 5.39). Interestingly, the M375 tumour volume was greater than that of the M285 cell line at 3005.85mm^3 and 635.70mm^3 respectively.

5.2.9 Mouse xenograft study

Based on the cell viability experiments and the subsequent calculated CI values, combined with the ability to form a palpable tumour, the M375 melanoma cell line was chosen to be used in the xenograft study. The M375 cells were injected into each mouse at 3×10^6 cells and were monitored until a palpable tumour developed which took approximately 4 weeks. The xenograft study had four arms to the experiment: vehicle alone, leflunomide alone, selumetinib alone and leflunomide and selumetinib in combination, with 10 SCID mice in each. The dosage regime comprised of leflunomide

being delivered at 7.5mg/kg once daily by intraperitoneal injection. Selumetinib was delivered twice daily by oral gavage at 30mg/kg. This was changed to once daily by oral gavage on day 3 because it was thought that the mice were becoming stressed due to the delivery of the drug. The tumour volume was measured every 3 days by callipers over a period of 12 days. At the end of the experiment, the mice were culled and the tumours excised and weighed.

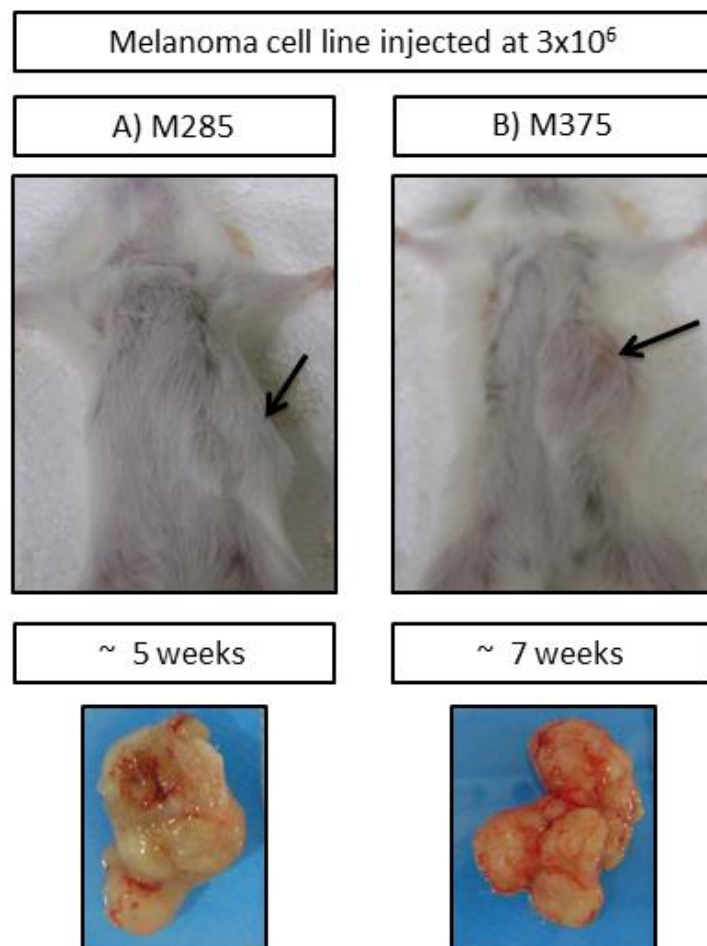


Figure 5.39. Results of the repeated pilot study showing tumours for the M285, and M375 cell lines. Black arrows indicate the location of the tumours.

During the 12 days of the xenograft study, 4 mice in the leflunomide arm and 3 in the combination had to be culled due to them becoming unhealthy. As a result, the subsequent analysis was done on the remaining mice. The tumour volume was measured every 3 days over a period of 12 days and the results can be seen in figure 5.40.

In the vehicle control arm, the average tumour volume increased from 46mm^3 on day 0 to 650mm^3 on day 12 (shown in black), indicating a steady increase in tumour growth. Interestingly in the leflunomide arm, the average tumour volume increased from 46mm^3 on day 0 to 712.83mm^3 on day 12 (shown in red). At day 12, this tumour volume is slightly greater than that of the vehicle control and the growth in tumour volume also overlaps with that of the vehicle control, though not significantly. This shows that leflunomide treatment did not reduce tumour volume when compared to the vehicle control. In contrast, selumetinib treatment showed a much greater effect on the average tumour volume (shown in blue). Again on day 0, the average tumour volume was 46mm^3 , but on day 12 this volume increased to just 169.7mm^3 . This is dramatically lower than the vehicle control, at almost a 4-fold decrease in tumour volume. This shows that selumetinib has the ability to reduce the tumour volume alone. In comparison, leflunomide was not able to reduce tumour volume alone. However, when leflunomide and selumetinib was administered in combination, the tumour volume decreased (shown in purple). On day 0 the average tumour volume was 46mm^3 , which decreased to 41mm^3 on day 12. Strikingly this decrease in tumour volume remained steady at this size over the 12 day period.

The results from the tumour volume analysis would suggest that the combination of leflunomide and selumetinib has the capability of not only reducing the tumour volume, but preventing the tumour further growing in size with selumetinib being the more potent drug in the combination

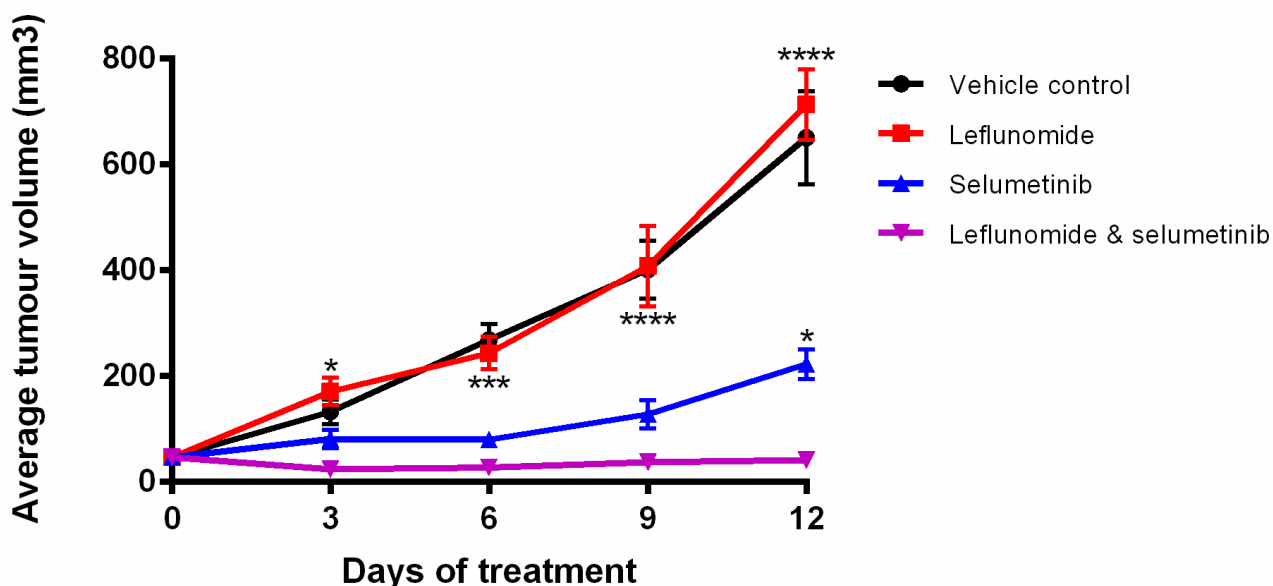


Figure 5.40. The combination of leflunomide and selumetinib reduced the average tumour volume greater than either drug alone. Data is presented as the mean \pm SD of one independent experiment. Statistical analysis compares either drug alone to them in combination determined by two-way ANOVA with Turkey's post-hoc test. * $P \leq 0.05$, ** $P \leq 0.01$, *** $P \leq 0.001$ and **** $P \leq 0.0001$.

The tumours from the culled mice at day 12 were excised and weighed (figures 5.41 and 5.42). In the vehicle control arm, the tumour weights ranged from 0.118g to 0.282g (figure 5.41). In the leflunomide arm the tumour weights ranged from 0.147 to 0.299g and on average the tumours in this arm were the heaviest. This correlates to the fact that in the leflunomide arm the average tumour volumes were also the largest. There is a remarkable drop in tumour weight seen in the selumetinib arm with tumour weights ranging from 0.02 to 0.084g. The tumour weight decreased further when leflunomide and selumetinib were used in combination as the weights ranged in this arm from 0.009 to 0.039g. The combination of leflunomide and selumetinib on the effect on the tumour weights was significantly better than either of the two drugs alone, with the p values for leflunomide and selumetinib being <0.0001 and <0.0494 respectively.

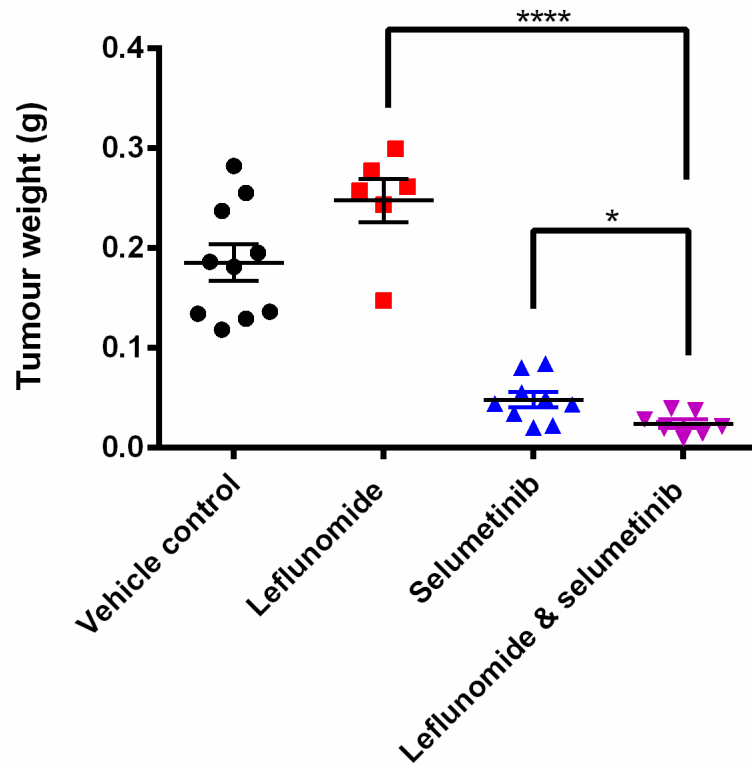


Figure 5.41. The combination of leflunomide and selumetinib reduced tumour weight greater than either drug alone. Data is presented as the mean \pm SD of one independent experiment. Asterisks indicate the degree of statistical difference comparing the combination of leflunomide and selumetinib to each drug alone determined by unpaired student t-test. * $P \leq 0.05$, ** $P \leq 0.01$, *** $P \leq 0.001$ and **** $P \leq 0.0001$.

Figure 5.42 clearly shows visually, the excised tumours. Again this figure reiterates what has been observed in figures 5.40 and 5.41. In figure 5.42 you can see that the leflunomide arm bears the largest tumours, with the vehicle arm holding the second largest tumours. Becoming more noticeable was the smaller sized tumours in the selumetinib arm and the smallest sized tumours being present in the leflunomide and selumetinib arm. Therefore the trend observed in the average tumour volume correlated to what was observed with the tumour weights.

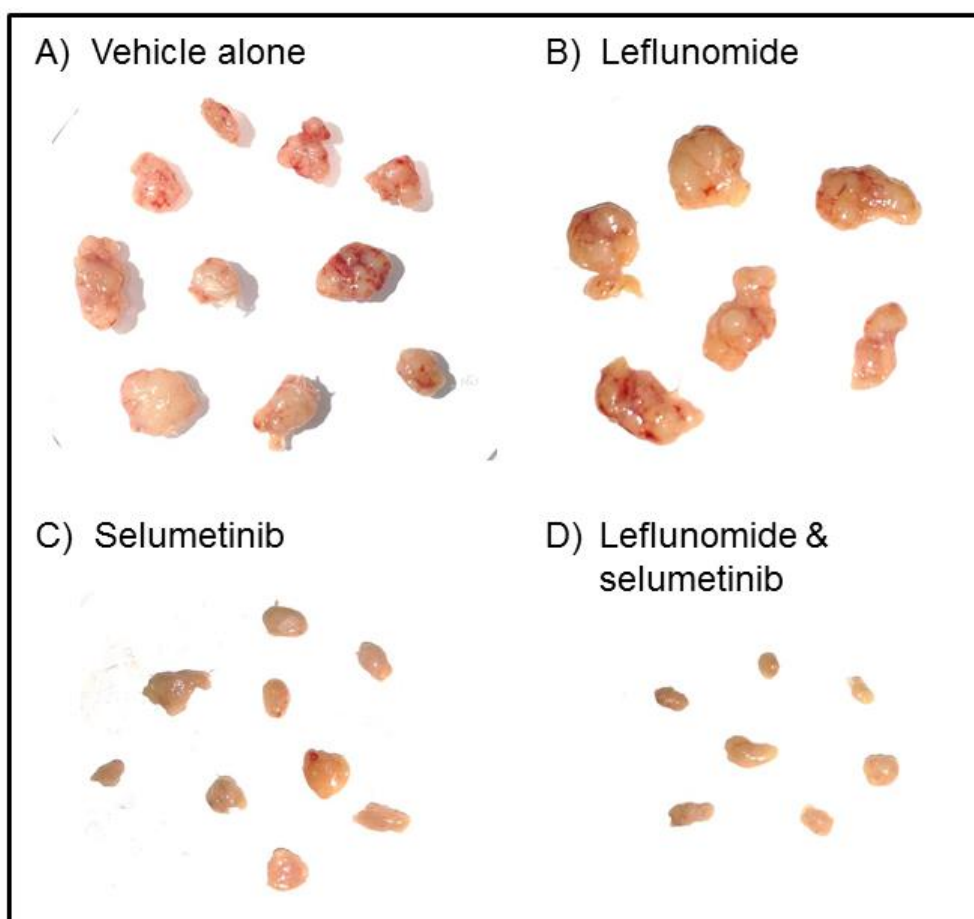


Figure 5.42. Visualisation of the excised tumours from the mouse xenograft study. Only nine out of ten tumours are shown for selumetinib arm due to one tumour being too small to be excised.

5.3 Discussion

Within the field of melanoma it is increasingly becoming accepted that monotherapy is not the way forward in developing treatments. This is due to a lack of treatments, and many of the currently available treatments only targeting a subset of patients whose tumours have a specific genotype. In addition, one of the key obstacles in treating melanoma is the acquisition of resistance to current treatments in a matter of months. To address this issue researchers are searching for combinations of drugs that are more efficacious, cause more durable clinical responses and improve the survival rate of patients. To try and contribute to this area of research, the aim of this chapter of the thesis was to determine if leflunomide could be used in combination with the MEK inhibitor selumetinib.

Initially cell viability assays were carried out on the bank of eight melanoma cell lines upon treatment with selumetinib alone. All of the eight melanoma cell lines exhibited a dose-dependent decrease in cell viability upon treatment with increasing concentrations of selumetinib. However it was noted that there was a substantial variation in response to selumetinib between the melanoma cell lines. This variation in sensitivity of melanoma cell lines in response to MEK inhibitors is consistent with other reports from other studies (Euw et al, 2012; Stones et al, 2013; Boussemart et al, 2014). One such study tested the sensitivity of the MEK inhibitor E6021 against a panel of 31 melanoma cell lines. This study quantified sensitivity in regards to the IC_{50} 's produced from the cell viability assays carried out. Sensitivity to E6201 was considered if the IC_{50} 's produced were <500 nM and hypersensitivity was considered if the IC_{50} 's produced were <100 nM. IC_{50} 's produced ranged from 0-10,000 nM. Of the 31 melanoma cell lines 24 were classified as being sensitive to E6201, 18 of which were also hypersensitive. However 7 of the cell lines produced IC_{50} 's >500 nM. This range in sensitivity seen in this study to the MEK inhibitor E6201 is in line with what was seen here in this thesis to the MEK inhibitor selumetinib. However what was investigated and concluded in the study with E6201, which was not in this

thesis, was that gene mutations in each cell line correlated with the sensitivity to E6201. Sensitivity to the E6201 was associated with a wildtype PTEN and mutant BRAF status. In comparison, resistance to E6201 was associated with a mutant RAS status and activation of the PI3K pathway (Byron et al. 2012).

Additional studies have also started to make such correlations. For example another study identified a subset of melanoma cell lines which were wildtype for NRAS mutations and resistant to vemurafenib, but were sensitive to treatment of trametinib. This suggests that patients that are wildtype for BRAF and NRAS could respond well to trametinib (Stones et al. 2013). In both of these studies, the genotype of the melanoma cell lines governed these specific responses to the MEK inhibitor. Although this was not investigated in this thesis, such experiments would be grounds for further studies. This highlights and brings forward the proposed model of personalised medicine in which the treatment given to patients is customised based upon genetic profiling of their tumour.

Cell viability assays on leflunomide and selumetinib had previously been carried out individually. The primary aim of this chapter was to determine if leflunomide could be used in combination with selumetinib to provide superior tumour cell growth inhibition. Therefore cell viability assays determining the effect of leflunomide in combination with selumetinib were carried out on all eight of the melanoma cell lines. One of the objectives of combinatorial studies is to be able to reduce the concentration of each individual drug, thus also reducing toxicities observed from when each drug is given alone. However a combination of drugs at lower concentration is hoped to elicit an enhanced effect therapeutically compared to either drug alone otherwise the combination of drugs is not worth following up further. The concentrations of leflunomide used in these combinatorial cell viability assays were 12.5, 25 and 50 μ M. This was based upon previous studies which had carried out cell viability assays testing leflunomide in combination

with vemurafenib (White et al. 2011). The concentrations of selumetinib used were 0.025, 0.05 and 0.1 μ M. This was determined from prior cell viability assays carried out with a range of selumetinib concentrations being tested against the leflunomide concentrations with these three concentrations being chosen (data not shown). It is to note that the maximum concentration of leflunomide being used in these combinatorial assays (50 μ M) was half that of the maximum concentration used in the cell viability assays of leflunomide alone (100 μ M). Likewise, the maximum concentration of selumetinib in these assays was considerably lower compared to that of the previous selumetinib alone cell viability assays (0.1 μ M vs 1 μ M).

All of the eight melanoma cell lines responded to the combination of leflunomide and selumetinib. But again, the variation in sensitivity across the cell lines that was observed in this set of experiments is likely due to the genotyping of each cell line as just described. However future experiments would confirm if this hypothesis holds true. For the majority of the cell lines upon treatment with the combinations of leflunomide and selumetinib there was a dose dependent decrease in the number of viable cells. The combinations of leflunomide and selumetinib tested, again for the majority of the cell lines and the combinations, appeared to enhance the reduction of the number of viable cells compared to either of the two drugs alone. The M285, M375 and M229 cell lines clearly exhibited this trend (figures 5.5, 5.6 and 5.9). For example all of the IC₅₀'s for the M375 cell for the combinations tested were all lower than compared to either drug alone. For instance the IC₅₀ for selumetinib alone was 0.064 μ M which was lowered to 0.026 μ M for the combination of 50 μ M leflunomide and 0.1 μ M selumetinib (figure 5.6). This finding is a trend that is desired from a drug combination. What also became apparent from these experiments was this particular combination of 50 μ M leflunomide and 0.1 μ M selumetinib was the most statistically significant across all eight of the melanoma cell lines. Overall, these combinatorial cell viability assays proved promising results. However the true significance of these combinatorial cell viability assays and the key and fundamental question that needed to be answered was whether this

combination of drugs was acting synergistically or not. Determining if this drug combination reflected synergy or not was the primary focus in how to analyse this set of experiments.

From reading the literature there is not a fixed definition of the term 'synergy'. Current existing definitions of the term synergy are not all agreed upon, which adds confusion in how to interpret synergy data and most importantly how to calculate synergy. This confusion encompassing the term synergy is noticeable and has been picked up by other researchers. One study investigated how valid synergy claims are by conducting a literature search for published papers between 2006-2010 citing the terms 'synergy' or 'synergistic' (Ocana et al, 2012). From these papers the preclinical data (*in vitro* and *in vivo*) was evaluated in order to see if this data and the methodology used was sufficient enough for them to justify using the term synergy. A total of 86 papers of clinical trials which were carried out based upon synergy claims from prior studies were identified. For these 86 clinical trial papers published, 132 preclinical papers were also identified as supporting papers for the clinical trials. Of these 132 papers, only 90 had used the term synergy (68%). This left 32% of the articles not actually citing the term synergy in evaluating their possible drug combination. Only 20% of the preclinical articles had used appropriate methods to determine synergy, which included either of the two most commonly methods in calculating synergy; Steel and Peckham isobologram method or Chou and Talalay combination index method. Surprisingly the majority of the preclinical studies used mouse models and claimed drug synergy without carrying out any methodology to validate such claims. What was interesting from this study was that from the minority of the studies which did use suitable methodology to determining drug synergy, there was no correlation found between using adequate methodology and the success of the clinical trial. This is perplexing as it could suggest that the success of a drug combination is irrespective of whether there is synergy between the two drugs or not. This then raises the question of whether calculation of drug synergy is necessary at all and how much value does synergy actually hold? However no definite conclusions

could be drawn from this study alone due to the identification of few studies that correctly evaluated drug synergy to be able to draw statistically significant conclusions from. What was also evident was a lack of the use of the term therapeutic index (TI) with only 4% of the preclinical studies using this term. TI compares the highest concentration at which a drug exerts a therapeutic effect to that which causes toxicity. Drugs with a high therapeutic index are preferred; however, those with a low profile are often drugs which do not progress to the end of the drug development process. Thus, regardless of whether the drug combination is synergistic, if the TI is poor, the combinations of drugs will unlikely make it through this process. This concept was emphasized in this study which states that studies should show a greater TI before pursuing such drug combination clinically to try and improve the efficacy. Overall, this study concluded that the majority of preclinical studies misuse the term synergy and do not use sufficient methods to evaluate drug synergy which could ultimately result in inadequately designed clinical trials and in part be a fundamental reason behind the failure of possible drug combinations in the drug development process (Ocana et al. 2012).

To evaluate synergy in this thesis for the combination of leflunomide and selumetinib, the methodology of Chou and Talalay was chosen to calculate combination index (CI) values. If a CI value of 1 is given, that drug combination is said to be acting additively. If the CI value is >1 this indicates the drug combination is acting antagonistically. If the CI value is <1 the drug combination is said to be working synergistically (Chou and Talalay, 1984). For all eight of the melanoma cell lines CI values were calculated. From table 4.2 showing all of the CI values it became apparent that the highest concentration of leflunomide, $50\mu\text{M}$, produced the majority of the synergistic values. This was not that unexpected given that from the previous cell viability assays it was apparent that leflunomide exerted its effects at higher concentrations. However there was variation in the CI values produced between the eight melanoma cell lines. For example, the M375 melanoma cell line produced all synergistic CI values, the M285 cell line produced all

bar one but the A375 cell line produced all antagonistic CI value which was an unexpected finding. The A375 cell line usually responds very well to selumetinib in melanoma studies, and observing no synergy between selumetinib and leflunomide was unexpected and potentially of significance. This might suggest that this cell line may not always be the best for studying melanoma and that a group of melanoma cell lines should be tested.

There could be a number of possible of reasons for the variation seen in the CI values produced. One possibility could be imparted due to the experimental design itself. Other studies have noted that a particular ratio of a drug combination could give rise to synergism, however a different ratio of the combined drugs could then cause antagonism (Chou, 2010; Chou 2006; Steel and Peckham 1979). Therefore it could be possible that if the combination of leflunomide and selumetinib was administered at a different ratio other to that used in this thesis of 1:1, antagonistic values could alter to become synergistic. For future work, altering the drug ratio of this drug combination would be interesting to see if this was the case here, in particular for the A375 cell line.

Another possible reason could be that the concentrations of both leflunomide and selumetinib may not have been optimised enough. For all cell viability assays carried out in this it thesis it became apparent that the sensitivity to either leflunomide or selumetinib varied amongst the eight melanoma cell lines. Therefore the sensitivity to a particular concentration of leflunomide and selumetinib may be more sensitive in some cell lines than others. This difference in sensitivity may be reflected in the CI values produced. Future studies could optimise the concentration range of the two drugs for each cell line. The only disadvantage of this would be that direct comparison could not be drawn between the cell lines. Nonetheless, one of the cell lines tested here for which this optimisation could prove to be successful is the SKmel5 cell line. The synergistic CI values produced for the SKmel5 cell line were only produced at 0.1 μ M selumetinib in combination with all of the

concentrations of leflunomide tested (figure 5.20). The strength of the synergism also improved with increasing doses of leflunomide. So if concentrations of selumetinib that were higher than 0.1 μ M were used in combination with the concentrations of leflunomide, one possibility is that even stronger synergism could be observed.

An alternative reason that needs to be taken into account is that for some of the melanoma cells used in this thesis, the history of any chemotherapy or radiotherapy received by the patient the cells derived from is unknown. Therefore if any resistance had developed from any prior treatment the genetic cause of this is not known. Thus, if this played a role in the sensitivity of any of the cell lines to leflunomide and selumetinib is also undetermined. This links in with the fact that the genotype of each cell line plays a pivotal role in the sensitivity to drug treatment and as a consequence the CI values produced. It also highlights the substantial heterogeneity of this type of cancer. Therefore future studies could sequence the melanoma cell lines for a broad range of potential genetic mutations and determine if any specific mutations (or not) have an effect on whether synergism or antagonism is seen with the combination of leflunomide and selumetinib.

Overall, given that a valid method was used in this thesis to evaluate synergy which is frequently used by other researchers, there is confidence in the validity of the results. However there is room for improvement in the experimental design but due to the discrepancy in the field over the term synergy and there being no guidelines on how to determine synergy it becomes troublesome in order to resolve any issues arisen.

A question was then posed if either pre-treating cells for 24 hours with leflunomide or selumetinib had an effect on the CI values produced. Four of the eight cell lines were tested in this next set of experiments; A375, M229, M285 and M375. Again variation was seen in the CI values produced and

this is likely due to the reasons as just described for the previous synergy experiments. However generally speaking, pre-treatment with either leflunomide or selumetinib did not improve the CI values for the A375, M229 and M375 cell lines ((with some exceptions) figures 5.29-5.34). In some cases the CI values worsened. Contrastingly, the CI values for the M285 cell line became more synergistic for both pre-treatment with leflunomide and selumetinib (figures 5.35 and 5.36). This highlights the importance of the dosing regime of drugs to patients and how vigilant experiments determining drug synergy need to be planned in order to obtain the greatest response.

To determine how leflunomide and selumetinib are mechanistically working synergistically together, western blots of pro-apoptotic and anti-apoptotic markers were carried out (figure 3.37). These experiments are very preliminary and the majority of the blots are still n=1 and some of the antibodies still need optimising (specifically BIM antibody). Therefore it is not possible to draw any conclusions. The concept behind using these markers was because it has been reported from other studies that selumetinib causes a G1 cell cycle arrest (Haas et al, 2008; Little et al, 2011). Therefore any effect this combination of drugs is causing on apoptosis is likely to be due to leflunomide and hopefully using these markers can help to identify how leflunomide is affecting apoptosis (see chapter 4). On the other hand it could also identify possible unidentified targets that both of these drugs target. These experiments are planned to be repeated and finalised and then a thorough analysis of the results will be performed and conclusions drawn.

To determine if this synergism observed *in vitro* between leflunomide and selumetinib had a similar effect *in vivo*, a mouse xenograft study was performed. The mouse xenograft was carried out using the M375 cell line and for the duration of 12 days. What was obvious from the results of the mouse xenograft study (figures 5.40 and 5.41) was that selumetinib was the more effective drug compared to leflunomide. This is said because leflunomide alone did not reduce the tumour volume or weight compared to

the vehicle control. However, when in combination with selumetinib the tumour volume and weight significantly decreased than compared to either drug alone. The efficacy of selumetinib over leflunomide could also be seen from the pre-treatment synergy experiments. For example, for the M229 cell line, 24 hour pre-treatment with leflunomide resulted in all antagonist CI values compared to the all (bar one) synergistic CI values when leflunomide and selumetinib were added at the same time. However when these cells were pre-treated with selumetinib, over half of the CI values returned back to synergistic, some were even stronger CI values (figures 5.31 and 5.32). The reasoning for this domineering potency of selumetinib over leflunomide is unknown. It could be feasible that leflunomide and selumetinib are competing in the liver to be metabolised by the same enzyme (such as cytochrome P450). In this instance the more predominate drug, i.e. selumetinib, would therefore exert its potent effects resulting in a decrease of the metabolism of the competing drug (leflunomide) and a decrease in its efficacy. It could also be possible that the enzymes responsible for metabolising leflunomide and selumetinib have counteractive activities. For example the enzyme that is responsible for metabolising leflunomide could be inhibited by selumetinib and vice versa causing an imbalance of the efficacy of the drugs in the *in vivo* setting.

From the xenograft study there was a decrease seen in the tumour weight which could be due to a number of factors. One possibility is that there could be a decrease in the blood vasculature present or because the number of cells has decreased. Dissecting each individual to examine the blood vasculature would answer this question, which was not done in this thesis.

From literature searches there appears to be no means of calculating drug synergy from *in vivo* experiments. Hence from this mouse xenograft it cannot be said that the drug synergy seen *in vitro* was also seen *in vivo*. But what can be said is that the combination of leflunomide and selumetinib

significantly decreased the growth of melanoma *in vitro* and *in vivo* compared to just using either drug alone.

Chapter 6: Overall Summary and future directions

6.1 Chapter 3: Chemical genetic screen of the NCI diversity set II library in *X.laevis* embryos succeeded by a cell-based screen

Marrying developmental biology, chemical genetic screening and molecular medicine, from this thesis, the chemical genetic screen of the NCI diversity set II library and subsequent cell viability screen was a success. It has led to the identification of 13 possible compounds of interest. The additional cell viability screen strengthened the data obtained from this chemical genetic screen. It has aided in narrowing down the compounds to those which appear to be specific towards inhibiting melanoma growth.

From this successfully conducted screen in this thesis, more evidence is provided to support the use of *Xenopus laevis* as a model organism in the drug discovery process. However it does also highlight the major disadvantage of these forward chemical genetic screens; namely that the targets of these 13 compounds are unknown. A current collaboration with Dr Andreas Bender is underway to try and combine chemoinformatics, the compound structures and the phenotypes produced from this thesis to predict the potential targets of these compounds (Liggi et al, 2013 and Drakakis et al, 2014).

Future work would involve carrying out cell viability assays on the 13 identified NCI compounds on more melanoma cell lines to strengthen the claim that these compounds appear to hold potential therapeutic value in the treatment of melanoma. Further experiments would involve cell cycle analysis via propidium iodide staining and cell death analysis via Annexin V/ propidium iodide staining with the 13 compounds. This would determine if

the reduction in cell viability seen for these compounds was due to either the cells becoming arrested in a particular phase of the cell cycle or if the compounds are having a more cytotoxic effect and cause cell death. The aim of these suggested further experiments is to try and narrow down these compounds even further to a select few of interest. The remaining compounds would then be tested in a mouse xenograft study to determine whether they have the same effect in an *in vivo* setting.

6.2 Chapter 4: Characterising the function of leflunomide as an effective melanoma drug

Previous studies have shown leflunomide to be a potential drug in treating melanoma (White et al, 2011). The further characterisation of leflunomide as an effective melanoma drug carried out in this thesis provided further evidence to support this claim. However, both White et al. (2011) and the results from this thesis suggest leflunomide may be best utilised in combination with another drug. In this thesis it was found that leflunomide is capable of reducing the cell viability in melanoma cell lines wildtype for BRAF and those harbouring the BRAF^{V600E} mutation. Therefore leflunomide in combination with another drug (such as vemurafenib, selumetinib or any other anti-melanoma drug), holds potential to enhance the treatment of all melanoma patients.

Experiments carried out in this thesis showed that leflunomide caused a decrease in cell proliferation, a G1 cell cycle arrest and induced apoptosis. All of these experiments were carried out on the A375 melanoma cell line. However the synergy analysis of the leflunomide and selumetinib combinatorial experiments showed this drug combination to be antagonistic in the A375 cell line, unlike all the other melanoma cell lines tested. Therefore the M375 melanoma cell line which showed the combination of leflunomide and selumetinib to be synergistic was used in the mouse xenograft study. Future studies would involve repeating the experiments

carried out in Chapter 4 of this thesis (such as cell cycle and cell death analysis) with the M375 cell line and/or other melanoma cell lines. Experiments using the A375 cell line should be treated carefully. A different melanoma cell line or better yet, a bank of melanoma cell lines needs to be tested in melanoma studies.

The data from this thesis indicates that leflunomide could be having a cytoprotective effect at 100 μ M. Therefore a useful further experiment would be to conduct a time course of the cell cycle and apoptosis assays to determine specifically at which time-point this effect starts to occur. For example, such time-course points could include 12, 24, 36, 48 and 60 hours post leflunomide treatment. In this thesis the cell cycle and apoptosis experiments were carried out 72 hours post treatment with leflunomide. At 100 μ M leflunomide a significantly pronounced G1 cell cycle arrest and a reduction in the amount of apoptosis was observed at this concentration compared to 25 and 50 μ M leflunomide. It would also be of interest to investigate mechanistically what is controlling this cytoprotective effect seen with leflunomide. One study has indicated that p53 has a role in the cytoprotective effect observed with teriflunomide (another DHODH inhibitor) and another study reporting that deficient biosynthesis of pyrimidines due to inhibition of DHODH initiates a p53 response (Hail et al, 2012; Khutornenko et al, 2010). Therefore carrying out western blots detecting p53 and would be a rational place to start to determine if p53-dependent pathways are a target of leflunomide.

It was noted in this thesis that when cells were treated with 100 μ M leflunomide the intensity of green fluorescence emitted from mitotracker green was 3-fold higher compared to the DMSO control. However it could not be concluded from this assay why this increase in fluorescence was observed at 100 μ M leflunomide. It could be that there was an increase in the number of mitochondria present, or that there was mitochondrial swelling. Imaging cells treated with leflunomide would need to be performed.

Mitotracker green dye is not well retained post fixation of cells, therefore live-cell imaging would be required.

6.3 Chapter 5: Investigating the possibility of using leflunomide in combination with selumetinib to treat melanoma

The combinatorial experiments carried out with leflunomide and selumetinib proved to be successful both *in vitro* and *in vivo*. From the synergy analysis of the combinatorial cell viability assays, synergy was observed between these drugs for the majority of the melanoma cell lines tested. The combination of leflunomide and selumetinib significantly reduced tumour growth in the mouse xenograft study compared to either drug alone. Although further analysis could be carried out on the excised tumours from the mouse xenograft study, it is plausible to look into pursuing this drug combination in a clinical trial.

The key future work to be completed from this chapter of the thesis would be to analyse the dissected tumours from the mouse xenograft study. Staining for a proliferation marker such as Ki67 or BrdU would reveal to what extent the combination of leflunomide and selumetinib inhibited tumour cell division. TUNEL staining should also be conducted on the tumour samples to determine the level of tumour cell death. Additionally, staining could also be performed with a phospho-ERK antibody to visualise and confirm that selumetinib was efficiently inhibiting its target MEK. Given how selumetinib and leflunomide appear to be working mechanistically, it would be interesting to conduct further staining for cell cycle and cell death proteins; such as the cyclin D and CDK4/6 complex, p16INK4A and caspase 3.

In Chapter 5 of this thesis, the only *in vitro* assay conducted prior to the mouse xenograft study was the cell viability assays performed with leflunomide and selumetinib treated melanoma cells. What could be of

interest for future studies would to elaborate on the *in vitro* assays in this chapter. For example, cell cycle (by PI staining) and cell death analysis (Annexin V/PI staining) could be conducted on a melanoma cell line treated with the combination of leflunomide and selumetinib. This would provide functional data as to how these two drugs exert their effects in combination. This additional data could also then be compared to the data obtained from leflunomide treated cells in chapter 4 of this thesis. Therefore any notable differences in the data obtained compared to that in chapter 4 would be due to the addition of selumetinib.

Further valuable *in vitro* experiments that could be conducted would to be to carry out cell work on primary tumour isolates directly from melanoma patients. Such experiments could offer more clinically relevant information regarding the efficacy of the combination of leflunomide and selumetinib. Although the efficacy of this drug combination was preliminarily tested in a xenograft model, this could be improved in the future by developing patient derived tumour xenografts (PDX) mouse models. One of the major disadvantages of xenograft models is that they have limited ability in predicting how a possible anti-cancer drug would clinically respond in a patient. PDX mouse models overcome this issue in that they implant cancerous tissue directly from a patient's primary tumour into an immunocompromised mouse. This maintains the tumours genetic, phenotypic and stromal components of the tumour and enables more reliable predictions in how patients would respond to a possible anti-cancer drug. However the major disadvantages of the PDX mouse model is that they are expensive and time-consuming (Tentler et al, 2012; Jung, 2014).

This thesis has shown that leflunomide's efficacy as a potential melanoma drug was strongly enhanced in combination with selumetinib. Future experiments could further test leflunomide's efficacy in combination with currently available melanoma chemotherapy drugs, such as dacarbazine. Furthermore with the current success of immunotherapies for treating

melanoma within the field, it would be of interest to investigate whether leflunomide in combination with an immunotherapy (such as ipilimumab) is also successful. Determining if leflunomide has the versatility to achieve similar results with an immunotherapy could reinforce the conclusion of this thesis that suggests leflunomide to be a promising drug in the battle against melanoma.

References

Ackerman A, McDermott DF, Lawrence DP, Gunturi LA, Flaherty KT, Giobbie-Hurder A, Hodi FS, Ibrahim N, Atkins MB, Cho DC and Sullivan RJ (2012) Outcomes of patients with malignant melanoma treated with immunotherapy prior to or after vemurafenib. *J Clin Oncol* **30**, (suppl; abstr 8569).

Alcalá AM and Flaherty KT (2012) BRAF inhibitors for the treatment of metastatic melanoma clinical trials and mechanisms of resistance. *Clin Cancer Res* **18**; 33-39.

Alessi DR, Saito Y, Campbell DG, Cohen P, Sithanandam G, Rapp U, Ashworth A, Marshall CJ and Cowley S (1994) Identification of the sites in MAP kinase kinase-1 phosphorylated by p74raf-1. *Embo J* **13**; 1610-1619.

Alessi DR, Cuend A, Cohen P, Dudley DT and Soltiel AR (1995) PD098059 is a specific inhibitor of the activation of mitogen-activated protein kinase kinase in vitro and in vivo. *J Biol Chem* **17**; 27489-94.

Atefi M, von Eeuw E, Attar N, Ng C, Chu C et al (2011) Reversing melanoma cross-resistance to BRAF and MEK inhibitors by co-targeting the AKT/mTOR pathway. *PloS one* **6**; e28973.

Ascierto PA, Simeone E, Giannarelli D, Grimaldi AM, Romano A and Mozzillo N (2012) Sequencing of BRAF inhibitors and ipilimumab in patients with metastatic melanoma: a possible algorithm for clinical use. *J Transl Med* **10**;

Ascierto PA, Schadendorf D, Berking C, Agarwala SS, van Herpen CM, Queirolo P, Blank CU, Hauschild A, Beck JT, St-Pierre A, Niazi F, Wandel S, Peters M, Zube A, Dummer R (2013) MEK162 for patients with advanced

melanoma harbouring NRAS or Val600 BRAF mutations: a non-randomised, open-label phase 2 study. *Lancet Oncol* **14**; 249-256.

Bandarchi B, Ma L, Navab R, Seth A and Rasty G (2010) From melanocyte to metastatic melanoma. *Dermatol Res and Pract* **2010**; 1-8.

Baumann P, Mandl-Weber S, Völkl A, Adam C, Bumeder I, Oduncu F, Schmidmaier R (2009) Dihydroorotate dehydrogenase inhibitor A771726 (leflunomide) induces apoptosis and diminishes proliferation of multiple myeloma cells. *Mol Cancer Ther* **8**; 366-375.

Bender RP, McGinniss MJ, Esmay P, Velazquez EF and Riemann JDR (2013) Identification of HRAS mutations and absence of GNAQ or GNA11 mutations in deep penetrating nevi. *Modern Pathology* **26**; 1320-1328.

Boussemart L, Malka-Mahieu H, Girault I, Allard D, Hemmingsson O, Tomasic G, Thomas M, Basmadjian C, Ribeiro N, Frédéric Thuaud F, Mateus C, Routier E, Kamsu-Kom N, Agoussi S, Eggermont AM, Laurent Désaubry L, Caroline Robert C and Vagner S (2014) eIF4F is a nexus of resistance to anti BRAF anti MEK cancer therapies. *Nature* **513**; 105-109.

Brtva TR, Drugan JK, Ghosh S, Terrell RS, Campbell Burk S, Bell RM and Der CJ (1995) Two distinct Raf domains mediate interaction with Ras. *J Biol Chem* **270**; 9806-9812.

Breedveld FC and Dayer JM (2000) Leflunomide: mode of action in the treatment of rheumatoid arthritis. *Ann Rheum Dis* **59**; 841–849.

Buday L, Warne PH and Downward J (1995) Downregulation of the Ras activation pathway by MAP kinase phosphorylation of Sos. *Oncogene* **11**; 1327-1331.

Byron SA, Loch DC, Wellens CL, Wortmann A, Wu J, Wang J, Nomoto K and Pollock PM (2012) Sensitivity to the MEK inhibitor E6201 in melanoma

cells is associated with mutant BRAF and wildtype PTEN status. *Mol Cancer* **5**;

Cancer Research UK, (2012) CancerStats. Key facts: Skin cancer. Available from:http://publications.cancerresearchuk.org/downloads/product/CS_KF_SKIN.pdf Accessed on March 3rd 2015.

Cárdenas-Navia LI, Cruz P, Lin JC, NISC Comparative Sequencing Programme, Rosenberg SA and Samules Y (2010) Novel somatic mutations in heterotrimeric G proteins in melanoma. *Cancer Biol Ther* **1**; 33-37.

Caunt CJ and Keyse SM (2013) Dual-specificity MAP kinase phosphatases (MKPs): shaping the outcome of MAP kinase signaling. *FEBS J* **280**; 489-504.

Caunt CJ, Sale MJ, Smith PD and Cook SJ (2015) MEK1 and MEK2 inhibitors and cancer therapy: the long and winding road. *Nature Reviews* **15**; 577-592.

Chambers CA, Kuhns MS, Egen JG and Allison JP (2001) CTLA-4 – mediated inhibition in regulation of T cell responses: mechanisms and manipulation in tumour immunotherapy. *Annu Rev Immunol* **19**; 565-594.

Chapman PB, Hauschild A, Robert C et al (2011) Improved survival with vemurafenib in patients with metastatic melanoma. *N Engl J Med* **364**; 2507-2516.

Chen RE and Thorner J (2007) Function and regulation in MAPK signaling pathways. *Biochem Biophys Acta* **1773**; 1311-1340.

Cherwinski HM, McCarley D, Schatzman R, Devens B and Ransom JT (1995) The immunosuppressant leflunomide inhibits lymphocyte progression through cell cycle by a novel mechanism. *J Pharmacol Exp Ther* **272**; 460–468.

Chin L (2003) The genetics of malignant melanoma: Lessons from mouse and man. *Nat Rev Cancer* **3**; 559-570.

Choi H, Kim JY, Chang YT, Nam HG (2014) Forward chemical genetic screening. *Methods Mol Biol* **1062**; 393-404.

Chou TC, Talalay P (1984) Quantitative analysis of dose-effect relationships: the combined effects of multiple drugs or enzyme inhibitors. *Adv Enzyme Regul.* **22**; 27-55.

Chou TC (2010) Drug combination studies and their synergy quantification using the Chou-Talalay method. *Cancer Res* **70**; 440-446.

Chou TC (2006) Theoretical basis, experimental design, and computerized simulation of synergism and antagonism in drug combination studies. *Pharmacol Rev* **58**; 621-681.

Chudnovsky Y, Khavari PA and Adams AE (2005) Melanoma genetics and the development of rational therapeutics. *J Clin Invest* **115**; 813-824.

Colanesi S, Taylor KL, Temperley ND, Lundegaard PR, Liu D, North TE, Idhizaki H, Kelsh RN and Patton E (2012) Small molecule screening identifies targetable zebrafish pigmentation pathways. *Pigment Cell Melanoma Res* **25**; 131-143.

Cong F, Cheung AK, and Huang SHA (2012) Chemical Genetics–Based Target Identification in Drug Discovery. *Annual Review of Pharmacology and Toxicology* **52**; 57-78.

Cooper CD and Raible DW (2009) Mechanisms for reaching the differentiated state: insights from neural crest derived melanocytes. *Semin Cell Dev Biol* **20**; 105-110.

Cully M, You H, Levine AJ and Mak TW (2006) Beyond PTEN mutations: the PI3K pathway as an integrator of multiple inputs during tumorigenesis. *Nature Reviews Cancer* **6**; 184-192.

Curtin JA, Busam K, Pinkel D and Bastian BC (2006) Somatic activation of KIT in distinct subtypes of melanoma. *J Clin Oncol* **24**; 4340-4346.

Davies H, Bignell GR, Cox C et al. (2002) Mutations of the BRAF gene in human cancer. *Nature* **417**; 949-954.

Dong C, Waters SB, Holt KH and Pessin JE (1996) SOS phosphorylation and dissociation of the Grb2-SOS complex by the ERK and JNK signalling pathways. *J Biol Chem* **271**; 6328-6332.

Dorsky RI, Moon RT and Raible DW (1998). Control of neural crest fate by the Wnt signalling pathway. *Nature* **369**; 370-373.

Dorsam RT and Gutkinds RT (2007) G-protein coupled receptors and cancers. *Nature Reviews Cancer* **7**; 79-94.

Doughty MK, Müller J, Ritt DA, Zhou M, Zhou XZ, Copeland TD, Conrads TP, Veenstra TD, Lu KP and Morrison DK (2005) Regulation of Raf-1 by direct feedback phosphorylation. *Mol Cell* **17**; 215-224.

Downward J (1996) Control of Ras activation. *Cancer Surv* **27**; 87-100.

Drakakis G, Hendry AE, Hanson KM, Brewerton SC, Bodkin MJ, Evans DA, Wheeler GN and Bender A (2014) Comparative mode-of-action analysis following manual and automated phenotype detection in *Xenopus laevis*. *Med. Chem. Commun* **5**; 389-396.

Drummer R and Flaherty KT (2012) Resistance patterns with tyrosine kinase inhibitors in melanoma: new insights. *Curr Opin Oncol* **24**; 150-154.

Dudley DT, Pang L, Decker SJ, Bridges AJ and Saltiel AR (1995) A synthetic inhibitor of the mitogen-activated protein kinase cascade. *Proc Natl Acad Sci* **15**; 7686-7689.

Erickson CA and Reedy MV (1998). Neural crest development: The interplay between morphogenesis and cell differentiation. *Curr Top Dev Bio* **40**; 177-209.

Euw EV, Atefi M, Attar N, Chu C, Zachariahs S, Burgess BL, Mok S, Ng C, Wong DJL, Chmielowski B, Litcher DI, Koya RC, McCannel TA, Izmailova E and Ribas A (2012) Antitumour effects of the investigational selective MEK inhibitor TAK733 against cutaneous and uveal melanoma cell lines. *Mol Cancer* **11**; 1-9.

Favata MF, Horiuchi KY, Manos EJ, Daulerio AJ, Stradley DA, Feeser WS, Van Dyk DE, Pitts WJ, Earl RA, Hobbs F, Copeland RA, Magolda RL, Scherle PA and Trzaskos JM (1998) Identification of a novel inhibitor of mitogen-activated protein kinase kinase. *J Biol Chem* **29**; 18623-32.

Ferrell JE and Bhatt RR (1997) Mechanistic studies of the dual phosphorylation of mitogen-activated protein kinase. *J Biol Chem* **272**; 19008-19016.

Flaherty KT, Puzanov J, Kim KB et al (2010a) Inhibition of mutated, activated BRAF in metastatic melanoma. *N Engl J Med* **363**; 809-819.

Flaherty K (2010b) Advances in drug development. BRAF validation in melanoma. *Clin Adv Hematol Oncol* **8**; 31-34.

Flaherty KT, Robert C, Hersey P, Nathan P, Garbe C, Milhem M, Demidov LV, Hassel JC, Rutkowski P, Mohr P, Dummer R, Trefzer U, Larkin JM, Utikal J, Dreno B, Nyakas M, Middleton MR, Becker JC, Casey M, Sherman LJ, Wu FS, Ouellet D, Martin AM, Patel K, Schadendorf D; METRIC Study

Group (2012a) Improved survival with MEK inhibition in BRAF-mutated melanoma. *N Engl J Med* **367**; 107-114.

Flaherty KT, Infante JR, Daud A, Gonzalez R, Kefford RF, Sosman J, Hamid O, Schuchter L, Cebon J, Ibrahim N, Kudchadkar R, Burris HA 3rd, Falchook G, Algazi A, Lewis K, Long GV, Puzanov I, Lebowitz P, Singh A, Little S, Sun P, Allred A, Ouellet D, Kim KB, Patel K, Weber J (2012b) Combined BRAF and MEK inhibition in melanoma with BRAF V600 mutations *N Engl J Med* **367**; 1694-1703.

Fox RI, Herrmann ML, Frangou CG, Wahl GM, Morris RE, Strand V, Kirschbaum BJ (1999) Mechanism of action for leflunomide in rheumatoid arthritis. *Clin Immunol* **93**; 198-208.

Gaggioli C and Sahai E (2007) Melanoma invasion - current knowledge and future. *Pigment cell res* **20**; 161-172.

Garraway LA, Widlund HR, Rubin MA, Getz G, Berger AJ, Ramaswamy S, Beroukhi R, Milner DA, Granter SR, Du J, Lee C, Wagner SN, Li C, Golub TR, Rimm DL, Meyerson ML, Fisher DE and Sellers WR (2005) Integrative genomic analyses identify MITF as a lineage survival oncogene amplified in malignant melanoma. *Nature* **436**; 112-122.

Georgescu MM (2010) PTEN tumour suppressor network in PI3K-Akt pathway control. *Genes and cancer* **1**; 1170-1177.

Gilley R, Lochhead PA, Balmanno K, Oxley D, Clark J and Cook SJ (2012) CDK1, not ERK1/2 or ERK5, is required for mitotic phosphorylation of BIM_{EL}. *Cellular signalling* **24**; 170-180.

Gilmartin AG, Bleam MR, Groy A, Moss KG, Minthorn EA, Kulkarni SG, Rominger CM, Erskine S, Fisher KE, Yang J, Zappacosta F, Annan R, Sutton D and Laquerre SG (2011) GSK1120212 (JTP-74057) is an inhibitor

of MEK activity and activation with favourable pharmacokinetic properties for sustained *in vivo* pathway inhibition. *Clin Cancer Res* **17**; 989-1000.

Goldsmith ZG and Dhanasekaran DN (2007) G protein regulation of MAPK networks. *Oncogene* **26**; 3122-3142.

Gray-Schopfer, Wellbrock C and Marais R (2007) Melanoma biology and new targeted therapy. *Nature* **445**; 851-857.

Hail N Jr, Chen P, Kepa JJ and Bushman LR (2012) Evidence supporting a role for dihydroorotate dehydrogenase, bioenergetics and p53 in selective teriflunomide-induced apoptosis in transformed versus normal human keratinocytes. *Apoptosis* **17**; 258-268.

Haass NK, Sproesser K, Nguyen TK, Contractor R, Medina CA, Nathanson KL, Herlyn M and Smalley KS (2008) The mitogen-activated protein/extracellular signal-related kinase kinase inhibitor AZD6244 (ARRY-142886) induces growth arrest in melanoma cells and tumour regression when combined with docetaxel. *Clin Cancer Res* **1**; 230-9.

Haq R and Fisher DE (2011) Biology and clinical relevance of the microphthalmia family of transcription factors in human cancer. *J Clinical Oncology* **29**; 3474-3482.

Hartman ML and Czyz M (2015) MITF melanoma: mechanisms behind its expression and activity. *Cell Mol Life Sci* **72**; 1249-1260.

Harvey RD (2014) Immunologic and clinical effects of targeting PD-1 in lung cancer. *Clin Pharmacol Ther* **96**; 214-223.

Hatzivassiliou G, Song K, Yen I et al (2010) RAF inhibitors prime wild-type RAF to activate MAPK pathway and enhance growth. *Nature* **464**; 431-436.

Hayflick L and Moorhead PS (1961) The serial cultivation of human diploid cell strains. *Exp Cell Res* **25**; 585-621.

Heidorn SJ, Milagre C, Whittaker S et al (2010) Kinase-dead BRAF and oncogenic RAS cooperate to drive tumour progression through CRAF. *Cell* **140**; 209-221.

Heisermann GJ, Wiley HS, Walsh BJ, Ingraham HA, Fiol CJ and Gill GN (1990) Mutational removal of the Thr669 and Ser671 phosphorylation sites alters substrate specificity and ligand-induced internalization of the epidermal growth factor receptor. *J Biol Chem* **265**; 12820-12827.

Herrmann ML, Schleyerback R and Kirschbaum BJ (2000) Leflunomide, an immunomodulatory drug for the treatment of rheumatoid arthritis and other autoimmune disease. *Immunopharmacology* **47**;:273–289.

Hino R, Kabashima K, Kato Y, Yagi H, Nakamura M, Honio T, Okazaki T and Tokura Y (2010) Tumor cell expression of programmed cell death-1 ligand 1 is a prognostic factor for malignant melanoma. *Cancer* **116**; 1757-1766

Hodi FS, O'Day SJ, McDermott DF (2010) Improved survival with ipilimumab in patients with metastatic melanoma. *N Engl J Med* **363**; 711-723.

Holderfield M, Deuker MM, McCormick F, McMahon M (2014) Targeting RAF kinases for cancer therapy: BRAF-mutated melanoma and beyond. *Nature Reviews Cancer* **14**; 455–467.

Hornyak TJ, Hayes DJ, Chiu LY and Ziff EB (2001) Transcription factors in melanocyte development: distinct roles for Pax-3 and Mitf. *Mechanisms of Development* **101**; 47-59.

Hu CD, Kanya K, Tamada M, Akasaka K, Shirouzu M, Yokoyama S and Kataoka T (1995) Cysteine rich region of Raf1 interacts with activator domain of post-translationally modified Ha-Ras. *J Biol Chem* **270**; 30274-30277.

Jakob JA, Bassett RL Jr, Ng CS, Curry JL, Joseph RW, Alvarado GC, Rohlfs ML, Richard J, Gershenwald JE, Kim KB, Lazar AJ, Hwu P, Davies MA (2012) NRAS mutation status is an independent factor in metastatic melanoma. *Cancer* **118**; 4014-4023.

Johannessen CM, Boehm JS, Kim SY et al (2010) COT drives resistance to RAF inhibition through MAP kinase pathway reactivation. *Nature* **468**; 968-972.

Johnson GL and Dahansekar N (1989) The G-protein family and their interaction with receptors. *Endocr Rev* **10**; 317-331.

Jung J (2014) Human tumor xenograft models for preclinical assessment of anticancer drug development. *Toxicol Res* **30**; 1-5.

Kalinec G, Nazarali AJ, Hermouet S, Xu N, Gutkind JS (1992) Mutated alpha subunit of the Gq protein induces malignant transformation NIH3T3 cells. *Mol Cell Biol* **12**; 4687-93.

Kawasumi M and Nghiem P (2007) Chemical genetics: elucidating biological systems with small-molecule compounds. *J Invest Dermatol* **127**; 1577-1584.

Khutornenko AA, Roudko VV, Chernyak BV, Vartapetian AB, Chumakov PM and Evstafieva AG (2010) Pyrimidine synthesis links mitochondrial respiration to the p53 pathway. *Proc Natl Acad Sci USA* **107**; 12828-12833.

Kier ME, Butte MJ, Freeman GJ and Sharpe AH (2008) PD-1 and its ligands in tolerance and immunity. *Annu Rev Immunol* **26**; 677-704.

Kirkwood JM, Bastholt L, Robert C, Sosman J, Larkin J, Hersey P, Middleton M, Cantarini M, Zazulina V, Kemsley K, Dummer R (2012) Phase II, open-label, randomized trial of the MEK 1/2 inhibitor selumetinib as monotherapy versus temozolomide in patients with advanced melanoma. *Clin Cancer Res* **18**; 555-567.

Kolch W (2000) Meaningful relationships: the regulation of the Ras/Raf/MEK/ERK pathway by protein interactions. *Bio Chem J* **351**; 289-305.

Kumar R, Angelini S, Snellman E and Hemminki K (2004) BRAF mutations are common somatic events in melanocytic nevi. *J Invest Dermatol* **122**; 342-348.

Landis CA, Masters SB, Spada A, Pace AM, Bourne HR, Vallar L (1989) GTPase inhibiting mutations activate the alpha chain of Gs and stimulate adenylyl cyclase in human pituitary tumours. *Nature* **31**; 692-696.

Lane DP (1992) p53, guardian of the genome. *Nature* **358**; 15–16.

Lang R, Wagner H and Heeg K (1995) Differential effects of the immunosuppressive agents cyclosporine and leflunomide in vivo *Transplantation* **59**; 382–389.

Larkin J, Chiarion-Sileni V, Gonzalez R, Grob JJ, Cowey CL, Lao CD, Schadendorf D, Dummer R, Smylie M, Rutkowski P, Ferrucci PF, Hill A, Wagstaff J, Carlino MS, Haanen JB, Maio M, Marquez-Rodas I, McArthur GA, Ascierto PA, Long GV, Callahan MK, Postow MA, Grossmann K, Sznol M, Dreno B, Bastholt L, Yang A, Rollin LM, Horak C, Hodi FS, Wolchok JD (2015) Combined Nivolumab and Ipilimumab or Monotherapy in Untreated Melanoma *N Engl J Med* (Ahead of print).

Law MH, Macgregor S and Hayward NK (2012) Melanoma Genetics: Recent Findings Take Us Beyond Well-Traveled Pathways. *Journal of Investigative Dermatology* **132**; 1763–1774.

Le Douarin NM, Calloni GW and Dupin E (2008). The stem cells of the neural crest. *Cell Cycle* **7**; 1013-1019.

Levy C, Khaled M and Fisher DE (2006) MITF: master regulator of melanocyte development and melanoma oncogene. *Trends in molecular medicine* **12**; 406-414.

Liggi S, Drakakis G, Hendry AE, Hanson KM, Brewerton SC, Wheeler GN, Bodkin MJ, Evans D A. and Bender A (2013). Extensions to In Silico Bioactivity Predictions Using Pathway Annotations and Differential Pharmacology Analysis: Application to *Xenopus laevis* Phenotypic Readouts. *Mol. Inf.* **32**, 1009-1024.

Li N, Batzer A, Daly R, Yajnik V, Skolnik E, Chardin P, Bar-Sagi D, Margolis B and Schlessinger J (1993) Guanine-nucleotide-releasing factor hSOS1 binds to Grb2 and links receptor tyrosine kinase to Ras signalling. *Nature* **363**; 85-88.

Li X, Huang Y, Jiang J and Frank SJ (2008) ERK-dependent threonine phosphorylation of EGF receptor modulates receptor downregulation and signalling. *Cell Signal* **20**; 2145-2155.

Linke SP, Clarkin KC, Di Leonardo A, Tsou A and Wahl GM (1996) A reversible, p53-dependent G0/G1 cell cycle arrest induced by ribonucleotide depletion in the absence of detectable DNA damage. *Genes Dev* **10**; 934–947.

Linke SP, Clarkin KC and Wahl GM (1997) p53 mediates permanent arrest over multiple cell cycles in response to gamma irradiation. *Cancer Res* **57**;1171–1179.

Lipson EJ and Drake CG (2011) Ipilimumab: An anti-CTLA-4 antibody for metastatic melanoma. *Clin Cancer Res* **17**; 6958-62.

Little AS, Balmanno K, Sale MJ, Newman S, Dry JR, Hampson M, Edwards PA, Smith PD and Cook SJ (2011) Amplification of the driving oncogene,

KRAS or BRAF, underpins acquired resistance to MEK1/2 inhibitors in colorectal cancer cells. *Sci Signaling* **4**; ra17.

Little AS, Smith PD and Cook SJ (2013) Mechanisms of acquired resistance to ERK1/2 pathway inhibitors. *Oncogene* **32**; 1207-1215.

Long GV, Stroyakovskiy D, Gogas H, Levchenko E, de Braud F, Larkin J, Garbe C, Jouary T, Hauschild A, Grob JJ, Chiarion Sileni V, Lebbe C, Mandalà M, Millward M, Arance A, Bondarenko I, Haanen JB, Hansson J, Utikal J, Ferraresi V, Kovalenko N, Mohr P, Probachai V, Schadendorf D, Nathan P, Robert C, Ribas A, DeMarini DJ, Irani JG, Casey M, Ouellet D, Martin AM, Le N, Patel K, Flaherty K (2014) Combined BRAF and MEK Inhibition versus BRAF Inhibition Alone in Melanoma *N Engl J Med* **371**;1877-1888.

Lorusso PM, Adjei AA, Varterasian M, Gadgeel S, Reid J, Mitchell DY, Hanson L, DeLuca P, Bruzek L, Piens J, Asbury P, Van Becelaere K, Herrera R, Sebolt-Leopold J, Meyer MB (2005) Phase I and pharmacodynamics study of the oral MEK inhibitor CI-1040 in patients with advanced malignancies. *J Clin Oncol* **23**; 5281-5293.

Mansh M (2011) Ipilimumab and cancer immunotherapy: A new hope for advanced stage melanoma. *Yale J Biol Med* **84**; 381-9.

Margarit SM, Sondermann H, Hall BE, Nagar B, Hoelz A, Pirruccello M, Bar-Sagi D and Kuriyan J (2003) Structural evidence for feedback activation by Ras. GTP if the Ras-specific nucleotide exchange factor SOS. *Cell* **112**; 685-695.

Marshall CJ (1996) Ras effectors. *Curr Opin Cell Biol* **8**; 197-204.

McArthur GA (2015) Combination therapies to inhibit the RAF/MEK/ERK pathway in melanoma; we are not done yet. *Front Oncol* **5**; 1-6.

McKay MM and Morrison DK (2007) Integrating signals from RTKs to ERK/MAPK. *Oncogene* **26**; 3113-3121.

Melanoma Research Foundation. It's a Fact. (2012). Available from: <http://www.melanoma.org/sites/default/files/u13882/It%27s%20a%20Fact%20Sheet%20-%20Updated.pdf>. Accessed on March 3rd 2015.

Metabolic database (2015) Available from: <http://www.metabolic-database.com/html/search.html> Accessed on 12th November 2015.

Monzon JG and Dancey J (2012) Targeted agents for the treatment of metastatic melanoma. *OncoTargets and Therapy* **5**; 31-46.

Morandell S, Stasyk T, Skvortsov S, Ascher S and Huber LA (2008) Quantitative proteomics and phosphoproteomics reveal novel insights into complexity and dynamics of the EGFR signaling network. *Proteomics* **8**; 4383-4401.

Nazarian R, Shi H, Wang Q et al (2010) Melanomas acquire resistance to BRAF(V600E) inhibition by RTK or N-RAS upregulation. *Nature* **468**; 973-977.

Neyns B, Seghers AC, Wilgenhof S and Lebbe C (2012) Successful rechallenge in two patients with BRAF-V600-mutant melanoma who experienced previous progression during treatment with selective BRAF inhibitor. *Melanoma Res* **22**; 466-472.

Ocana A, , Amir E, Yeung C, Seruga B and Tannock IF (2012) How valid are claims for synergy in published clinical studies? *Annals of Oncology* **23**; 2161-2166.

Okazaki T and Honjo T (2007) PD-1 and PD-1 ligands: from discovery to clinical application. *Int Immunol* **19**; 813-824.

Onken MD, Worley LA, Long MD, Duan S, Council ML, Bowcock AM and Harbour JW (2008) Oncogenic mutations in GNAQ occur early in uveal melanoma. *Invest Ophthalmol Vis Sci* **49**; 5230-5234.

Owens DM and Keyse SM (2007) Differential regulation of MAP kinase signaling by dual-specificity protein phosphatases. *Oncogene* **26**; 3203-3213.

Paraiso KH, Xiang Y, Rebecca VW et al (2011) PTEN loss confers BRAF inhibitor resistance to melanoma cells through the suppression of BIM expression. *Cancer Res* **71**; 2750-2619.

Pardoll DM (2012) The blockade of immune checkpoints in cancer. *Nat Rev Cancer* **12**; 252-264.

Pawson T (2002) Regulation and targets of receptor tyrosine kinases. *Eur J Cancer* **38**; S3-10.

Peggs KS, Quezada SA, Korman AJ et al (2006) Principles and use of anti-CTLA4 antibody in human cancer. *Curr Opin Immunol* **16**; 206-13.

Porfiri E and McCormick F (1996) Regulation of epidermal growth factor receptor signaling by phosphorylation of the ras exchange factor hSOS1. *J Biol Chem* **271**; 5971-5877.

Quilliam LA, Khosrovi-Far R, Huff SY and Der CJ (1995) Guanine nucleotide exchange factors; activators of the RAS superfamily of proteins. *BioEssays* **17**; 395-404.

Puzanov I, Callahan MK, Linette GP, Patel SP, Luke JJ, Sosman JA, Wolchok JD, Hamid O, Minor DR, Orford KW, Hug BA, Ma B, Matthys GM and Hoos A (2014) Phase 1 study of the BRAF inhibitor dabrafenib (D) with or without the MEK inhibitor trametinib (T) in combination with ipilimumab (Ipi) for V600E/K mutation–positive unresectable or metastatic melanoma (MM). *J Clin Oncol* 32:5s, (suppl; abstr 2511).

Rinehart J, Adjei AA, Lorusso PM, Waterhouse D, Hecht JR, Natale RB, Hamid O, Varterasian M, Asbury P, Kaldjian EP, Gulyas S, Mitchell DY, Herrera R, Sebolt-Leopold JS, Meyer MB (2004) Multicentre phase II study of the oral MEK inhibitor CI-1040, in patients with advanced non-small-cell lung, breast, colon and pancreatic cancer/.. *J Clin Oncol*. **22**; 4456-4462.

Peterson RT, Link BA, Dowling JE and Schreiber SL (2000) Small molecule developmental screens reveal the logic and timing of vertebrate development. *Proc Natl Acad Sci* **97**; 12965-12969.

Poulikakos Pi, Zhang C, Bollag G et al (2010) RAF inhibitors transactivate RAF dimers and ERK signaling in cells with wild-type BRAF. *Nature* **464**; 427-430.

Poulikos IP and Rosen N (2011) Mutant BRAF melanomas-dependence and resistance. *Cancer Cell* **19**; 11-15.

Ribas A, Kim KB, Schuchter LM et al (2011) BRIM-2: an open-label multicenter phase II study of vemurafenib in previously treated patients with BRAFV600E mutation-positive melanoma. *J Clin Oncol* **29**; Suppl:8509 abstract.

Ribas A and Flaherty KT (2011) BRAF targeted therapy changes the treatment paradigm in melanoma. *Nat Rev Clin Oncol* **24**; 426-433.

Ribas A, Hodi SF, Callahan M, Konto C and Wolchok J (2013) Hepatotoxicity with Combination of Vemurafenib and Ipilimumab. *N Engl J Med* **368**;1365-1366.

Ritt DA, Monson DM, Specht SI, Morrison DK (2010) Impact of feedback phosphorylation and Raf-1 heterodimerization on normal and mutant B-Raf signaling. *Mol Cell Biol* **30**; 806-819.

Robert C and Ghiringhelli F (2009) What is the role of cytotoxic T lymphocyte-associated antigen 4 blockade in patients with metastatic melanoma? *Oncologist* **14**; 848-61.

Robert C, Thomas L, Bondarenko I et al (2011) Ipilimumab plus dacarbazine for previously untreated metastatic melanoma. *N Engl J Med* **364**; 2517-2526.

Robert C, Long GV, Brady B, Dutriaux C, Maio M, Mortier L, Hassel JC, Rutkowski P, McNeil C, Kalinka-Warzocho E, Savage KJ, Hernberg MM, Lebbé C, Charles J, Mihalciou C, Chiarion-Sileni V, Mauch C, Cognetti F, Arance A, Schmidt H, Schadendorf D, Gogas H, Lundgren-Eriksson L, Horak C, Sharkey B, Waxman IM, Atkinson V, Ascierto PA (2015) Nivolumab in previously untreated melanoma without BRAF mutation. *N Engl J Med* **372**; 320-330.

Rushworth LK, Hindley AD, O'Neill E and Kolch W (2006) Regulation and role of Raf-1/B-Raf heterodimerization. *Mol Cell Biol* **26**; 2262-2272.

Schadendorf D, Hodi FS, Robert C, Weber JS, Margolin K, Hamid O, Patt D, Chen TT, Berman DM and Wolchok JD (2015) Pooled analysis of long-term survival data from Phase II and Phase III trials of ipilimumab in unresectable or metastatic melanoma. *J Clin Oncol* **10**; 1889-1894.

Schapler KA (2014) PD-L1 expression and tumor-infiltrating lymphocytes: Revisiting the antitumor immune response potential in breast cancer. *Oncoimmunology* **3**; e29288.

Sclessinger J (2000) Cell signalling by receptor tyrosine kinases. *Cell* **103**; 211-225.

Sebolt-Leopold JS, Dudley DT, Herrera R, Becelaere KV, Wiland A, Gowan RC, Teclé H, Barretts D, Bridges A, Przybranski S, Leopold WR and

Saltiel AR (1999) Blockade of the MAP kinase pathway suppresses growth of colon tumours in vivo. *Nature Medicine* **5**; 810-816.

Shoemaker RH (2006) The NCI60 human tumour cell line anticancer drug screen. *Nature Reviews* **6**; 813-823.

Siemasko KF, Chong ASF, Williams JW, Bremer EG and Finnegan A (1996) Regulation of B cell function by the immunosuppressive agent leflunomide. *Transplantation* **61**; 635–642.

Shull AY, Latham-Schwark, Ramasamy P et al. (2012) Novel somatic mutations to PI3K pathway genes in metastatic melanoma. *PLOS ONE* **7**; e43369.

Skin Cancer Foundation. (2012). Available from: <http://www.skincancer.org/skin-cancer-information/melanoma>. Accessed on March 3rd 2015.

Slominski A, Tobin DJ, Shibahara S and Wortsman J (2004) Melanin pigmentation in mammalian skin and its hormonal regulation. *Physiol. Rev* **84**; 1155-1228.

Solit DB, Garraway LA, Pratilas CA, Sawai A, Getz G, Basso A, Ye Q, Lobo JM, She Y, Osman I, Golub TR, Sebolt-Leopold J, Sellers WR, Rosen N (2006) BRAF mutation predicts sensitivity to MEK inhibition. *Nature* **439**; 358-362.

Solit DB and Rosen N (2010) Oncogenic RAF: a brief history of time. *Pigment Cell Res* **23**; 760-762.

Sommer L (2011) Generation of melanocytes from neural crest cells. *Pigment Cell Res* **24**; 411-421.

Sosman JA, Kim KB, Schuchter L et al (2012) Survival in BRAF V600-mutant advance melanoma treated with vemurafenib. *N Engl J Med* **366**; 707-714.

Spring DR (2005) Chemical genetics to chemical genomics: small molecules offer big insights. *Chem Soc Rev* **34**; 472-482.

Stahl JM, Sharma A, Cheung M et al (2004) Deregulated Akt3 activity promotes development of malignant melanoma. *Cancer Res* **64**; 7002-7010.

Steck PA, Pershouse MA, Jasser SA et al (1997) Identification of a candidate tumour suppressor gene, MMAC1, at chromosome 10q23.3 that is mutated in multiple advanced cancers. *Nat Genet* **15**; 56-62.

Stagg J and Allard B (2013) Immunotherapeutic approaches in triple-negative breast cancer: latest research and clinical prospects. *Ther Adv Med Oncol* **5**; 169-181.

Steel GG and Peckham MJ (1979) Exploitable mechanisms in combined radiotherapy-chemotherapy: the concept of additivity. *Int J Radiat Oncol Biol Phys* **5**; :85-91.

Stones CJ, Kim JE, Joseph WR, Leung E, Marshall ES, Finlay GJ, Shelling AN and Baguley BC. (2013) Comparison of responses of human melanoma cell lines to MEK and BRAF inhibitors. *Front. Genet.* **4:66**.

Sturm OE, Orton R, Grindlay J, Birtwistle M, Vyshemirsky V, Gilbert D, Calder M, Pitt A, Kholodenko B, Kolch W (2010) The mammalian MAPK/ERK pathway exhibits properties of a negative feedback amplifier. *Sci Signal* **3**; ra90.

Sznol M, Kluger HM, Callahan MK, Postow MA, Gordon RA, Segal NH, Rizvi NA, Lesokhin AM, Atkins MB, Kirkwood JM, Burke MM, Ralabate AL, Rivera AL, Kronenberg SA, Agunwamba B, Feely W, Hong Q, Krishnan S, Gupta AK, Wolchok JD (2014) *J Clin Oncol* 32:5s (suppl; abstr LBA9003^).

Tarhini A, Lo E and Minor DR (2010) Releasing the brake on the immune system: Ipilimumab in melanoma and other tumours. *Cancer Biother Radiopharm* **25**; 601-13.

Das Thakur, Salangsang F, Landman AS, Sellers WR, Pryer NK, Levesque MP, Dummer R, McMahon M and Stuart DD (2013) Modelling vemurafenib resistance in melanoma reveals a strategy to forestall drug resistance. *Nature* **494**; 251-256.

Das Thakur M and Stuart DD (2013) The evolution of melanoma resistance reveals therapeutic opportunities. *Cancer Res* **73**; 6106-6110.

Tentler JJ, Tan AC, Weekes CD, Jimeno A, Leong S, Pitts TM, Arcaroli JJ, Messersmith WA and Eckhardt SG (2012) Patient-derived tumour xenograft as models for oncology drug development. *Nature Reviews Clinical Oncology* **9**; 338-350.

Tomlinson ML, Field RA and Wheeler GN (2005) *Xenopus* as a model organism in developmental chemical genetic screens. *Mol Biosyst* **1**; 223-228.

Tomlinson ML, Rejzek M, Fidock M, Field RA and Wheeler GN (2009) Chemical genomics identifies compounds affecting *Xenopus laevis* pigment cell development. *Mol Biosyst* **5**; 376-384.

Topalian SL, Hodi FS, Brahmer JR, Gettinger SN, Smith DC, McDermott DF, Powderly JD, Carvajal RD and Sosman JA (2012) Safety, activity and immune correlates of anti-PD-1 antibody in cancer. *N Engl J Med* **366**; 2443-2454.

Tran SL, Haferkamp S, Scurr LL et al (2012) Absence of distinguishing senescence traits in human melanocytic nevi. *J Invest Dermatol* **132**; 2226-2234.

Trump BE, Berezsky IK, Chang SH and Phelps PC (1997) The Pathways of Cell Death: Oncosis, Apoptosis, and Necrosis. *Toxicologic Pathology* **25**; 82-88.

Tsao H, Chin L, Garraway LA and Fisher DE (2012) Melanoma: from mutations to medicine. *Genes and Development* **26**; 1131-1155.

Tykodi SS (2014) PD-1 as an emerging therapeutic target in renal cell carcinoma: current evidence. *OncoTargets Ther* **7**; 1349-1359.

Ulrich A and Schlessinger J (1990) Signal transduction by receptors with tyrosine kinase activity. *Cell* **61**; 203-212.

U.S. Food and Drug Administration (2013) Available from: <http://www.fda.gov/drugs/informationondrugs/approveddrugs/ucm376547.htm>. Accessed on September 21st 2015.

Uong A and Zon LI (2010). Melanocytes in development and cancer. *J. Cell. Physiol* **222**; 38-41.

Van Raamsdonk CD, Bezrookove V, Green G, Bauer J, Gaugler L, O'Brien JM, Simpson EM, Barsh GS and Bastian BC (2009) Frequent somatic mutations of GNAQ in uveal melanoma and blue nevi. *Nature* **29**; 599-602.

Van Raamsdonk CD, Griewank KG, Crosby MB, Garrido MC, Vemula S, Wiesner T, Obenaus AC, Wackernagel W, Green G, Bouvier N, Sozen MM, Baimukanova G, Roy R, Heguy A, Dolgalev I, Khanin R, Busam K, Speicher MR, O'Brien J, Bastian BC (2010) Mutations in GNA11 in uveal melanoma. *N Engl J Med* **363**; 2191-9.

Verschraegen C (2012) The monoclonal antibody to cytotoxic T lymphocyte antigen 4, ipilimumab, in the treatment of melanoma. *Cancer Management and Research* **4**; 1-8.

Villanueva J, Vultur A, Lee JT et al (2010) Acquired resistance to BRAF inhibitors mediated by a RAF kinase switch in melanoma can be overcome by cotargeting MEK and IGF-1R/PI3K. *Cancer Cell* **18**; 683-695.

Wagle N, Emery C, Berger MF et al (2011) Dissecting therapeutic resistance to RAF inhibition in melanoma by tumour genomic profiling. *J Clin Oncol* **29**; 3085-3096.

Wahl GM, Linke SP, Paulson TG and Huang L-C (1997) Maintaining genetic stability through TP53 mediated checkpoint control. *Cancer Surv* **29**; 183–219.

Wang N and Herbert DN (2006) Tyrosinase maturation through the mammalian secretory pathway: bringing color to life. *Pigment Cell Res* **19**; 3-18.

Wheeler GN and Brändli AW (2009) Simple vertebrate models for chemical genetics and drug discovery screens: lessons from zebrafish and *Xenopus*. *Developmental Dynamics* **238**; 1287-1308.

Wheeler GN and Lui KJ (2012) *Xenopus*: an ideal system for chemical genetics. *Genesis* **50**; 207-218.

White RM, Cech J, Ratanasirintrawoot S et al (2011) DHODH modulates transcriptional elongation in the neural crest and melanoma. *Nature* **471**; 518-522.

Wolchok JD¹, Kluger H, Callahan MK, Postow MA, Rizvi NA, Lesokhin AM, Segal NH, Ariyan CE, Gordon RA, Reed K, Burke MM, Caldwell A, Kronenberg SA, Agunwamba BU, Zhang X, Lowy I, Inzunza HD, Feely W, Horak CE, Hong Q, Korman AJ, Wigginton JM, Gupta A, Sznol M (2013) Nivolumab plus ipilimumab in advanced melanoma. *N Engl J Med* **369**; 122-133.

Xu X, Williams JW, Bremer EG, Finnegan A and Chong ASF (1995) Inhibition of protein tyrosine phosphorylation in T cells by a novel immunosuppressive agent, leflunomide. *J Biol Chem* **270**; 12398–12403.

Yajima I, Kumasaka MY, Thang ND et al. (2011) RAS/RAF/MEK/ERK and PI3K/PTEN/AKT signalling in malignant melanoma progression and therapy. *Dermatology Research and Practice* **2012**; 1-5.

Yazdi AS, Palmedo G, Flaig MJ, Puchta U, Reckwerth A, Rutten A, Mentzel T, Hugel H, Hantschke M and Schmid-Wendtner MH (2003) Mutations of the BRAF gene in benign and malignant melanocytic lesions. *J Invest Dermatol* **121**; 1160-1162.

Zaidi MR, Day CP and Merlino G (2008) From UVs to metastases: Modeling melanoma initiation and progression in the mouse. *J Invest Dermatol* **128**; 2381-2391.

Zhang G and Herlyn M (2012) Human nevi: No longer precursors of melanomas? *J Invest Dermatol* **132**; 2133-2134.

Zheng CF and Guank L (1994) Activation of MEK family kinases requires phosphorylation of two conserved ser/thr residues. *Embo J* **13**; 1123-1131.

Zhou B, Wang ZX, Zhao Y, Brautigam DL and Zhang ZY (2002) The specificity of extracellular signal-regulated kinase 2 dephosphorylation by protein phosphatases. *J Biol Chem* **277**; 31818-31825.

Zhu S, Yan X, Xiang Z, Ding HF and Cui H (2013) Leflunomide reduces proliferation and induces apoptosis in neuroblastoma cells *In Vitro* and *In Vivo*. *PLOS ONE* **8**;